60 TGS ($(NH_2CH_2COOH)_3 \cdot H_2SO_4$) family

60A Pure compounds

No. 60A-1 $(NH_2CH_2COOH)_3 \cdot H_2SO_4$, Triglycine sulfate (TGS)

(M = 323.28; [D: 340.38])

1a Ferroelectricity in TGS was discovered by Matthias et al. in 1956. 56Mat

b

phase	II	I	
state	F	P	
crystal system	monoclinic	monoclinic	
space group	$P2_1 - C_2^{2}$ [a])	$P2_1/m - C_{2h}^{2}$ [a])	[a]) 57Woo
Θ [°C]	49.42 [b]) [D: 60 [c])]		[b]) 66Gon [c]) 61Sil

Transition temperature for the deuterated crystal: see Fig. 60A-1-034 in 5a and Fig. 60B-2-001 in No. 60B-2.

$P_s \parallel [010]$. 56Mat

$\rho = 1.69 \cdot 10^3$ kg m^{-3} at RT. 57Woo

Transparent, colorless. 58Nit

Cleavage plane: (010). 57Woo

2a Crystal growth: evaporation method and cooling method from aqueous solution. 66Kol, 58Nit

Solubility in H_2O: Fig. 60A-1-001; see also 71Bre

Crystal growth in space: see 94Lal1

Epitaxial growth of oriented thin film: see 81Had

b Crystal form: Fig. 60A-1-002, Fig. 60A-1-003, Fig. 60A-1-004.

3a Unit cell parameters:

Axial system by Wood et al.: a = 9.15 Å, b = 12.69 Å, c = 5.73(3) Å, β = 105° 40′ (20′) at RT. 57Woo

Axial system by Hoshino et al.: a' = 9.41$_7$ Å, b' = 12.64$_3$ Å, c' = 5.73$_5$ Å, β' = 110° 23′ at RT. 59Hos

They are related by $\boldsymbol{a'} = \boldsymbol{a} + \boldsymbol{c}$, $\boldsymbol{b'} = -\boldsymbol{b}$, $\boldsymbol{c'} = -\boldsymbol{c}$.

See Fig. 60A-1-004.

In the following tables and figures, Wood et al's system will be used without any special reference.

Other axial systems according to various authors: Fig. 60A-1-005.

b Z = 2 in phases I and II. 57Woo

Crystal structure: Fig. 60A-1-006.

Positional and temperature parameters: Table 60A-1-001, Table 60A-1-002, Table 60A-1-003, Table 60A-1-004, Table 60A-1-005, Table 60A-1-006; see also 85Sol, 91Mos

Effect of X-ray irradiation: see 76Fle2

Interatomic distances and bond angles: Table 60A-1-007, Table 60A-1-008.

Structure change associated with phase transition: Table 60A-1-009, Table 60A-1-010, Table 60A-1-011; Fig. 60A-1-007, Fig. 60A-1-008.

4	Thermal expansion: Fig. 60A-1-009, Fig. 60A-1-010, Fig. 60A-1-011, Fig. 60A-1-012; see also	62Shi, 80Sta, 94Kor
	Effect of irradiation: see	74Ste, 91Kas
	Thermal expansion of α-alanine-doped crystal: see	87Jim, 90Kas
	Thermal expansion of Cr^{3+}-doped crystal: see	94Jim
5a	Dielectric constants: Fig. 60A-1-013, Fig. 60A-1-014, Fig. 60A-1-015, Fig. 60A-1-016, Fig. 60A-1-017, Fig. 60A-1-018.	
	Dielectric constant of powdered specimen: see	80Mot, 84Ami, 86Kur
	Effect of X-ray irradiation: see	85Nak1
	Effect of acoustic wave: see	90Dya
	Effect of electric field normal to the *b* axis: see	84Sto
	Dielectric dispersion: Fig. 60A-1-019, Fig. 60A-1-020, Fig. 60A-1-021, Fig. 60A-1-022, Fig. 60A-1-023, Fig. 60A-1-024, Fig. 60A-1-025, Fig. 60A-1-026; see also	80Vol, 80Dev
	Dielectric dispersion at low frequency: Fig. 60A-1-027, Fig. 60A-1-028.	
	Effect of γ-irradiation on dielectric dispersion: see	79Paw
	Effect of amplitude of measuring ac field: Fig. 60A-1-029.	
	Change of Θ determined by dielectric constant measurement: Table 60A-1-012; Fig. 60A-1-030, Fig. 60A-1-031, Fig. 60A-1-032, Fig. 60A-1-033, Fig. 60A-1-034, Fig. 60A-1-035; see also	60Jon, 88Mro
	See also Fig. 60B-2-001 in No. 60B-2.	
	Dielectric properties of α-alanine-doped crystal: Fig. 60A-1-036; see also	71Kev, 85Bre2, 91Nak
	For crystals doped with other amino-acids: see	85Pyk, 90Sta, 95Sta, 95Jin2
	For crystals doped with metallic ions such as Sn^{2+}, Ni^{2+}, Co^{2+}, Cu^{2+}, Pt^{2+}, Cu^{3+}, Fe^{3+} and Cr^{6+}: see	61Toy, 80Pol, 87Bre, 95Fan
	For crystals doped with rare earth: see	88Zhe, 95Mih
b	Nonlinear dielectric properties: Fig. 60A-1-037, Fig. 60A-1-038, Fig. 60A-1-039, Fig. 60A-1-040, Fig. 60A-1-041, Fig. 60A-1-042; see also Fig. 60A-1-029 and	76Ehs, 86Zio

Coefficient of power series expansion of electric field strength $E = (1/\chi_P)P + \xi P^3 + \zeta P^5$:

ξ [$\cdot 10^{11}$ V m^5 C^{-3}]	ζ [$\cdot 10^{14}$ V m^9 C^{-5}]	
6.5	3.6	58Tri
5.6	6.0	68Gon
5.6	10.4	74Zer
6.25	4.02	77Cho

Microwave nonlinearity: see 73Mat
Nonlinear properties of α-alanine-doped crystal: see 91Cac
Nonlinear properties of Cu^{2+}-doped crystal: see 88Fug

c Spontaneous polarization: Fig. 60A-1-043, Fig. 60A-1-044, Fig. 60A-1-045, Fig. 60A-1-046.
Coercive field: Fig. 60A-1-047, Fig. 60A-1-048, Fig. 60A-1-049, Fig. 60A-1-050, Fig. 60A-1-051, Fig. 60A-1-052.

d Pyroelectric properties: Fig. 60A-1-053, Fig. 60A-1-054, Fig. 60A-1-055.
Effect of γ-irradiation: Fig. 60A-1-056.
Pyroelectric properties at low temperature: see 91Nov, 83Man
Nonlinear pyroelectric effects: see 91Bog
Pyroelectric properties of α-alanine-doped crystal: Fig. 60A-1-057; see also 75Kev, 91Jim
For aniline-doped crystal: see 80Kra, 87Zha
For metallic-ion-doped crystal: see 81Rud, 84Bha
Effect of simultaneous organic and inorganic dopants: see 94Lal2
Electrocaloric effect: Fig. 60A-1-058, Fig. 60A-1-059, Fig. 60A-1-060.
α-alanine-doped crystal: see 92Jim
Figure of merit at 25 °C: 75Bee

	p_2 [$\cdot 10^{-4}$ C K^{-1} m^{-2}]	F.M.$_R$ [$\cdot 10^{-12}$ C m J^{-1}]	F.M.$_{D^*}$ [$\cdot 10^{-6}$ C m$^{3/2}$ J^{-1} Ω$^{1/2}$]
TGS	4	4.6	2.1
DTGS	2.7	6	2.4

6a Heat capacity: Fig. 60A-1-061, Fig. 60A-1-062, Fig. 60A-1-063, Fig. 60A-1-064, Fig. 60A-1-065;
see also 79Ema2, 83Nov
Low temperature heat capacity: Fig. 60A-1-066; see also 86Vil
Effect of γ-ray irradiation: Fig. 60A-1-067, Fig. 60A-1-068.
Effect of doping: Fig. 60A-1-069;
see also 87Jim, 83Nov

Transition heat, transition entropy:

ΔQ_m [J mol^{-1}]	ΔS_m [J K mol^{-1}]	
1446	4.60	64Str
1409	4.47	70Tel
1629	5.06	77Tar

b	Thermal conductivity: Fig. 60A-1-070, Fig. 60A-1-071, Fig. 60A-1-072; see also	91Str
	α-alanine-doped crystal: see	87Jim
	Fe^{3+}-doped crystal: Table 60A-1-013.	
	Thermal diffusivity: Fig. 60A-1-073, Fig. 60A-1-074.	
	For crystals doped with Ni^{2+}, Co^{2+}, Cu^{2+}, Cr^{3+} and Fe^{3+}: see	87Gaf
7a	Piezoelectric constant: Fig. 60A-1-075, Fig. 60A-1-076, Fig. 60A-1-077; see also	82Tyl, 61Gil
	Effect of γ-irradiation: see	85Bal, 62Sil
	Nonlinear piezoelectric constant: see	87Yus
b	Electrostrictive constant: Table 60A-1-014; Fig. 60A-1-078; see also	80Ehs2
8a	Elastic constant: Table 60A-1-015, Table 60A-1-016; Fig. 60A-1-079, Fig. 60A-1-080, Fig. 60A-1-081, Fig. 60A-1-082;	
	see also	61Gil, 77Hau
	For crystals doped with Cu^{2+} and Cr^{3+}: see	85Wol, 89Wol
	Effect of doping of some organic compounds: see	93Dzi, 91Wol
	See also subsection 10b.	
	Hydrostatic pressure derivatives of elastic stiffness constants: Table 60A-1-017.	
	Acoustic surface wave: Fig. 60A-1-083, Fig. 60A-1-084; see also	90Hal
	Ultrasonic wave velocity and attenuation: Table 60A-1-018; Fig. 60A-1-085, Fig. 60A-1-086, Fig. 60A-1-087, Fig. 60A-1-088, Fig. 60A-1-089, Fig. 60A-1-090, Fig. 60A-1-091, Fig. 60A-1-092, Fig. 60A-1-093, Fig. 60A-1-094, Fig. 60A-1-095, Fig. 60A-1-096, Fig. 60A-1-097; see also	92Dzi2
	Effect of irradiation: Fig. 60A-1-098, Fig. 60A-1-099; see also	88Kon1
	α-alanine-doped crystal: Fig. 60A-1-100, Fig. 60A-1-101; see also	77Tyl
	For crystals doped with metallic ions: Fig. 60A-1-101; see also	85Vin, 86Vik
	Phosphate-doped crystal: see	94Sre
	Nitroaniline-doped crystal: see	77Tyl
b	Third order elastic constant: Fig. 60A-1-102, Fig. 60A-1-103; see also	89Dvo
	Acoustic second harmonics: Fig. 60A-1-104.	
9a	Orientation of optic plane: see	59Dio, 86Mey
	Refractive indices: Fig. 60A-1-105, Fig. 60A-1-106, Fig. 60A-1-107, Fig. 60A-1-108.	
	Rotation angle of optical indicatrix and optical axial angle: Fig. 60A-1-109, Fig. 60A-1-110, Fig. 60A-1-111, Fig. 60A-1-112.	
	Effect of X-ray irradiation on the refractive indices: see	81Rom1
	Birefringence: Fig. 60A-1-113, Fig. 60A-1-114, Fig. 60A-1-115, Fig. 60A-1-116.	
	Reflection in infrared region: Fig. 60A-1-117, Fig. 60A-1-118.	
	Ultraviolet spectra: Fig. 60A-1-119, Fig. 60A-1-120; see also	81Rom2
	Effect of X-ray irradiation on ultraviolet spectra: see	84Vas
	Far-infrared spectra: Fig. 60A-1-121.	
	Infrared spectra of phosphate-doped crystal: see	94Hub
	Infrared spectra of urea-doped crystal: see	96Cha
	Ultraviolet spectra of Fe^{3+}-doped crystal: see	91Mon
b	Electrooptic effect: Fig. 60A-1-122, Fig. 60A-1-123, Fig. 60A-1-124, Fig. 60A-1-125, Fig. 60A-1-126, Fig. 60A-1-127, Fig. 60A-1-128, Fig. 60A-1-129, Fig. 60A-1-130; see also Fig. 60A-1-137.	

c	Piezooptic effect: Table 60A-1-019, Table 60A-1-020; Fig. 60A-1-131, Fig. 60A-1-132.	
	For crystal doped with α-alanine: see	90Myt
d	Optical activity: Fig. 60A-1-133, Fig. 60A-1-134.	
	For crystal doped with α-alanine: see	92Kor
	Electrogyration: Fig. 60A-1-135, Fig. 60A-1-136, Fig. 60A-1-137;	
	see also Fig. 60A-1-130 and	84Kor, 93Kus, 94Kam
e	Nonlinear optical susceptibility: $d_{23} / d_{36}^{KDP} = 0.07$ for $\lambda = 693.4$ nm.	67Son3
	See also	62Sav
10a	Raman scattering: Fig. 60A-1-138, Fig. 60A-1-139, Fig. 60A-1-140, Fig. 60A-1-141, Fig. 60A-1-142; see also Fig. 60A-1-118.	
	α-alanine-doped crystal: see	94San, 95Jin1
	Phosphate-doped crystal: see	94Hub
b	Brillouin scattering: Table 60A-1-020; Fig. 60A-1-143, Fig. 60A-1-144, Fig. 60A-1-145, Fig. 60A-1-146.	
	45° Brillouin scattering: see	84Tsu
	Brillouin scattering in γ-irradiated crystal: see	81Kit, 81Yur
	Elastic constant from Brillouin scattering: see Table 60A-1-016; Fig. 60A-1-081.	
11	Electric conduction: Fig. 60A-1-147, Fig. 60A-1-148, Fig. 60A-1-149, Fig. 60A-1-150, Fig. 60A-1-151;	
	see also	61Gur, 86Mil
	Effect of irradiation: Table 60A-1-021; see also	83Ami, 92Elk
	For crystals doped with α-alanine: see	89Oka
	For crystals doped with metallic ions: Table 60A-1-021; see also	83Jar
	Electric breakdown strength: $2.2 \cdot 10^4$ kV m^{-1} at RT.	69Gur
	Thermally excited light emission: see	73Jaq, 89Pop
13a	NMR: Table 60A-1-022, Table 60A-1-023, Table 60A-1-024, Table 60A-1-025, Table 60A-1-026; Fig. 60A-1-152, Fig. 60A-1-153, Fig. 60A-1-154, Fig. 60A-1-155, Fig. 60A-1-156, Fig. 60A-1-157, Fig. 60A-1-158;	
	see also	76Buc, 89Slo
b	ESR and ENDOR: Table 60A-1-027.	
	Cr^{3+}-doped crystal: Table 60A-1-028; Fig. 60A-1-159, Fig. 60A-1-160, Fig. 60A-1-161, Fig. 60A-1-162;	
	see also	74Kat, 74Sta2, 75Win, 76Yur, 91Sch
	Cu^{2+}-doped crystal: Table 60A-1-029, Table 60A-1-030, Table 60A-1-031, Table 60A-1-032, Table 60A-1-033;	
	see also	65Los, 77Bot, 86Bot

	Fe^{3+}-doped crystal: see	85Fer
	VO^{2+}-doped crystal: Table 60A-1-034, Table 60A-1-035; Fig. 60A-1-162; see also	75Fuj, 75Wie, 79Bot
	Irradiated crystal: Table 60A-1-036; Fig. 60A-1-163; see also	76Kot, 78Wel, 69Kat, 91Vol
c	Mössbauer effect: Table 60A-1-037.	
14	Integrated intensity of Bragg reflection: Fig. 60A-1-164, Fig. 60A-1-165, Fig. 60A-1-166, Fig. 60A-1-167. Diffuse scattering: Fig. 60A-1-168, Fig. 60A-1-169, Fig. 60A-1-170.	
15a	Domain structure: Fig. 60A-1-171, Fig. 60A-1-172. Domains have been observed by various methods:	
	Etching method.	62Kon, 60Chy1
	Powder pattern technique.	58Pea, 73Hat
	Decoration method.	75Mey, 89Hil, 76Dis, 90Wic
	Dew method.	66Fou
	Scanning electron microscope.	71LeB, 89LeB, 89Sog
	Nematic liquid crystal.	79Glo, 80Tik, 81Nak
	Cleavage.	75Nak, 89Nak
	Pyroelectric-probe technique.	75Had1, 84Pra
	X-ray topography.	69Pet, 78Tak, 70Tak
	Domain pattern evolution after heat treatment: see	68Mor, 81Don, 85Nak2, 89Tom
	Irradiation effect on domain structure: see	86Nak, 95Mel
	Fractal aspect of domain structure: see	95Oza
b	Domain switching: Fig. 60A-1-173, Fig. 60A-1-174, Fig. 60A-1-175, Fig. 60A-1-176, Fig. 60A-1-177, Fig. 60A-1-178, Fig. 60A-1-179, Fig. 60A-1-180.	
	Analysis of switching current: see	59Fat, 74Lop, 90del, 87Per
	Domain wall motion: Fig. 60A-1-181.	

	Domain wall motion was observed by	
	successive etching,	69Hay
	powder pattern technique,	59Chy
	liquid crystal method,	86Tik, 89Don, 89Mat
	pyroelectric-probe technique.	75Had2, 95Nak
	Light emission induced by domain switching: see	74God, 81Mon
	Electron emission induced by domain switching: see	95Bie, 90Ros
	Interaction of domain wall motion and crystal defects: see	62Nak, 77Kom
	Optical gyration study of domain switching: see	91Kob, 84Kor
	Effect of acoustic wave on domain switching: see	65Rud
	Chaotic behavior of domain switching:	90Bei, 92Dro
	Domain switching in α-alanine-doped crystal: see	88Tik, 89DeL
	Domain switching in Cr^{2+} doped-crystal: see	95Kam
16	Etchant for revealing domain structure and etch pits due to dislocations: H_2O, ethylalcohol.	60Toy, 67Saw, 77Sus
	X-ray topographic study of crystal defects: see	72Izr, 73Pol, 81Par
	Dielectric properties of thin film and surface layer: see	68Chi, 76Wur, 84Had
	Examination of crystal surface with atomic force microscope: see	94Lut, 95Blu, 96Ohg

Table 60A-1-001. $(NH_2CH_2COOH)_3 \cdot H_2SO_4$ (TGS). Structure of phase I [73Ito]. Fractional coordinates and temperature parameters at 57 °C. U_{ij} is defined by Eq. (d) in Introduction. Crystallographic axes are referred to those of Hoshino et al., see subsection 3a.

Atom	*x*	*y*	*z*	U_{11}	U_{22}	U_{33}	U_{23}	U_{31}	U_{12}
				[10^{-2} Å^2]					
Sulfate ion									
S	1.0003(1)	0.2500(0)	0.2252(2)	1.8(0)	1.8(0)	1.9(0)	0.0(0)	0.8(0)	0.0(0)
O(1)	0.8585(4)	0.2538(37)	0.0058(7)	2.1(2)	4.8(7)	2.4(2)	0.9(8)	0.4(1)	1.1(8)
O(2)	0.9651(5)	0.2396(28)	0.4549(7)	4.1(2)	2.3(12)	2.4(2)	–0.1(3)	1.6(2)	0.0(3)
O(3)	1.0864(3)	0.1550(2)	0.2100(5)	3.5(1)	2.5(1)	4.6(2)	0.1(1)	1.7(1)	0.9(1)
Glycine I									
O(11)	0.6077(5)	0.2626(18)	1.0709(8)	2.3(2)	3.6(10)	3.3(2)	–0.6(3)	0.8(2)	–0.1(2)
O(12)	0.4937(6)	0.2568(33)	0.6609(10)	4.1(3)	9.6(11)	3.8(3)	0.5(8)	1.2(2)	–2.4(9)
C(11)	0.4885(7)	0.2600(33)	0.8682(12)	2.7(2)	1.6(14)	3.6(3)	–0.3(3)	1.2(2)	–0.3(4)
C(12)	0.3375(7)	0.2543(19)	0.9096(12)	2.5(2)	4.4(5)	3.8(3)	–0.5(7)	0.9(2)	–2.3(6)
N(1)	0.3576(7)	0.2136(6)	1.1602(13)	2.8(3)	6.6(6)	4.7(4)	0.6(3)	2.1(3)	1.0(3)
Glycine II									
O(21)	0.7817(3)	0.4994(3)	0.2313(5)	3.3(1)	5.3(2)	3.5(1)	1.2(1)	0.9(1)	–0.3(1)
O(22)	0.5439(3)	0.4741(3)	0.2186(6)	2.7(1)	6.2(2)	4.9(2)	0.9(2)	0.7(1)	0.9(1)
C(12)	0.6903(4)	0.4722(3)	0.3254(7)	3.1(2)	2.8(2)	3.1(2)	0.1(1)	0.7(1)	0.1(1)
C(22)	0.7381(4)	0.4297(3)	0.5879(7)	3.1(2)	4.4(2)	3.1(2)	0.7(1)	1.1(1)	–0.1(2)
N(2)	0.9061(3)	0.4282(3)	0.7009(5)	3.4(2)	3.2(2)	2.3(1)	0.3(1)	0.3(1)	–0.4(1)

Table 60A-1-002. $(NH_2CH_2COOH)_3 \cdot H_2SO_4$ (TGS). Structure of phase II [76Fle1]. Fractional coordinates of the non-hydrogen atoms. Crystallographic axial system by Hoshino et al. is adopted, see subsection 3a. $a' = 9.419(1)$ Å, $b' = 12.647(1)$ Å, $c' = 5.727(1)$ Å, $\beta' = 110.32°$ at RT. See also Fig. 60A-1-006.

Atom	*x*	*y*	*z*
S	0.99956(8)	0.25	0.22648(13)
O(1)	0.8572(3)	0.2470(4)	0.0072(5)
O(2)	0.9649(3)	0.2500(4)	0.4565(5)
O(3)	1.0847(5)	0.3455(3)	0.2091(8)
O(4)	1.0873(4)	0.1550(3)	0.2131(8)
O(11)	0.6068(3)	0.2379(4)	1.0798(5)
O(12)	0.4946(4)	0.2292(4)	0.6677(6)
C(11)	0.4883(4)	0.2367(5)	0.8727(8)
C(12)	0.3398(4)	0.2418(6)	0.9164(7)
N(1)	0.3580(4)	0.2856(4)	1.1643(8)
O(21)	0.7790(5)	0.4927(4)	0.2232(8)
O(22)	0.5387(5)	0.4659(4)	0.1974(8)
C(21)	0.6825(5)	0.4659(4)	0.3118(8)
C(22)	0.7273(5)	0.4290(4)	0.5764(9)
N(2)	0.8934(5)	0.4284(3)	0.6989(8)
O(31)	0.2138(5)	0.4958(4)	0.7611(8)
O(32)	0.4475(5)	0.5164(4)	0.7527(9)
C(31)	0.2997(5)	0.5229(4)	0.6560(9)
C(32)	0.2472(5)	0.5665(4)	0.3979(9)
N(3)	0.0810(5)	0.5727(4)	0.2949(8)

Table 60A-1-003. $(NH_2CH_2COOH)_3 \cdot H_2SO_4$ (TGS). Structure of phase II [76Fle1]. Anisotropic temperature parameters and principal value of root mean square amplitudes of thermal vibration. Anisotropic temperature parameter: see Table 60A-1-001. U_{ij} is defined by Eq. (d) in Introduction. Values of U_{ij} [Å^2] are $\times 10^4$ for S and $\times 10^3$ for O, N, and C.

Atom	U_{11}	U_{22}	U_{33}	U_{12}	U_{13}	U_{23}	Min.	Inter.	Max.
	[Å^2]						[Å]		
S	117(9)	95(9)	145(9)	–8(4)	67(4)	–3(5)	0.094	0.100	0.123
O(1)	14(1)	35(2)	20(1)	–4(2)	5(1)	–2(2)	0.115	0.147	0.188
O(2)	30(2)	27(2)	19(1)	–4(2)	16(1)	–1(2)	0.107	0.158	0.184
O(3)	29(2)	9(2)	39(2)	–8(2)	19(2)	0(2)	0.069	0.160	0.203
O(4)	20(2)	16(2)	36(2)	6(2)	11(2)	1(2)	0.108	0.152	0.189
O(11)	15(1)	42(2)	27(2)	2(2)	7(1)	–2(2)	0.121	0.167	0.205
O(12)	31(2)	56(4)	27(2)	9(2)	11(1)	–1(2)	0.158	0.170	0.245
C(11)	19(2)	17(3)	29(2)	4(2)	10(1)	1(2)	0.115	0.147	0.169
C(12)	15(2)	26(2)	29(2)	0(2)	6(1)	–4(3)	0.121	0.154	0.181
N(1)	16(2)	47(3)	29(2)	–7(2)	14(2)	–3(2)	0.101	0.172	0.220
O(21)	25(2)	38(2)	29(2)	–1(2)	10(2)	12(2)	0.137	0.160	0.218
O(22)	19(2)	41(2)	31(2)	5(2)	4(2)	7(2)	0.129	0.181	0.211
C(21)	21(2)	15(2)	17(2)	1(2)	4(2)	4(2)	0.110	0.137	0.156
C(22)	18(2)	30(3)	27(3)	–1(2)	11(2)	1(2)	0.121	0.165	0.176
N(2)	21(2)	14(2)	15(2)	–1(2)	5(2)	3(2)	0.105	0.132	0.151
O(31)	25(2)	41(2)	25(2)	–3(2)	10(2)	10(2)	0.130	0.161	0.217
O(32)	18(2)	64(3)	39(2)	12(2)	9(2)	11(2)	0.121	0.194	0.262
C(31)	22(2)	17(2)	33(2)	2(2)	9(2)	–2(2)	0.126	0.151	0.184
C(32)	22(2)	25(2)	24(2)	2(2)	10(2)	6(2)	0.130	0.147	0.176
N(3)	19(2)	19(2)	16(2)	–2(2)	5(2)	2(2)	0.124	0.130	0.153

Table 60A-1-004. $(NH_2CH_2COOH)_3 \cdot H_2SO_4$ (TGS). Structure of phase II [76Fle1]. Fractional coordinates and mean square displacements of hydrogen atoms. Crystallographic axial system by Hoshino et al. is adopted, see subsection 3a.

Atom	x	y	z	$\overline{u^2}$ [Å^2]
H(11)	0.432(7)	0.335(6)	1.235(12)	0.04(2)
H(12)	0.273(8)	0.285(6)	1.186(12)	0.05(2)
H(13)	0.403(8)	0.250(10)	1.275(12)	0.06(2)
H(14)	0.272(5)	0.286(4)	0.798(8)	0.01(1)
H(15)	0.293(5)	0.174(4)	0.908(8)	0.01(1)
H(16)	0.691(9)	0.273(8)	1.015(14)	0.08(3)
H(21)	0.922(6)	0.484(5)	0.719(10)	0.02(1)
H(22)	0.911(6)	0.394(5)	0.846(10)	0.02(1)
H(23)	0.929(6)	0.383(5)	0.608(11)	0.02(2)
H(24)	0.694(8)	0.478(6)	0.707(12)	0.03(2)
H(25)	0.662(7)	0.372(5)	0.572(12)	0.03(2)
H(26)	0.511(7)	0.489(5)	0.054(9)	0.02(1)
H(31)	0.014(14)	0.521(10)	0.290(22)	0.12(4)
H(32)	0.044(7)	0.596(5)	0.104(12)	0.03(2)
H(33)	0.043(8)	0.629(7)	0.402(14)	0.05(2)
H(34)	0.286(8)	0.533(6)	0.322(13)	0.04(2)
H(35)	0.286(6)	0.637(5)	0.388(10)	0.02(1)

Table 60A-1-005. $(NH_2CH_2COOH)_3 \cdot H_2SO_4$ (TGS). Structure of phase II determined by neutron diffraction [73Kay]. Fractional coordinates and temperature parameters. B_{ij} is defined by Eq. (a) in Introduction. Inverse polarity of the structure is shown in Fig. 60A-1-006. Crystallographic axial system by Hoshino et al. is adopted, see subsection 3a.

				B_{ij} [10^4]					
	x	y	z	B_{11}	B_{22}	B_{33}	B_{12}	B_{13}	B_{23}
Sulfate group									
S	0.0002(12)	0.2500(22)	0.2282(19)	37(15)	25(10)	104(39)	–27(40)	25(40)	101(66)
O(1)	0.8568(6)	0.2472(14)	0.0046(11)	38(8)	49(6)	160(22)	–2(24)	12(22)	110(39)
O(2)	0.9652(7)	0.2468(15)	0.4579(11)	86(10)	41(6)	151(24)	–16(24)	115(25)	–95(38)
O(4)	0.0836(13)	0.1497(11)	0.2064(26)	96(16)	7(8)	286(54)	14(17)	122(42)	–27(30)
O(3)	0.0882(12)	0.3397(14)	0.2172(27)	52(13)	33(9)	282(54)	–5(18)	103(39)	36(32)
Glycine groups									
O(11)	0.6086(9)	0.2548(15)	1.0777(12)	57(10)	54(7)	166(27)	4(25)	34(28)	42(42)
O(12)	0.4953(19)	0.2653(14)	0.6660(15)	76(10)	86(14)	204(31)	5(20)	77(27)	–55(38)
C(11)	0.4890(6)	0.2571(12)	0.8732(10)	47(8)	35(6)	177(23)	–30(15)	54(23)	–10(27)
C(12)	0.3409(7)	0.2510(14)	0.9182(12)	34(8)	42(6)	230(28)	24(21)	80(26)	76(40)
N(1)	0.3584(8)	0.2092(11)	1.1645(14)	38(9)	110(11)	245(31)	21(13)	94(26)	00(24)
H_1	0.707(2)	0.253(2)	1.049(2)	73(18)	71(12)	225(42)	122(40)	59(46)	134(64)
H_2	0.292(3)	0.330(2)	0.897(5)	215(44)	98(23)	694(15)	77(53)	478(140)	264(85)
H_3	0.263(2)	0.198(2)	0.777(4)	82(24)	133(22)	286(77)	–90(37)	86(72)	–71(64)
H_4	0.415(3)	0.143(2)	1.192(4)	224(42)	56(17)	303(75)	56(43)	297(83)	154(59)
H_5	0.252(2)	0.189(2)	1.178(31)	63(22)	120(18)	357(70)	–2(29)	173(65)	61(50)
H_6	0.411(2)	0.260(4)	1.301(4)	118(27)	187(32)	336(74)	120(60)	41(75)	–240(128)
O(31)	0.2202(11)	0.5020(12)	0.7774(22)	40(13)	59(10)	167(43)	–7(17)	–4(40)	116(34)
O(32)	0.4600(11)	0.5298(13)	0.7973(22)	23(12)	79(10)	125(39)	–3(17)	–19(32)	–47(29)
C(31)	0.3190(10)	0.5302(11)	0.6898(17)	96(15)	20(6)	150(35)	–10(15)	99(36)	19(22)
C(32)	0.2683(13)	0.5653(13)	0.4166(21)	74(14)	44(10)	230(49)	–42(22)	88(47)	82(31)
N(3)	0.1046(8)	0.5673(8)	0.3017(15)	53(9)	39(8)	52(34)	–19(13)	–42(27)	21(23)
H_8	0.327(3)	0.525(3)	0.327(5)	97(28)	143(30)	313(91)	21(41)	120(80)	–49(72)
H_9	0.319(2)	0.645(2)	0.417(5)	94(27)	97(23)	415(105)	–167(44)	33(79)	121(68)
H_{10}	0.064(3)	0.495(3)	0.295(4)	176(35)	62(22)	284(88)	–36(47)	20(81)	252(69)
H_{11}	0.062(3)	0.600(2)	0.121(5)	227(42)	70(20)	165(109)	24(47)	260(115)	40(75)
H_{12}	0.056(3)	0.614(2)	0.385(5)	161(40)	66(21)	327(101)	102(40)	132(106)	35(65)
O(21)	0.7848(14)	0.4972(13)	0.2405(26)	100(18)	42(9)	280(50)	–15(20)	150(52)	19(36)
O(22)	0.5515(16)	0.4808(15)	0.2480(32)	99(19)	91(12)	342(59)	51(23)	166(54)	67(42)
C(21)	0.6991(10)	0.4727(11)	0.3404(19)	22(10)	40(8)	212(41)	17(12)	41(35)	11(22)
C(22)	0.7485(12)	0.4273(13)	0.5982(19)	99(17)	41(96)	162(43)	34(22)	134(47)	–42(33)
N(2)	0.9192(10)	0.4232	0.7088(22)	98(13)	21(7)	264(45)	–35(16)	151(46)	–5(28)
H_7	0.515(2)	0.501(2)	1.050(4)	53(20)	58(12)	387(114)	28(24)	28(26)	144(62)
H_{13}	0.716(2)	0.482(2)	0.731(4)	111(32)	113(21)	309(83)	52(37)	129(85)	–118(67)
H_{14}	0.715(2)	0.355(3)	0.606(6)	109(31)	72(22)	586(128)	–60(39)	–30(94)	328(81)
H_{15}	0.960(3)	0.502(3)	0.711(5)	169(38)	59(23)	483(113)	–193(45)	112(94)	–200(72)
H_{16}	0.947(3)	0.394(2)	0.870(7)	125(35)	34(18)	371(127)	59(34)	–272(100)	–54(78)
H_{17}	0.950(2)	0.373(2)	0.589(5)	99(28)	110(26)	240(85)	14(36)	262(84)	64(67)

Table 60A-1-006. $[(NH_2CH_2COOH)_3 \cdot H_2SO_4]_{0.16}[(ND_2CH_2COOD)_3 \cdot D_2SO_4]_{0.84}$ ($TGS_{0.16}DTGS_{0.84}$). Fractional coordinates of phase II determined by neutron diffraction [86Che]. Crystallographic axial system by Hoshino et al. is adopted, see subsection 3a. a' = 9.462 Å, b' = 12.706 Å, c' = 5.746 Å, β' = 110.35° at RT.

	x	*y*	*z*
S	–0.0109	0.2482	0.2212
O(1)	0.8546	0.2443	0.0131
O(2)	0.9638	0.2845	0.4584
O(3)	0.0909	0.1517	0.2048
O(4)	0.0861	0.3432	0.2178
O(11)	0.6093	0.2538	1.0833
O(12)	0.4939	0.2702	0.6768
C(11)	0.4900	0.2619	0.8803
C(12)	0.3384	0.2530	0.9213
N(1)	0.3622	0.2106	1.1680
$D(H)_1$	0.7054	0.2479	1.0471
H_2	0.2956	0.3342	0.8973
H_3	0.2561	0.1978	0.7766
$D(H)_4$	0.4226	0.1418	1.1936
$D(H)_5$	0.2585	0.1891	1.1828
$D(H)_6$	0.4151	0.2518	1.3082
O(21)	0.2253	0.5058	0.7696
O(22)	0.4594	0.5315	0.8001
C(21)	0.3200	0.5286	0.6872
C(22)	0.2693	0.5656	0.4190
N(2)	0.1062	0.5672	0.3018
H_8	0.3269	0.5264	0.3168
H_9	0.3078	0.6492	0.3997
$D(H)_{10}$	0.0603	0.4906	0.2851
$D(H)_{11}$	0.0702	0.5961	0.1099
$D(H)_{12}$	0.0538	0.6076	0.3870
O(31)	0.7822	0.4952	0.2423
O(32)	0.5557	0.4814	0.2459
C(31)	0.6984	0.4750	0.3355
C(32)	0.7507	0.4257	0.6031
N(3)	0.9229	0.4219	0.7064
$D(H)_7$	0.5108	0.5043	1.0513
H_{13}	0.7185	0.4773	0.7337
H_{14}	0.7212	0.3534	0.6000
$D(H)_{15}$	0.9685	0.4976	0.7174
$D(H)_{16}$	0.9528	0.3916	0.8788
$D(H)_{17}$	0.9555	0.3707	0.5987

Table 60A-1-007. $(NH_2CH_2COOH)_3 \cdot H_2SO_4$ (TGS). Structure of phase II [76Fle1]. Interatomic distances [Å] and bond angles [deg].

Sulfate ion	
S–O(1)	1.486(2)
S–O(2)	1.463(3)
S–O(3)	1.472(4)
S–O(4)	1.476(4)
O(1)–S–O(2)	110.1(2)
O(1)–S–O(3)	108.5(2)
O(1)–S–O(4)	107.0(2)
O(2)–S–O(3)	111.0(3)
O(2)–S–O(4)	110.5(3)
O(3)–S–O(4)	109.7(2)

Glycine I		Glycine II		Glycine III	
C(11)–O(11)	1.316(4)	C(21)–O(21)	1.232(8)	C(31)–O(31)	1.214(9)
C(11)–O(12)	1.200(6)	C(21)–O(22)	1.284(6)	C(31)–O(32)	1.310(7)
C(11)–C(12)	1.506(6)	C(21)–C(22)	1.499(8)	C(31)–C(32)	1.492(9)
C(12)–N(1)	1.477(7)	C(22)–N(2)	1.475(7)	C(32)–N(3)	1.471(7)
O(11)–C(11)–O(12)	124.6(4)	O(21)–C(21)–O(22)	126.0(5)	O(31)–C(31)–O(32)	124.5(6)
O(11)–C(11)–C(12)	113.3(4)	O(21)–C(21)–C(22)	120.9(5)	O(31)–C(31)–C(32)	123.2(5)
O(12)–C(11)–C(12)	122.0(3)	O(22)–C(21)–C(22)	113.1(6)	O(32)–C(31)–C(32)	112.3(6)
C(11)–C(12)–N(1)	111.8(3)	C(21)–C(22)–N(2)	111.2(6)	C(31)–C(32)–N(3)	110.9(6)

Table 60A-1-008. $(NH_2CH_2COOH)_3 \cdot H_2SO_4$ (TGS). Structure of phase II [76Fle1]. Interatomic distances and bond angles involving hydrogen atoms.

Donor-acceptor	D–A [Å]	D–H [Å]	H–A [Å]	D–H–A [deg]
O(11)–H(16)–O(1)^{I}	2.536(4)	1.08(9)	1.62(8)	139(6)
N(1)–H(11)–O(22)^{I}	2.812(7)	0.92(7)	1.98(8)	149(6)
N(1)–H(12)–O(3)^{II}	2.780(7)	0.85(8)	1.98(8)	156(7)
N(1)–H(13)–O(12)^{I}	2.811(5)	0.78(8)	2.13(7)	147(7)
C(12)–H(14)		0.94(5)		
C(12)–H(15)		0.96(5)		
O(22)–H(26)–O(32)^{III}	2.473(7)	0.82(6)	1.65(7)	171(7)
N(2)–H(21)–O(4)^{IV}	2.904(6)	0.74(8)	2.21(8)	156(8)
N(2)–H(22)–O(1)^{I}	2.986(7)	0.91(6)	2.21(6)	143(4)
N(2)–H(22)–O(3)^{I}	3.037(6)	0.92(6)	2.23(5)	146(5)
N(2)–H(23)–O(2)	2.850(7)	0.92(9)	1.96(8)	160(7)
C(22)–H(24)		1.10(9)		
C(22)–H(24)		0.95(7)		
N(3)–H(31)–O(2)^{V}	2.911(7)	0.91(9)	2.13(9)	143(8)
N(3)–H(31)–O(3)^{V}	2.918(6)	0.91(9)	2.41(10)	116(7)
N(3)–H(32)–O(4)^{VI}	2.976(6)	1.07(7)	1.95(6)	159(6)
N(3)–H(33)–O(2)^{VII}	2.769(7)	1.08(8)	1.74(8)	156(7)
C(32)–H(34)	0.78(7)			
C(32)–H(35)	0.98(7)			

Superscripts I…VII stand for atoms whose coordinates are:
(I) $x, y, 1 + z$
(II) $x - 1, y, 1 + z$
(III) $x, y, z - 1$
(IV) $2 - x, 1/2 + y, 1 - z$
(V) $x - 1, y, z$
(VI) $1 - x, 1/2 + y, - z$
(VII) $1 - x, 1/2 + y, 1 - z$

The coordinates x, y, z are given in Table 60A-1-002 and Table 60A-1-004.

Table 60A-1-009. $(NH_2CH_2COOH)_3 \cdot H_2SO_4$ (TGS). Temperature variation of lattice constants [73Ito]. Crystallographic axial system by Hoshino et al. is adopted, see subsection 3a.

	19 °C	37 °C	57 °C
a' [Å]	9.42_4	9.41_3	9.41_5
b' [Å]	12.64_3	12.64_1	12.64_3
c' [Å]	5.73_5	5.74_1	5.74_0
β' [°]	110.3_6	110.3_5	110.3_3

Table 60A-1-010. $(NH_2CH_2COOH)_3 \cdot H_2SO_4$ (TGS). Temperature variation of bond lengths and angles in the glycine molecules [73Ito]. i = 1, 2, 3.

		19 °C	37 °C	57 °C
Bond lengths [Å]				
O(i1)–C(i1)	Glycine I	1.306(5)	1.309(6)	1.307(7)
	Glycine II	1.213(7)	1.197(16)	1.214(6)
	Glycine III	1.218(8)	1.238(16)	1.214(6)
O(i2)–C(i1)	Glycine I	1.198(7)	1.209(9)	1.208(10)
	Glycine II	1.299(5)	1.332(13)	1.300(4)
	Glycine III	1.305(6)	1.263(12)	1.300(4)
C(i1)–C(i2)	Glycine I	1.527(7)	1.518(9)	1.522(11)
	Glycine II	1.544(8)	1.520(16)	1.514(5)
	Glycine III	1.494(7)	1.509(16)	1.514(5)
C(i2)–N(i)	Glycine I	1.478(8)	1.485(11)	1.477(13)
	Glycine II	1.540(7)	1.543(15)	1.487(4)
	Glycine III	1.460(6)	1.457(14)	1.487(4)
Bond angles [deg]				
O(i1)–C(i1)–O(i2)	Glycine I	125.4(5)	124.1(6)	124.2(7)
	Glycine II	125.7(5)	125.5(10)	125.8(4)
	Glycine III	126.1(5)	125.2(11)	125.8(4)
O(i1)–C(i1)–C(i2)	Glycine I	113.0(4)	114.7(6)	115.0(6)
	Glycine II	122.7(4)	124.1(9)	122.1(3)
	Glycine III	122.1(4)	120.8(8)	122.1(3)
O(i2)–C(i1)–C(i2)	Glycine I	121.5(4)	121.1(5)	120.7(6)
	Glycine II	111.5(5)	110.4(11)	112.1(4)
	Glycine III	111.7(5)	113.9(11)	112.1(4)
C(i1)–C(i2)–N(i)	Glycine I	111.5(4)	110.1(6)	111.0(8)
	Glycine II	106.2(5)	107.7(11)	110.0(3)
	Glycine III	113.1(5)	111.4(11)	110.0(3)

Table 60A-1-011. $(NH_2CH_2COOH)_3 \cdot H_2SO_4$ (TGS). Temperature variation of bond lengths and angles in the sulfate ion [73Ito].

	19 °C	37 °C	57°C
Bond lengths [Å]			
S–O(1)	1.488(2)	1.488(3)	1.485(4)
S–O(2)	1.469(3)	1.467(5)	1.473(6)
S–O(3)	1.472(4)	1.475(9)	1.468(3)
S–O(4)	1.477(4)	1.469(8)	1.468(3)
Bond angles [deg]			
O(1)–S–O(2)	110.2(2)	110.0(2)	110.3(3)
O(1)–S–O(3)	108.4(3)	108.1(5)	109.2(15)
O(1)–S–O(4)	107.5(3)	107.0(5)	109.2(15)
O(2)–S–O(3)	109.5(3)	111.6(6)	106.3(12)
O(2)–S–O(4)	111.0(3)	110.1(6)	106.3(12)
O(3)–S–O(4)	110.2(2)	109.8(5)	109.8(2)

Table 60A-1-012. $(NH_2CH_2COOH)_3 \cdot H_2SO_4$ (TGS), $(NH_2CH_2COOH)_3 \cdot H_2SeO_4$ (TGSe), $(NH_2CH_2COOH)_3 \cdot H_2BeF_4$ (TGFB). Values of γ_i, $\Sigma\gamma_i$ and $d\Theta_f/dp$ [$\cdot 10^{-8}$ K N^{-1} m^2] [78Sta1]. γ_i: the Curie point pressure coefficient measured under uniaxial pressure acting various directions, $d\Theta_f/dp$: measured under hydrostatic pressure. Coordinate system of Fig. 60A-1-003 is adopted.

Crystal	γ_x	γ_y	γ_z	$\Sigma\gamma_i$	$\frac{d\Theta_f}{dp}$
TGS	–6.7	–9.3	+19.0	+3.0	+2.6
TGFB	+2.9	–12.4	+13.5	+4.0	+2.6
TGSe	–16.6	–9.4	+30.0	+4.0	+3.6

Table 60A-1-013. $(NH_2CH_2COOH)_3 \cdot H_2SO_4$ (TGS). Thermal conductivity λ for pure and Fe^{3+}-doped TGS crystals [80Jar]. $T = 25$ °C.

Fe^{3+} dopants concentration in TGS crystal [wt %]	λ [Js^{-1} m^{-1} K^{-1}] in the crystallographic direction		
	[100]	[010]	[001]
0	0.775	0.726	0.714
$6 \cdot 10^{-4}$	0.567	0.548	0.540
$10 \cdot 10^{-4}$	0.515	0.446	0.439
$18 \cdot 10^{-4}$	0.425	0.352	0.345

Table 60A-1-014. $(NH_2CH_2COOH)_3 \cdot H_2SO_4$ (TGS). $Q_{\lambda\mu}$ [m^4 C^{-2}] at RT. Coordinate system: see Fig. 60A-1-003.

Q_{12}	Q_{22}	Q_{32}	Q_{44}	Q_{46}	Q_{52}	Q_{64}	Q_{66}	Q_{h2}*)	Ref.
1.35	2.25	–4	–3.9	0.54	–0.36	3.8	2	–0.4	63Ike
1.6	2.4	–4.45			<0.1			–0.45	63Sch

*) Volume electrostrictive constant: $Q_{h2} = Q_{12} + Q_{22} + Q_{32}$.

Table 60A-1-015. $(NH_2CH_2COOH)_3 \cdot H_2SO_4$ (TGS). Elastic stiffness constants [$\cdot 10^{10}$ N m^{-2}] [84Dun]. Coordinate system: see Fig. 60A-1-003.

c_{11}^E	c_{22}^D	c_{33}^E	c_{44}^D	c_{55}^E	c_{66}^D	c_{12}^D	c_{13}^E	c_{23}^D	c_{15}^E	c_{25}^D	c_{35}^E	c_{46}^D	Ref.
4.55	3.21	2.63	0.95	1.11	0.62	1.72	1.98	2.08	–0.30	–0.036	–0.50	–0.026	59Kon
4.71	3.35	2.75	1.02	1.03	0.61	1.50	2.10	1.85	–0.18	–0.20	0.05	–0.02	77Lus
4.41	3.34	2.73	1.04	1.08	0.61	1.89	1.67	1.97	–0.21	–0.19	–0.18	0.05	84Dun
4.61	–	2.79	–	1.12	–	–	2.10	–	–0.22	–	0.15	–	81Tyl1

Table 60A-1-016. Deuterated triglycine sulfate (DTGS). Elastic stiffness obtained by Brillouin scattering [77Vaz]. c_{ij} in [$\cdot 10^{10}$ N m^{-2}]. Coordinate system: see Fig. 60A-1-003.

c_{11}	c_{22}	c_{33}	c_{44}	c_{55}	c_{66}	c_{12}	c_{13}	c_{15}	c_{23}	c_{25}	c_{35}	c_{46}
5.06	3.51	2.81	1.10	1.21	0.73	2.04	2.05	-	2.40	-	-	+0.02

Table 60A-1-017. $(NH_2CH_2COOH)_3 \cdot H_2SO_4$ (TGS). Hydrostatic pressure derivatives of the elastic stiffness constants $c_{\lambda\mu}$ [84Dun]. Coordinate system: see Fig. 60A-1-003.

$\left(\frac{\partial c_{11}}{\partial p}\right)_{p=0} = 9.5$	$\left(\frac{\partial c_{12}}{\partial p}\right)_{p=0} = 8.9$	$\left(\frac{\partial c_{13}}{\partial p}\right)_{p=0} = 6.0$
$\left(\frac{\partial c_{15}}{\partial p}\right)_{p=0} = -0.40$	$\left(\frac{\partial c_{22}}{\partial p}\right)_{p=0} = 13.4$	$\left(\frac{\partial c_{23}}{\partial p}\right)_{p=0} = 6.9$
$\left(\frac{\partial c_{25}}{\partial p}\right)_{p=0} \approx 0$	$\left(\frac{\partial c_{33}}{\partial p}\right)_{p=0} = 5.9$	$\left(\frac{\partial c_{35}}{\partial p}\right)_{p=0} = 0.43$
$\left(\frac{\partial c_{44}}{\partial p}\right)_{p=0} = 0.92$	$\left(\frac{\partial c_{46}}{\partial p}\right)_{p=0} = 0.07$	$\left(\frac{\partial c_{55}}{\partial p}\right)_{p=0} = 1.2$
	$\left(\frac{\partial c_{66}}{\partial p}\right)_{p=0} = 0.58$	

Table 60A-1-018. $(NH_2CH_2COOH)_3 \cdot H_2SO_4$ (TGS). Change of the sound velocity Δv_l relative to the sound velocity at 50.0 °C [64OBr]. Pulse method. All measurements are for longitudinal waves perpendicular to ($\bar{1}$ 0 1).

T	Δv_l [10 m s^{-1}]		
[°C]	f = 15 MHz	f = 45 MHz	f = 65 MHz
49.50	–0.55	0	0
49.20	–1.4	–1.2	–1.2
49.15	–1.8	–1.5	–2.1
49.10	–2.7	–1.9	–2.6
49.00	–6.9	–6.0	–6.5
48.90	–8.9	–9.5	–10.30
48.80	–9.9	–11.0	–11.1
48.00	–11.3	–11.0	–11.7

Table 60A-1-019. $(NH_2CH_2COOH)_3 \cdot H_2SO_4$ (TGS). Piezooptic constants [83Str]. T = RT. λ = 633 nm.

p_{11}	p_{12}	p_{13}	p_{21}	p_{22}	p_{23}	p_{31}	p_{32}	p_{33}
0.204	0.162	0.175	0.172	0.208	0.150	0.204	0.169	0.151

Table 60A-1-020. $(NH_2CH_2COOH)_3 \cdot H_2SO_4$ (TGS), $(NH_2CH_2COOH)_3 \cdot H_2BeF_4$ (TGFB). Pockels (piezooptic) coefficients determined from Brillouin scattering intensity [73Mer]. λ = 633 nm.

Crystal	p_{21}	p_{23}	p_{25}
TGFB	$20 \cdot 10^{-2}$	$20 \cdot 10^{-2}$	~ 0
TGS	$27 \cdot 10^{-2}$	$27 \cdot 10^{-2}$	~ 0

Table 60A-1-021. $(NH_2CH_2COOH)_3 \cdot H_2SO_4$ (TGS). Effect of radiation damage and impurity doping on ρ and ΔU [61Toy]. In the X-ray irradiation, the X-ray is excited by 35 kV; in the neutron irradiation, the dose is $3 \cdot 10^{16}$ nvt. Asterisks (*) indicate that the crystals were grown from aqueous solutions containing 0.2 mol% of Fe^{3+} or Cr^{3+} ions. Activation energy ΔU is estimated from the relation $\rho \propto (\Delta U/kT)$.

Direction of E	Treatment	ρ [Ωm]		ΔU [eV]	
		27 °C	48 °C	Ferroelectric phase	Paraelectric phase
b	Normal	$1.5 \cdot 10^{12}$	$8.5 \cdot 10^{10}$	1.5	0.7
b	X-ray 15 min	$1.9 \cdot 10^{11}$	$6.5 \cdot 10^{9}$	1.35	0.73
b	X-ray 1 h	$2 \cdot 10^{11}$	$6.5 \cdot 10^{9}$	1.39	0.84
b	X-ray 4 h	$2.1 \cdot 10^{11}$	$6.0 \cdot 10^{9}$	1.52	0.92
b	Neutron	$1.8 \cdot 10^{11}$	$6.2 \cdot 10^{9}$	1.58	0.9
b	*Fe^{3+}	$3 \cdot 10^{12}$	$1 \cdot 10^{11}$	1.47	0.9
b	*Cr^{3+}	$3.5 \cdot 10^{12}$	$7 \cdot 10^{10}$	1.68	0.9
b	*Cr^{3+} X-ray 4 h	$3.5 \cdot 10^{11}$	$8 \cdot 10^{9}$	1.6	0.9
c	Normal	$2.7 \cdot 10^{11}$	$1.2 \cdot 10^{10}$	1.3	0.75
c	X-ray 15 min	$7 \cdot 10^{9}$	$1.4 \cdot 10^{8}$	1.9	0.6
c	X-ray 1 h	$8.5 \cdot 10^{9}$	$1.5 \cdot 10^{8}$	1.86	0.67
c	X-ray 4 h	$7 \cdot 10^{9}$	$2.5 \cdot 10^{8}$	1.65	0.71
c	*Fe^{3+}	$1.3 \cdot 10^{10}$	$3.1 \cdot 10^{8}$	1.65	0.6
c	*Fe^{3+} X-ray 1 h	$8.5 \cdot 10^{9}$	$1.6 \cdot 10^{8}$	1.84	0.68

Table 60A-1-022. $(ND_2CH_2COOD)_3 \cdot D_2SO_4$ (DTGS). Eigenvalues $3eQ\phi_{ij}/2h$ [kHz] and direction cosines λ, μ, ν of the largest principal axes for the O–D- -O and ND_3 electric quadrupole coupling constant tensors [67Bli]. G: Glycine. Coordinate system of Fig. 60A-1-003 is adopted.

O–D- -O (2.55 Å) *)				O–D- -O (2.44 Å)			
T = 20 °C		T = 73 °C		T = 20 °C		T = 73 °C	
$3eQ\phi_{ij}/2h$	λ μ ν	$3eQ\phi_{ij}/2h$	λ μ ν	$3eQ\phi_{ij}/2h$	λ μ ν	$3eQ\phi_{ij}/2h$	λ μ ν
195.8	0.861 0.022 0.508	197.5	0.860 0.012 0.510	118.3	±0.313 0.275 ±0.909	127.9	±0.325 0.237 ±0.901
–115.5	–0.206 0.928 0.309	–114.6	–0.122 0.975 0.184	–70.5	±0.141 0.933 ±0.331	–78.2	±0.026 0.955 ±0.295
–80.3	–0.464 –0.371 0.804	–83.0	–0.495 –0.221 0.840	–47.8	±0.939 0.232 ±0.253	–49.7	±0.945 0.072 ±0.318
$(e^2qQ)/h$ = 131.0 η = 0.160		$(e^2qQ)/h$ = 130.5 η = 0.180		$(e^2qQ)/h$ = 78.8 η = 0.192		$(e^2qQ)/h$ = 85.0 η = 0.223	

*) Since the two R_{O-O} = 2.54 Å H-bonds have nearly the same direction, only the average direction cosines of the coupling tensor for this bond are given.

GI				GII, GIII		GII		GIII	
T = 73 °C		T = 20 °C		T = 73 °C		T = 20 °C		T = 20 °C	
$3eQ\phi_{ij}/2h$	λ μ ν	$3eQ\phi_{ij}/2h$	λ μ ν	$3eQ\phi_{ij}/2h$	λ μ ν	$3eQ\phi_{ij}/2h$	λ μ ν	$3eQ\phi_{ij}/2h$	λ μ ν
56.0	±0.024 0 ±0.997	70.5	±0.039 –0.400 ±0.916	77.9	±0.995 –0.067 ±0.076	80.7	±0.990 –0.135 ±0.035	79.2	±0.997 –0.075 ±0.025
–28.6	±0.997 0 ±0.0236	–43.9	±0.442 0.828 ±0.343	–44.7	±0.013 –0.676 ±0.736	–45.7	±0.075 0.729 ±0.680	–45.4	±0.070 –0.686 ±0.724
–27.4	0 1 0	–26.5	±0.896 0.392 0.209	–33.2	±0.098 0.734 ±0.672	–35.0	±0.117 0.671 ±0.732	–33.7	±0.037 0.724 ±0.689
$(e^2qQ)/h$ = 37.3 η = 0.021		$(e^2qQ)/h$ = 47.0 η = 0.247		$(e^2qQ)/h$ = 51.9 η = 0.148		$(e^2qQ)/h$ = 54.8 η = 0.133		$(e^2qQ)/h$ = 52.8 η = 0.147	

Table 60A-1-023. $(ND_2CH_2COOD)_3 \cdot D_2SO_4$ (DTGS). ND_3^+ deuteron electric field gradient eigenvalues, $3eQ\phi_{ij}/2h$ [kHz], and direction cosines λ, μ, ν for each eigenvalue [67Bjo]. $|\phi_{ZZ}| > |\phi_{YY}| > |\phi_{XX}|$; the orientational accuracy is within ±1°; A_1, A_2, B_1, B_2, C_1, C_2 associate with $N_{II}D_3^+$, $N_{III}D_3^+$, and $N_ID_3^+$, respectively. Coordinate system of Fig. 60A-1-003 is adopted.

Site	T = 65 °C			Site	T = 30 °C	
		λ				0.895
	$3eQ\phi_{ij}/2h$	μ			76.3	∓ 0.084
		ν				0.057
						– 0.102
				A_1, A_2	–44.9	∓ 0.749
						0.658
			0.995			– 0.013
		79.6	∓ 0.054		–31.4	∓ 0.663
			0.078			– 0.751
			– 0.097			
$A_1(B_1)$, $A_2(B_2)$		–46.2	∓ 0.617			
			0.782			0.993
					79.3	∓ 0.027
			0.015			0.112
		–33.4	∓ 0.780			
			0.622			– 0.109
				B_1, B_2	–46.3	∓ 0.625
						0.773
						0.043
					–33.0	∓ 0.782
						– 0.662
			0			0.023
		56.6	0		69.0	∓ 0.386
			1			0.922
			1			0.441
C		–29.6	0	C_1, C_2	–42.7	± 0.832
			0			0.337
			0			– 0.897
		–27.0	1		–26.3	± 0.397
			0			0.189

Table 60A-1-024. $(NH_2CH_2COOH)_3 \cdot H_2SO_4$ (TGS). Components of ^{14}N quadrupole coupling tensors $eQ\phi_{ij}/h$ [kHz] expressed in the crystal fixed coordinate system a' sin β', b', c' [71Bli]. Crystallographic axial system by Hoshino et al. is adopted, see subsection 3a.

	$T < \Theta_f$			$T > \Theta_f$		
	α' sin β'	b'	c'	α' sin β'	b'	c'
Glycine I	–747	0	280	–740	0	208
	0	–107	±350	0	–140	0
	280	±350	853	208	0	880
Glycine II	960	0	–243	960	0	–208
	0	–493	±73	0	–480	±52
	–243	±73	–467	–208	±52	–480
Glycine III	880	0	–243	960	0	–208
	0	–467	±73	0	–480	±52
	–243	±73	–453	–208	±52	–480

Table 60A-1-025. $(NH_2CH_2COOH)_3 \cdot H_2SO_4$ (TGS). ^{14}N and $-ND_3^+$ deuteron quadrupole coupling constants e^2qQ/h [kHz], asymmetry parameters η and direction cosines λ, μ, ν of the largest principal axis of the electric field gradient tensors [71Bli]. The direction cosines of the C–N bond directions, taken from the structural data on the ferroelectric phase, are listed as well. Coordinate system of Fig. 60A-1-003 is adopted.

		$(^{14}N)_{65°C}$	$(^{14}N)_{20°C}$	$(–ND_3)_{70°C}$	$(–ND_3)_{20°C}$	$(–C–N–)_{20°C}$
Glycine I	e^2qQ/h	906	1008	37.3	47.0	–
	η	0.691	0.586	0.021	0.247	–
	λ	±0.125	±0.150	±0.024	±0.039	±0.150
	μ	0.000	0.296	0	0.400	0.218
	ν	±0.992	±0.943	±0.997	±0.916	±0.964
Glycine II	e^2qQ/h	990	983	51.9	54.8	–
	η	0.10	0.137	0.148	0.133	–
	λ	0.990	0.985	0.995	0.990	0.999
	μ	±0.005	±0.009	±0.067	±0.135	±0.054
	ν	0.140	–0.175	0.076	0.035	0.005
Glycine III	e^2qQ/h	990	1020	51.9	52.8	–
	η	0.10	0.130	0.148	0.147	–
	λ	0.990	0.986	0.995	0.997	0.996
	μ	±0.05	±0.008	±0.068	±0.075	±0.009
	ν	0.140	–0.164	0.076	0.025	0.088

Table 60A-1-026. $(ND_2CH_2COOD)_3 \cdot D_2SO_4$ (DTGS). e^2qQ/h and η of the ND_3 group deuterons [79Hof]. The data of [67Bli] (see Table 60A-1-022) are given in parentheses.

Glycine	Ferro (294 K)		Para (354 K)	
	e^2qQ/h [kHz]	η	e^2qQ/h [kHz]	η
I	47.2(47.0)	0.291(0.247)	38.09(37.3)	0.033(0.021)
II	53.6(54.8)	0.217(0.133)	52.3(51.9)	0.212(0.148)
III	52.3(52.8)	0.212(0.147)		

Table 60A-1-027. $(NH_2CH_2COOH)_3 \cdot H_2SO_4$ (TGS). Relaxation time τ for the exchange of protons in the radical [70Kat, 72Kat]. $\tau^{-1} = f_0 \exp(-E/kT)$.

Radical	E [eV]	f_0 [s^{-1}]	Ref.
CH_2COO^-	0.16(3)	$1.2 \cdot 10^{12}$	70Kat
NH_3CHCOO^-	0.17	$5 \cdot 10^{11}$	72Kat

Table 60A-1-028. $(NH_2CH_2COOH)_3 \cdot H_2SO_4$ (TGS), $(NH_2CH_2COOH)_3 \cdot H_2SeO_4$ (TGSe), $(NH_2CH_2COOH)_3 \cdot H_2BeF_4$ (TGFB). Spin Hamiltonian parameters g, D, E for the Cr^{3+} ion in TGS type crystals in the paraelectric phase [78Sta2]. Spin Hamiltonian parameters in the form: $H = g\mu_B H_z S_z + D\{S_z^2 - S(S+1)/3\} + E(S_x^2 - S_y^2)$. See Fig. 60A-1-161.

Crystal	g	D [10^2 m^{-1}]	E [10^2 m^{-1}]	E/D
TGFB	1.981	0	0	–
TGS	1.987	0.435	0.063	0.14
TGSe	1.985	0.634	0.127	0.20

Table 60A-1-029. $(NH_2CH_2COOH)_3 \cdot H_2SO_4$ (TGS):Cu^{2+}. g and A values [73Kat]. A: hyperfine structural factor. T = 77K. λ, μ, ν: direction cosines of the principal axes with respect to the coordinate system of Fig. 60A-1-003. $A_s^N = 10.0 \cdot 10^{-2}$ m^{-1}, $A_s^H = 10.0 \cdot 10^{-2}$ m^{-1}; A_s^N, A_s^H **:** super hyperfine factors due to Fermi contact interaction at nitrogen nucleus and hydrogen nucleus, respectively.

	Principal value	Direction cosine λ	μ	ν
Spectrum I				
g	2.4332	0.712	∓ 0.703	∓ 0.006
	2.0379	0.556	0.558	± 0.617
	2.1748	–0.430	∓ 0.442	0.787
A [10^{-2} m^{-1}]	127.3	0.735	∓ 0.675	0.063
	77.7	± 0.588	0.589	∓ 0.555
	17.7	0.338	± 0.444	0.830
Spectrum II				
g	2.092	0.792	∓ 0.266	–0.549
	2.259	∓ 0.081	0.846	∓ 0.527
	2.027	0.605	± 0.462	0.649
A [10^{-2} m^{-1}]	24.2	0.756	± 0.332	0.564
	165.4	∓ 0.008	0.867	∓ 0.499
	84.8	–0.654	± 0.373	0.658

Table 60A-1-030. $(NH_2CH_2COOH)_3 \cdot H_2SO_4$ (TGS):Cu^{2+}. Spin Hamiltonian parameters of $^{63}Cu^{2+}$ [74Sta3].

$g_\parallel$	2.261	$A_\parallel^{Cu}$	$150.1 \cdot 10^{-2}$ m^{-1}
$g_\perp$	2.054	$A_\perp^{Cu}$	$30 \cdot 10^{-2}$ m^{-1}
$A_\parallel^N$	$7.4 \cdot 10^{-2}$ m^{-1}	A^H	$3.6 \cdot 10^2$ A m^{-1}
$A_\perp^N$	$11.4 \cdot 10^{-2}$ m^{-1}		

Table 60A-1-031. Deuterated triglycine sulfate (DTGS):Cu^{2+}. Spin Hamiltonian parameters for Cu^{2+} [85Bot]. T = 4.2 K. Direction cosines with respect to the coordinate system of Fig. 60A-1-003.

Principal values		Direction cosines		
g-tensor	$\mathbf{A}^{Cu}$-tensor $[10^{-2}\ m^{-1}]$	λ	μ	ν
$g_z = 2.257$	$A_z = -152(2)$	∓ 0.142	0.848	± 0.511
$g_y = 2.064$	$A_y = 10(4)$	∓ 0.964	0	∓ 0.267
$g_x = 2.057$	$A_x = -29(3)$	± 0.225	0.552	∓ 0.834

Table 60A-1-032. Deuterated triglycine sulfate (DTGS):Cu^{2+}. Deuteron hyperfine spin Hamiltonian parameters [85Bot]. T = 4.2 K. Direction cosines with respect to the principal axes of the **g**-tensor in Table 60A-1-031.

Deuteron	Principal values [kHz]	Direction cosines		
		λ	μ	ν
D_1	$A_{11} = 800$	0.776	–0.104	0.622
	$A_{22} = -1248$	–0.572	0.298	0.764
	$A_{33} = -2231$	0.264	0.949	–0.172
	$A_{iso} = -893$			
	$A_{aniso} = 1693, -355, -1338$			
D_2	$A_{11} = 811$	0.784	–0.087	0.614
	$A_{22} = -1203$	–0.563	0.314	0.764
	$A_{33} = -2256$	0.259	0.945	–0.196
	$A_{iso} = -881$			
	$A_{aniso} = 1692, -332, -1375$			
D_3	$A_{11} = 997$	0.910	0.365	–0.195
	$A_{22} = -971$	–0.414	0.782	–0.466
	$A_{33} = -1928$	–0.017	0.505	0.865
	$A_{iso} = -634$			
	$A_{aniso} = 1631, -337, -1294$			
D_4	$A_{11} = 942$	0.981	0.082	–0.176
	$A_{22} = -1080$	–0.162	0.843	–0.513
	$A_{33} = -1632$	0.107	0.532	0.840
	$A_{iso} = -590$			
	$A_{aniso} = 1532, -490, -1042$			

Table 60A-1-033. Deuterated triglycine sulfate (DTGS):Cu^{2+}. Deuteron quadrupole coupling tensor [85Bot]. T = 4.2 K. Direction cosines with respect to the principal axes of the **g**-tensor in Table 60A-1-031.

Deuteron	Principal values [kHz]	Direction cosines		
		λ	μ	ν
$D_{1,2}$	$eQ\phi_{zz}/h = 94$	0.176	0.050	0.983
	$eQ\phi_{yy}/h = -55$	0.979	0.098	–0.180
	$eQ\phi_{xx}/h = -38$	–0.105	0.994	–0.032
	$e^2qQ/h = 188$	$\eta = 0.18$		
$D_{3,4}$	$eQ\phi_{zz}/h = 90$	0.698	0.530	–0.481
	$eQ\phi_{yy}/h = -49$	0.666	–0.236	0.708
	$eQ\phi_{xx}/h = -41$	–0.262	0.814	0.518
	$e^2qQ/h = 180$	$\eta = 0.09$		

Table 60A-1-034. $(ND_2CH_2COOD)_3 \cdot D_2SO_4$ (DTGS):VO^{2+}. Spin Hamiltonian parameters of $(VO^{2+})_1$ and $(VO^{2+})_2$ at room temperature and direction cosines of the principal axes of **g** and **A** tensors [74Fuj]. $(VO^{2+})_1$, $(VO^{2+})_2$: observed centers after the annealing process. Reference axes of the direction cosines are shown in Fig. 60A-1-003. $A_\perp$, $A_\parallel$ in units of 10^{-2} m^{-1}.

Tensors		Principal values	Direction cosines		
g_1	$g_{1\perp}$	1.9852	0.712,	∓0.674,	0.188
		1.9982	–0.305,	∓0.058,	0.949
	$g_{1\parallel}$	1.9288	±0.631,	0.736,	±0.246
g_2	$g_{2\perp}$	1.9854	0.745,	∓0.661,	∓0.096
		1.9981	–0.146,	∓0.132,	0.976
	$g_{2\parallel}$	1.9289	±0.648,	0.737,	±0.195
$^{51}V_1$	$A_{1\perp}$	71.2	0.611,	∓0.540,	±0.565
		73.7	∓0.407,	0.410,	0.806
	$A_{1\parallel}$	177.8	±0.662,	0.730,	±0.169
$^{51}V_2$	$A_{2\perp}$	70.1	–0.446,	±0.380,	0.810
		73.9	∓0.567,	0.581,	∓0.568
	$A_{2\parallel}$	178.2	±0.692,	0.719,	±0.044

Table 60A-1-035. $(ND_2CH_2COOD)_3 \cdot D_2SO_4$ (DTGS):VO^{2+}. Spin Hamiltonian parameters of $(VO^{2+})_s$ at room temperature and direction cosines of the principal axes of **g** and **A** tensors [74Fuj]. $(VO^{2+})_s$: vanishing complex during annealing process. Reference axes of the direction cosines are shown in Fig. 60A-1-003. $A_\perp$, $A_\parallel$ in units of 10^{-2} m^{-1}.

Tensors		Principal values	Direction cosines		
g	$g_\perp$	1.9939	0.735,	∓ 0.394,	–0.552
		1.9850	∓ 0.607,	0.745,	∓ 0.277
	$g_\parallel$	1.9296	0.302,	∓ 0.539,	0.787
^{51}V	$A_\perp$	68.9	0.803,	∓ 0.581,	0.135
		57.1	∓ 0.560,	0.655,	∓ 0.507
	$A_\parallel$	173.0	0.206,	∓ 0.483,	0.851

Table 60A-1-036. $(NH_2CH_2COOH)_3 \cdot H_2SO_4$ (TGS). ESR data for irradiated crystals. See also [61Bli, 61Ove].

Paramagnetic center	S	**H**	ν [GHz]	T [K]	g-factor	FS D, E [10^{-2} m^{-1}]	HFS $^nA, {}^nA_\lambda, Q_z$ [10^{-2} m^{-1}]	Ref.
diglycine-Cr^{3+}-chelate*)	3/2	(5)	9.4	RT	I: 1.985(5)	I: $\|D\| = 4252(15)$ $\|E\| = 668(10)$	$\|^{53}A\| < 13$ [1])	66 War
					II: 1.985(5)	II: $\|D\| = 3964(15)$ $\|E\| = 489(10)$		
diglycine-Cu^{2+}-chelate*)	1/2	(10)	9	77	$g_x = 2.048(5)$		$^{63}A_x = -37(4)$ [2])	
					$g_y = 2.063(5)$		$\|^{63}A_y\| \leqq 10$	67Win
					$g_z = 2.252(5)$		$^{63}A_z = -150(3)$	65Los
				300	$g_x = 2.052(5)$		$^{63}A_x = -28(4)$ [2])	66Sta
					$g_y = 2.064(3)$		$\|^{63}A_y\| \leqq 9$	
					$g_z = 2.259(5)$		$^{63}A_z = -150(3)$	
				77, 300			$\|(^{14}A_N)_\parallel\| = 10.8(6)$ [2]) $\|(^{14}A_N)_\perp\| = 7.7(4)$ $\|^1A_H\| \approx 5$ $\|Q_z\| \leqq 5$ [2])	

*) Formula:

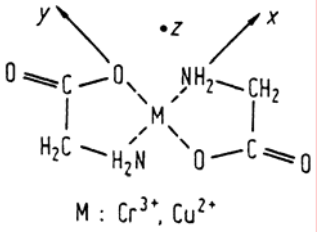

[1]) Orientation of the principal axes x, y, z relative to the a', b', c' axes, which are the crystallographic axes according to Hoshino et al. (see 1b).
I: $\alpha = 17.5(25)°$, $\gamma = 23(2)°$
II: $\alpha = 17.5(25)°$, $\gamma = 20(2)°$

[2]) Orientation of the principal axes x, y, z, $\|, \perp$: parallel, perpendicular to x.

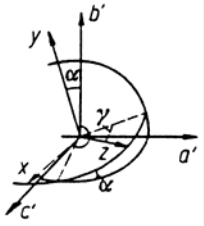

Table 60A-1-037. $(NH_2CH_2COOH)_3 \cdot H_2SO_4$ (TGS):^{57}Fe. Mössbauer data [76Mor]. δ: isomer shift. ΔE_{quad}: quadrupole splitting. Γ: line width.

	T [K]	δ [mm s^{-1}]	ΔE_{quad} [mm s^{-1}]	Γ [mm s^{-1}]
Iron-doped TGS	80	0.542(3)	0.598(6)	0.23(1)
	180	0.493(7)	0.706(6)	0.26(2)
	315	0.419(7)	0.687(8)	0.26(3)
	325	0.413(7)	0.684(8)	0.24(2)
	335	0.408(9)	0.678(9)	0.25(2)
	345	0.394(5)	0.718(5)	0.260(5)
Iron-doped TGS after heating	330	0.413(5)	0.720(5)	0.274(5)
	315	0.419(5)	0.708(5)	0.267(5)

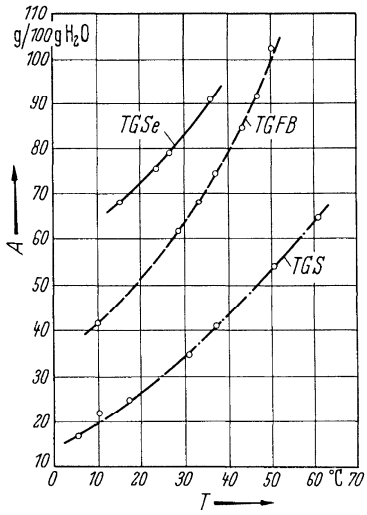

Fig. 60A-1-001. $(NH_2CH_2COOH)_3 \cdot H_2SO_4$ (TGS), $(NH_2CH_2COOH)_3 \cdot H_2SeO_4$ (TGSe), $(NH_2CH_2COOH)_3 \cdot H_2BeF_4$ (TGFB). *A* vs. *T* [58Nit]. *A*: solubility in H_2O.

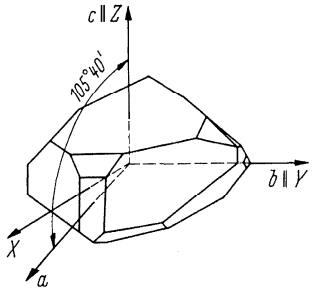

Fig. 60A-1-002. $(NH_2CH_2COOH)_3 \cdot H_2SO_4$ (TGS). Crystal form and the reference system of coordinate [62Ike].

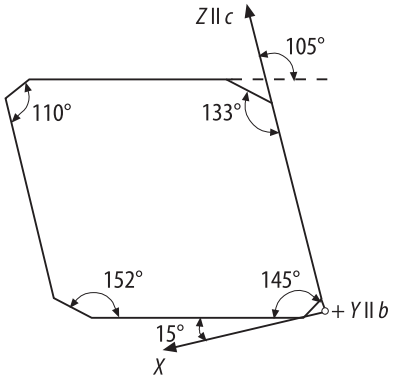

Fig. 60A-1-003. $(NH_2CH_2COOH)_3 \cdot H_2SO_4$ (TGS). Reference system of coordinate in a single crystal [59Kon].

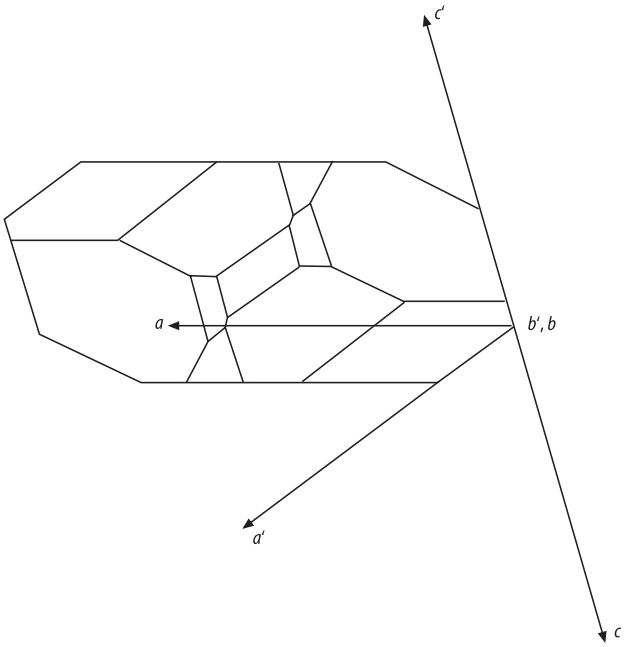

Fig. 60A-1-004. $(NH_2CH_2COOH)_3 \cdot H_2SO_4$ (TGS). Crystal form and the crystallographic directions [90Nak]. *a*, *b*, *c* and *a*′, *b*′, *c*′ represent the crystallographic axes of the systems of Wood et al. [57Woo] and of Hoshino et al. [59Hos], respectively.

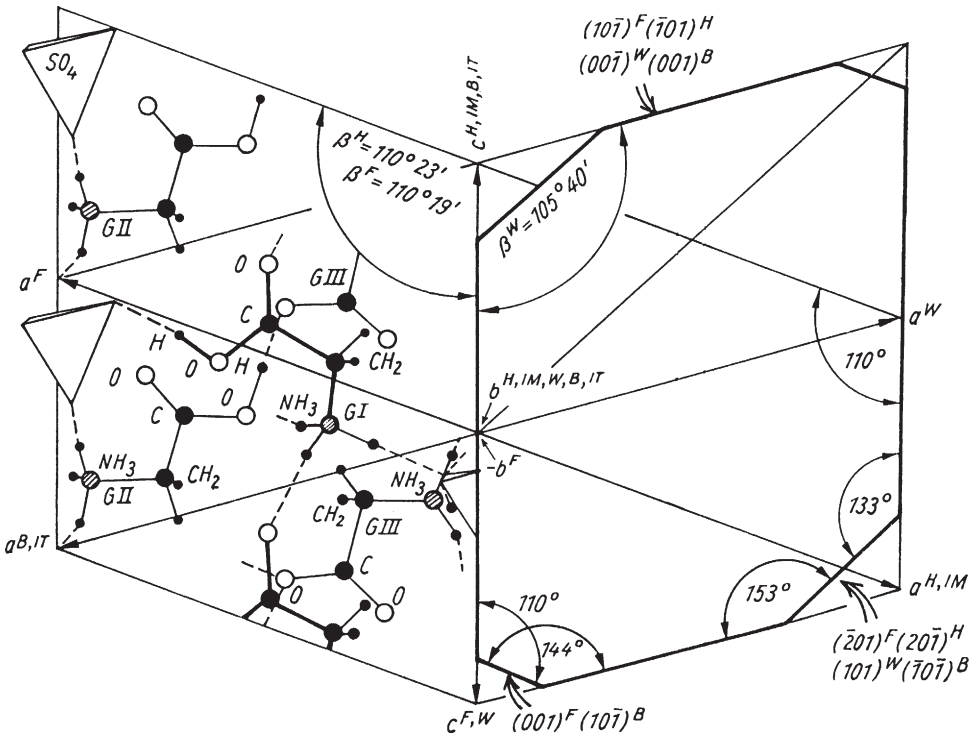

Fig. 60A-1-005. $(NH_2CH_2COOH)_3 \cdot H_2SO_4$ (TGS). Axial systems by various authors and [010] projection of crystal structure [85Bre1]. The superscripts: B [71Bre], F [76Fle1], H [59Hos], IT [62Ike], IM [73Ito], W [57Woo].

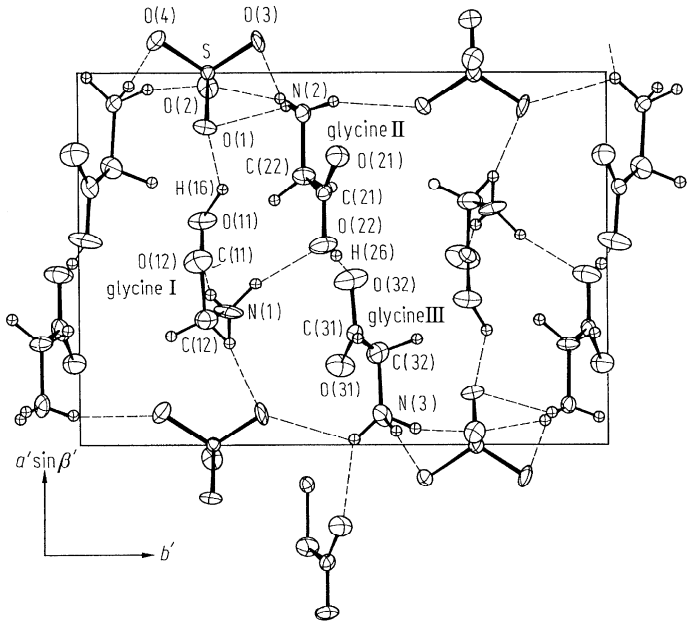

Fig. 60A-1-006. $(NH_2CH_2COOH)_3 \cdot H_2SO_4$ (TGS). Structure of phase II [76Fle1]. [001] projection. Hydrogen bonds are indicated by broken lines and thermal vibration ellipsoids are scaled to enclose 50 % probability.

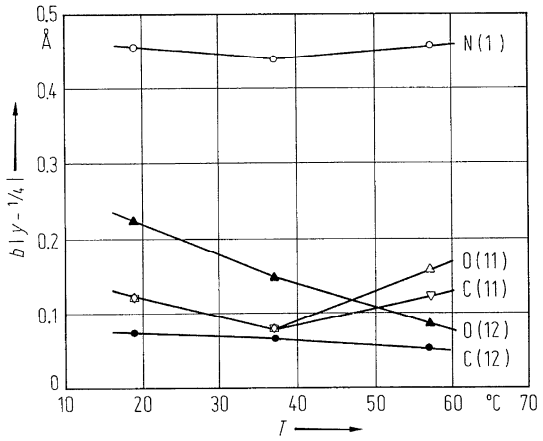

Fig. 60A-1-007. $(NH_2CH_2COOH)_3 \cdot H_2SO_4$ (TGS). $b|y - 1/4|$ vs. T [73Ito]. y: fractional coordinate of atoms in the glycine I molecule, b: lattice constant.

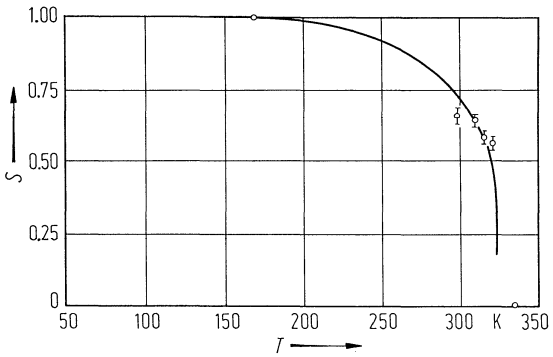

Fig. 60A-1-008. $(NH_2CH_2COOH)_3 \cdot H_2SO_4$ (TGS). S vs. T [85Ito]. S: long range order parameter obtained by X-ray structure analysis.

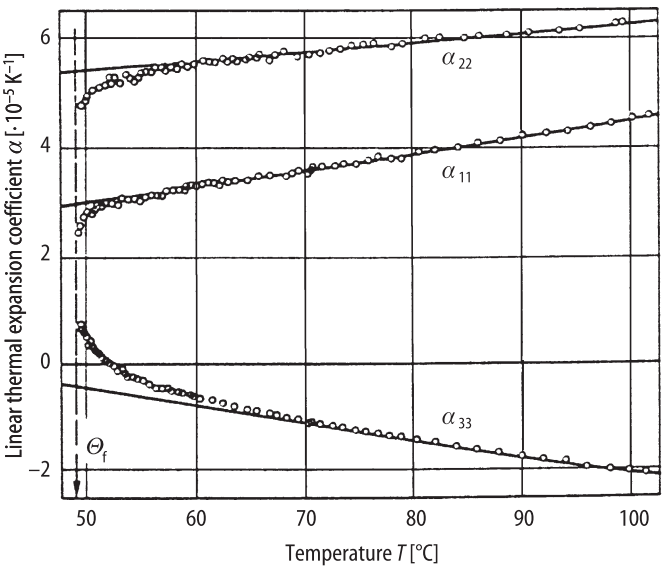

Fig. 60A-1-009. $(NH_2CH_2COOH)_3 \cdot H_2SO_4$ (TGS). α_{11}, α_{22}, α_{33} vs. T [79Ema1]. The orthogonal axial system of Fig. 60A-1-003 is adopted.

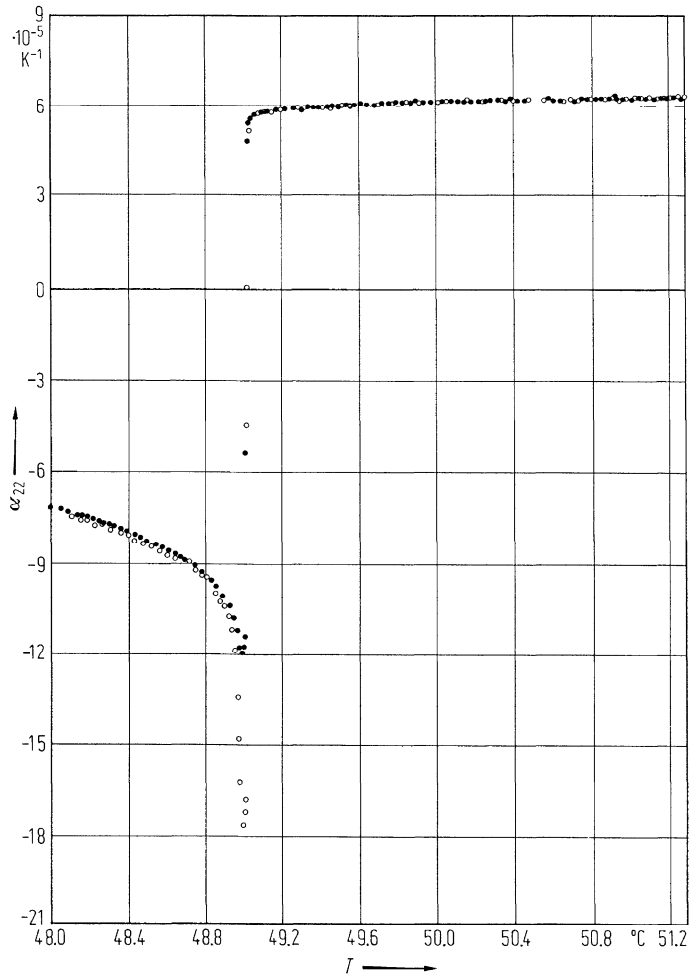

Fig. 60A-1-010. $(NH_2CH_2COOH)_3 \cdot H_2SO_4$ (TGS). α_{22} vs. T [79Deg]. α_{22}: linear thermal expansion coefficient along the b axis.

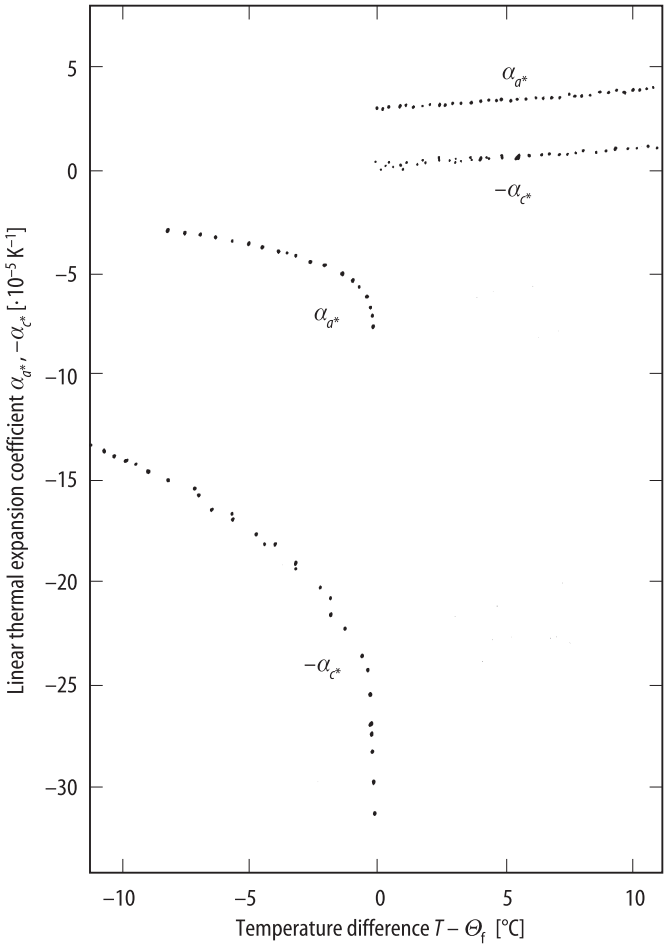

Fig. 60A-1-011. $(NH_2CH_2COOH)_3 \cdot H_2SO_4$ (TGS). α_{a^*}, $-\alpha_{c^*}$ vs. $T - \Theta_f$ [80Ehs1]. α_{a^*}, α_{c^*}: linear thermal expansion coefficient along the *a** and *c** axis, respectively. *a** axis: normal to the *bc* plane, *c** axis: normal to the *ab* plane.

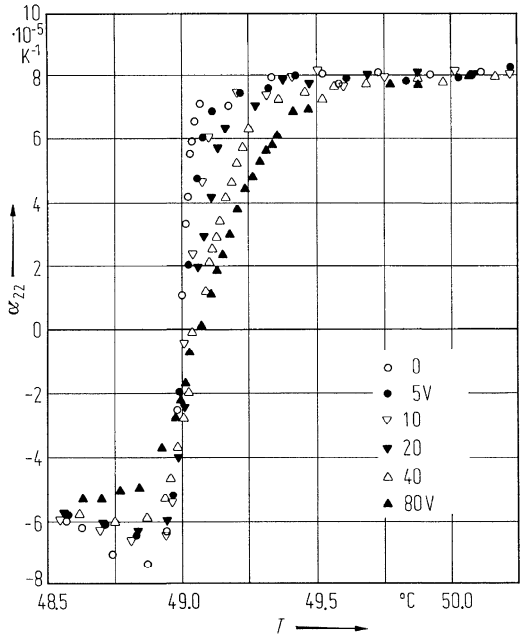

Fig. 60A-1-012. $(NH_2CH_2COOH)_3 \cdot H_2SO_4$ (TGS). α_{22} vs. T [74Gil]. Parameter: applied voltage. An applied voltage of 80 V corresponds to a field of 17.8 kV m^{-1}.

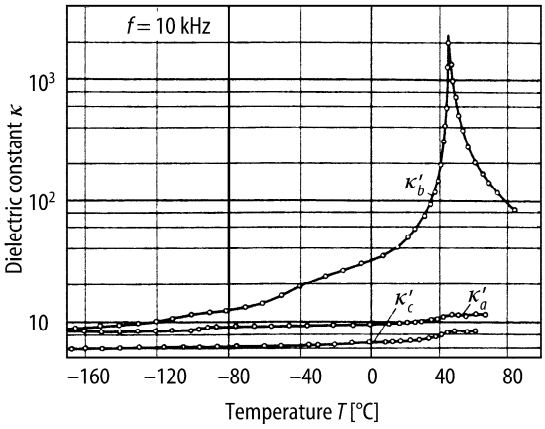

Fig. 60A-1-013. $(NH_2CH_2COOH)_3 \cdot H_2SO_4$ (TGS). $\kappa_{a'}$, $\kappa_{b'}$, $\kappa_{c'}$ vs. T [57Hos].

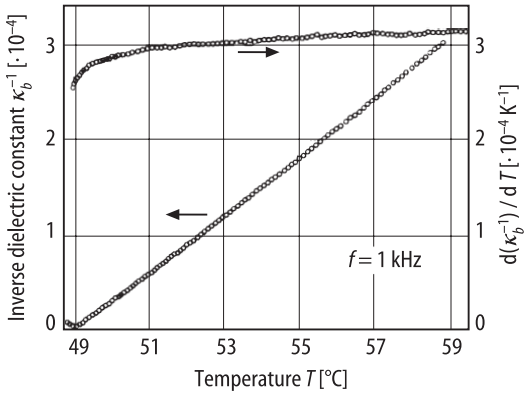

Fig. 60A-1-014. $(NH_2CH_2COOH)_3 \cdot H_2SO_4$ (TGS). κ_b^{-1}, $d(\kappa_b^{-1}) / dT$ vs. T in the vicinity of Θ_f [79Deg].

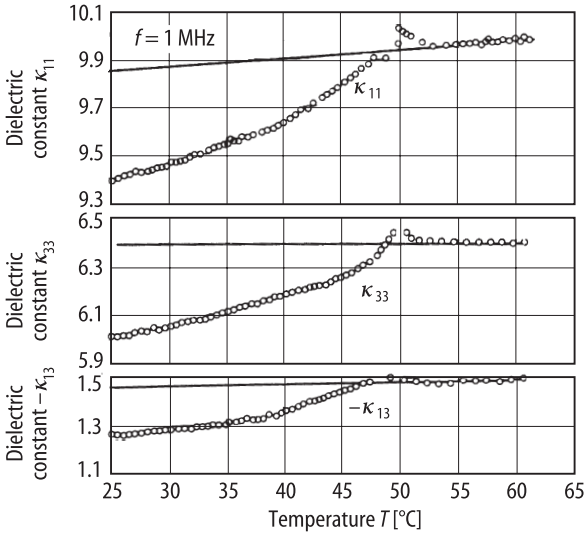

Fig. 60A-1-015. $(NH_2CH_2COOH)_3 \cdot H_2SO_4$ (TGS). κ_{11}, κ_{33}, $-\kappa_{13}$ vs. T [72Bro]. The orthogonal axial system of Fig. 60A-1-003 is adopted.

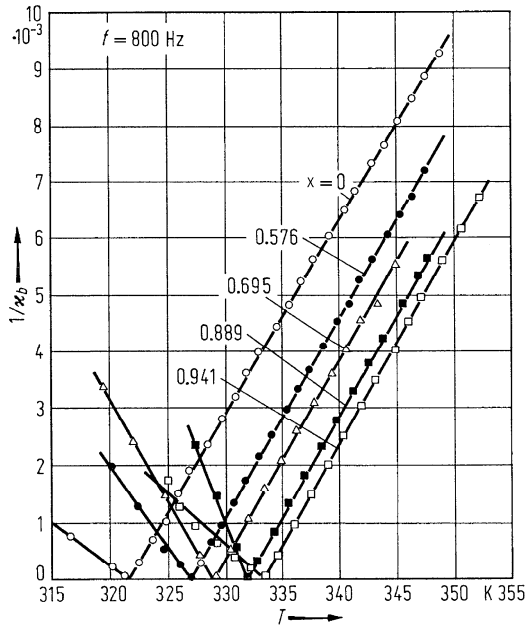

Fig. 60A-1-016. $[(NH_2CH_2COOH)_3 \cdot H_2SO_4]_{1-x}[(ND_2CH_2COOD)_3 \cdot D_2SO_4]_x$ ($TGS_{1-x}DTGS_x$). κ_b^{-1} vs. T [68Bre2]. Parameter: x.

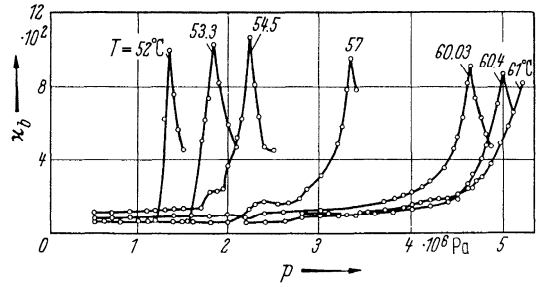

Fig. 60A-1-017. $(NH_2CH_2COOH)_3 \cdot H_2SO_4$ (TGS). κ_b vs. p [62Leo]. Parameter: T.

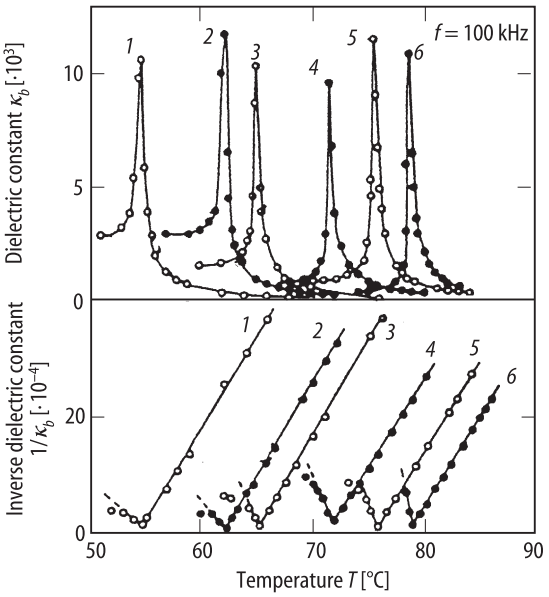

Fig. 60A-1-018. $[(NH_2CH_2COOH)_3 \cdot H_2SO_4]_{0.32}[(ND_2CH_2COOD)_3 \cdot D_2SO_4]_{0.68}$ ($TGS_{0.32}DTGS_{0.68}$). κ_b, κ_b^{-1} vs. T [90Yao]. Parameter: p. Curve *1*: $p = 0$, *2*: 0.25 GPa, *3*: 0.31 GPa, *4*: 0.61 GPa, *5*: 0.8 GPa, *6*: 1 GPa.

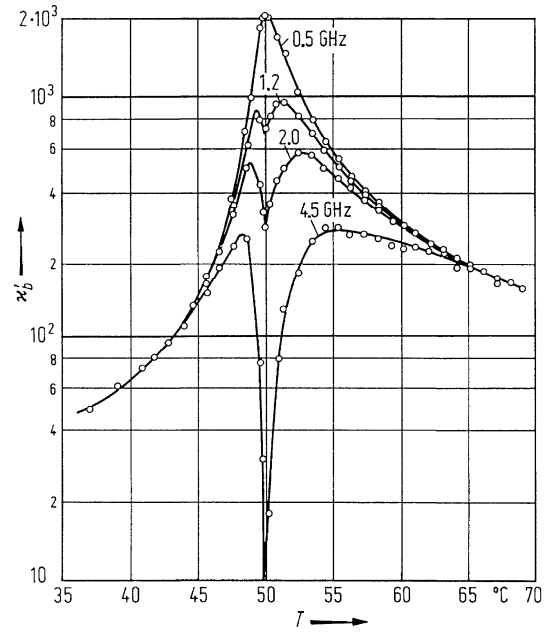

Fig. 60A-1-019. $(NH_2CH_2COOH)_3 \cdot H_2SO_4$ (TGS). κ_b' vs. T [69Lut]. Parameter: f.

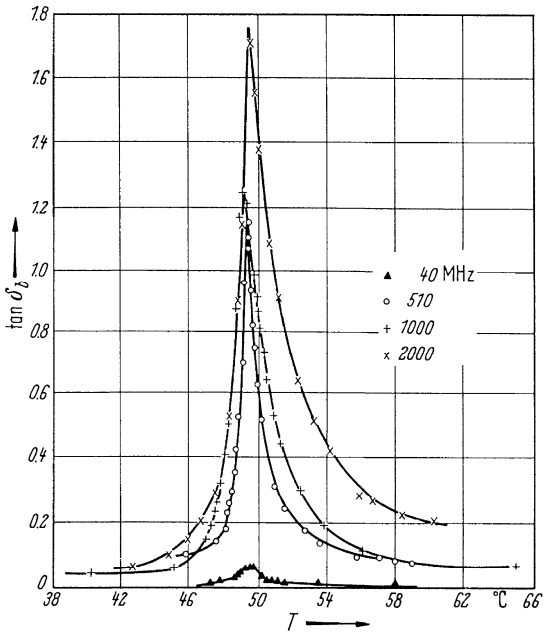

Fig. 60A-1-020. $(NH_2CH_2COOH)_3 \cdot H_2SO_4$ (TGS). tan δ_b vs. T [60Lur]. Parameter: f.

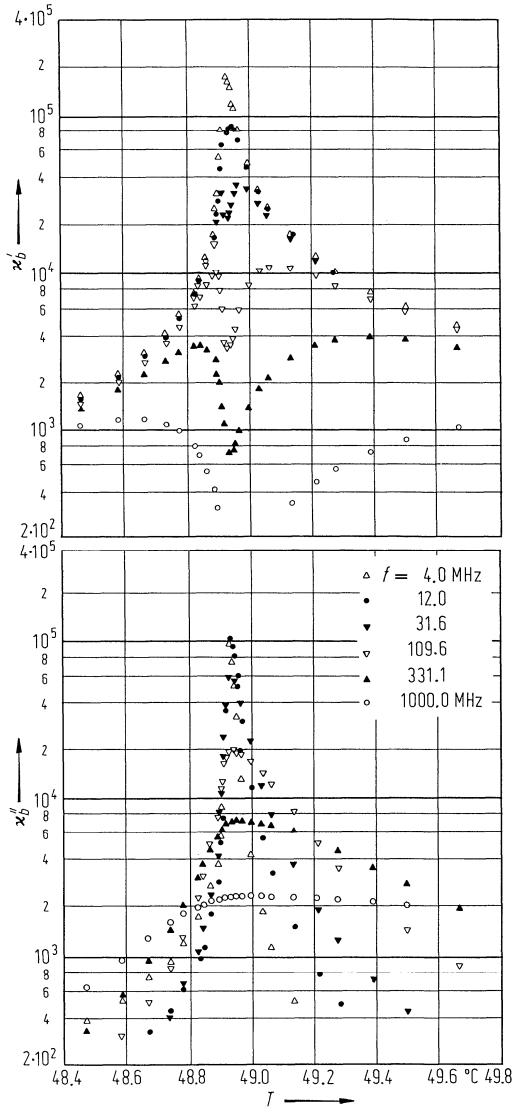

Fig. 60A-1-021. $(NH_2CH_2COOH)_3 \cdot H_2SO_4$ (TGS). κ_b', κ_b'' vs. T in the vicinity of Θ_f [84Tak]. Parameter: f.

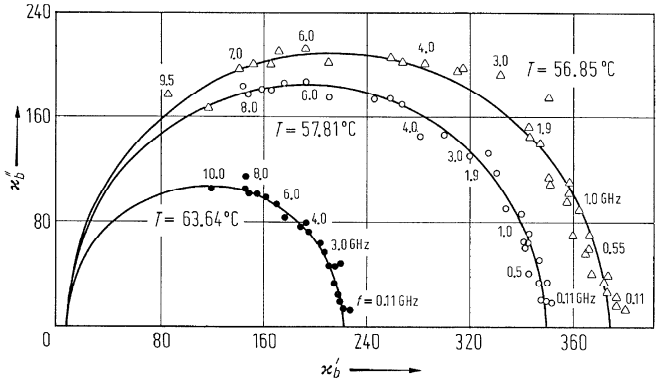

Fig. 60A-1-022. $(NH_2CH_2COOH)_3 \cdot H_2SO_4$ (TGS). Cole-Cole plot of the complex dielectric constant in the paraelectric phase [73Lut]. Parameter: T.

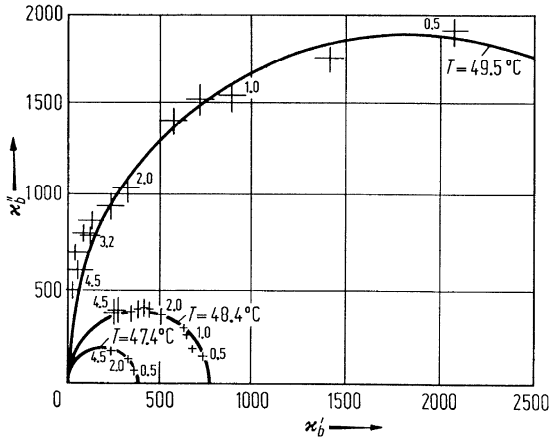

Fig. 60A-1-023. $(NH_2CH_2COOH)_3 \cdot H_2SO_4$ (TGS). Cole-Cole plot of the complex dielectric constant in the ferroelectric phase [69Lut]. Parameter: *T*. Frequencies are in GHz.

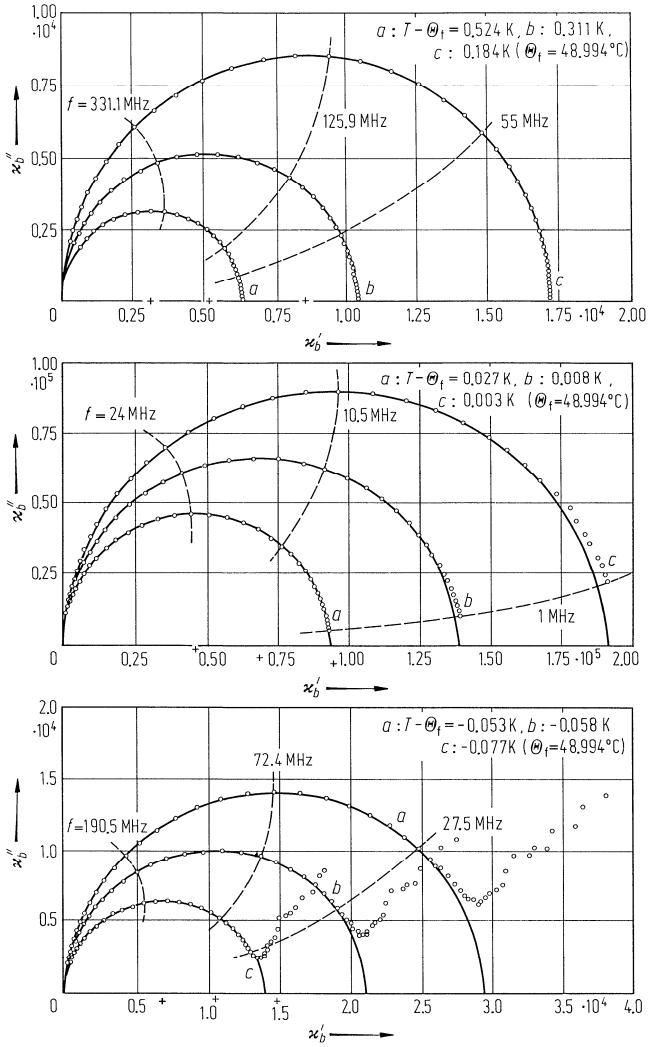

Fig. 60A-1-024. $(NH_2CH_2COOH)_3 \cdot H_2SO_4$ (TGS). Cole-Cole plot of the complex dielectric constant [84Tak]. Parameter: *T*.

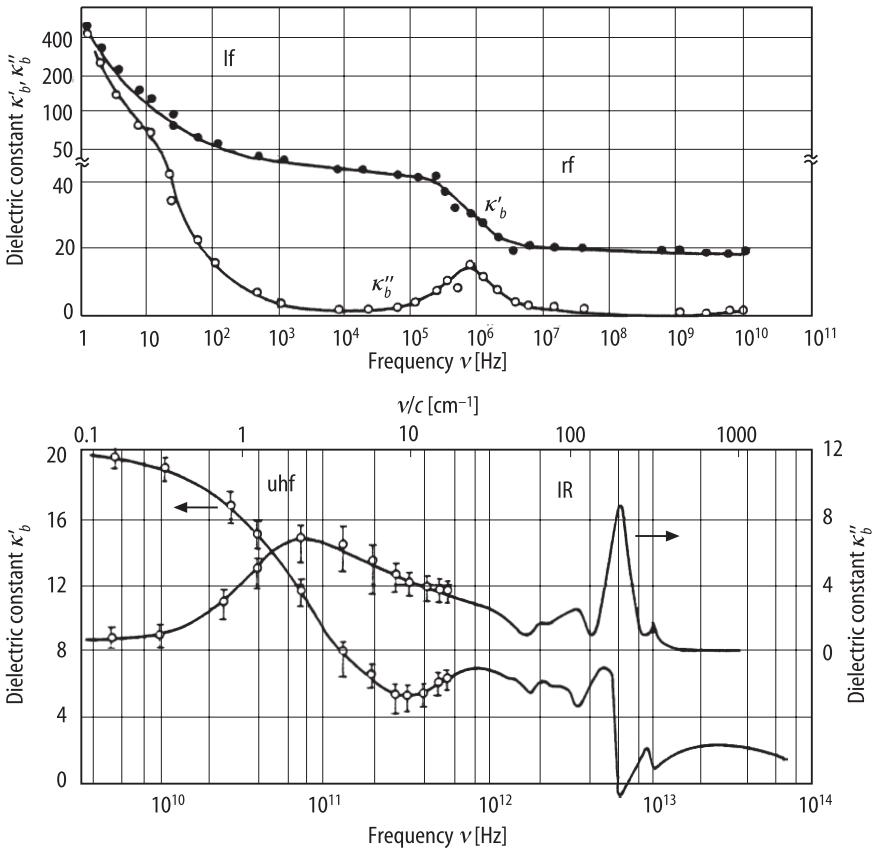

Fig. 60A-1-025. $(NH_2CH_2COOH)_3 \cdot H_2SO_4$ (TGS). κ'_b, κ''_b vs. ν at about 20 °C [73Pop]. lf: low frequency; rf: radio frequency; uhf: ultra high frequency. Note change of scale of ordinate.

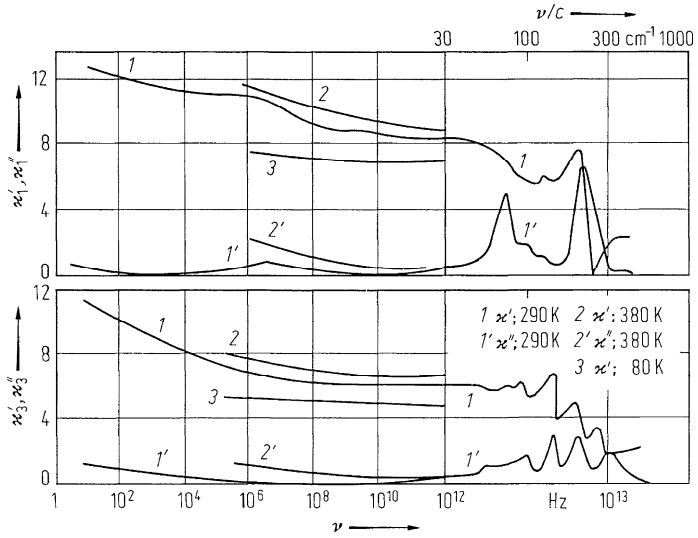

Fig. 60A-1-026. $(NH_2CH_2COOH)_3 \cdot H_2SO_4$ (TGS). κ', κ'' vs. ν [74Pop]. Parameter: T. κ_1 and κ_3 are the principal dielectric constants along the axes perpendicular to the b axis.

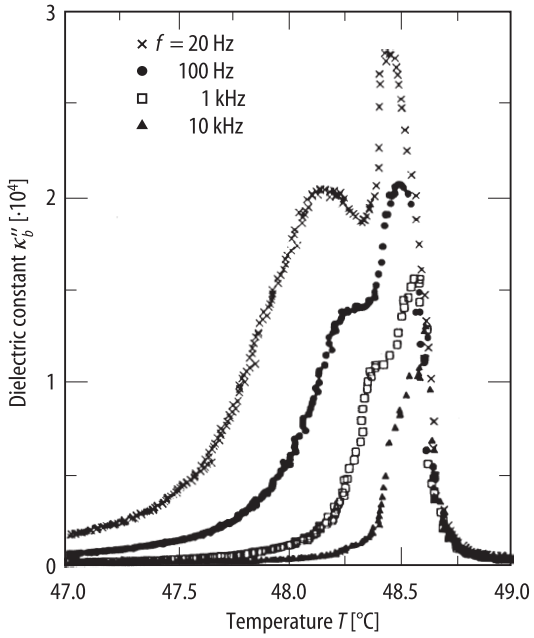

Fig. 60A-1-027. $(NH_2CH_2COOH)_3 \cdot H_2SO_4$ (TGS). κ_b'' vs. T [94Prz]. Parameter: f. Amplitude of measuring field: 10^3 V m^{-1}.

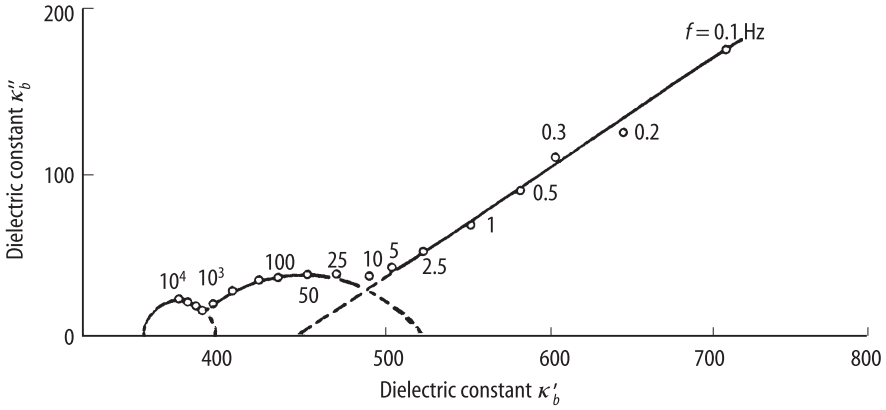

Fig. 60A-1-028. $(NH_2CH_2COOH)_3 \cdot H_2SO_4$ (TGS). Cole-Cole plot of the complex dielectric constant at low frequency [89Gal]. T = 317.83 K.

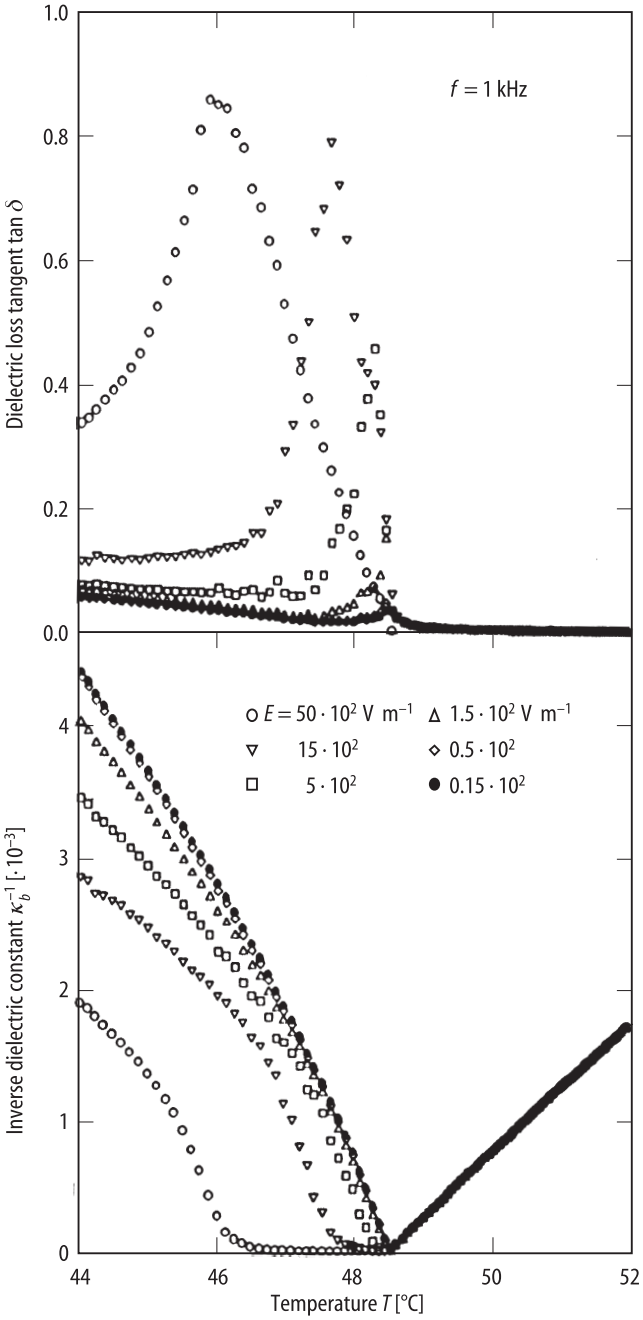

Fig. 60A-1-029. $(NH_2CH_2COOH)_3 \cdot H_2SO_4$ (TGS). $\tan\delta$, κ_b^{-1} vs. T [94Igl]. Parameter: amplitude of measuring ac field E.

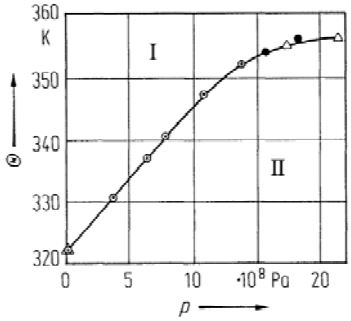

Fig. 60A-1-030. $(NH_2CH_2COOH)_3 \cdot H_2SO_4$ (TGS). Θ vs. p [74Sta1]. Different marks correspond to different runs of experiments.

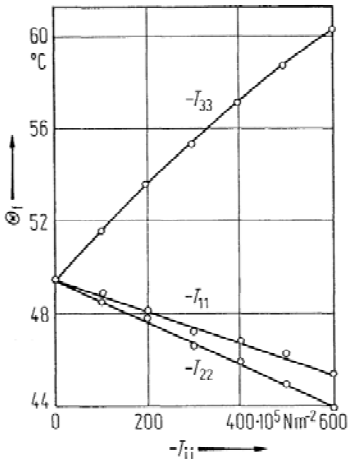

Fig. 60A-1-031. $(NH_2CH_2COOH)_3 \cdot H_2SO_4$ (TGS). Θ_f vs. $-T_{ii}$ [74Ima]. Θ_f: ferroelectric Curie temperature, $-T_{ii}$: uniaxial stress. The orthogonal axial system of Fig. 60A-1-003 is adopted.

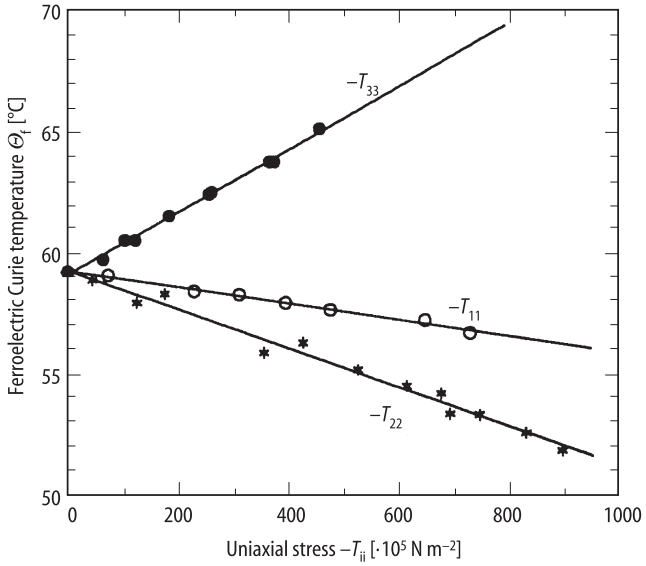

Fig. 60A-1-032. Deuterated triglycine sulfate (DTGS). Θ_f vs. $-T_{ii}$ [93Kor]. Θ_f: ferroelectric Curie temperature, $-T_{ii}$: uniaxial stress. The orthogonal axial system ($X \parallel a$, $Y \parallel b$, $Z \parallel c^*$) is adopted. Degree of deuteration is ≈ 90 %.

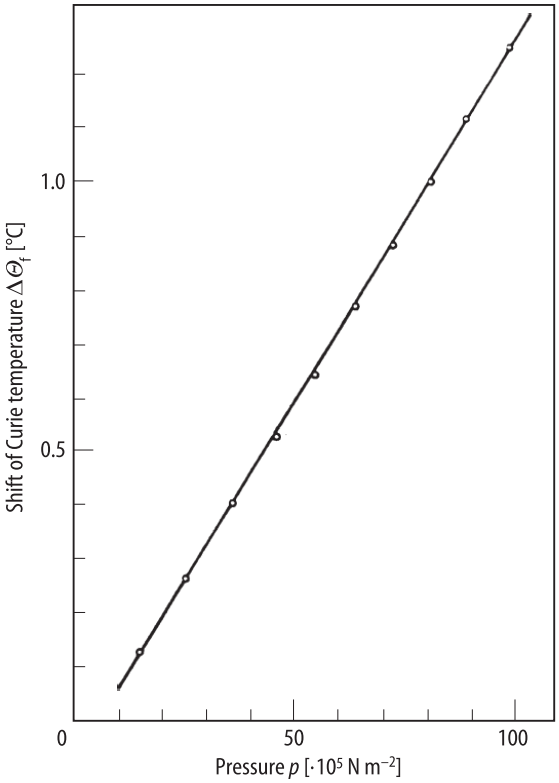

Fig. 60A-1-033. $(NH_2CH_2COOH)_3 \cdot H_2SO_4$ (TGS). $\Delta\Theta_f$ vs. p [72Mor]. $\Delta\Theta_f$: shift of Curie temperature. p: two-dimensional pressure perpendicular to the b axis.

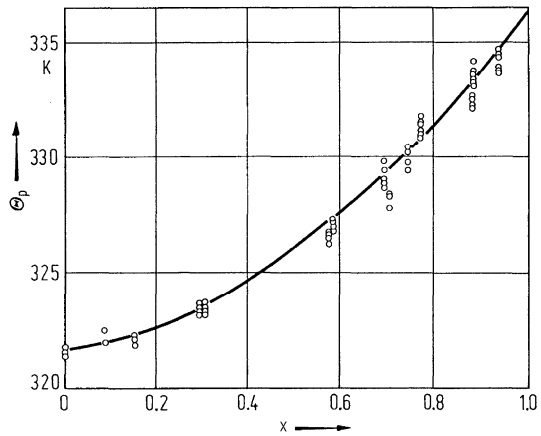

Fig. 60A-1-034. $[(NH_2CH_2COOH)_3 \cdot H_2SO_4]_{1-x}[(ND_2CH_2COOD)_3 \cdot D_2SO_4]_x$ ($TGS_{1-x}DTGS_x$). Θ_p vs. x [68Bre2]. Θ_p: paraelectric Curie temperature.

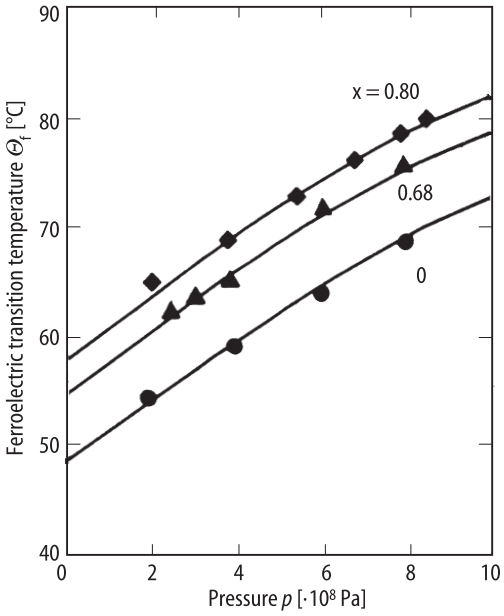

Fig. 60A-1-035. $[(NH_2CH_2COOH)_3 \cdot H_2SO_4]_{1-x}[(ND_2CH_2COOD)_3 \cdot D_2SO_4]_x$ ($TGS_{1-x}DTGS_x$). Θ_f vs. p [90Yao]. Parameter: x.

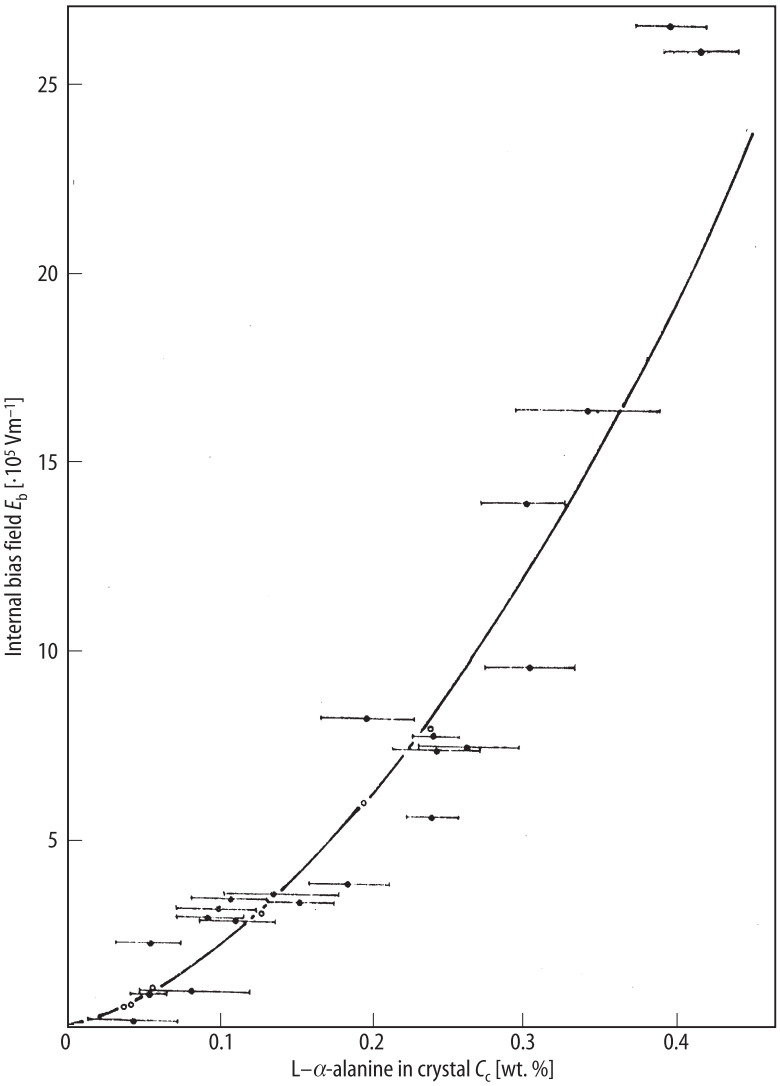

Fig. 60A-1-036. L-α-alanine-doped TGS (LATGS). E_b vs C_c [87Sta]. C_c: wt. % of L-α-alanine in crystal. E_b: intensity of internal bias field. Full circle: [87Sta], open circle: [78Lil].

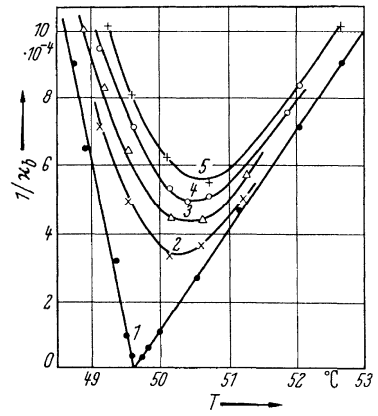

Fig. 60A-1-037. $(NH_2CH_2COOH)_3 \cdot H_2SO_4$ (TGS). $1/\kappa_b$ vs. T [61Sil]. Parameter: E_{bias}.

Curve	*1*	*2*	*3*	*4*	*5*
E_{bias} [kV m^{-1}]	0	50	80	120	180

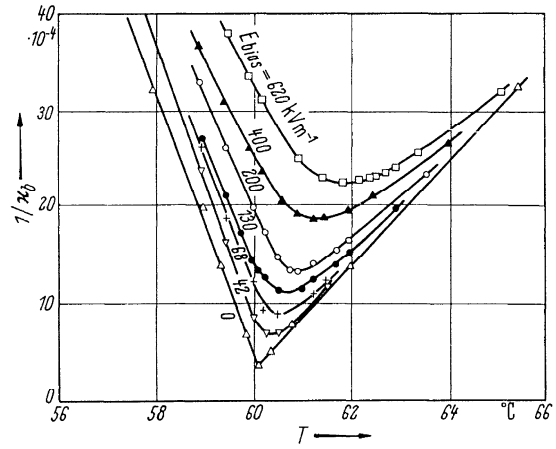

Fig. 60A-1-038. Deuterated triglycine sulfate (DTGS). $1/\kappa_b$ vs. T [61Sil]. Parameter: E_{bias}.

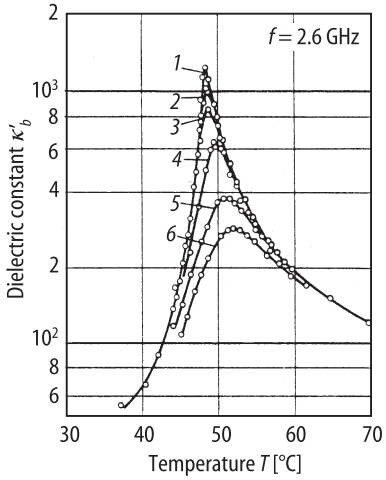

Fig. 60A-1-039. $(NH_2CH_2COOH)_3 \cdot H_2SO_4$ (TGS). κ'_b vs. T [63Hil]. Parameter: E_{bias}.

Curve	*1*	*2*	*3*	*4*	*5*	*6*
E_{bias} [kV m^{-1}]	0	60	120	240	640	1060

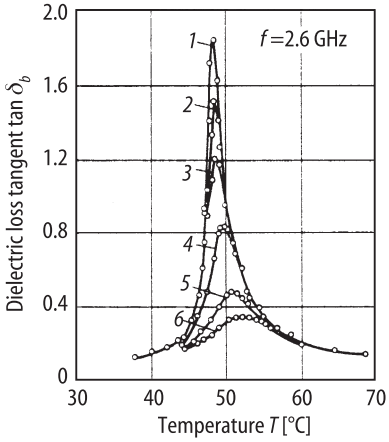

Fig. 60A-1-040. $(NH_2CH_2COOH)_3 \cdot H_2SO_4$ (TGS). tan δ_b vs. T [63Hil]. Parameter: E_{bias}.

Curve	*1*	*2*	*3*	*4*	*5*	*6*
E_{bias} [kV m^{-1}]	0	60	120	240	640	1060

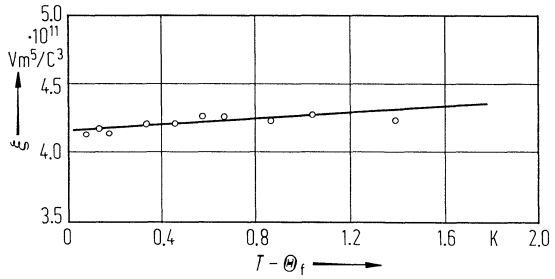

Fig. 60A-1-041. Deuterated TGS (47 % deuterated). ξ vs. $T - \Theta_f$ [80Sch]. ξ: coefficient of power series expansion of electric field strength, $E = (1/\chi_p)P + \xi P^3 + \zeta P^5$.

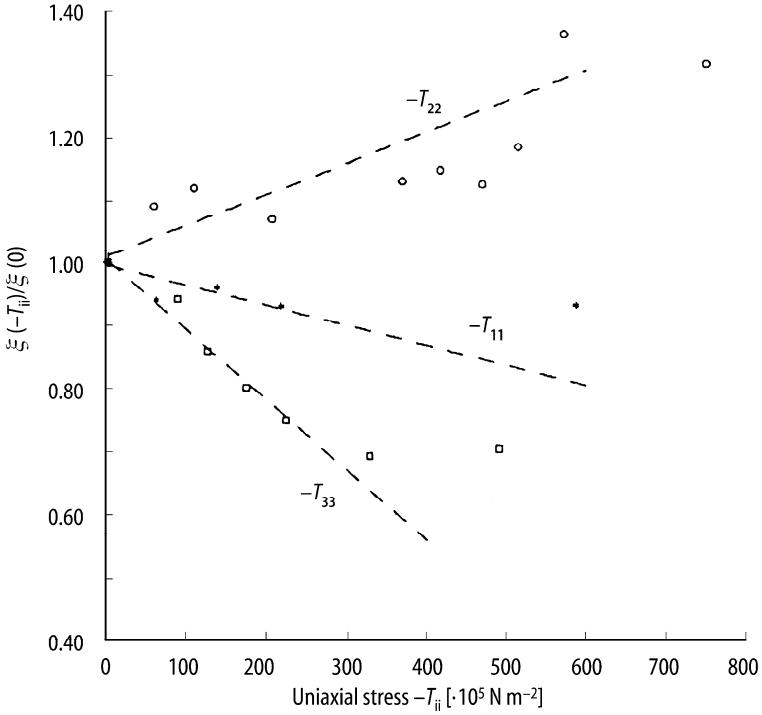

Fig. 60A-1-042. $(NH_2CH_2COOH)_3 \cdot H_2SO_4$ (TGS). $\xi(-T_{ii})/\xi(0)$ vs. $-T_{ii}$ [92FeL]. ξ: coefficient of power series expansion of electric field strength, $E = (1/\chi_p)P + \xi P^3 + \zeta P^5$. $-T_{ii}$: uniaxial stress. The orthogonal axial system ($X \parallel a$, $Y \parallel b$, $Z \parallel c^*$) is adopted.

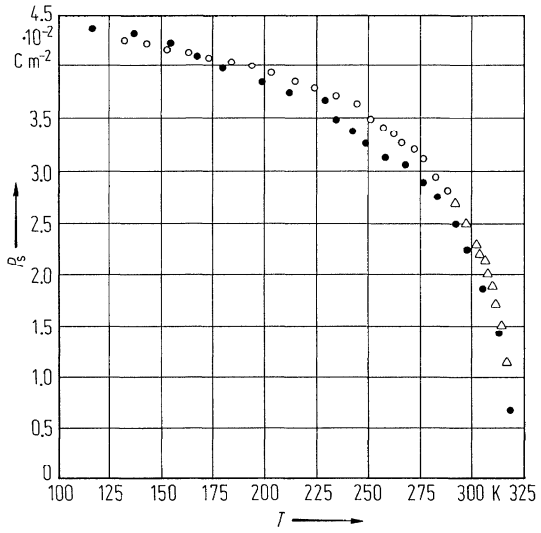

Fig. 60A-1-043. $(NH_2CH_2COOH)_3 \cdot H_2SO_4$ (TGS). P_s vs. T [64Gon]. Open circles: pyroelectric [60Chy2]. Triangles: hysteresis loop [58Tri]. Full circles: hysteresis loop [64Gon].

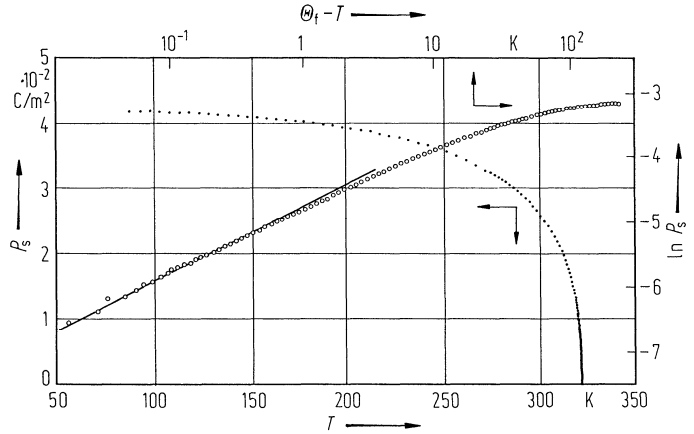

Fig. 60A-1-044. $(NH_2CH_2COOH)_3 \cdot H_2SO_4$ (TGS). Temperature dependence of P_s [80Ima]. Dots: P_s vs. T, open circles: ln P_s vs. $\Theta_f - T$.

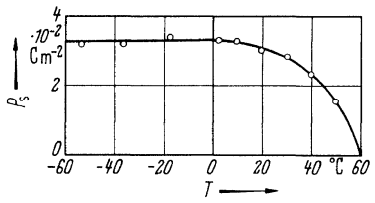

Fig. 60A-1-045. Deuterated triglycine sulfate (DTGS). P_s vs. T [60Kon].

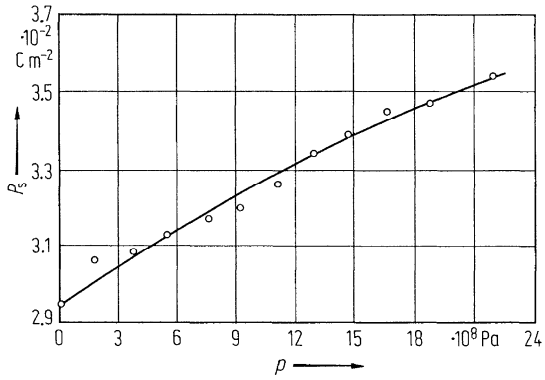

Fig. 60A-1-046. $(NH_2CH_2COOH)_3 \cdot H_2SO_4$ (TGS). P_s vs. p at RT [74Sta1].

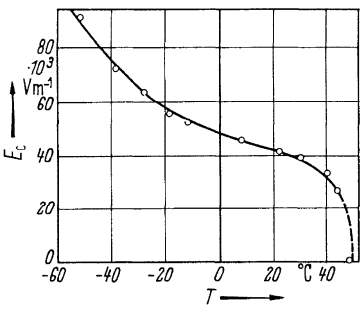

Fig. 60A-1-047. $(NH_2CH_2COOH)_3 \cdot H_2SO_4$ (TGS). E_c vs. T [58Dom].

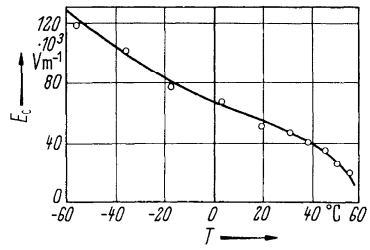

Fig. 60A-1-048. Deuterated triglycine sulfate (DTGS). E_c vs. T [60Kon]. f = 50 Hz.

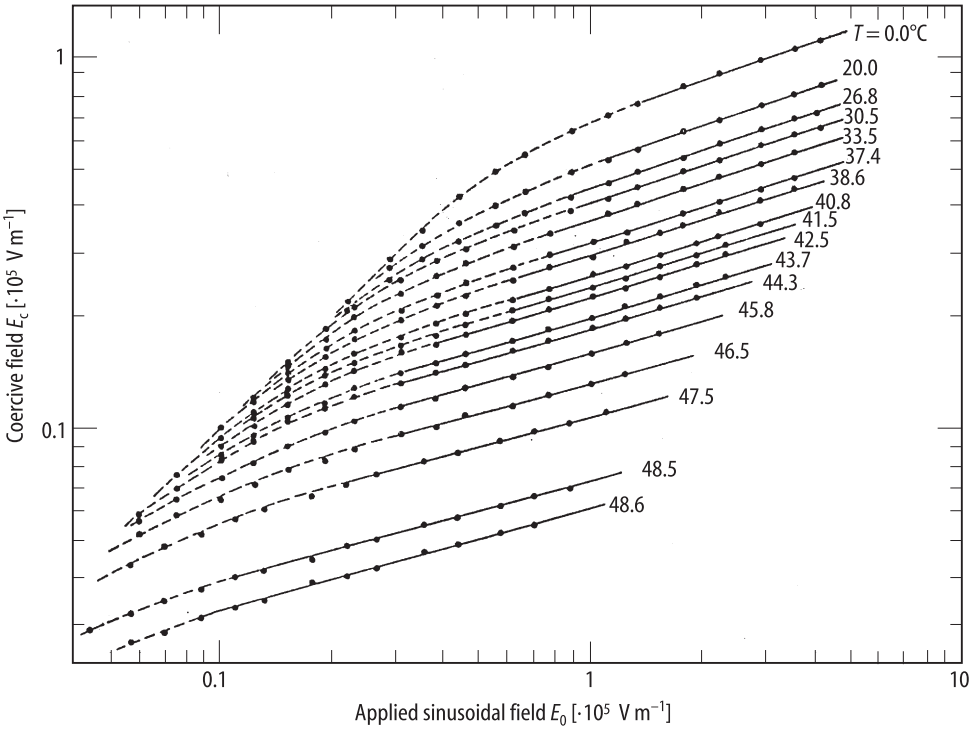

Fig. 60A-1-049. $(NH_2CH_2COOH)_3 \cdot H_2SO_4$ (TGS). E_c vs. E_0 [72Nak]. Parameter: T. E_0: amplitude of applied sinusoidal field. f = 60 Hz.

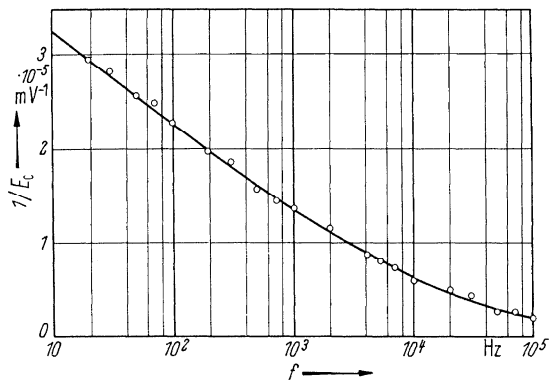

Fig. 60A-1-050. $(NH_2CH_2COOH)_3 \cdot H_2SO_4$ (TGS). E_c^{-1} vs. f [58Pul].

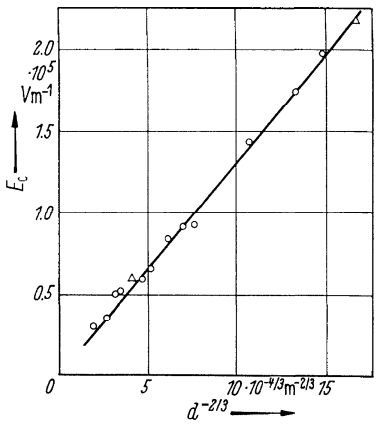

Fig. 60A-1-051. $(NH_2CH_2COOH)_3 \cdot H_2SO_4$ (TGS). E_c vs. $d^{-2/3}$ [62Kay]. d: crystal thickness. Circle and triangle: by different specimens.

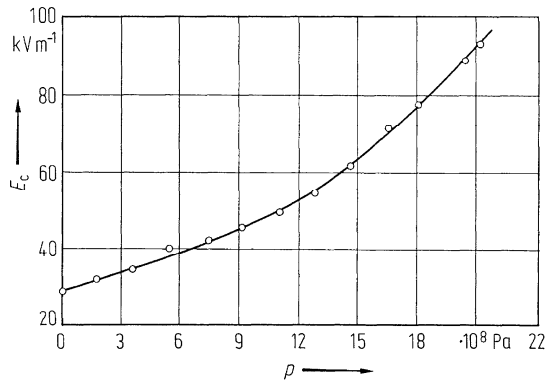

Fig. 60A-1-052. $(NH_2CH_2COOH)_3 \cdot H_2SO_4$ (TGS). E_c vs. p at RT [74Sta1].

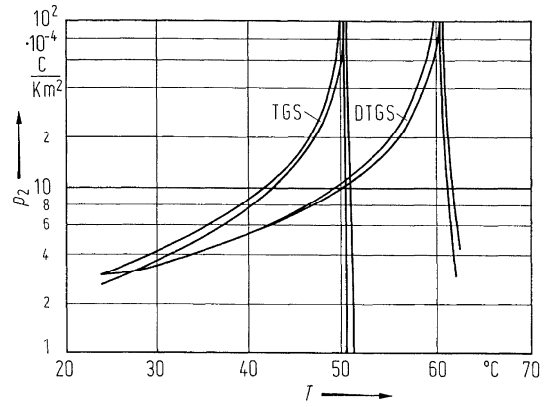

Fig. 60A-1-053. $(NH_2CH_2COOH)_3 \cdot H_2SO_4$ (TGS), deuterated triglycine sulfate (DTGS). p_2 vs. T [78Fel]. p_2: pyroelectric coefficient along the [010] axis. Two curves for TGS and DTGS are the extreme values obtained for several samples.

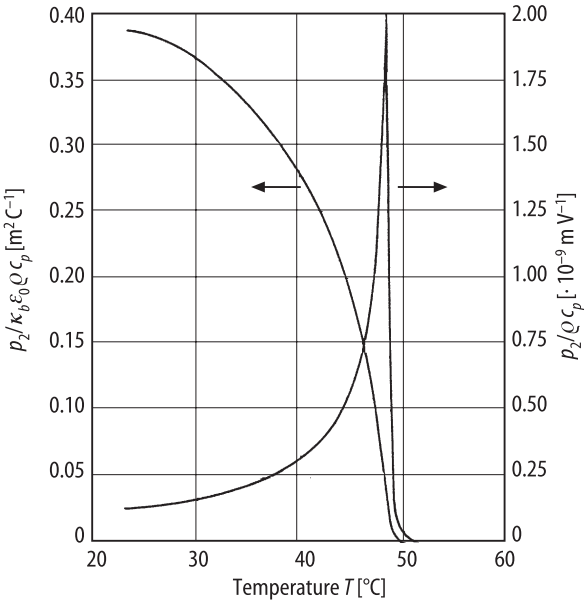

Fig. 60A-1-054. $(NH_2CH_2COOH)_3 \cdot H_2SO_4$ (TGS). $p_2/\kappa_b\varepsilon_0\rho c_p$, $p_2/\rho c_p$ vs. T [79Sha]. p_2: pyroelectric coefficient along the b axis, ρ: density, c_p: specific heat capacity at constant pressure.

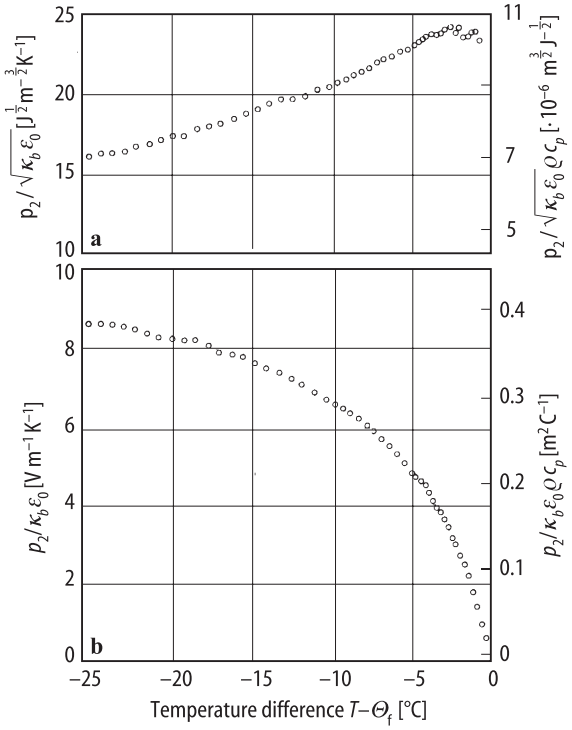

Fig. 60A-1-055. $(NH_2CH_2COOH)_3 \cdot H_2SO_4$ (TGS). Pyroelectric properties [79Sha]. (**a**) $p_2/\sqrt{\kappa_b\varepsilon_0}$, $p_2/\sqrt{\kappa_b\varepsilon_0}\,\rho c_p$ vs. $T-\Theta_f$, (**b**) $p_2/\kappa_b\varepsilon_0$, $p_2/\kappa_b\varepsilon_0\rho c_p$ vs. $T-\Theta_f$. p_2: pyroelectric coefficient along the b axis, ρ: density, c_p: specific heat capacity at constant pressure.

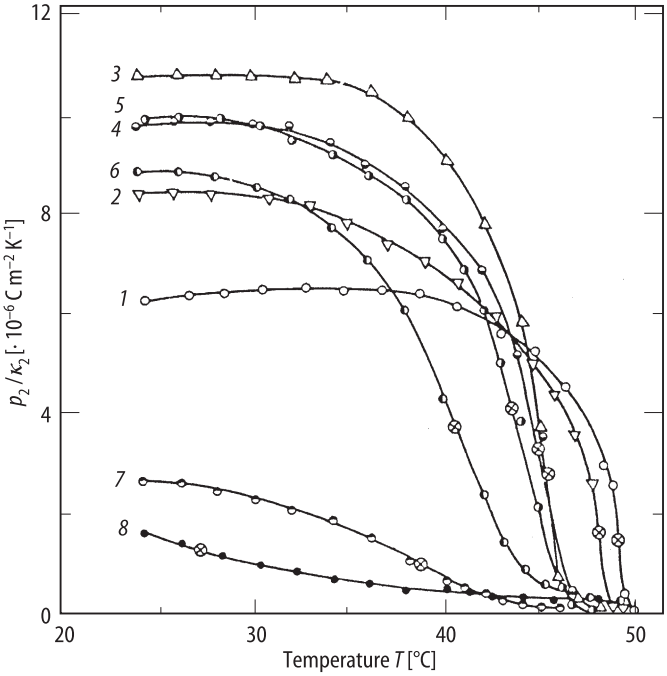

Fig. 60A-1-056. $(NH_2CH_2COOH)_3 \cdot H_2SO_4$ (TGS). p_2/κ_2 vs. T [89Tse]. p_2: pyroelectric coefficient along the b axis. Parameter: γ-irradiation dose. *1*: before irradiation, *2*: 0.01 MR, *3*: 0.1 MR, *4*: 0.5 MR, *5*: 1 MR, *6*: 5 MR, *7*: 10 MR, *8*: 20 MR. 1 R = $2.58 \cdot 10^{-4}$ C kg^{-1}.

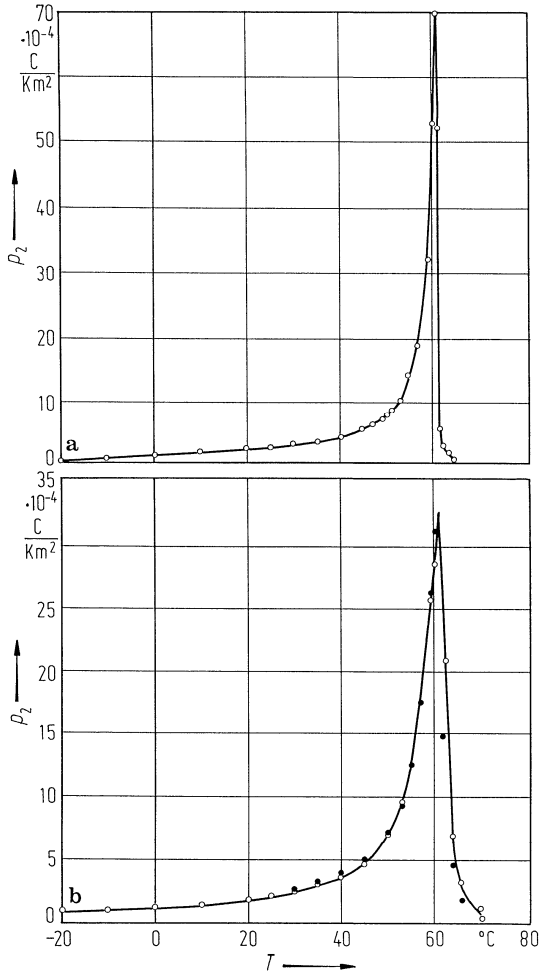

Fig. 60A-1-057. $(ND_2CH_2COOD)_3 \cdot D_2SO_4$ (DTGS). p_2 vs. T [79Lil]. p_2: pyroelectric coefficient along the b axis. (**a**): L-α-alanine doped DTGS crystal, (**b**): undoped DTGS crystal. Open circles, full circles: by different specimens

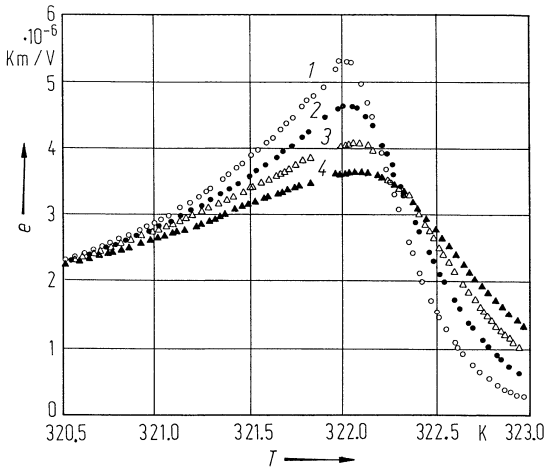

Fig. 60A-1-058. $(NH_2CH_2COOH)_3 \cdot H_2SO_4$ (TGS). e vs. T [82Ram]. e: electrocaloric coefficient along the b axis. Parameter: *E. 1*: $E = 1.6 \cdot 10^4$ V m^{-1}, *2*: $3.0 \cdot 10^4$ V m^{-1}, *3*: $5.0 \cdot 10^4$ V m^{-1}, *4*: $8.0 \cdot 10^4$ V m^{-1}.

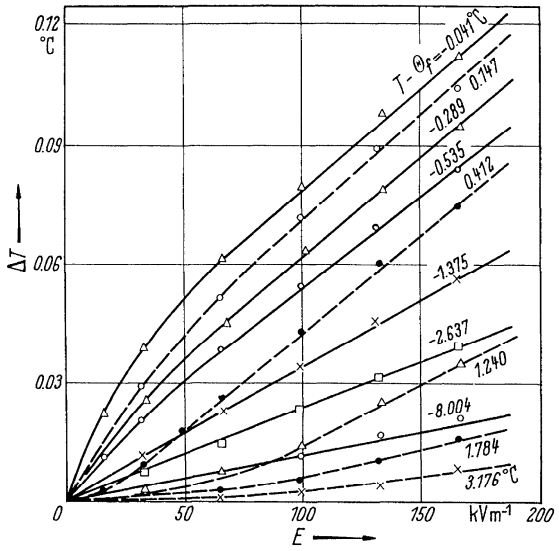

Fig. 60A-1-059. $(NH_2CH_2COOH)_3 \cdot H_2SO_4$ (TGS). ΔT vs. E [66Str]. Parameter: $T - \Theta_f$. ΔT: electrocaloric temperature change.

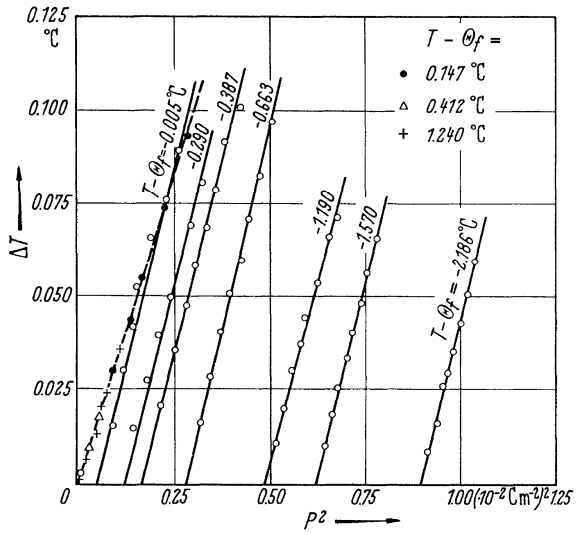

Fig. 60A-1-060. $(NH_2CH_2COOH)_3 \cdot H_2SO_4$ (TGS). ΔT vs. P^2 [66Str]. Parameter: $T - \Theta_f$. ΔT: electrocaloric temperature change.

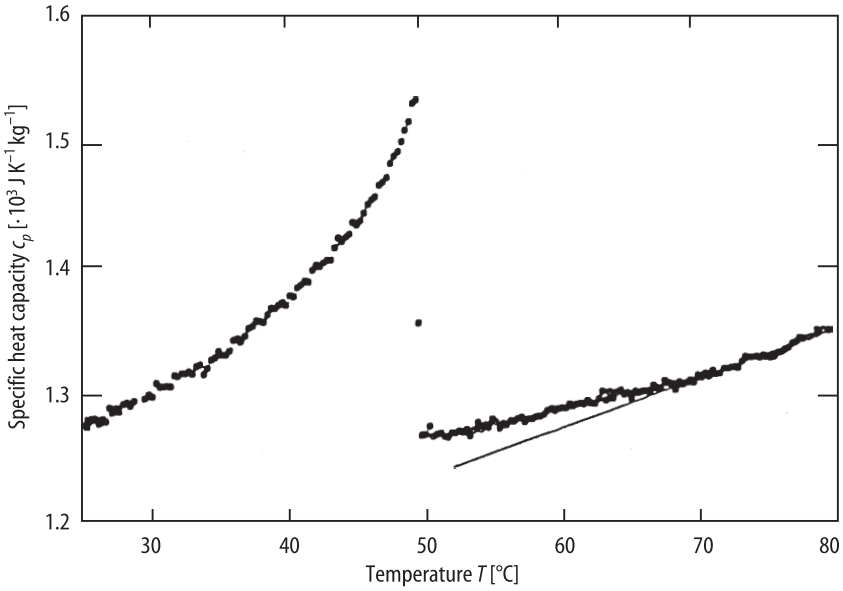

Fig. 60A-1-061. $(NH_2CH_2COOH)_3 \cdot H_2SO_4$ (TGS). c_p vs. T [89Ram]. c_p: specific heat capacity at constant pressure.

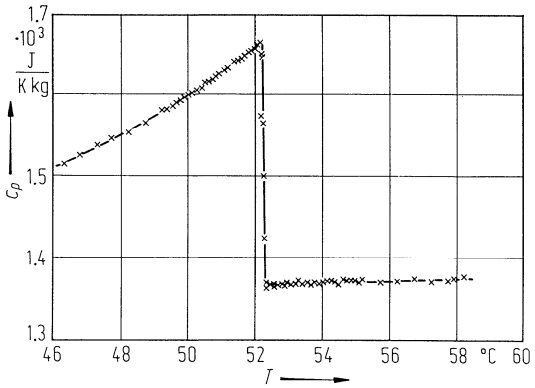

Fig. 60A-1-062. Deuterated TGS (47 % deuterated). c_p vs. T [80Mus]. c_p: specific heat capacity at constant pressure.

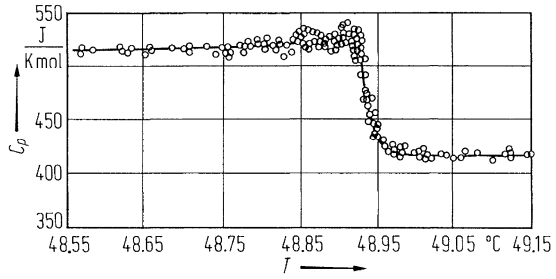

Fig. 60A-1-063. $(NH_2CH_2COOH)_3 \cdot H_2SO_4$ (TGS). C_p vs. T in the close vicinity of Θ_f [70Tar]. C_p: molar heat capacity at constant pressure.

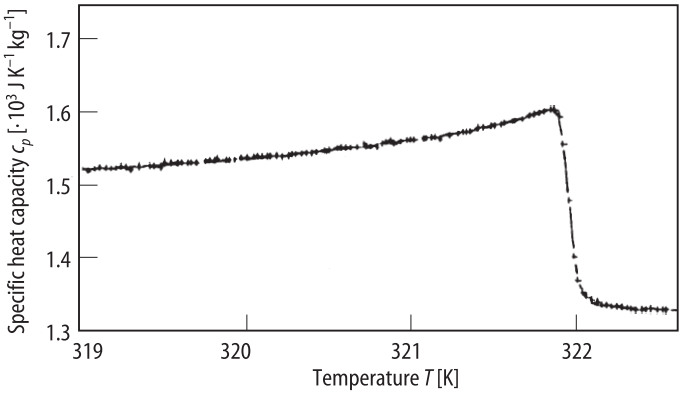

Fig. 60A-1-064. $(NH_2CH_2COOH)_3 \cdot H_2SO_4$ (TGS). c_p vs. T [80Ram]. c_p: specific heat capacity at constant pressure.

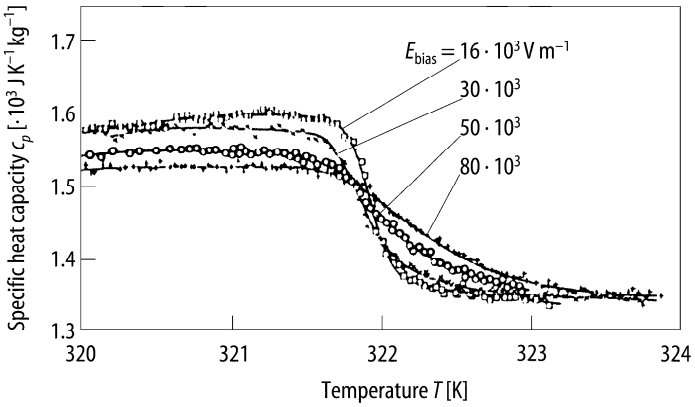

Fig. 60A-1-065. $(NH_2CH_2COOH)_3 \cdot H_2SO_4$ (TGS). c_p vs. T [80Ram]. c_p: specific heat capacity at constant pressure. Parameter: E_{bias}.

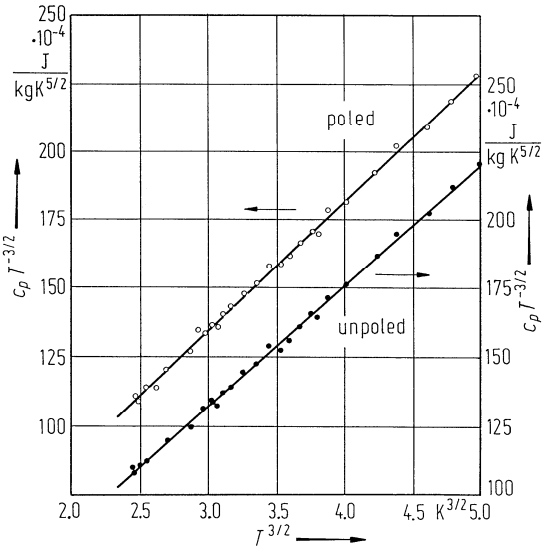

Fig. 60A-1-066. $(NH_2CH_2COOH)_3 \cdot H_2SO_4$ (TGS). $c_p T^{-3/2}$ vs. $T^{3/2}$ [81Law]. c_p: specific heat capacity at constant pressure.

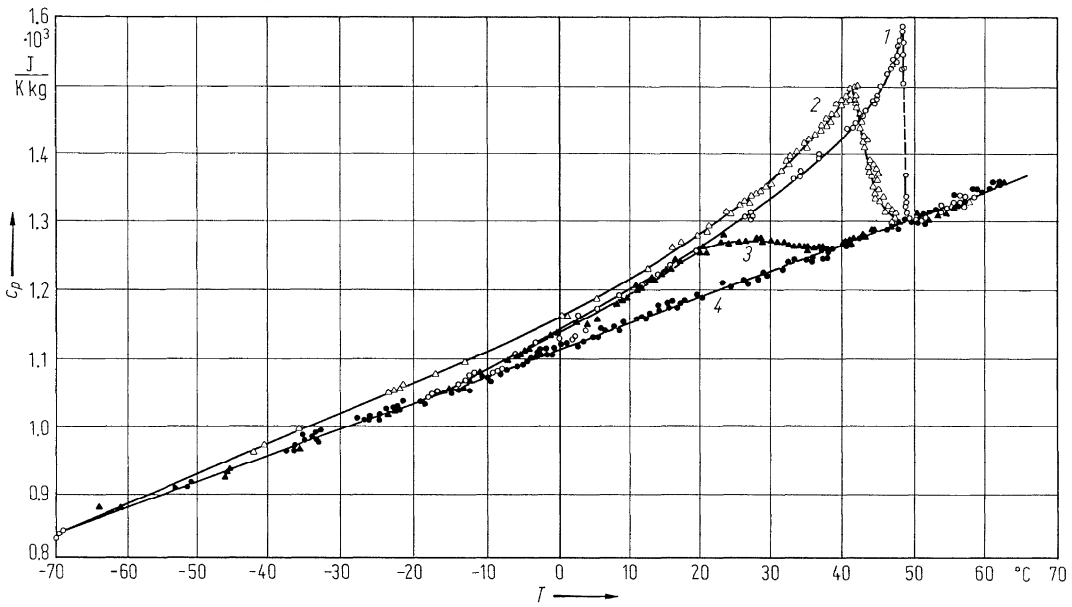

Fig. 60A-1-067. $(NH_2CH_2COOH)_3 \cdot H_2SO_4$ (TGS). c_p vs. T [77Tar]. Parameter: γ-ray irradiation dose. Curve *1*: 0, *2*: 3 mR, *3*: 15 mR, *4*: 30 mR. 1 R = $2.58 \cdot 10^{-4}$ C kg^{-1}.

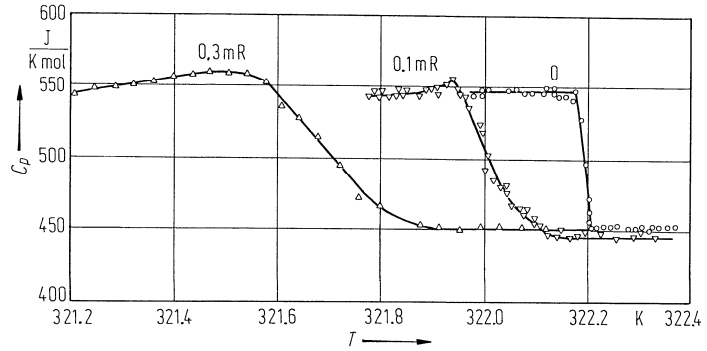

Fig. 60A-1-068. $(NH_2CH_2COOH)_3 \cdot H_2SO_4$ (TGS). C_p vs. T [80Str]. Parameter: γ-ray irradiation dose. C_p: molar heat capacity at constant pressure.

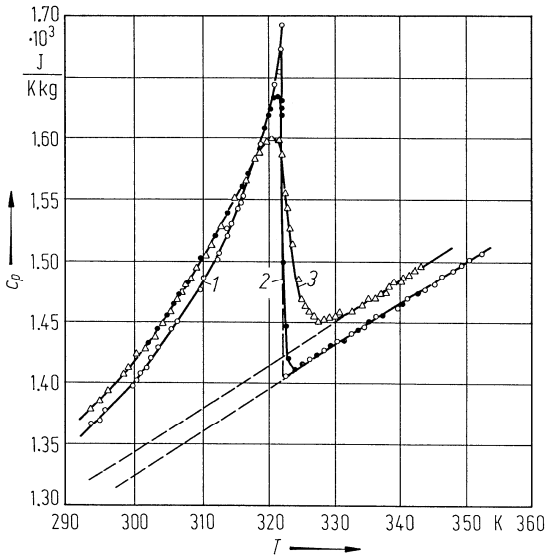

Fig. 60A-1-069. $(NH_2CH_2COOH)_3 \cdot H_2SO_4$ (TGS). c_p vs. T [82Str]. c_p: specific heat capacity at constant pressure. *1*: pure crystal, *2*: Cr^{3+} doped crystal (3 % in solution), *3*: α-alanine doped crystal (10 % in solution). The sound velocity data for the same specimens are shown in Fig. 60A-1-101.

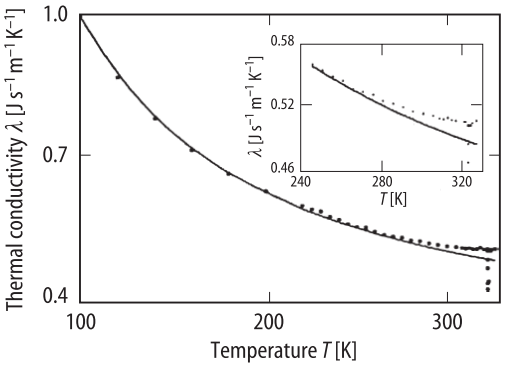

Fig. 60A-1-070. $(NH_2CH_2COOH)_3 \cdot H_2SO_4$ (TGS). λ vs. T [92Str]. λ: thermal conductivity along the c axis.

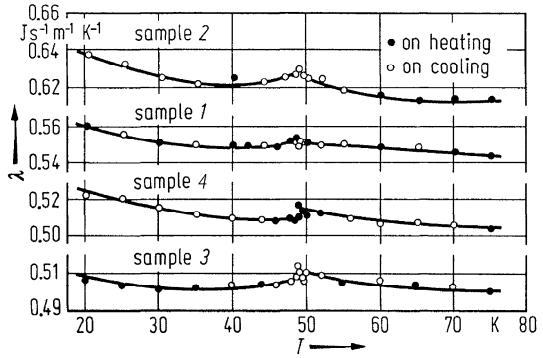

Fig. 60A-1-071. $(NH_2CH_2COOH)_3 \cdot H_2SO_4$ (TGS). λ vs. T [71Hel]. λ: thermal conductivity.

Sample No.	*1*	*2*	*3*	*4*
Direction	*y*	*x*	*z*	$\perp y$, 45° from *z*

See the axial system of Fig. 60A-1-003.

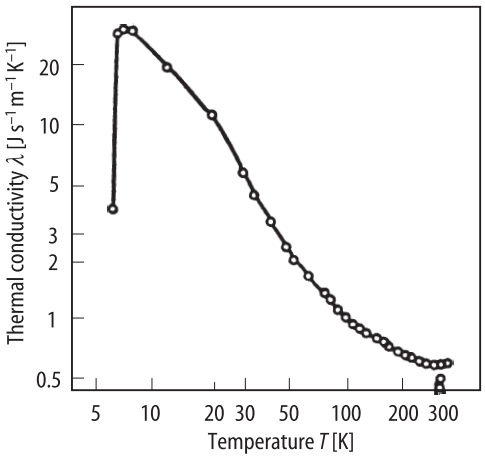

Fig. 60A-1-072. $(NH_2CH_2COOH)_3 \cdot H_2SO_4$ (TGS). λ vs. T [90Str]. λ: thermal conductivity along the c axis.

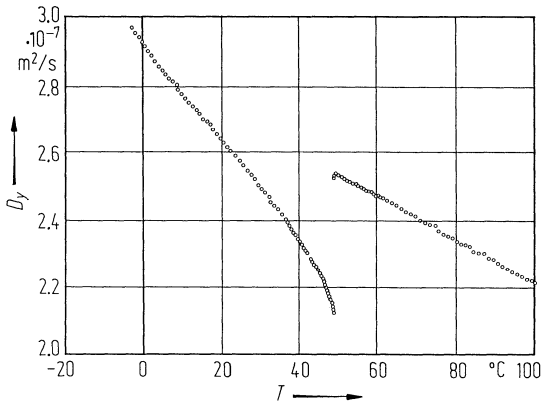

Fig. 60A-1-073. $(NH_2CH_2COOH)_3 \cdot H_2SO_4$ (TGS). D_y vs. T [86Hat]. D_y: thermal diffusivity along the b axis.

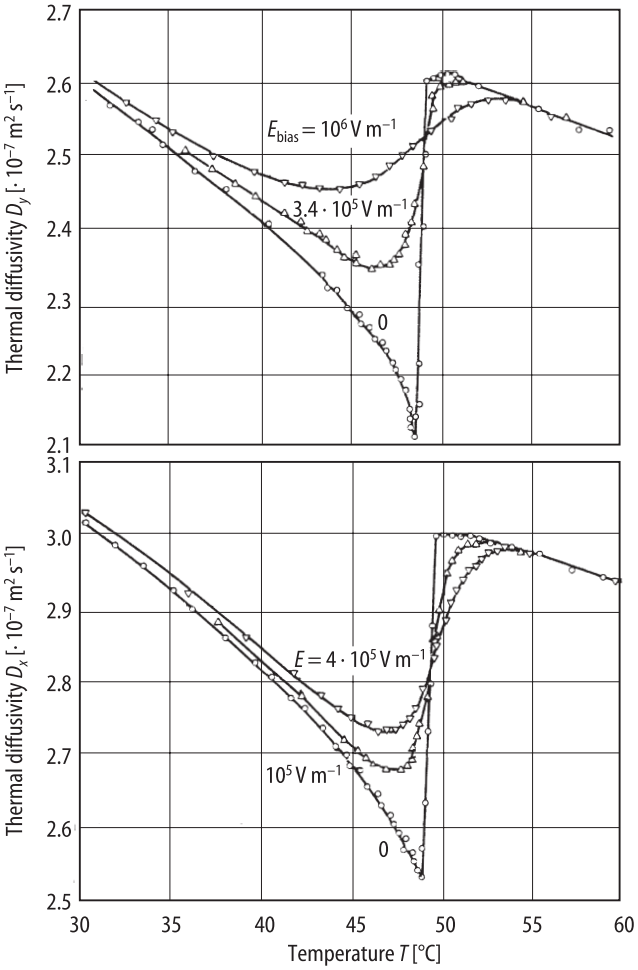

Fig. 60A-1-074. $(NH_2CH_2COOH)_3 \cdot H_2SO_4$ (TGS). D_x, D_y vs. T near Θ_f [85Zav]. Parameter: E_{bias}. D_x, D_y: thermal diffusivities along the *a* and *b* axes.

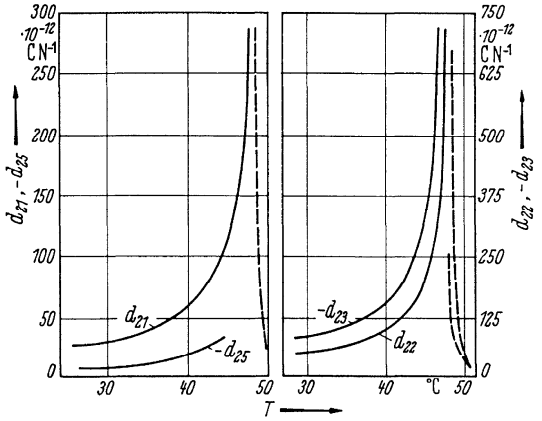

Fig. 60A-1-075. $(NH_2CH_2COOH)_3 \cdot H_2SO_4$ (TGS). $d_{i\lambda}$ vs. T [62Ike]. Broken lines show apparent piezoelectricities caused by electrostriction.

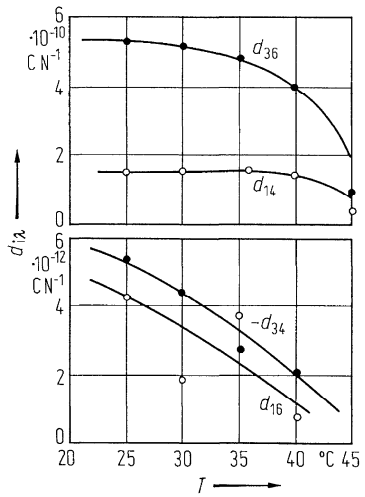

Fig. 60A-1-076. $(NH_2CH_2COOH)_3 \cdot H_2SO_4$ (TGS). $d_{i\lambda}$ ($\lambda = 4$ and 6) vs. T [62Ike].

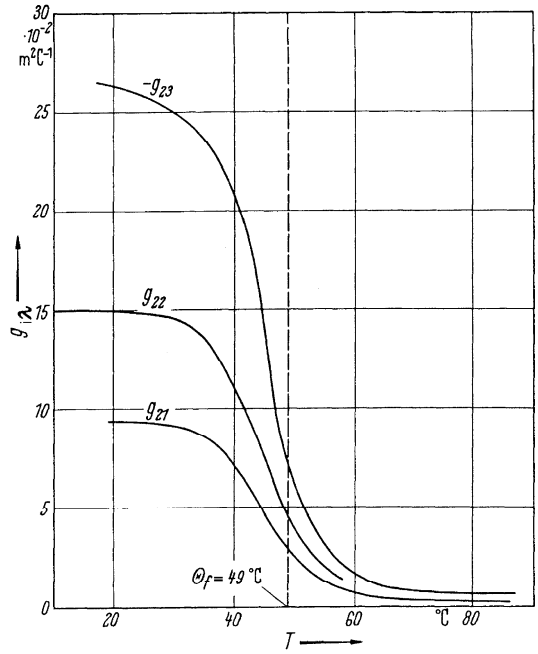

Fig. 60A-1-077. $(NH_2CH_2COOH)_3 \cdot H_2SO_4$ (TGS). $g_{i\lambda}$ vs. T [63Sch].

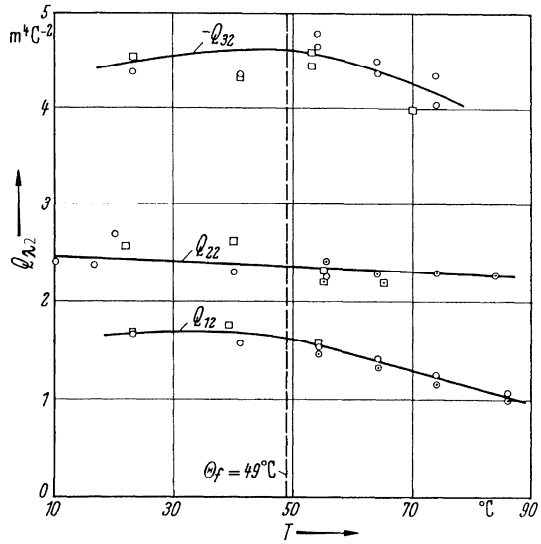

Fig. 60A-1-078. $(NH_2CH_2COOH)_3 \cdot H_2SO_4$ (TGS). $Q_{\lambda\mu}$ vs.T [63Sch]. Different symbols correspond to different measurements.

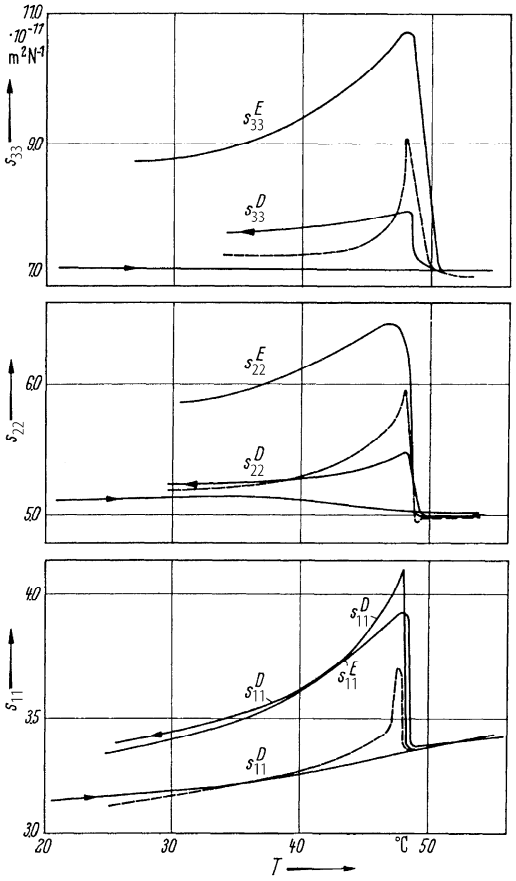

Fig. 60A-1-079. $(NH_2CH_2COOH)_3 \cdot H_2SO_4$ (TGS). $s^{D}_{\lambda\mu}$, $s^{E}_{\lambda\mu}$ vs. T [62Ike]. s^{E}: resonance method. s^{D}: calculated values from s^{E} (broken lines). The lowest flat lines show the values observed by composite-bar method (heating). The remaining curves show the values of the unpoled crystals observed by composite-bar method (cooling). See also [61Shu, 62Min].

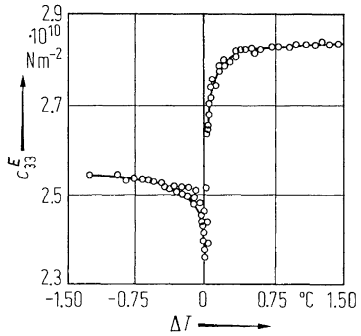

Fig. 60A-1-080. $(NH_2CH_2COOH)_3 \cdot H_2SO_4$ (TGS). c_{33}^{E} vs. ΔT [75Str]. $\Delta T = T - \Theta_f$. $f = 10$ MHz.

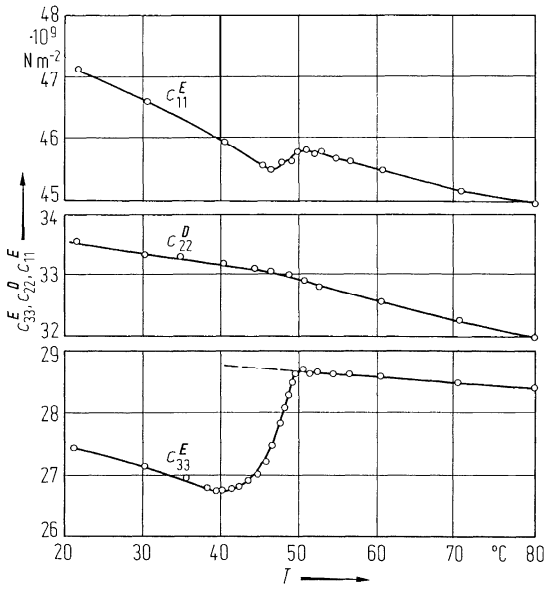

Fig. 60A-1-081. $(NH_2CH_2COOH)_3 \cdot H_2SO_4$ (TGS). $c_{11}^{E}, c_{22}^{D}, c_{33}^{E}$ vs. T [77Lus]. $c_{11}^{E}, c_{22}^{D}, c_{33}^{E}$ were obtained by Brillouin scattering.

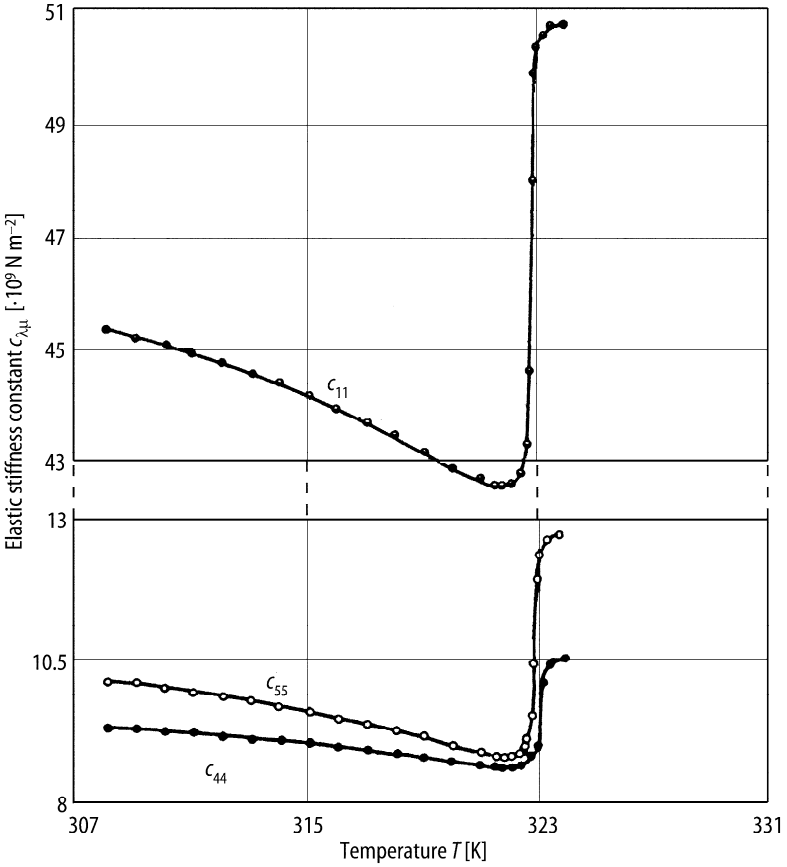

Fig. 60A-1-082. $(NH_2CH_2COOH)_3 \cdot H_2SO_4$ (TGS). $c_{\lambda\mu}$ vs. T [92Dzi1]. $c_{\lambda\mu}$: elastic stiffness constant obtained by resonance method.

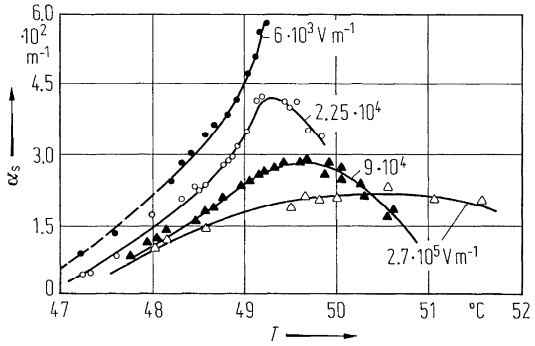

Fig. 60A-1-083. $(NH_2CH_2COOH)_3 \cdot H_2SO_4$ (TGS). α_s vs. T [76Sad]. α_s: acoustic surface wave attenuation in the a' axis on the b plane. Parameter: externally applied field.

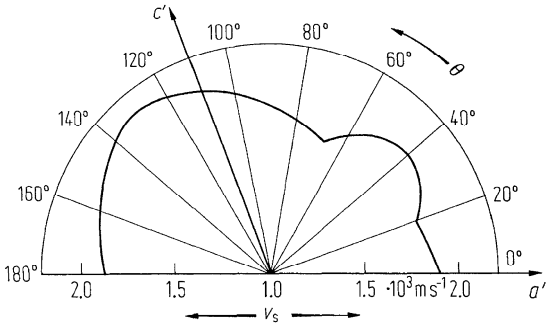

Fig. 60A-1-084. $(NH_2CH_2COOH)_3 \cdot H_2SO_4$ (TGS). v_s vs. θ [77Sad]. v_s: acoustic surface wave velocity in the *b* plane, θ: angle between the propagation direction and the a' axis.

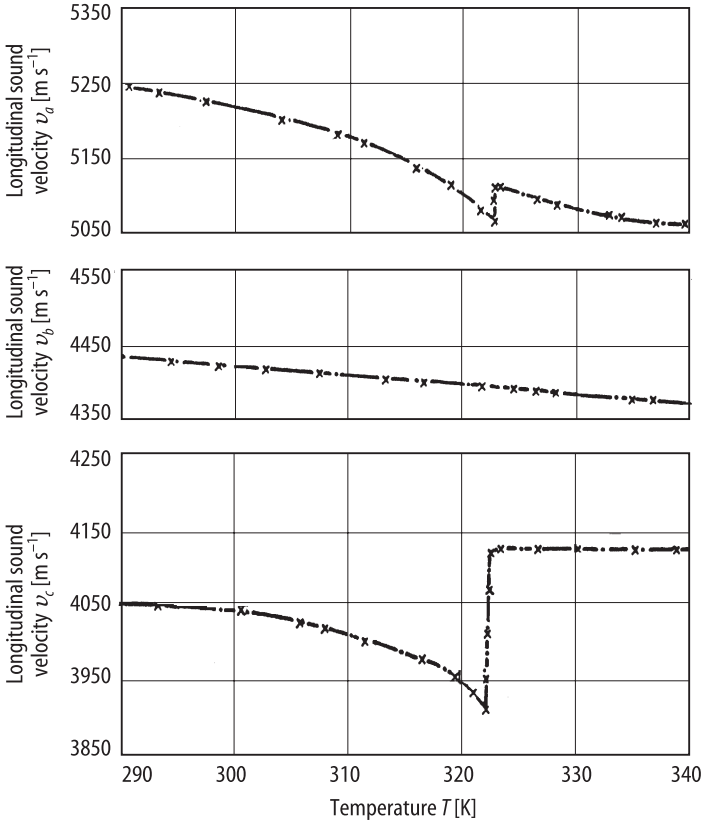

Fig. 60A-1-085. $(NH_2CH_2COOH)_3 \cdot H_2SO_4$ (TGS). v_a, v_b, v_c vs. T [83Szu]. v_a, v_b, v_c: longitudinal sound velocities propagating along the *a*, *b*, *c* axes. f = 9.8, 15.1, and 29.4 MHz.

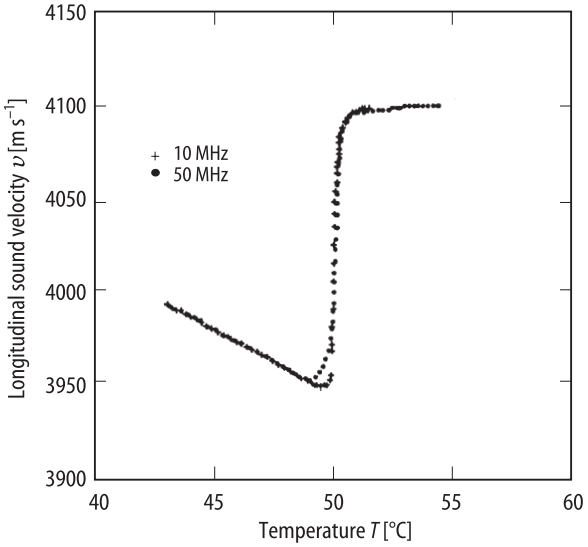

Fig. 60A-1-086. $(NH_2CH_2COOH)_3 \cdot H_2SO_4$ (TGS). v vs. T [92del]. v: longitudinal sound velocity propagating along the c axis.

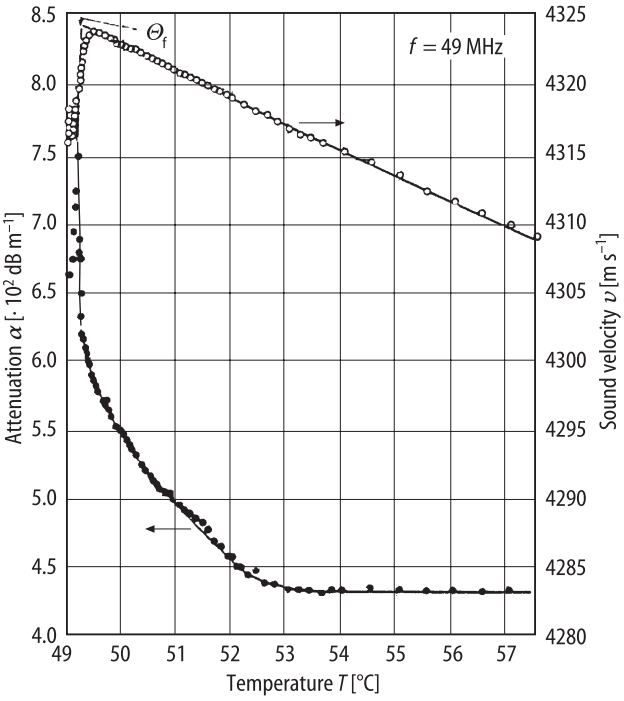

Fig. 60A-1-087. $(NH_2CH_2COOH)_3 \cdot H_2SO_4$ (TGS). α, v vs. T [77Kaw]. α: attenuation of longitudinal sound wave propagating along the b axis. v: sound velocity.

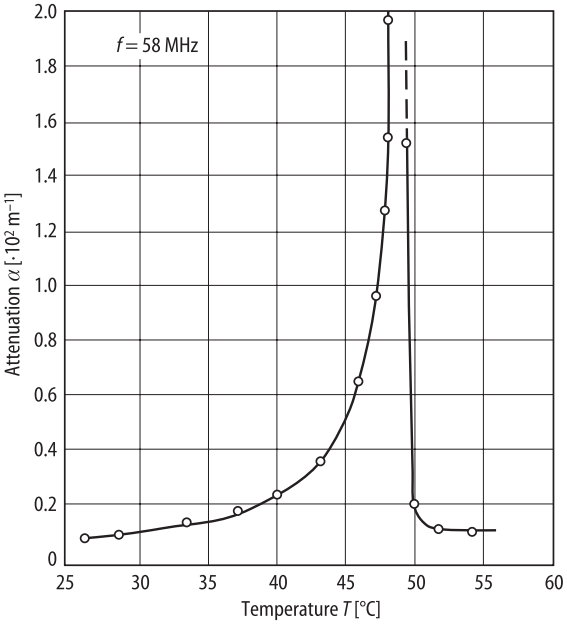

Fig. 60A-1-088. $(NH_2CH_2COOH)_3 \cdot H_2SO_4$ (TGS). α vs. T [71Baj]. α: attenuation coefficient of quasi-longitudinal wave propagating along the c axis.

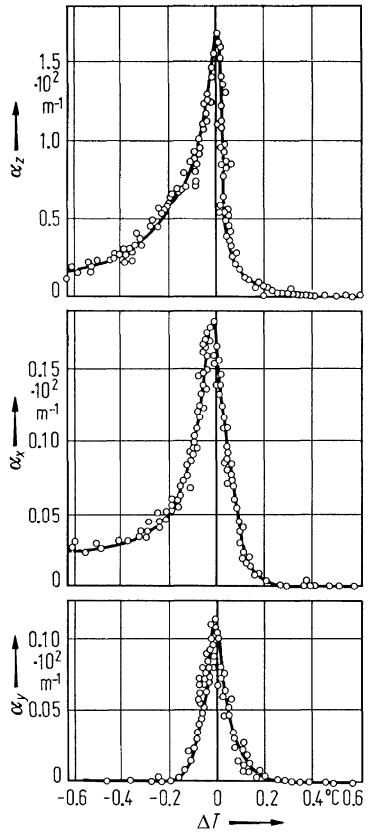

Fig. 60A-1-089. $(NH_2CH_2COOH)_3 \cdot H_2SO_4$ (TGS). α_x, α_y, α_z vs. ΔT [68Min]. α_j: attenuation coefficient for quasi-longitudinal ultrasonic wave propagating along the x, y, z axes. $\Delta T = T - \Theta_t$. See Fig. 60A-1-003.

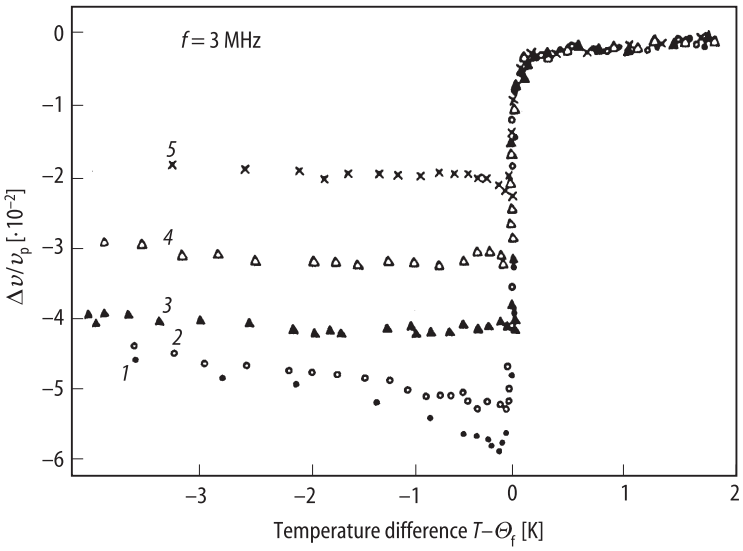

Fig. 60A-1-090. $(NH_2CH_2COOH)_3 \cdot H_2SO_4$ (TGS). $\Delta v/v_p$ vs. $T - \Theta_f$ [87Suc]. Δv: discontinuity near the phase transition in the longitudinal sound velocity in the *bc* plane. v_p: velocity in the paraelectric phase. Parameter: angle of propagating direction to the *c* axis. *1*: 0°, *2*: 2°, *3*: 6°, *4*: 10°, *5*: 18°.

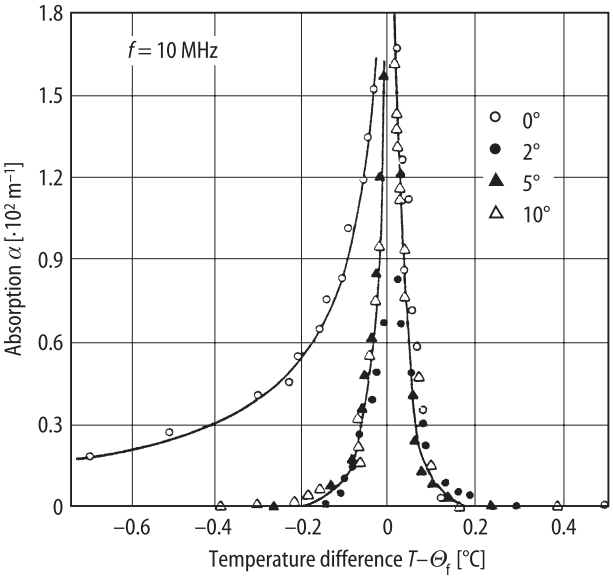

Fig. 60A-1-091. $(NH_2CH_2COOH)_3 \cdot H_2SO_4$ (TGS). α vs. $T - \Theta_f$ [69Min]. α: absorption coefficient of quasi-longitudinal ultrasonic waves propagating in the *bc* plane with angles 0°, 2°, 5° and 10° to the *c* axis.

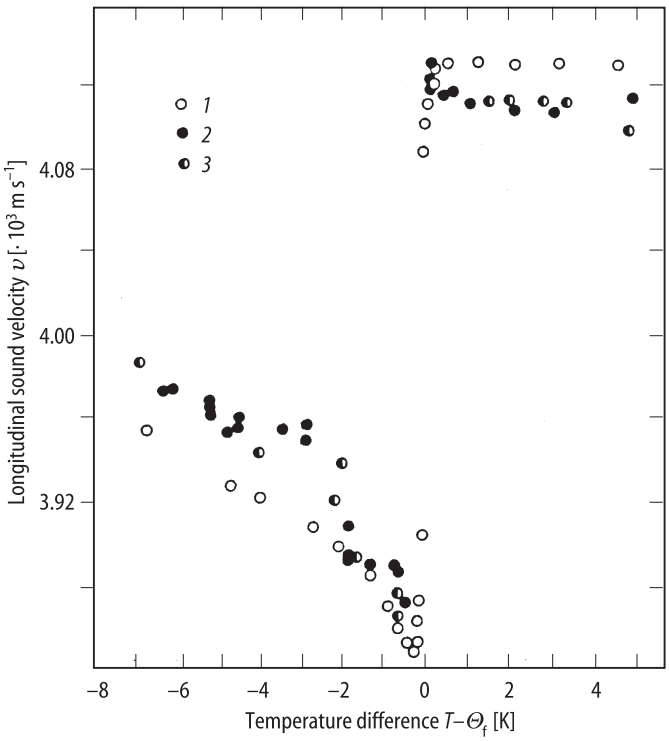

Fig. 60A-1-092. $(NH_2CH_2COOH)_3 \cdot H_2SO_4$ (TGS). v vs. $T - \Theta_f$ [93Cha]. v: longitudinal sound velocity propagating along the c axis. Parameter: *f. 1*: f = 17 MHz; *2*, *3*: 154 MHz. *1*, *2*: heating process; *3*: cooling process.

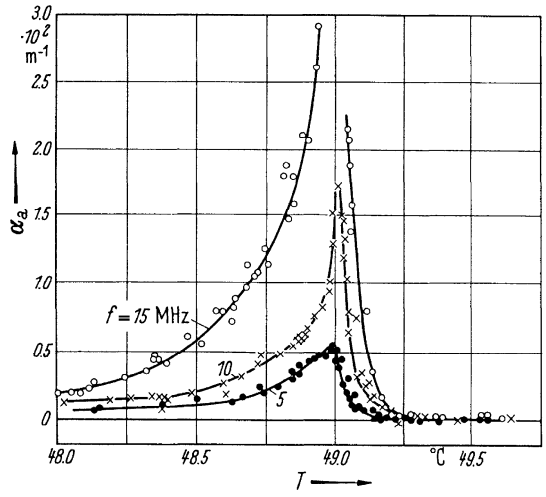

Fig. 60A-1-093. $(NH_2CH_2COOH)_3 \cdot H_2SO_4$ (TGS). α_a vs. T [65Min]. Parameter: f. Pulse method. Longitudinal waves along the c axis. α_a: ultrasonic absorption coefficient.

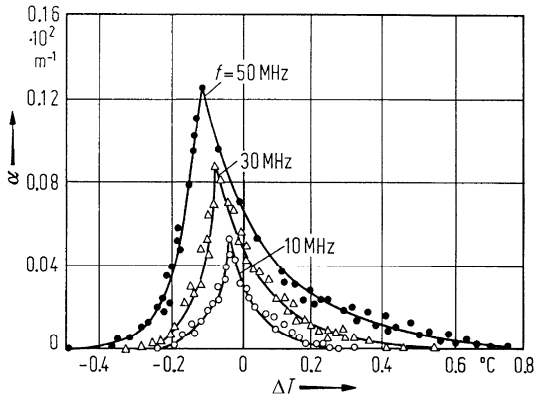

Fig. 60A-1-094. $(NH_2CH_2COOH)_3 \cdot H_2SO_4$ (TGS). α vs. ΔT [70Min]. Parameter: *f.* α: absorption coefficient of longitudinal ultrasonic waves propagating along the *b* axis. $\Delta T = T - \Theta_f$.

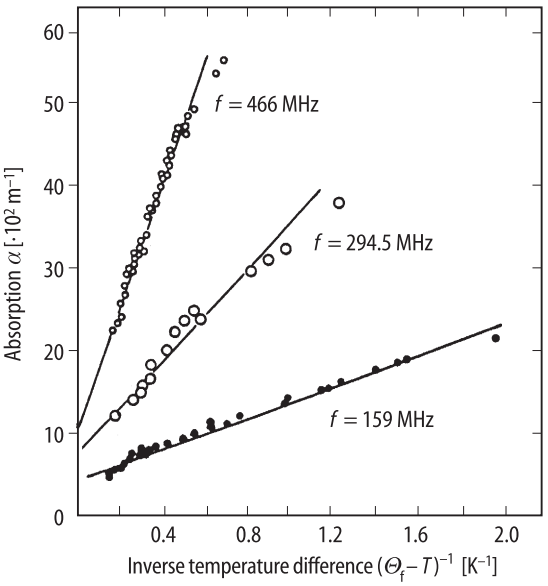

Fig. 60A-1-095. $(NH_2CH_2COOH)_3 \cdot H_2SO_4$ (TGS). α vs. $(\Theta_f - T)^{-1}$ [93Cha]. Parameter: *f.* α: absorption coefficient of longitudinal ultrasonic waves propagating along the *c* axis.

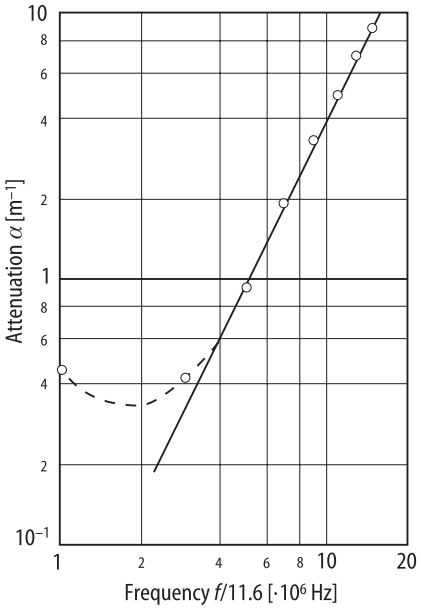

Fig. 60A-1-096. $(NH_2CH_2COOH)_3 \cdot H_2SO_4$ (TGS). α vs. f/ 11.6 [71Baj]. α: attenuation coefficient of quasi-longitudinal ultrasonic waves propagating along the *c* axis.

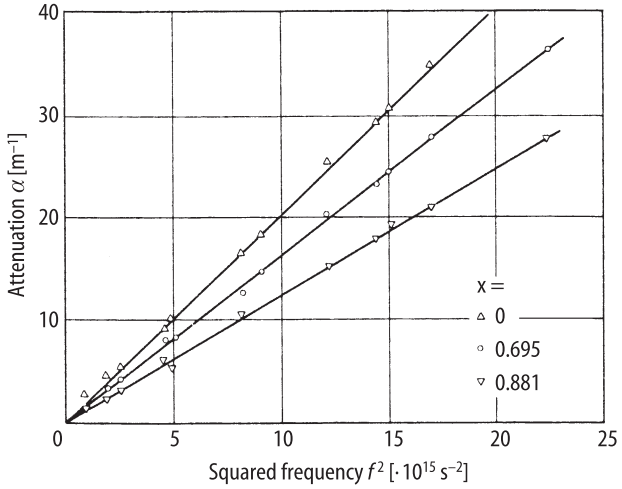

Fig. 60A-1-097. $[(NH_2CH_2COOH)_3 \cdot H_2SO_4]_{1-x}[(ND_2CH_2COOD)_3 \cdot D_2SO_4]_x$ ($TGS_{1-x}DTGS_x$). α vs. f^2 [80Baj]. Parameter: x. α: ultrasonic attenuation coefficient of the quasi-longitudinal wave propagating along the [001] direction. *f*: frequency. *T* = RT.

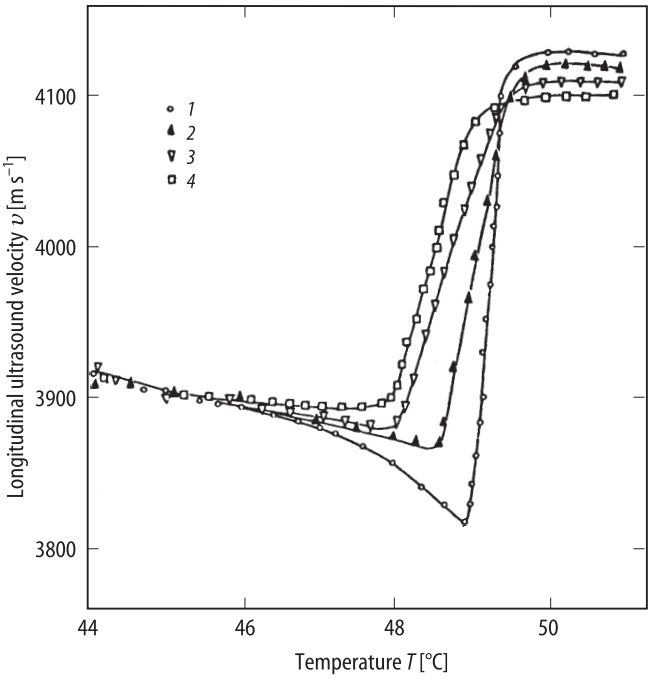

Fig. 60A-1-098. $(NH_2CH_2COOH)_3 \cdot H_2SO_4$ (TGS). v vs. T [85Vol]. v: longitudinal ultrasound velocity propagating along the c axis. f = 17.2 MHz. Parameter: X-ray dose. *1*: no irradiation, *2*: 1.3 MR, *3*: 2 MR, *4*: 4 MR. 1 R = $2.58 \cdot 10^{-4}$ C kg^{-1}.

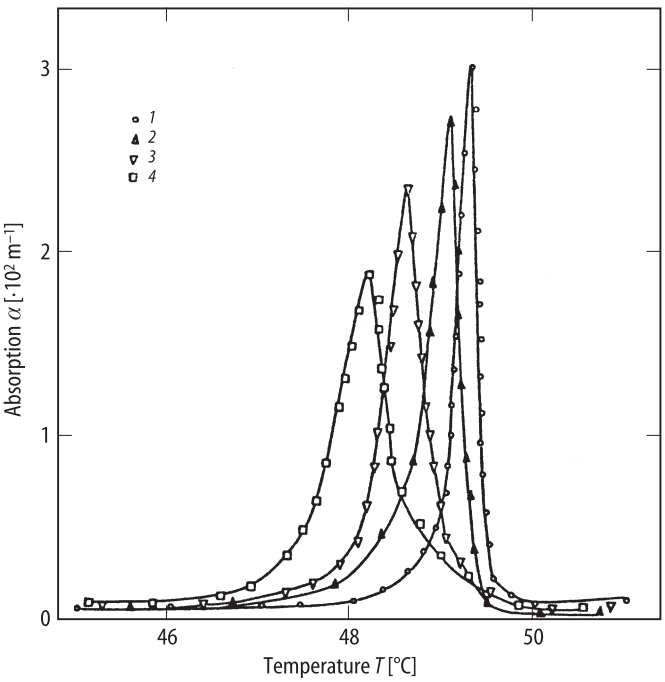

Fig. 60A-1-099. $(NH_2CH_2COOH)_3 \cdot H_2SO_4$ (TGS). α vs. T [85Vol]. α: absorption coefficient of longitudinal ultrasound propagating along the c axis. f = 17.2 MHz. Parameter: X-ray dose. *1*: no irradiation, *2*: 1.3 MR, *3*: 2 MR, *4*: 4 MR. 1 R = $2.58 \cdot 10^{-4}$ C kg^{-1}.

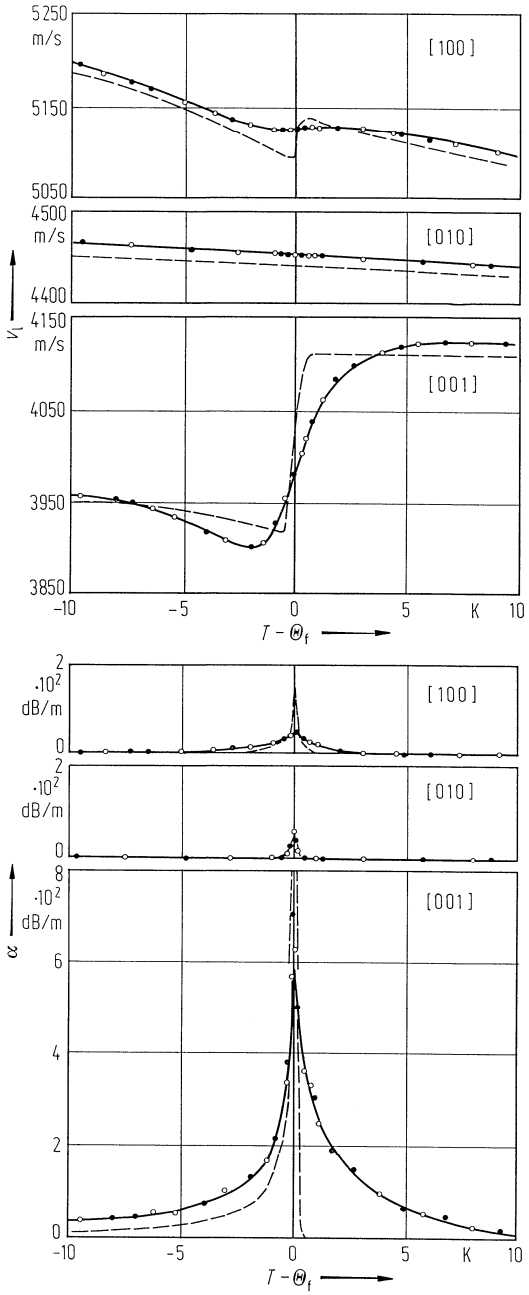

Fig. 60A-1-100. $(NH_2CH_2COOH)_3 \cdot H_2SO_4$ (TGS, $2 \cdot 10^{-4}$ % L-α-alanine doped). v_1, α vs. $T - \Theta_f$ [81Tyl2]. v_1, α: longitudinal sound velocity and attenuation coefficients along the [100], [010], and [001] directions. Broken lines represent the values for pure TGS crystals. f = 14.6 MHz. Full circles: aged crystal, heating; open circles: annealed crystals, cooling.

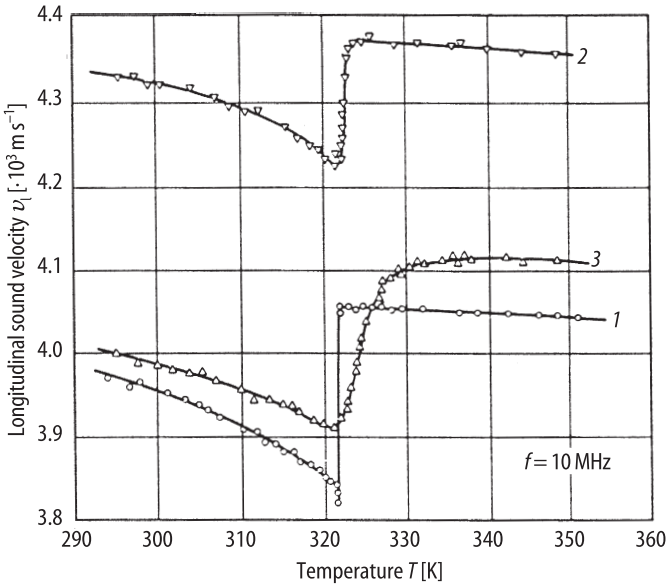

Fig. 60A-1-101. $(NH_2CH_2COOH)_3 \cdot H_2SO_4$ (TGS). v_l vs. T [82Str]. v_l: longitudinal sound velocity propagating along the [001] direction. *1*: pure crystal, *2*: Cr^{3+}-doped crystal (3 % in solution), *3*: α-alanine-doped crystal (10 % in solution). The specific heat data for the corresponding specimens are shown in Fig. 60A-1-069.

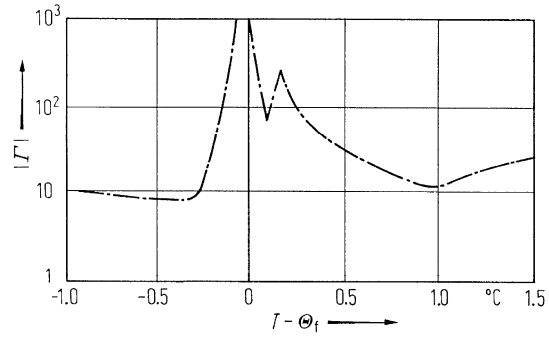

Fig. 60A-1-102. $(NH_2CH_2COOH)_3 \cdot H_2SO_4$ (TGS). $|\Gamma|$ vs. $T - \Theta_f$ [72Ser]. $|\Gamma|$: $|3 + c_{333}/c_{33}|$. c_{333}: third order elastic constant. $E = 0$.

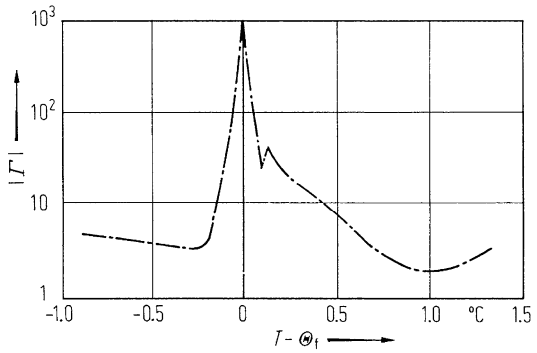

Fig. 60A-1-103. $(NH_2CH_2COOH)_3 \cdot H_2SO_4$ (TGS). $|\Gamma|$ vs. $T - \Theta_f$ [72Ser]. $|\Gamma|$: $|3 + c_{333}/c_{33}|$. c_{333}: third order elastic constant. $E_b = 1.5 \cdot 10^2$ kV m^{-1}; E_b: field along the ferroelectric *b* axis.

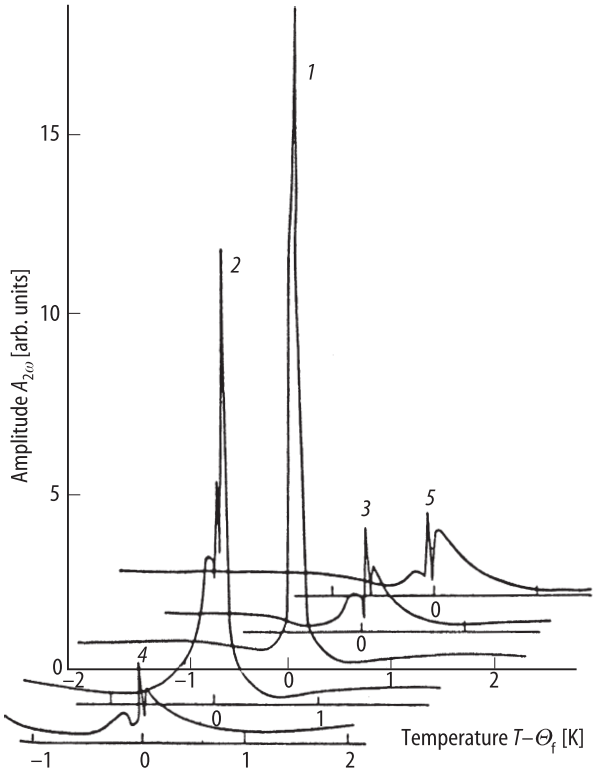

Fig. 60A-1-104. $(NH_2CH_2COOH)_3 \cdot H_2SO_4$ (TGS). $A_{2\omega}$ vs. $T - \Theta_f$ [88Kon2]. $A_{2\omega}$: amplitude of the second harmonic of the longitudinal ultrasound wave propagating along the *c* axis. $f \cong 10$ MHz. Parameter: external static electric field in the *b* axis. *1*: 0, *2*: –45 kV m^{-1}, *3*: +45 kV m^{-1}, *4*: –85 kV m^{-1}, *5*: +85 kV m^{-1}.

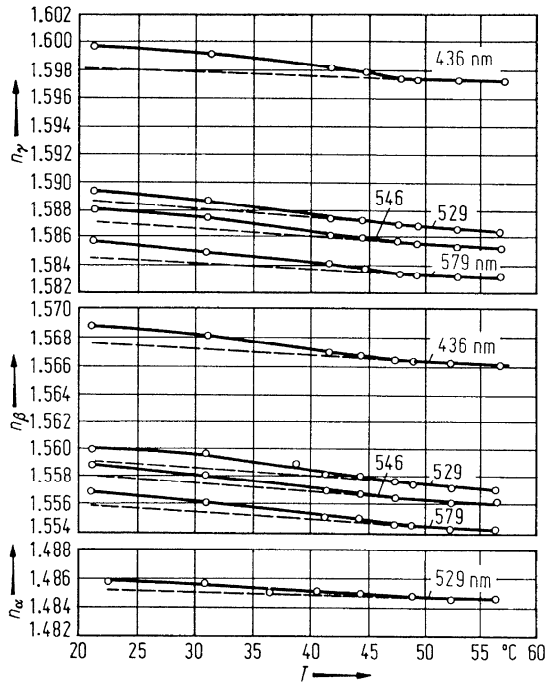

Fig. 60A-1-105. $(NH_2CH_2COOH)_3 \cdot H_2SO_4$ (TGS). n_α, n_β, n_γ vs. T [68Lom]. Parameter: λ. $n_\alpha = n_b$.

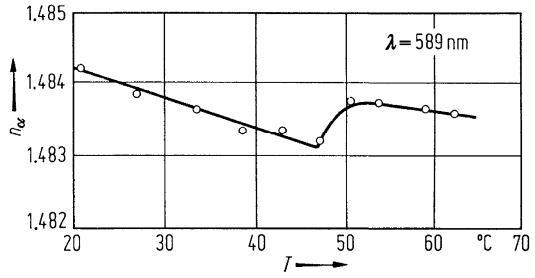

Fig. 60A-1-106. $(NH_2CH_2COOH)_3 \cdot H_2SO_4$ (TGS). n_α vs. T [68Iwa]. $n_\alpha = n_b$.

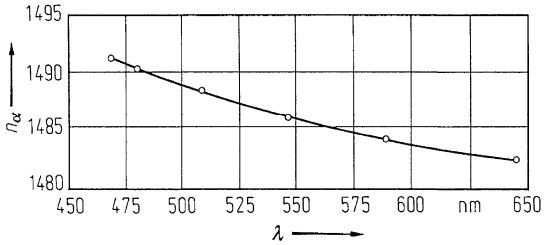

Fig. 60A-1-107. $(NH_2CH_2COOH)_3 \cdot H_2SO_4$ (TGS). n_α vs. λ at RT [68Iwa]. $n_\alpha = n_b$.

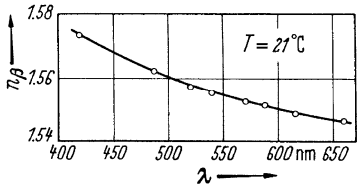

Fig. 60A-1-108. $(NH_2CH_2COOH)_3 \cdot H_2SO_4$ (TGS). n_β vs. λ [66Iva1].

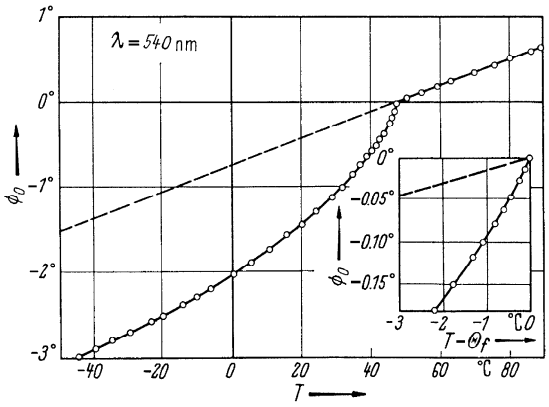

Fig. 60A-1-109. $(NH_2CH_2COOH)_3 \cdot H_2SO_4$ (TGS). ϕ_o vs. T [66Iva1]. ϕ_o: rotation angle of the optical indicatrix around the b axis.

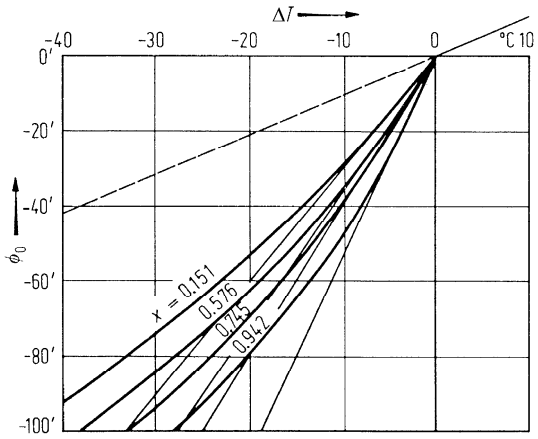

Fig. 60A-1-110. $[(NH_2CH_2COOH)_3 \cdot H_2SO_4]_{1-x}[(ND_2CH_2COOD)_3 \cdot D_2SO_4]_x$ ($TGS_{1-x}DTGS_x$). ϕ_o vs. ΔT [68Bre1]. ϕ_o: rotation angle of the optical indicatrix around the b axis. Parameter: x. $\Delta T = T - \Theta_{II-I}$.

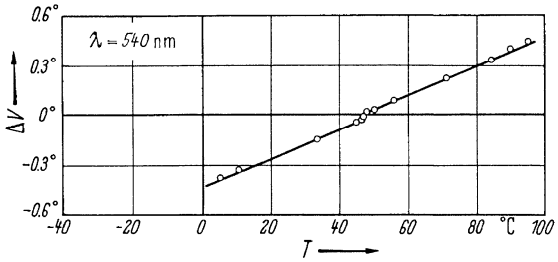

Fig. 60A-1-111. $(NH_2CH_2COOH)_3 \cdot H_2SO_4$ (TGS). ΔV vs. T [66Iva2]. $\Delta V = V(T) - V(\Theta)$. $2V(T)$: optical axial angle at T [°C].

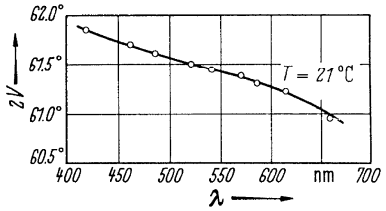

Fig. 60A-1-112. $(NH_2CH_2COOH)_3 \cdot H_2SO_4$ (TGS). $2V$ vs. λ [66Iva1]. $2V$: optical axial angle.

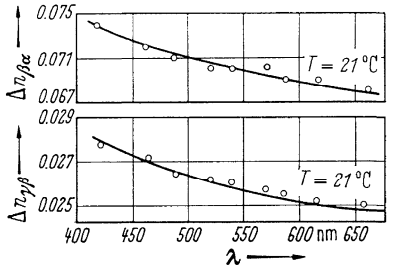

Fig. 60A-1-113. $(NH_2CH_2COOH)_3 \cdot H_2SO_4$ (TGS). $\Delta n_{\gamma\beta}$, $\Delta n_{\beta\alpha}$ vs. λ [66Iva1]. $\Delta n_{\gamma\beta} = n_\gamma - n_\beta$, $\Delta n_{\beta\alpha} = n_\beta - n_\alpha$.

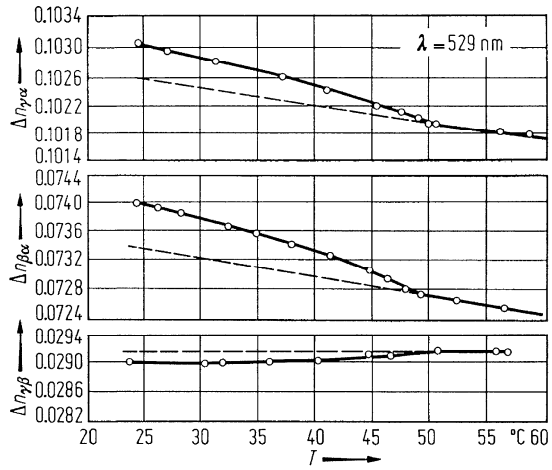

Fig. 60A-1-114. $(NH_2CH_2COOH)_3 \cdot H_2SO_4$ (TGS). $\Delta n_{\gamma\beta}$, $\Delta n_{\beta\alpha}$, $\Delta n_{\gamma\alpha}$ vs. T [68Lom]. $\Delta n_{\lambda\mu} = n_\lambda - n_\mu$.

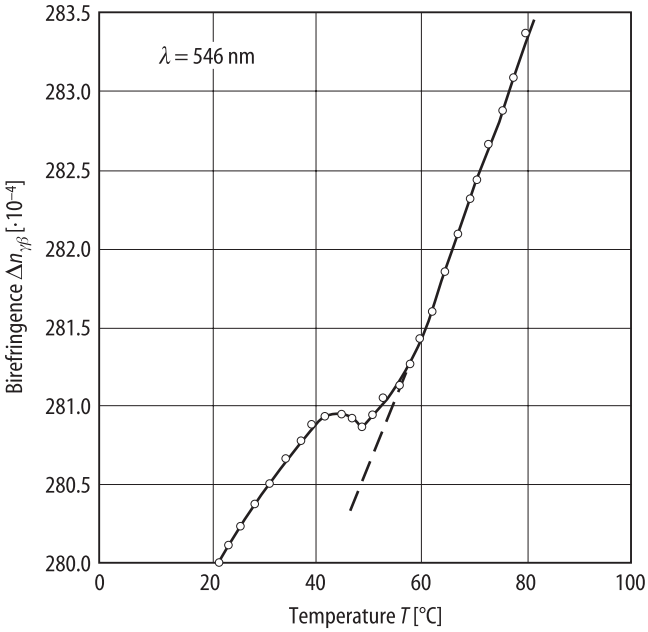

Fig. 60A-1-115. $(NH_2CH_2COOH)_3 \cdot H_2SO_4$ (TGS). $\Delta n_{\gamma\beta}$ vs. T [83Kus]. $\Delta n_{\gamma\beta} = n_\gamma - n_\beta$.

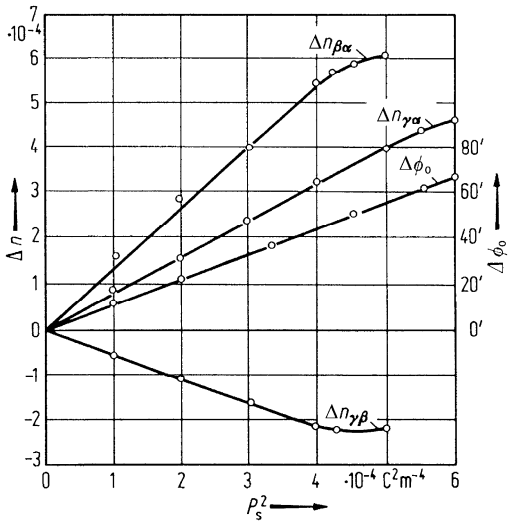

Fig. 60A-1-116. $(NH_2CH_2COOH)_3 \cdot H_2SO_4$ (TGS). Δn, $\Delta\phi_o$ vs. P_s^2 [68Lom]. $\Delta n_{\lambda\mu} = n_\lambda - n_\mu$. $\Delta\phi_o$: change in rotation angle of the optical indicatrix around the *b* axis.

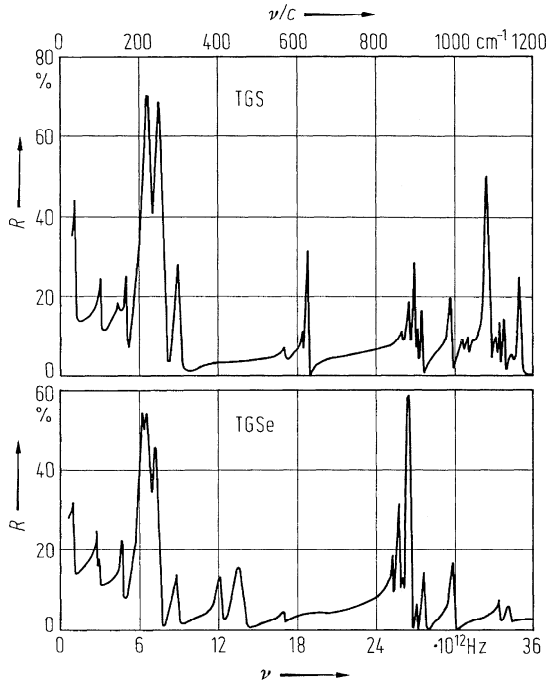

Fig. 60A-1-117. $(NH_2CH_2COOH)_3 \cdot H_2SO_4$ (TGS), $(NH_2CH_2COOH)_3 \cdot H_2SeO_4$ (TGSe). *R* vs. ν [77Win]. *R*: infrared reflectivity at 80 K. Polarization of the incident radiation is parallel to the *b* axis.

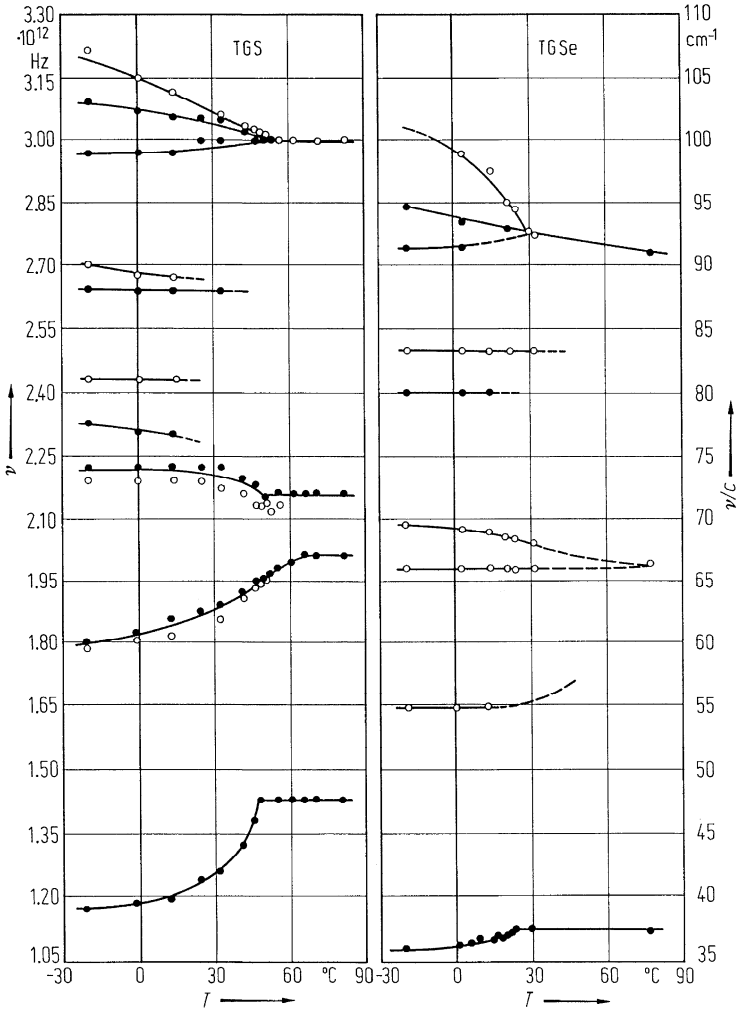

Fig. 60A-1-118. $(NH_2CH_2COOH)_3 \cdot H_2SO_4$ (TGS), $(NH_2CH_2COOH)_3 \cdot H_2SeO_4$ (TGSe). ν vs. T [77Win]. ν: frequency of the lattice vibration modes. Open circles: B-symmetry mode by IR spectra. Full circles: A-symmetry mode by Raman spectra.

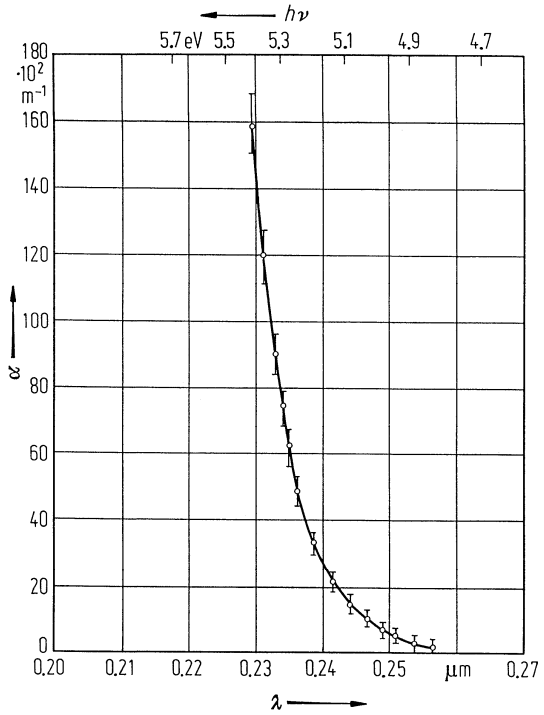

Fig. 60A-1-119. $(NH_2CH_2COOH)_3 \cdot H_2SO_4$ (TGS). α vs. λ [85Aba]. α: optical absorption coefficient along the *b* axis.

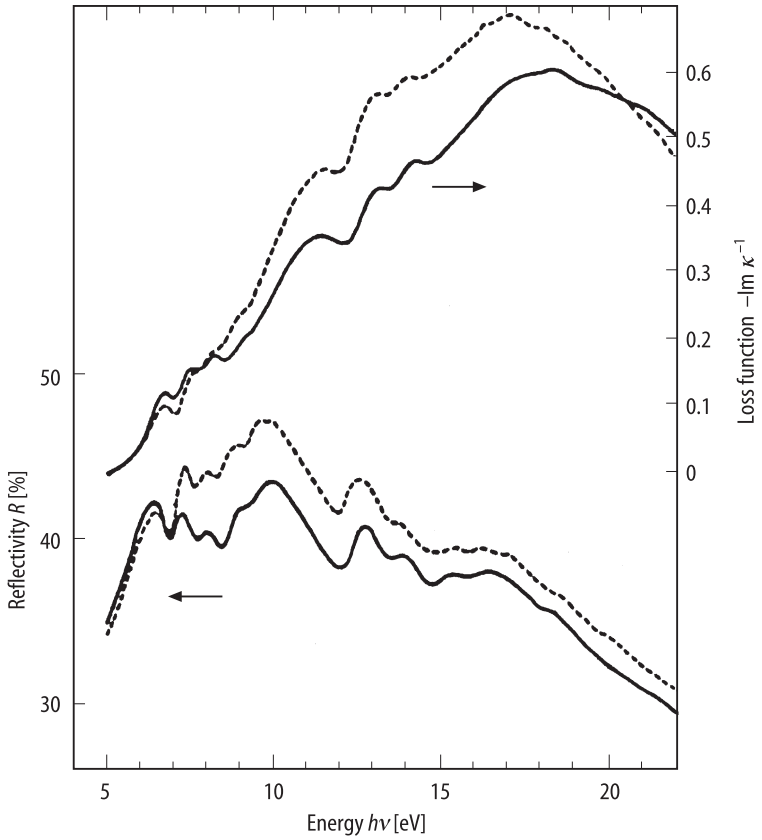

Fig. 60A-1-120. $(NH_2CH_2COOH)_3 \cdot H_2SO_4$ (TGS). R, –Im κ^{-1} vs. $h\nu$ [78Rom]. R: reflectivity. –Im κ^{-1}: loss function. Parameter: T. Solid curve: 20 °C, dotted curve: 80 °C.

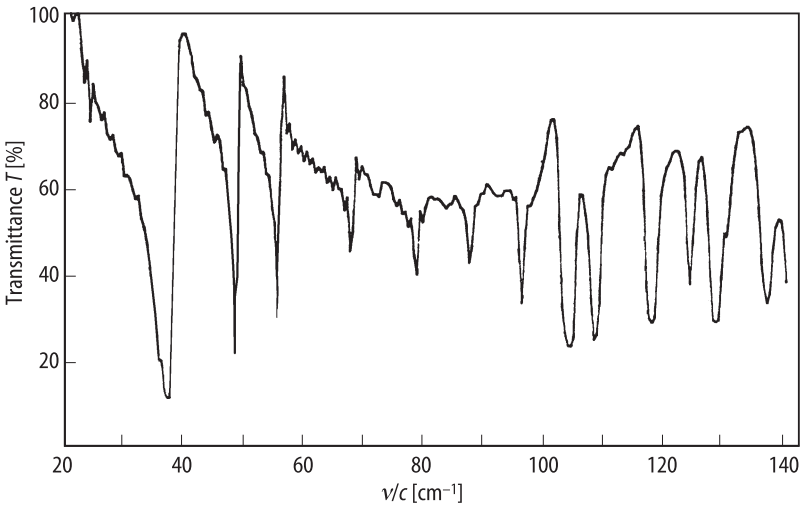

Fig. 60A-1-121. $(NH_2CH_2COOH)_3 \cdot H_2SO_4$ (TGS). T vs. ν/c [86Ger]. T: transmittance for far-infrared radiation at 4 K. Polarization of the incident radiation is parallel to the b axis. Sample: bc plate. Sample thickness: 13 µm.

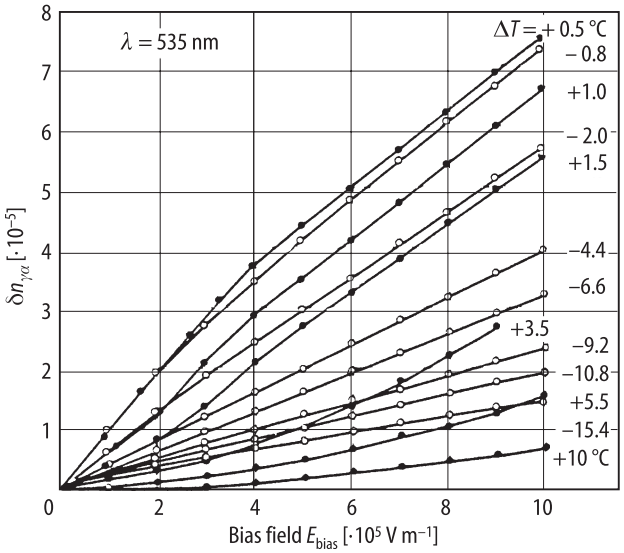

Fig. 60A-1-122. $(NH_2CH_2COOH)_3 \cdot H_2SO_4$ (TGS). $\delta n_{\gamma\alpha}$ vs. E_{bias} [67Son1]. $\delta n_{\gamma\alpha} = \delta(n_\gamma - n_\alpha)$. $E_{bias} \parallel c$. Parameter: $\Delta T = T - \Theta_f$.

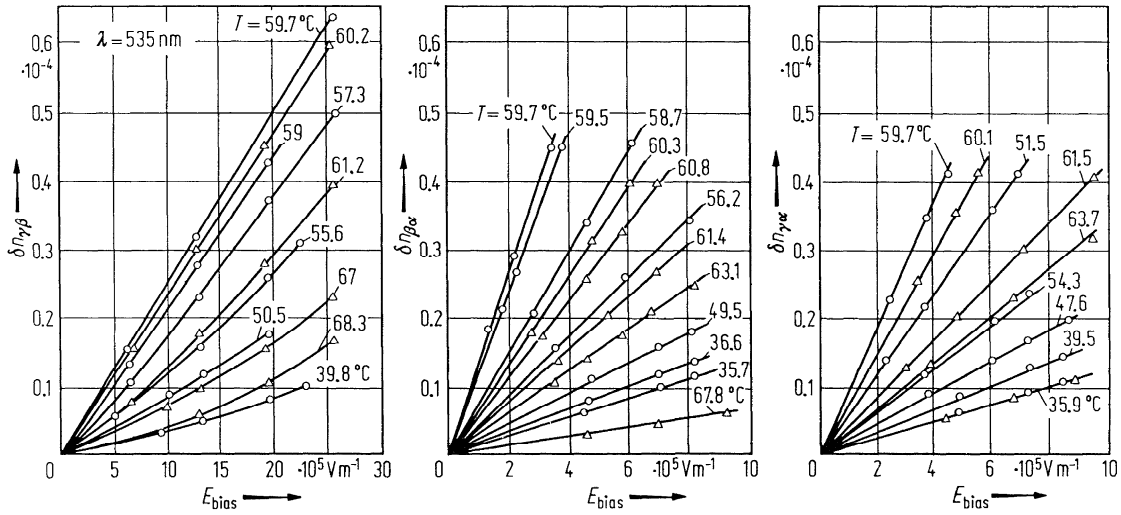

Fig. 60A-1-123. Deuterated triglycine sulfate (DTGS). $\delta n_{\gamma\beta}$, $\delta n_{\beta\alpha}$, $\delta n_{\gamma\alpha}$ vs. E_{bias} [67Son2]. Parameter: T. $\delta n_{\lambda\mu} = \delta(n_\lambda - n_\mu)$. $E_{bias} \parallel b$.

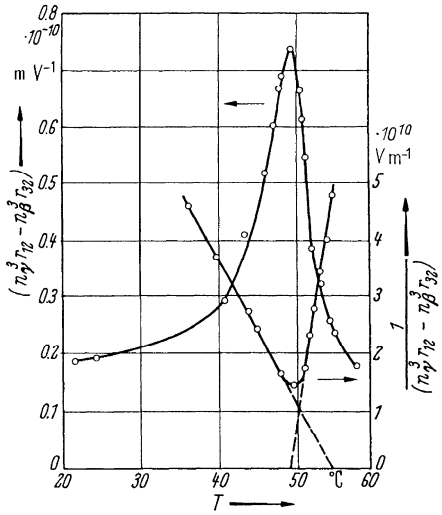

Fig. 60A-1-124. $(NH_2CH_2COOH)_3 \cdot H_2SO_4$ (TGS). $n_\gamma^3 r_{12} - n_\beta^3 r_{32}$, $(n_\gamma^3 r_{12} - n_\beta^3 r_{32})^{-1}$ vs. T [66Vas].

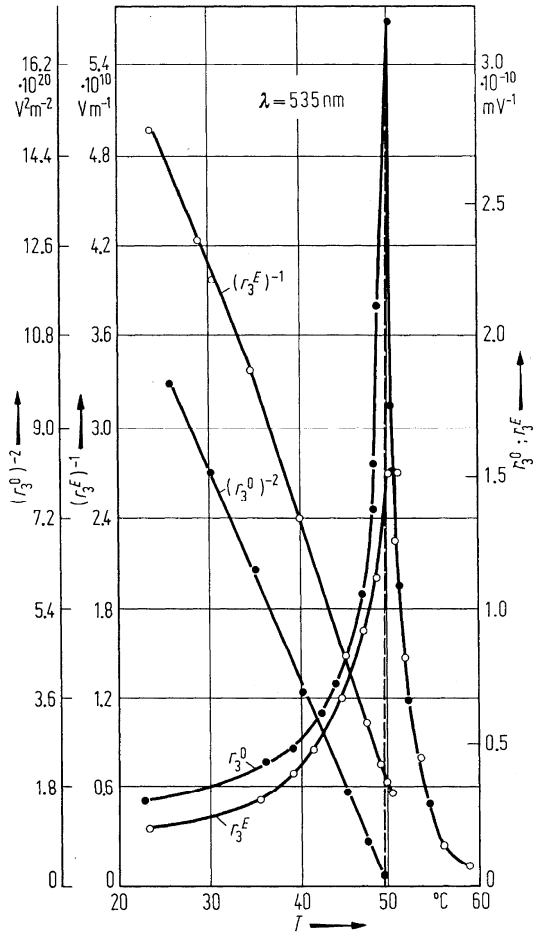

Fig. 60A-1-125. $(NH_2CH_2COOH)_3 \cdot H_2SO_4$ (TGS). r_3^0, r_3^E, $(r_3^0)^{-2}$, $(r_3^E)^{-1}$ vs. T [67Son1]. $r_3 = n_\gamma^3 r_{12} - n_\alpha^3 r_{22} \cdot r_3^0$: measured by weak fields. r_3^E : measured by strong fields.

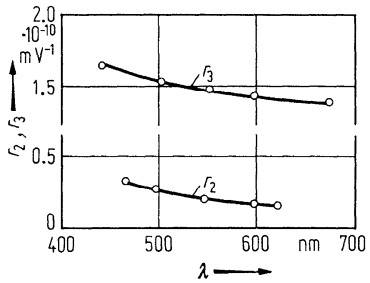

Fig. 60A-1-126. Deuterated triglycine sulfate (DTGS). r_2, r_3 vs. λ [67Son2]. $r_2 = n_\gamma^3 r_{12} - n_\beta^3 r_{32}$, $r_3 = n_\gamma^3 r_{12} - n_\alpha^3 r_{22}$.

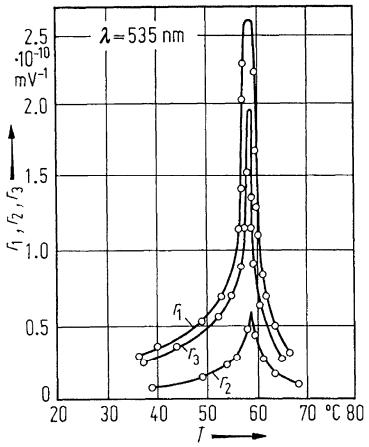

Fig. 60A-1-127. Deuterated triglycine sulfate (DTGS). r_1, r_2, r_3 vs. T [67Son2]. $r_1 = n_\beta^3 r_{32} - n_\alpha^3 r_{22}$, $r_2 = n_\gamma^3 r_{12} - n_\beta^3 r_{32}$, $r_3 = n_\gamma^3 r_{12} - n_\alpha^3 r_{22}$.

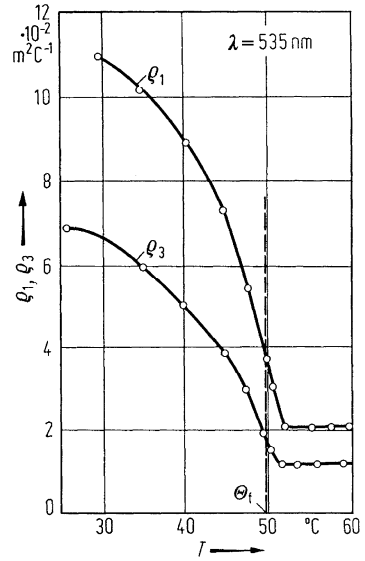

Fig. 60A-1-128. $(NH_2CH_2COOH)_3 \cdot H_2SO_4$ (TGS). ρ_1, ρ_3 vs. T [67Son1]. $\rho_1 = n_\beta^3 \rho_{32} - n_\alpha^3 \rho_{22}$, $\rho_3 = n_\gamma^3 \rho_{12} - n_\alpha^3 \rho_{22}$.

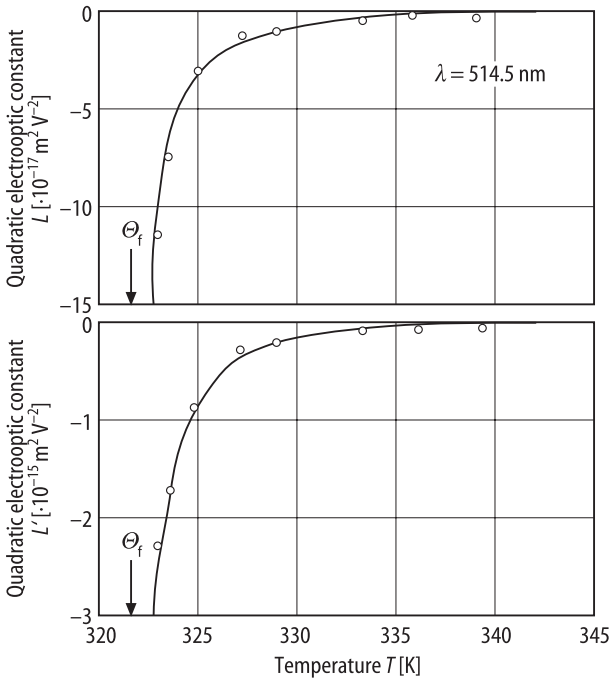

Fig. 60A-1-129. $(NH_2CH_2COOH)_3 \cdot H_2SO_4$ (TGS). L, L' vs. T [83Kob]. L, L': quadratic electrooptic constants for $\boldsymbol{E}$, $L = -(L_{32}n_3^3 - L_{12}n_1^3)/2$, $L' = -(n_1 n_3)^2 (n_3^2 - n_1^2)^{-1} L_{52}$.

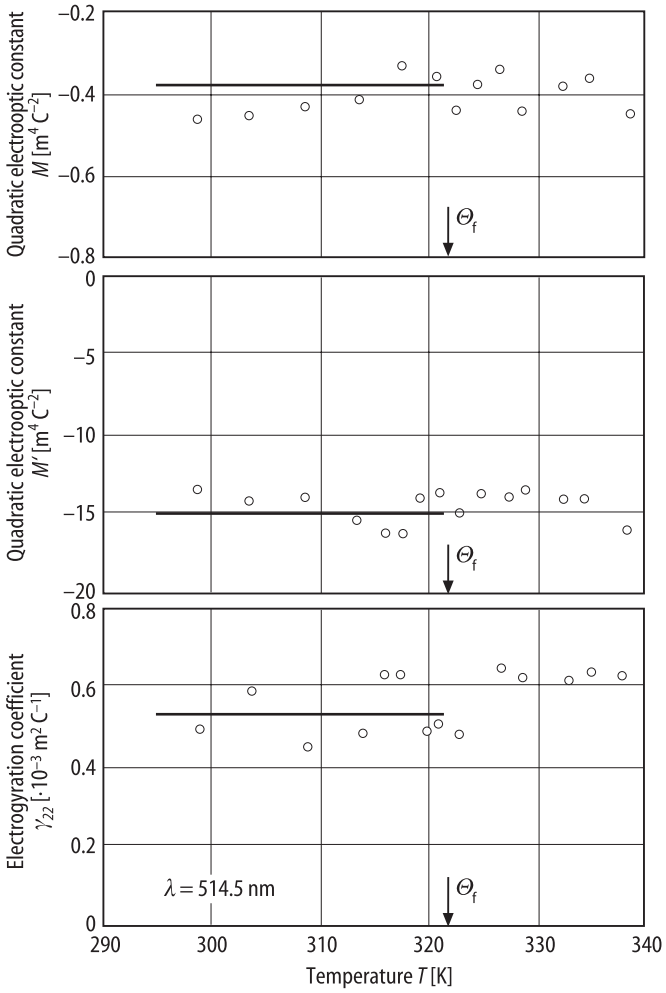

Fig. 60A-1-130. $(NH_2CH_2COOH)_3 \cdot H_2SO_4$ (TGS). M, M', γ_{22} vs. T [83Kob]. M, M': quadratic electrooptic constants for $\boldsymbol{P}$, $M = -(M_{32}n_3^3 - M_{12}n_1^3)/2$, $M' = -(n_1 n_3)^2 (n_3^2 - n_1^2)^{-1} M_{52}$. γ_{22}: electrogyration coefficient for $\boldsymbol{P}$, defined by $g_{22} = \gamma_{22} P_2$.

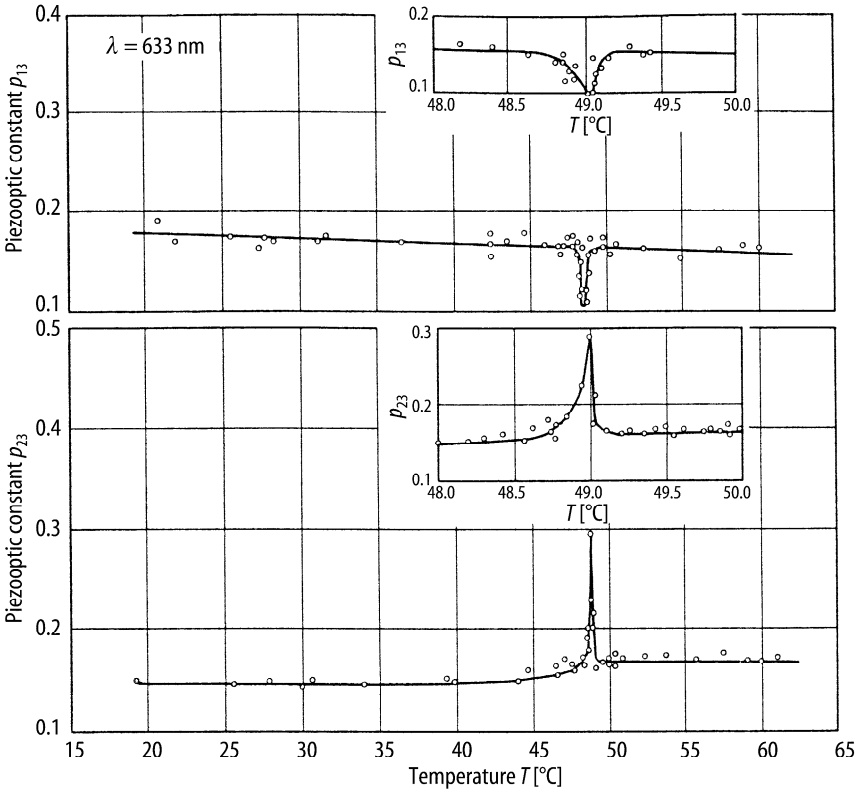

Fig. 60A-1-131. $(NH_2CH_2COOH)_3 \cdot H_2SO_4$ (TGS). p_{13}, p_{23} vs. T [83Str]. $p_{\lambda\mu}$: piezooptic constant.

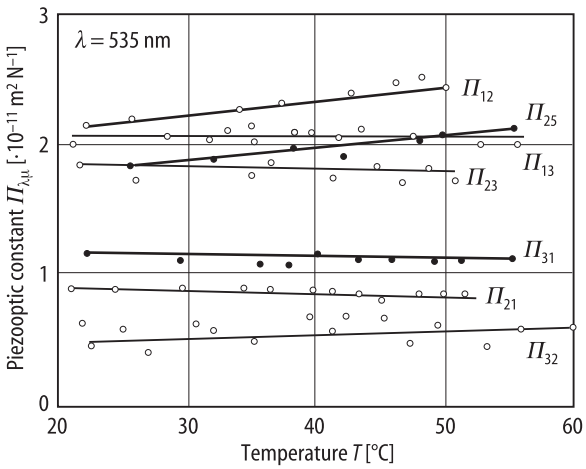

Fig. 60A-1-132. $(NH_2CH_2COOH)_3 \cdot H_2SO_4$ (TGS). $\Pi_{\lambda\mu}$ vs. T [67Vas].

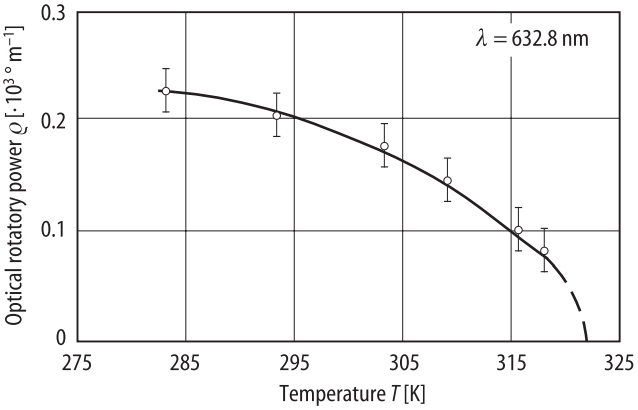

Fig. 60A-1-133. $(NH_2CH_2COOH)_3 \cdot H_2SO_4$ (TGS). ρ vs. T [81Hab]. ρ: optical rotatory power.

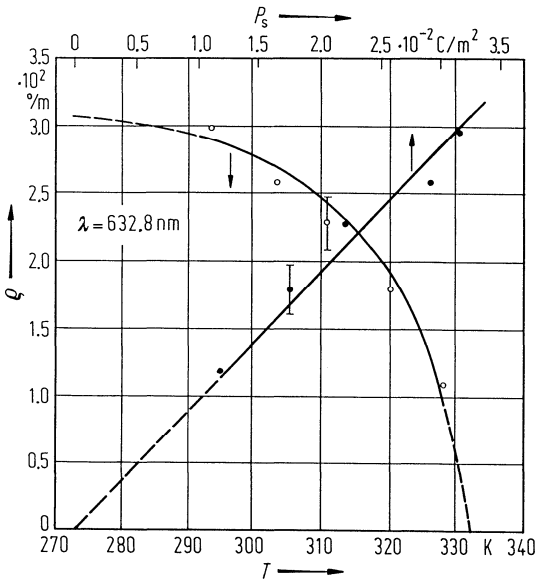

Fig. 60A-1-134. Deuterated triglycine sulfate (DTGS). ρ vs. T, P_s [82Kor]. Open circles: ρ vs. T, full circles: ρ vs. P_s. Degree of deuteration is about 90 %.

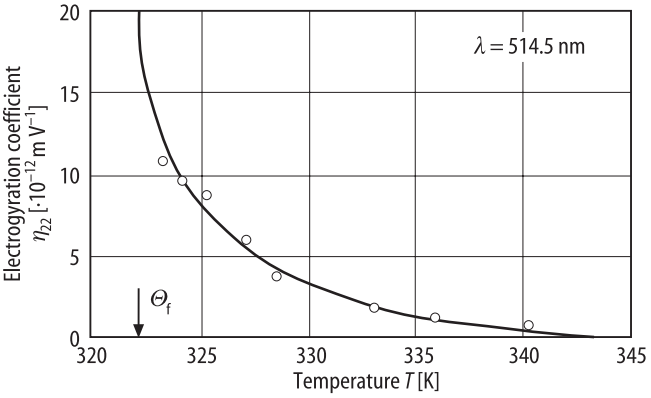

Fig. 60A-1-135. $(NH_2CH_2COOH)_3 \cdot H_2SO_4$ (TGS). η_{22} vs. T [83Kob]. η_{22}: electrogyration coefficient for $\boldsymbol{E}$, defined by $g_{22} = \eta_{22} E_2$.

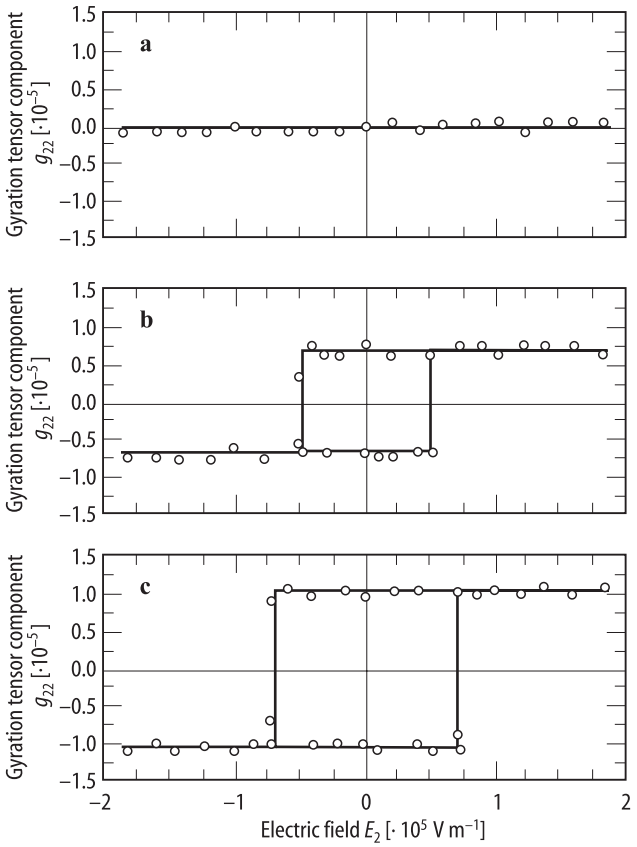

Fig. 60A-1-136. $(NH_2CH_2COOH)_3 \cdot H_2SO_4$ (TGS). g_{22} vs. E_2 [91Kob]. g_{22}: gyration tensor component. (**a**) T = 57.0 °C, (**b**) 43.0 °C, (**c**) 32.0 °C.

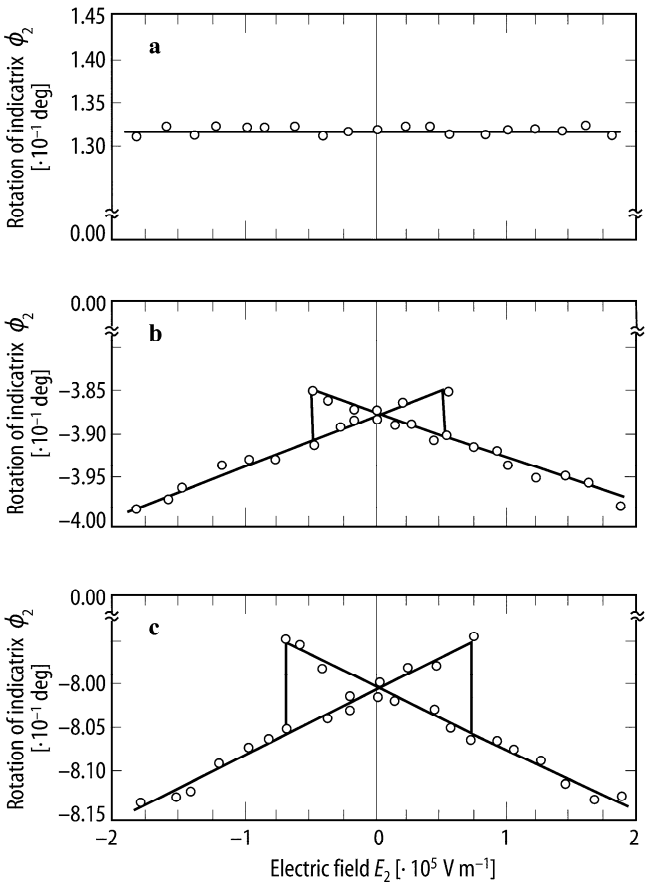

Fig. 60A-1-137. $(NH_2CH_2COOH)_3 \cdot H_2SO_4$ (TGS). ϕ_2 vs. E_2 [91Kob]. ϕ_2: rotation angle of optical indicatrix around the *b* axis. (**a**) $T = 57.0$ °C, (**b**) 43.0 °C, (**c**) 32.0 °C.

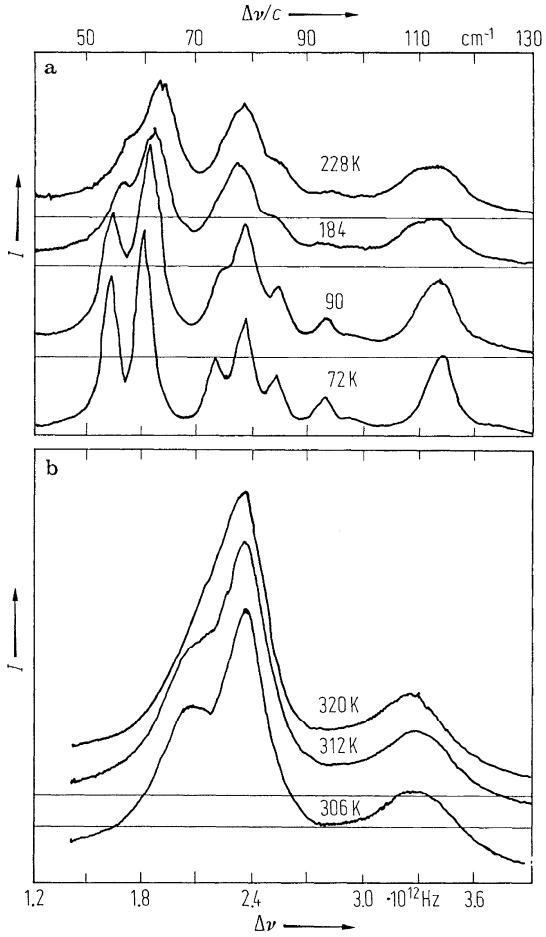

Fig. 60A-1-138. $(NH_2CH_2COOH)_3 \cdot H_2SO_4$ (TGS). I vs. $\Delta\nu$ [76Cer]. I: Raman scattering intensity for the scattering geometry $X(ZX)Z$. Parameter: T. (**a**) $T <$ RT, (**b**) $T >$ RT.

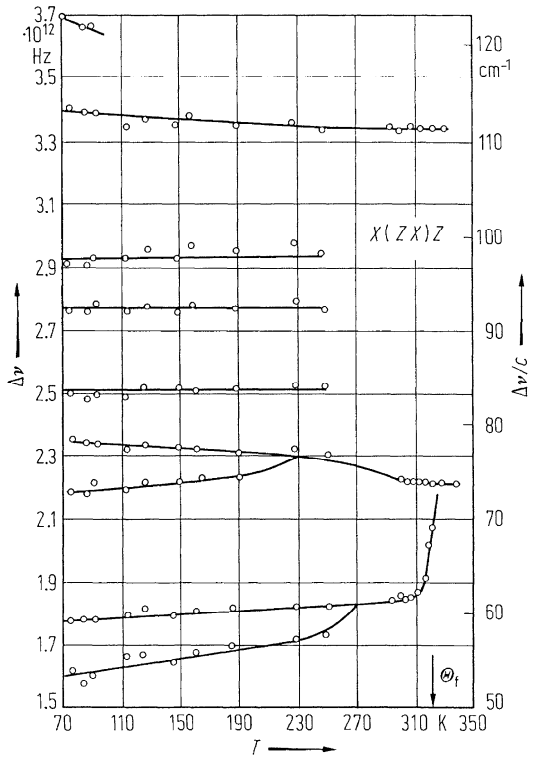

Fig. 60A-1-139. $(NH_2CH_2COOH)_3 \cdot H_2SO_4$ (TGS). $\Delta\nu$ vs. T [76Cer]. $\Delta\nu$: Raman frequency shift in the scattering geometry of $X(ZX)Z$.

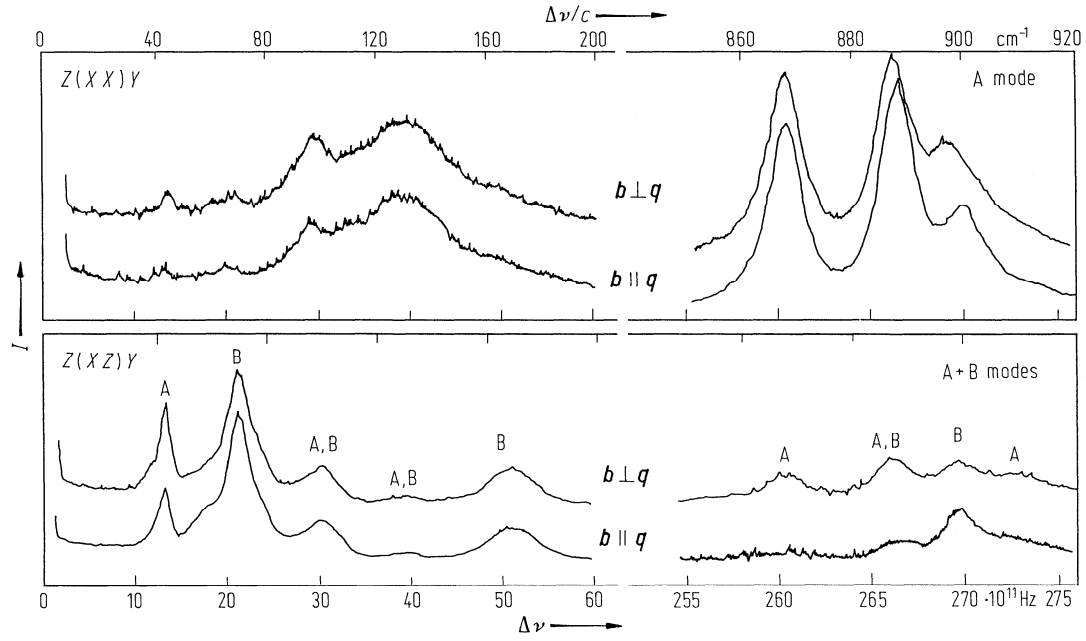

Fig. 60A-1-140. $(NH_2CH_2COOH)_3 \cdot H_2SO_4$ (TGS). I vs. $\Delta\nu$ [87Tas]. I: Raman intensity, $\Delta\nu$: Raman shift. $T = 300$ K. The Cartesian coordinate is defined as $Y \parallel \boldsymbol{q}_s$, $Z \parallel \boldsymbol{q}_i$, and $X \perp (Y, Z)$, where $\boldsymbol{q}_i$ and $\boldsymbol{q}_s$ are the wavenumber vectors for the incident and scattering phonons, respectively. $X \parallel c$ axis.

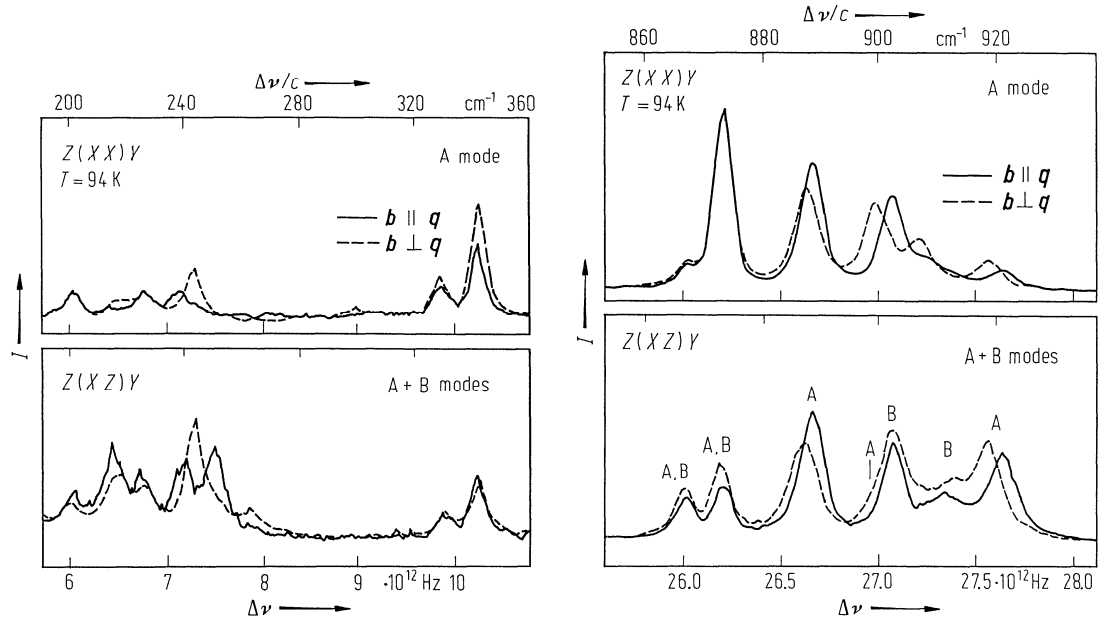

Fig. 60A-1-141. $(NH_2CH_2COOH)_3 \cdot H_2SO_4$ (TGS). I vs. $\Delta\nu$ [87Tas]. I: Raman intensity, $\Delta\nu$: Raman shift. $T = 94$ K. For the scattering geometry, see Fig. 60A-1-140.

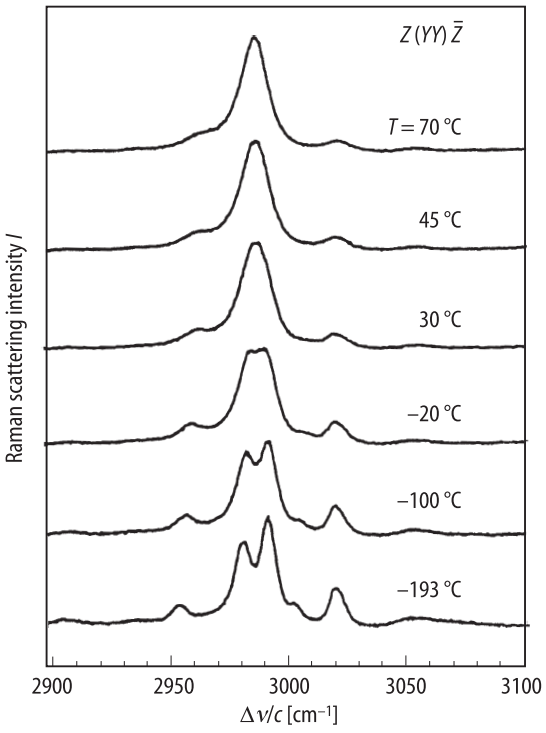

Fig. 60A-1-142. $(NH_2CH_2COOH)_3 \cdot H_2SO_4$ (TGS). I vs. $\Delta\nu/c$ [96Sak]. I: Raman scattering intensity in the $Z(YY)\bar{Z}$ geometry. $\Delta\nu$: frequency shift. Parameter: T. The mode at about 2990 cm^{-1} is assigned to a CH_2 symmetric stretching vibration in the glycine molecule.

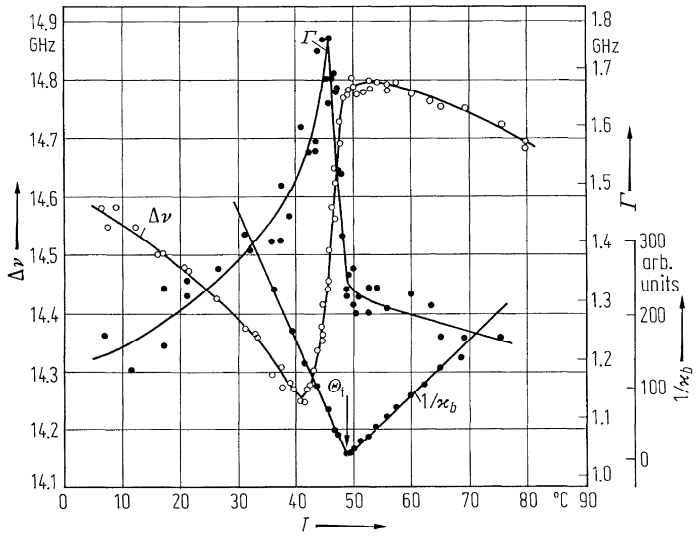

Fig. 60A-1-143. $(NH_2CH_2COOH)_3 \cdot H_2SO_4$ (TGS). $\Delta\nu$, Γ, κ_b^{-1} vs. T [76Yag]. $\Delta\nu$: frequency shift of Brillouin scattering of c_{33} mode. Γ: full line width at half maximum.

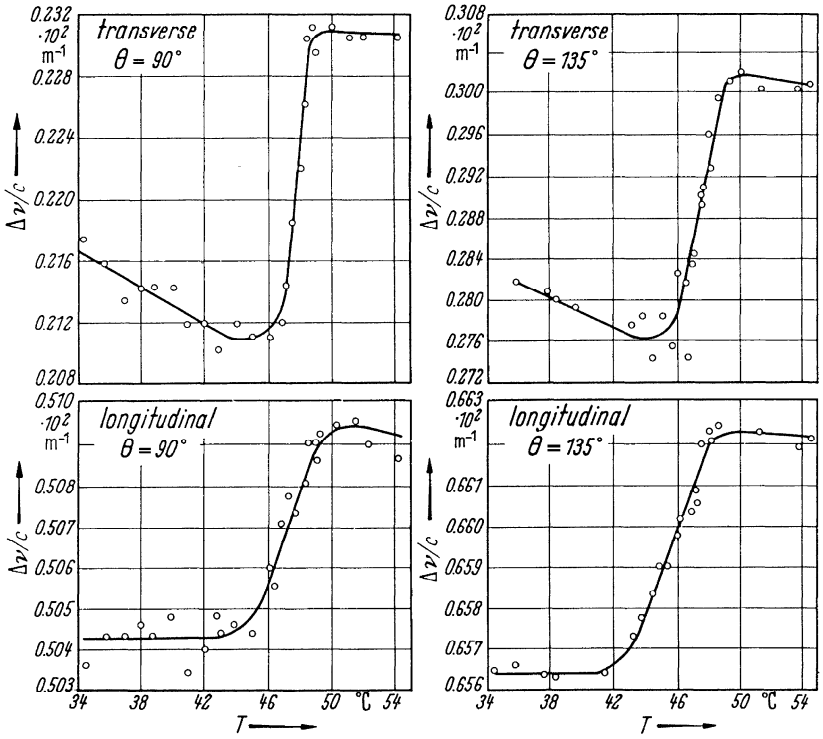

Fig. 60A-1-144. $(NH_2CH_2COOH)_3 \cdot H_2SO_4$ (TGS). $\Delta\nu/c$ vs. T [66Gam]. $\Delta\nu/c$: Brillouin shift from visible He–Ne laser frequency. θ: scattering angle.

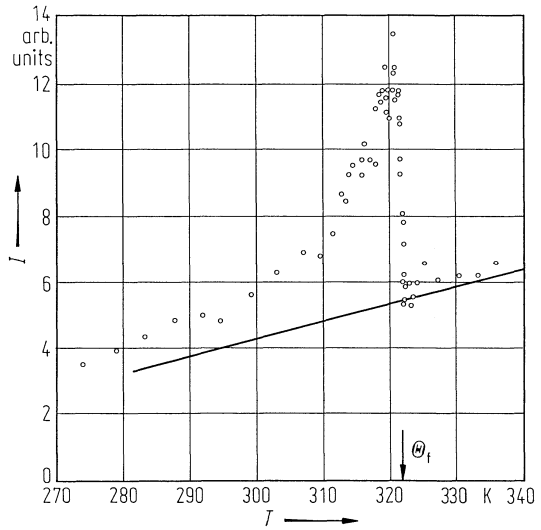

Fig. 60A-1-145. $(NH_2CH_2COOH)_3 \cdot H_2SO_4$ (TGS). I vs. T [80Miy]. I: height of a central peak. $\boldsymbol{q} \parallel c$. Full line represents the background elastic scattering.

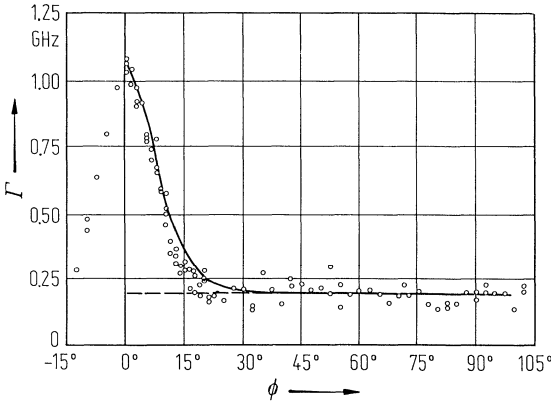

Fig. 60A-1-146. $(NH_2CH_2COOH)_3 \cdot H_2SO_4$ (TGS). Γ vs. ϕ [83Tsu]. Γ: full width of Brillouin spectrum of a quasi-longitudinal phonon propagating in the bc plane. ϕ: angle between $\boldsymbol{q}$ and c axis in the bc plane. T = 44.94 °C. Full line shows a calculated one and dashed line background one. λ = 488 nm.

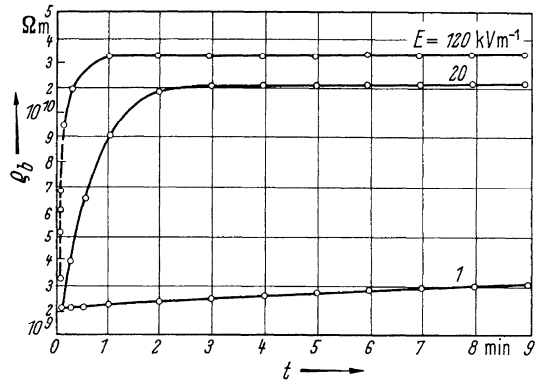

Fig. 60A-1-147. $(NH_2CH_2COOH)_3 \cdot H_2SO_4$ (TGS). ρ_b vs. t [60Gur]. Parameter: E. Crystal size 10 × 10 × 0.5 mm^3. The low initial resistances are caused by changes in the domain structure.

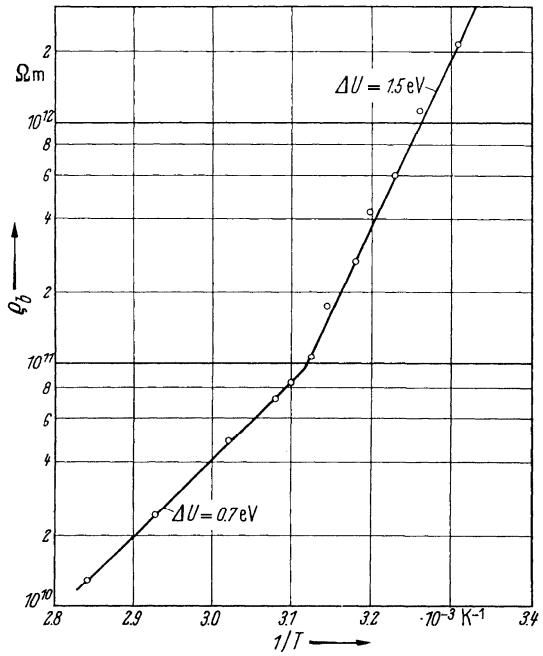

Fig. 60A-1-148. $(NH_2CH_2COOH)_3 \cdot H_2SO_4$ (TGS). ρ_b vs. $1/T$ [61Toy]. Activation energies are presented in the figure.

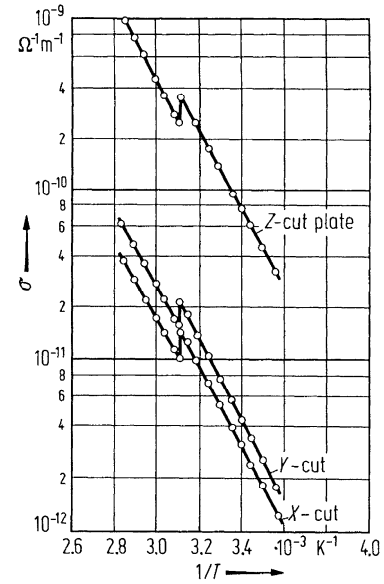

Fig. 60A-1-149. $(NH_2CH_2COOH)_3 \cdot H_2SO_4$ (TGS). σ vs. $1/T$ for *X*-cut, *Y*-cut, and *Z*-cut single crystals [69Gur]. Three-electrodes system with shielding electrode was adopted. $E = 120$ kV m^{-1}. Thickness of samples were 1 mm.

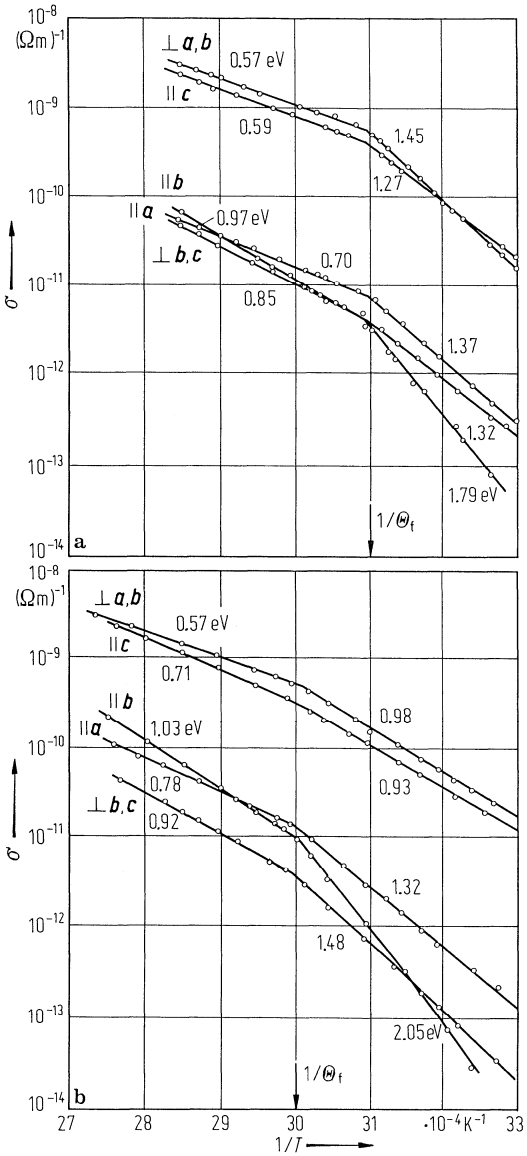

Fig. 60A-1-150. $(NH_2CH_2COOH)_3 \cdot H_2SO_4$ (TGS), deuterated triglycine sulfate (DTGS). σ vs. $1/T$ [81Pol]. (**a**) for TGS, (**b**) for DTGS. $E = 10^6$ V m^{-1}. The activation energies are presented in the figure.

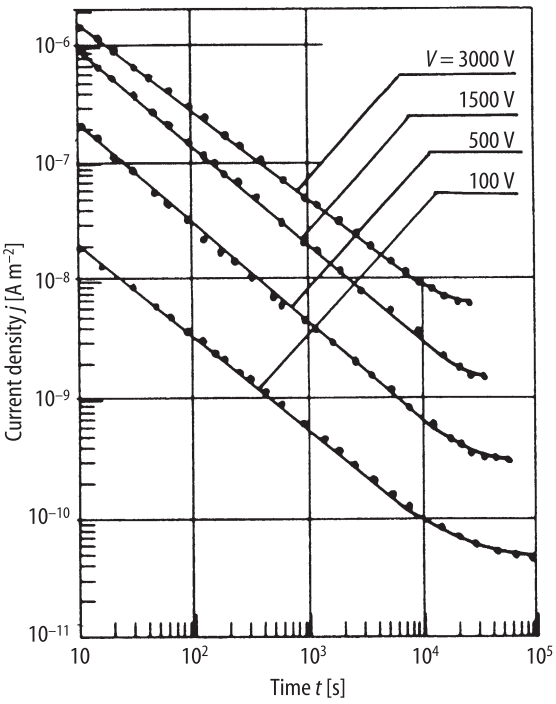

Fig. 60A-1-151. $(NH_2CH_2COOH)_3 \cdot H_2SO_4$ (TGS). j vs. t [94Osa]. j: current density of b plate. Sample thickness: 1.5 mm. $T = -193$ °C. Parameter: V.

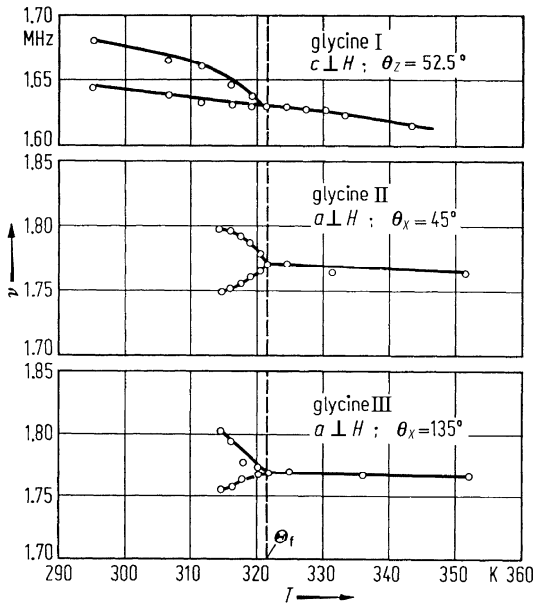

Fig. 60A-1-152. $(NH_2CH_2COOH)_3 \cdot H_2SO_4$ (TGS). ν vs. T [71Bli]. ν: double NMR ^1H–^{14}N, ^{14}N, transition frequency. θ_X: $\boldsymbol{H}$ direction measured from the Z axis in the Y–Z plane. θ_Z: $\boldsymbol{H}$ direction measured from the Y axis in the X–Y plane. The orthogonal axial system of Fig. 60A-1-003 is adopted.

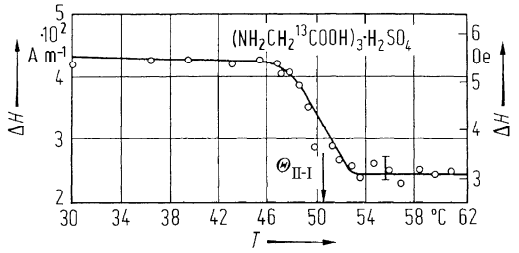

Fig. 60A-1-153. $(NH_2CH_2COOH)_3 \cdot H_2SO_4$ (TGS). ΔH vs. T [76Mul1]. ΔH: NMR line width of ^{13}C.

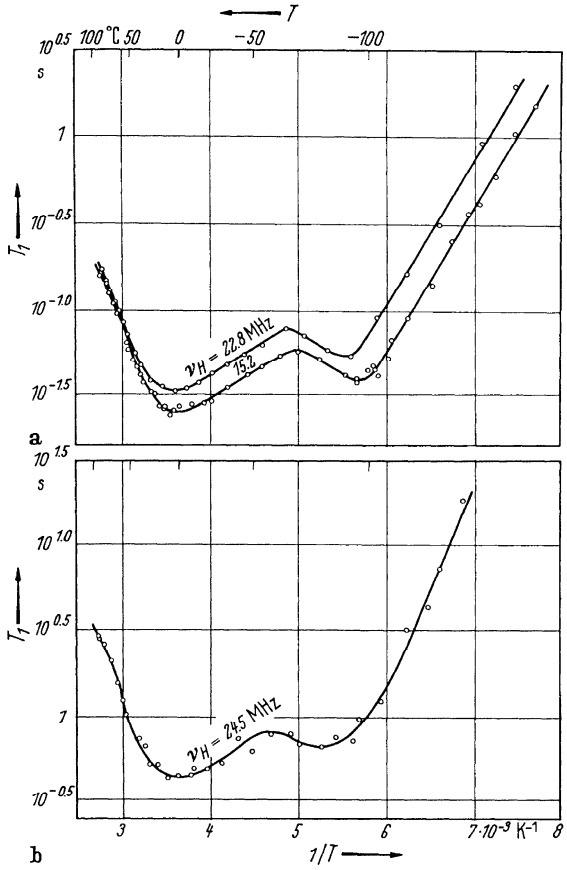

Fig. 60A-1-154. $(NH_2CH_2COOH)_3 \cdot H_2SO_4$ (TGS). T_1 vs. $1/T$ [66Bli]. T_1: proton spin-lattice relaxation time. (**a**) powdered TGS, (**b**) partially deuterated TGS. ν_H: Larmor frequency of proton.

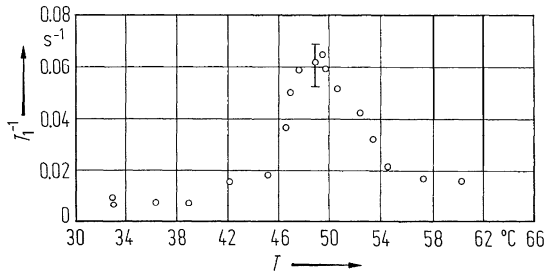

Fig. 60A-1-155. $(NH_2CH_2COOH)_3 \cdot H_2SO_4$ (TGS). T_1^{-1} vs. T [76Mul2]. T_1: spin-lattice relaxation time of ^{13}C at 22.63 MHz.

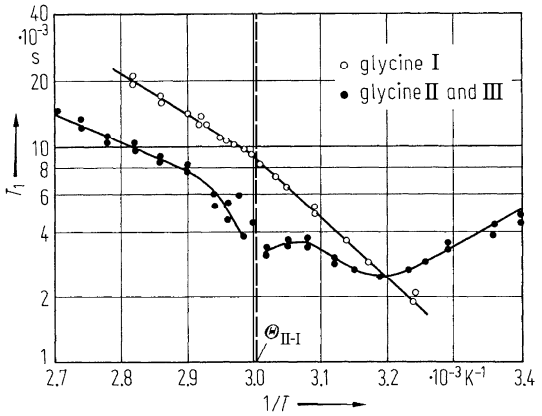

Fig. 60A-1-156. Deuterated triglycine sulfate (DTGS). T_1 vs. T^{-1} [75Ste]. T_1: ND_3 deuteron spin-lattice relaxation time.

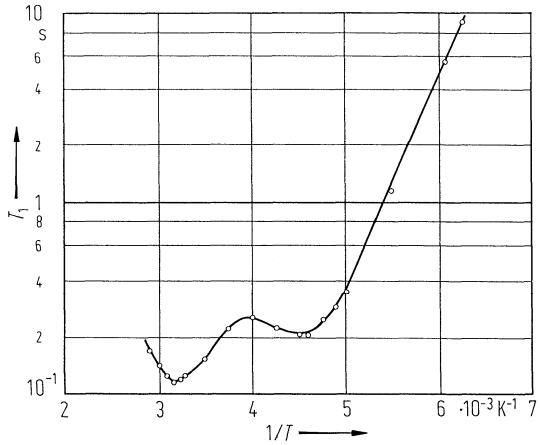

Fig. 60A-1-157. $(NH_2CH_2COOH)_3 \cdot H_2SO_4$ (powder). T_1 vs. $1/T$ [82Slo]. T_1: proton spin-lattice relaxation time. $f = 90$ MHz.

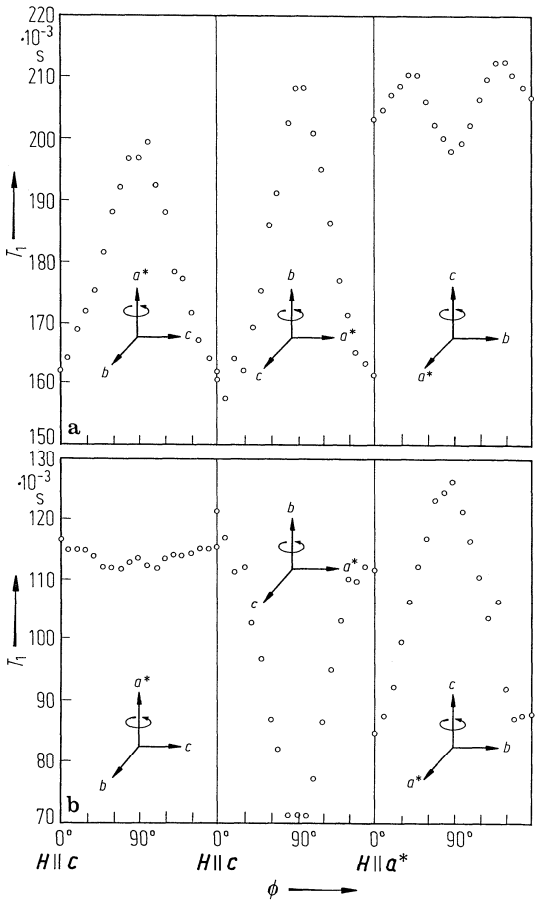

Fig. 60A-1-158. $(NH_2CH_2COOH)_3 \cdot H_2SO_4$ (TGS). T_1 vs. ϕ [82Slo]. T_1: proton spin-lattice relaxation time. ϕ: rotation angle. (**a**) $T = 217$ K, (**b**) $T = 302$ K.

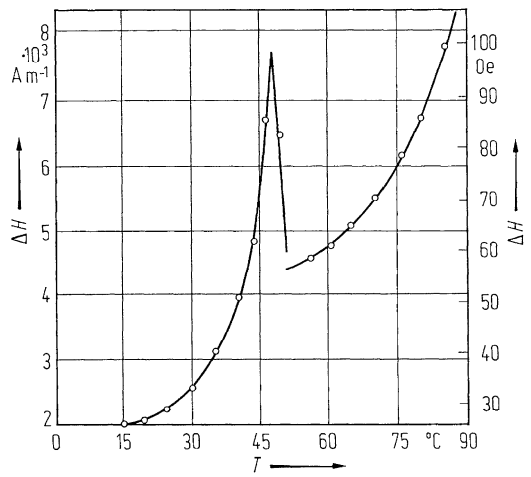

Fig. 60A-1-159. $(NH_2CH_2COOH)_3 \cdot H_2SO_4$ (TGS):Cr^{3+}. ΔH vs. T [78Owe]. ΔH: line width of the resonance due to the $M_s = 1/2$ to $M_s = 3/2$ transition. dc magnetic field is parallel to the z axis of the spin Hamiltonian tensor.

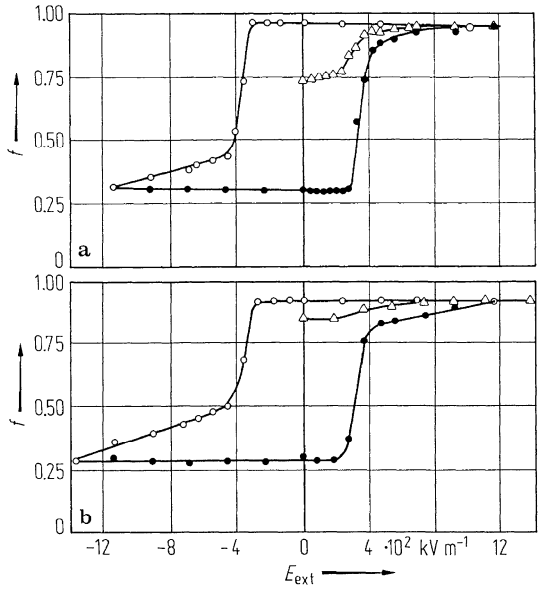

Fig. 60A-1-160. $(NH_2CH_2COOH)_3 \cdot H_2SO_4$ (TGS):Cr^{3+}. f vs. E_{ext} [74Win]. $f = I_1/(I_1 + I_2)$. I_1, I_2: normalized intensity of the $M = -1/2 \leftrightarrow -3/2$ transition, which corresponds to the opposite polarized domains, respectively. $\boldsymbol{E}_{ext} \parallel [010]$, $\boldsymbol{H} \perp c'$ sin β'. (**a**) –30 °C, (**b**) –60 °C.

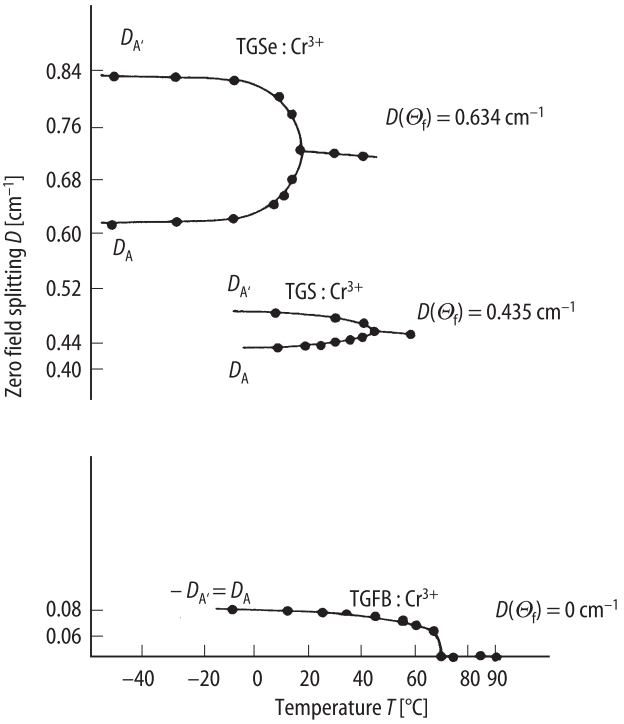

Fig. 60A-1-161. $(NH_2CH_2COOH)_3 \cdot H_2SO_4$ (TGS):Cr^{3+}, $(NH_2CH_2COOH)_3 \cdot H_2SeO_4$ (TGSe):Cr^{3+}, $(NH_2CH_2COOH)_3 \cdot H_2BeF_4$ (TGFB):Cr^{3+}. D vs. T [78Sta2]. D: zero field splitting. $D_A(T) = D(T_c) - \delta D(P_s)$, $D_{A'} = D(T_c) + \delta D(P_s)$. $\delta D(P_s)$: variation in D by mutual orientation interaction between the dipole cluster and the dipole moment of glycine I. See alsoTable 60A-1-028.

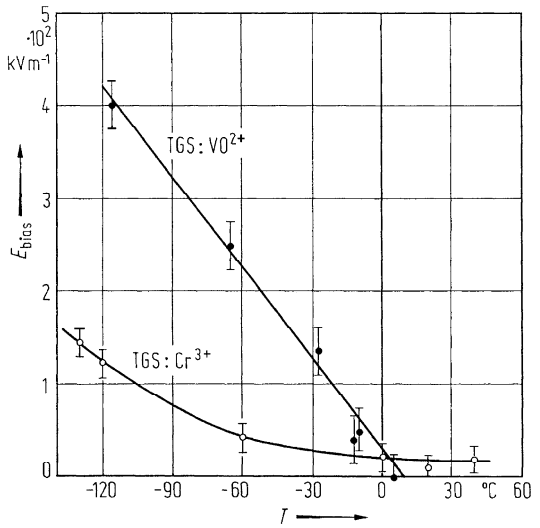

Fig. 60A-1-162. $(NH_2CH_2COOH)_3 \cdot H_2SO_4$ (TGS):VO^{2+}; :Cr^{3+}. E_{bias} vs. T [78Win]. E_{bias}: bias field of ESR intensity hysteresis loop.

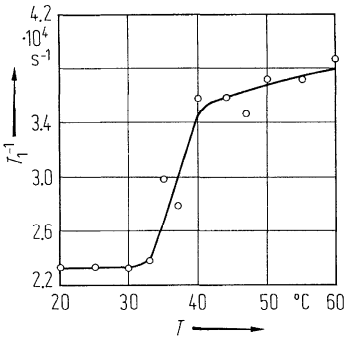

Fig. 60A-1-163. $(NH_2CH_2COOH)_3 \cdot H_2SO_4$ (TGS). T_1^{-1} vs. T of X-irradiated crystal [74Vol]. T_1: electron spin-lattice relaxation time of radical produced by X-irradiation.

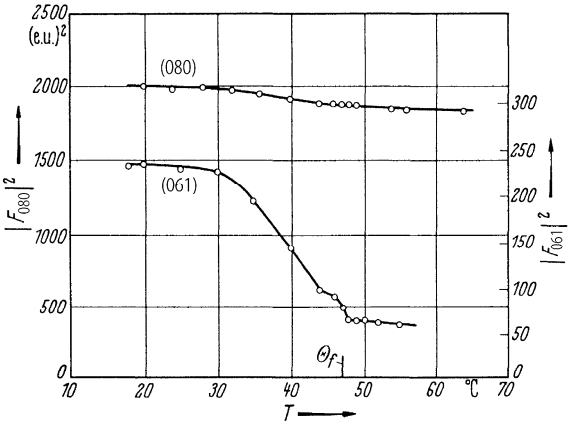

Fig. 60A-1-164. $(NH_2CH_2COOH)_3 \cdot H_2SO_4$ (TGS). $|F_{080}|^2$, $|F_{061}|^2$ vs. T [61Shi]. The Miller indices should follow the crystallographic axes chosen by Hoshino et al., see subsection 3a. F_{hkl}: structure factor in electron unit, e.u.

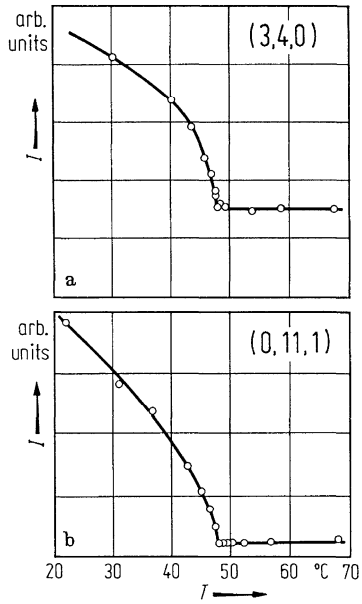

Fig. 60A-1-165. $(NH_2CH_2COOH)_3 \cdot H_2SO_4$ (TGS). *I* vs. *T* [71Fuj]. (**a**) (3, 4, 0) reflection. (**b**) (0, 11, 1) reflection. *I*: integrated intensity of Bragg reflection. The Miller indices should follow the crystallographic axes chosen by Hoshino et al., see subsection 3a.

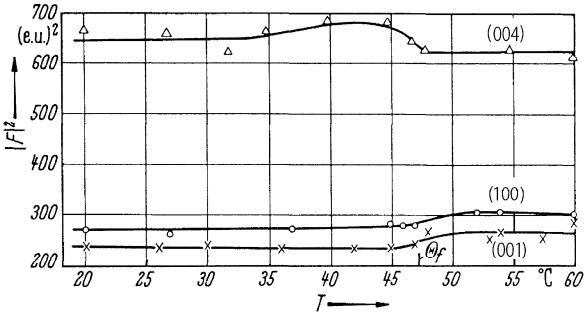

Fig. 60A-1-166. $(NH_2CH_2COOH)_3 \cdot H_2SO_4$ (TGS). $|F_{004}|^2$, $|F_{100}|^2$, $|F_{001}|^2$ vs. *T* [61Shi]. The Miller indices should follow the crystallographic axes chosen by Hoshino et al., see subsection 3a. F_{hkl}: structure factor in electron unit, e.u.

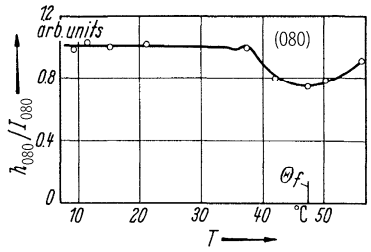

Fig. 60A-1-167. $(NH_2CH_2COOH)_3 \cdot H_2SO_4$ (TGS). h_{080}/I_{080} vs. *T* [61Shi]. h_{080}: peak height of (080) Bragg reflection. *I*: integrated intensity.

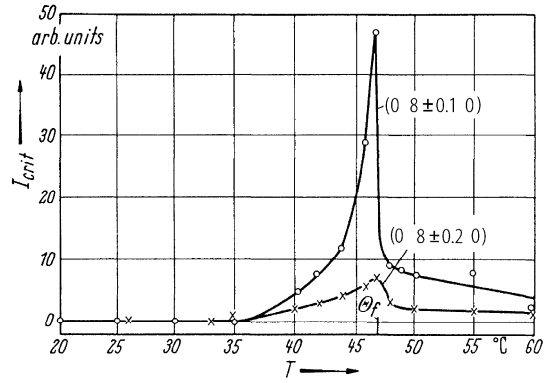

Fig. 60A-1-168. $(NH_2CH_2COOH)_3 \cdot H_2SO_4$ (TGS). I_{crit} at (0, 0.8 ± 0.1, 0) and (0, 0.8 ± 0.2, 0) vs. T [61Shi]. I_{crit}: critical X-ray scattering intensity.

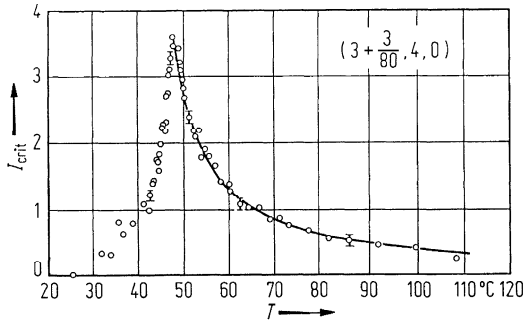

Fig. 60A-1-169. $(NH_2CH_2COOH)_3 \cdot H_2SO_4$ (TGS). I_{crit} at (3+3/80, 4, 0) vs. T [71Fuj]. I_{crit}: critical X-ray scattering intensity. The Miller indices should follow the crystallographic axes chosen by Hoshino et al., see subsection 3a.

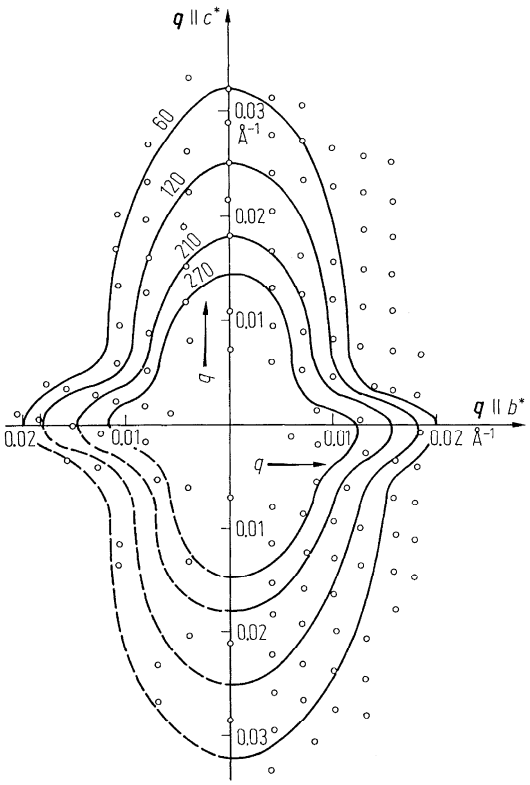

Fig. 60A-1-170. $(NH_2CH_2COOH)_3 \cdot H_2SO_4$ (TGS). X-ray diffuse scattering at 48.4 °C [73Pur]. Constant intensity curves in the reciprocal lattice space around (040). The open circles denote points where intensities were measured. The numbers at the curve give counts for 5 min. Transition temperature of the sample is 48 °C.

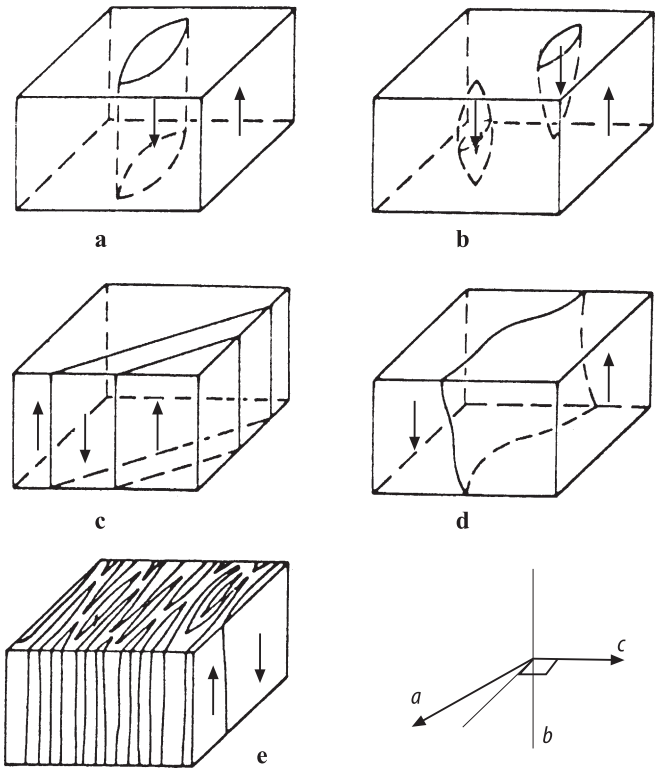

Fig. 60A-1-171. $(NH_2CH_2COOH)_3 \cdot H_2SO_4$ (TGS). Typical domain configurations [78Tak]. Arrows indicate the direction of spontaneous polarization. (**a**) Cylindrical domain with a lenticular cross section. (**b**) Domains in a cigar and in a spike shape. (**c**) Plate-like domain. (**d**) Complex shape domain. (**e**) Lamellar domains.

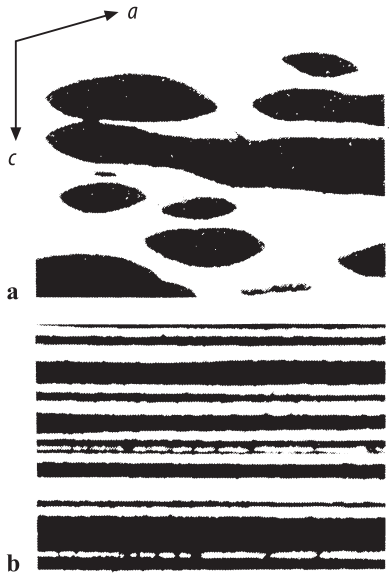

Fig. 60A-1-172. $(NH_2CH_2COOH)_3 \cdot H_2SO_4$ (TGS). Domain patterns on the (010) surface [77Hat]. Black regions are negative domains covered by the carbon powder. (**a**) Lenticular domains in a virgin crystal. (**b**) Lamellar domains revealed after heat treatment.

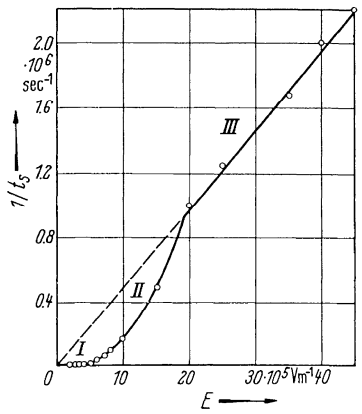

Fig. 60A-1-173. $(NH_2CH_2COOH)_3 \cdot H_2SO_4$ (TGS). $1/t_s$ vs. E [59Fat]. t_s: switching time. I, II, and III merely distinguishes three parts of the curve of different behavior.

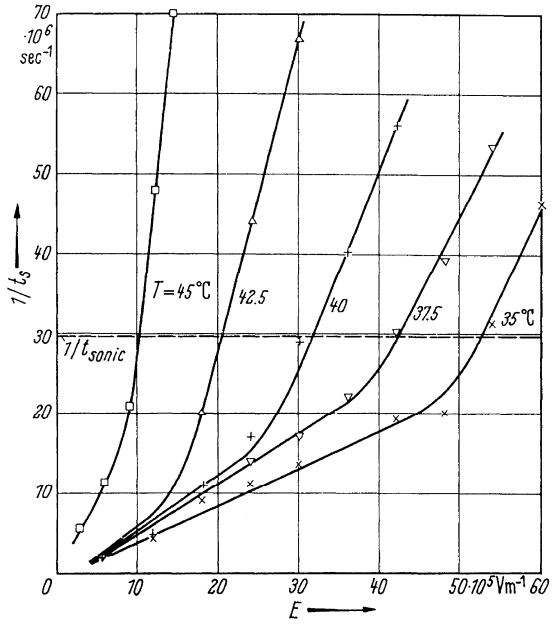

Fig. 60A-1-174. $(NH_2CH_2COOH)_3 \cdot H_2SO_4$ (TGS). $1/t_s$ vs. E [65Bin]. Parameter: T. t_s: switching time. t_{sonic}: transit time of a longitudinal sound wave. Transit time: time necessary for growing of domain walls from one electrode to the opposite electrode.

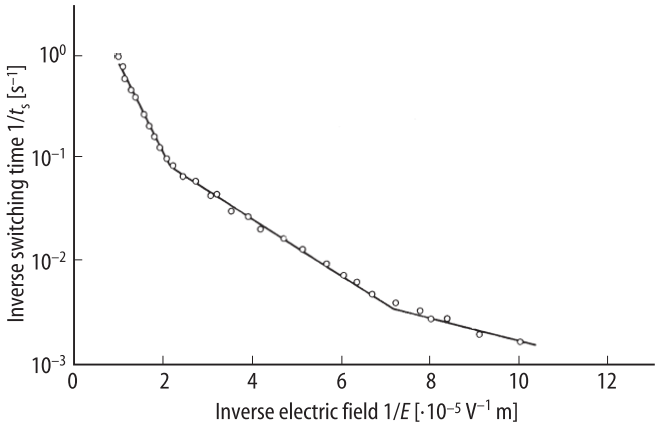

Fig. 60A-1-175. $(NH_2CH_2COOH)_3 \cdot H_2SO_4$ (TGS). $1/t_s$ vs. $1/E$ [89Mat]. t_s: switching time measured by means of liquid crystal.

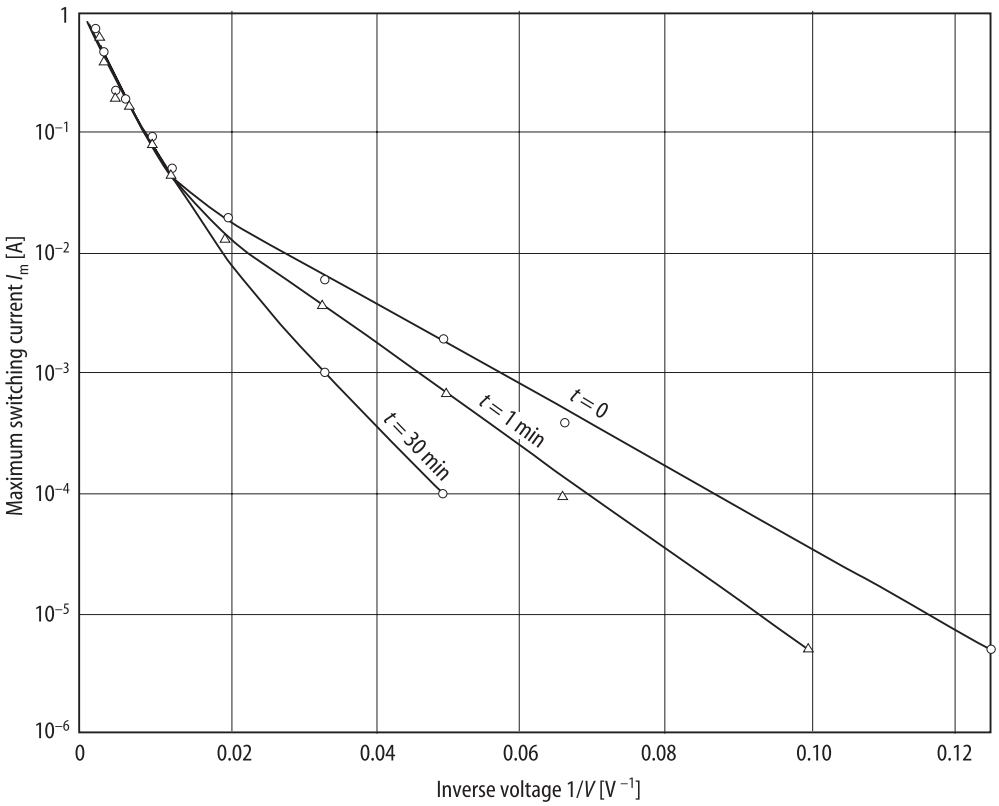

Fig. 60A-1-176. $(NH_2CH_2COOH)_3 \cdot H_2SO_4$ (TGS). I_m vs. $1/V$ [58Fat]. Parameter: waiting time t. I_m: maximum switching current.

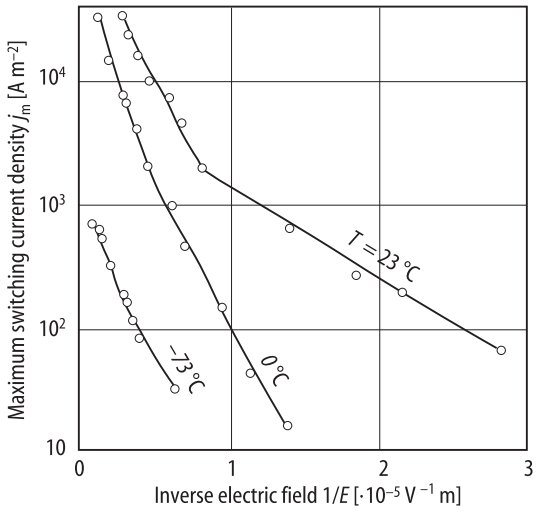

Fig. 60A-1-177. $(NH_2CH_2COOH)_3 \cdot H_2SO_4$ (TGS). j_m vs. $1/E$ [59Toy]. Parameter: T. j_m: maximum switching current density.

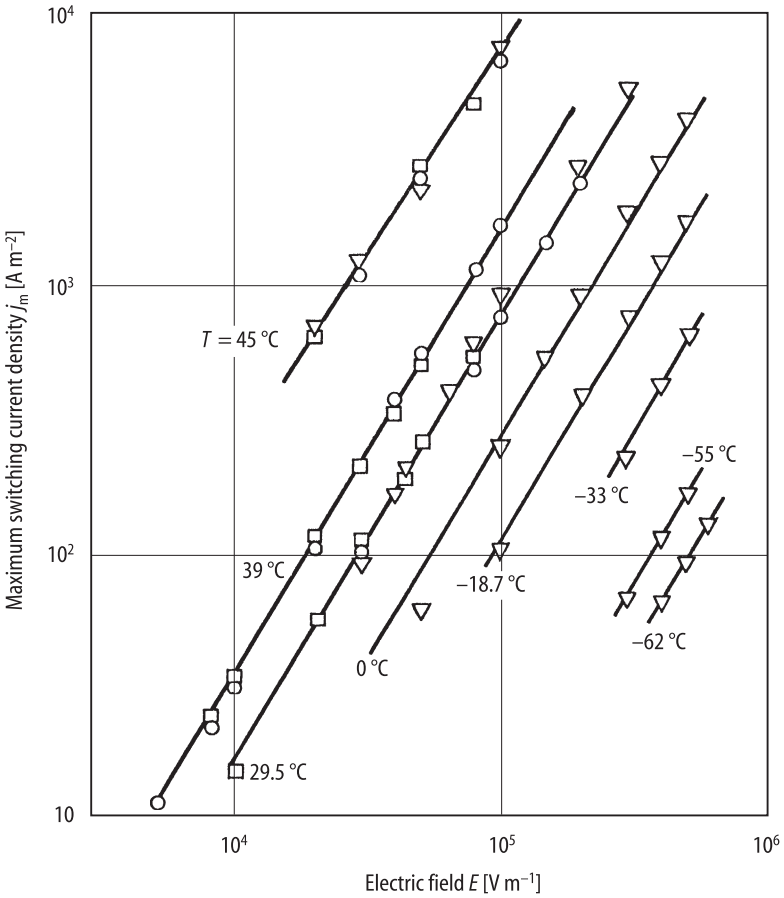

Fig. 60A-1-178. $(NH_2CH_2COOH)_3 \cdot H_2SO_4$ (TGS). j_m vs. E [71Cha]. Parameter: T. j_m: maximum switching current density. Sample thickness, downside triangle: 0.68 mm; circle: 1.45 mm; square: 4.45 mm.

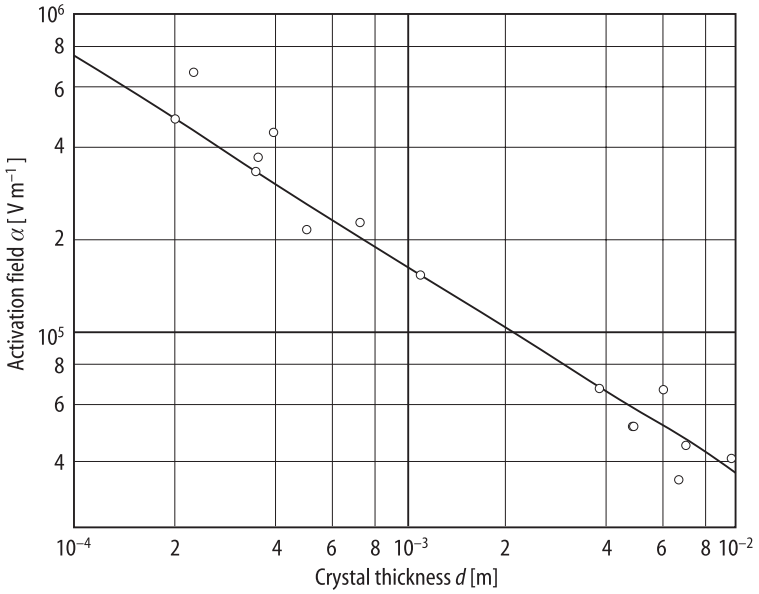

Fig. 60A-1-179. $(NH_2CH_2COOH)_3 \cdot H_2SO_4$ (TGS). α vs. d [64Wie]. α: activation field. d: crystal thickness.

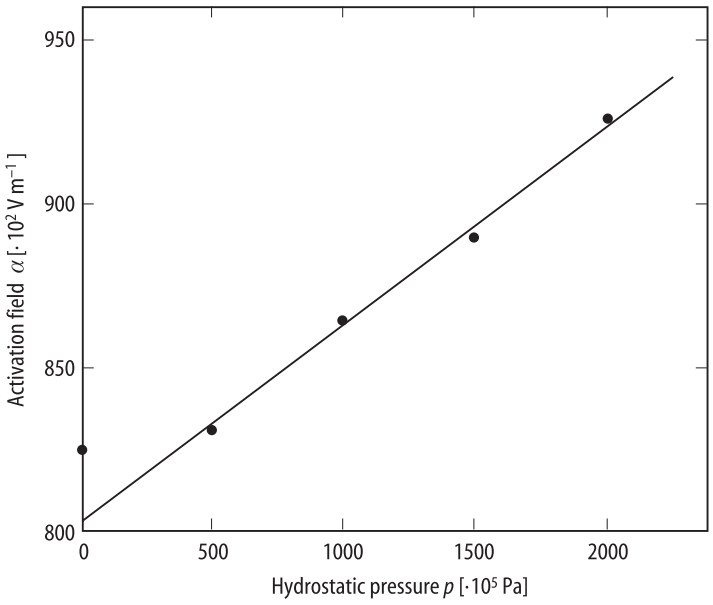

Fig. 60A-1-180. $(NH_2CH_2COOH)_3 \cdot H_2SO_4$ (TGS). α vs. p [71Hay]. α: activation field. p: hydrostatic pressure.

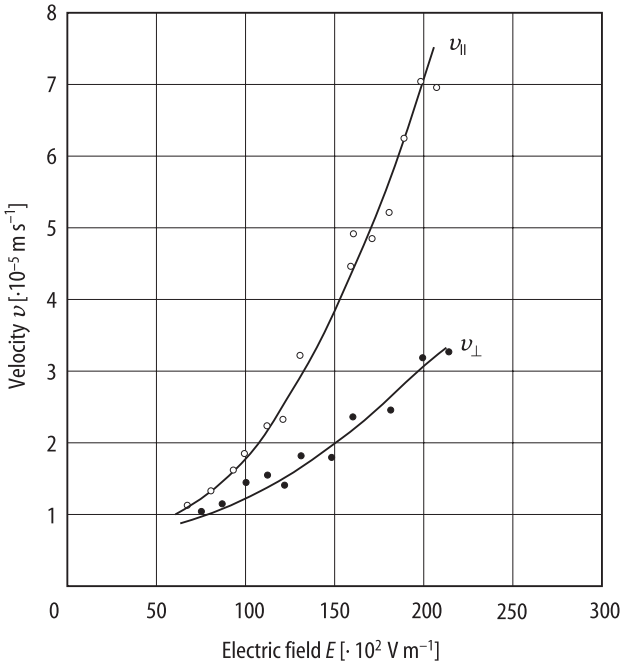

Fig. 60A-1-181. $(NH_2CH_2COOH)_3 \cdot H_2SO_4$ (TGS). $v_{\parallel}$, $v_{\perp}$ vs. E [80Tik]. $v_{\parallel}$, $v_{\perp}$: velocities of the sideward domain motion along the [$\bar{1}$02] direction, i. e. along the large axis of the lenticular domain, and the [001] direction. $T = 27$ °C.

References

56Mat Matthias, B.T., Miller, C.E., Remeika, J.P.: Phys. Rev. **104** (1956) 849.
57Hos Hoshino, S., Mitsui, T., Jona, F., Pepinsky, R.: Phys. Rev. **107** (1957) 1255.
57Woo Wood, E.A., Holden, A.N.: Acta Crystallogr. **10** (1957) 145.
58Dom Domanski, S.: Proc. Phys. Soc. London **72** (1958) 306.
58Fat Fatuzzo, E.: Helv. Phys. Acta **31** (1958) 309.
58Nit Nitsche, R.: Helv. Phys. Acta **31** (1958) 306.
58Pea Pearson, G.L., Feldmann, W.L.: J. Phys. Chem. Solids **9** (1958) 28.
58Pul Pulvari, C.F., Kuebler, W.: J. Appl. Phys. **29** (1958) 1742.
58Tri Triebwasser, S.: IBM J. Res. Dev. **2** (1958) 212.
59Chy Chynoweth, A.G., Abel, J.L.: J. Appl. Phys. **30** (1959) 1073.
59Dio Dion, I.M.: Acta Crystallogr. **12** (1959) 259.
59Fat Fatuzzo, E., Merz, W.J.: Phys. Rev. **116** (1959) 61.
59Hos Hoshino, S., Okaya, Y., Pepinsky, R.: Phys. Rev. **115** (1959) 323.
59Kon Konstantinova, V.P., Sil'vestrova, I.M., Aleksandrov, K.S.: Kristallografiya **4** (1959) 70; Sov. Phys. Crystallogr. (English Transl.) **4** (1959) 63.
59Toy Toyoda, H., Waku, S., Shibata, H., Tanaka, Y.: J. Phys. Soc. Jpn. **14** (1959) 109.
60Chy1 Chynoweth, A.G., Feldmann, W.L.: J. Phys. Chem. Solids **15** (1960) 225.
60Chy2 Chynoweth, A.G.: Phys. Rev. **117** (1960) 1235.
60Gur Gurevich, V.M., Zheludev, I.S., Rez, I.S.: Kristallografiya **5** (1960) 142; Sov. Phys. Crystallogr. (English Transl.) **5** (1960) 133.
60Jon Jona, F., Shirane, G.: Phys. Rev. **117** (1960) 139.
60Kon Konstantinova, V.P., Sil'vestrova, I.M., Shuvalov, L.A., Yurin, V.A.: Izv. Akad. Nauk SSSR, Ser. Fiz. **24** (1960) 1203; Bull. Acad. Sci. USSR, Phys. Ser. (English Transl.) **24** (1960) 1206.
60Lur Lurio, A., Stern, E.: J. Appl. Phys. **31** (1960) 1125.
60Toy Toyoda, H.: J. Phys. Soc. Jpn. **15** (1960) 1539.
61Bli Blinc, R., Detoni, S., Levstek, I., Pintar, M., Poberaj, S., Schara, M.: J. Phys. Chem. Solids **20** (1961) 187.
61Gil Gilletta, M.F.: C. R. Acad. Sci. (Paris) **253** (1961) 1556.
61Gur Gurevich, V.M., Zheludev, I.S.: Kristallografiya **6** (1961) 135; Sov. Phys. Crystallogr. (English Transl.) **6** (1961) 110.
61Ove Ovenall, D.W., Müller, K.A.: Helv. Phys. Acta **34** (1961) 786.
61Shi Shibuya, I., Mitsui, T.: J. Phys. Soc. Jpn. **16** (1961) 479.
61Shu Shuvalov, L.A., Pluzhnikov, K.A.: Kristallografiya **6** (1961) 692; Sov. Phys. Crystallogr. (English Transl.) **6** (1962) 555.
61Sil Sil'vestrova, I.M.: Kristallografiya **6** (1961) 582; Sov. Phys. Crystallogr. (English Transl.) **6** (1962) 466.
61Toy Toyoda, H., Tanaka, Y., Shiokawa, W.: Rev. Electr. Commun. Lab. **9** (1961) 485.
62Ike Ikeda, T., Tanaka, Y., Toyoda, H.: Jpn. J. Appl. Phys. **1** (1962) 13.
62Kay Kay, H.F., Dunn, J.W.: Philos. Mag. [8] **7** (1962) 2027.
62Kon Konstantinova, V.P.: Kristallografiya **7** (1962) 748; Sov. Phys. Crystallogr. (English Transl.) **7** (1963) 605.
62Leo Leonidova, G.G., Polandov, I.N., Golentovskaya, I.P.: Fiz. Tverd. Tela **4** (1962) 3337; Sov. Phys. Solid State (English Transl.) **4** (1963) 2443.
62Min Minaeva, K.A.: Kristallografiya **7** (1962) 425; Sov. Phys. Crystallogr. (English Transl.) **7** (1962) 335.
62Nak Nakamura, T., Nakamura, H.: Jpn. J. Appl. Phys. **1** (1962) 253.
62Sav Savage, A., Miller, R.C.: Appl. Opt. **1** (1962) 661.
62Shi Shibuya, I., Hoshino, S.: Jpn. J. Appl. Phys. **1** (1962) 249.
62Sil Sil'vestrova, I.M., Yurin, V.A.: Fiz. Tverd. Tela **4** (1962) 2319; Sov. Phys. Solid State (English Transl.) **4** (1963) 1698.
63Hil Hill, R.M., Ichiki, S.K.: Phys. Rev. **132** (1963) 1603.
63Ike Ikeda, T., Tanaka, Y., Toyoda, H.: Jpn. J. Appl. Phys. **2** (1963) 199.

63Sch Schmidt, G., Pfannschmidt, P.: Phys. Status Solidi **3** (1963) 2215.
64Gon Gonzalo, J.A., Lopez-Alonso, J.R.: J. Phys. Chem. Solids **25** (1964) 303.
64OBr O′Brien, E.J., Litovitz, T.A.: J. Appl. Phys. **35** (1964) 180.
64Str Strukov, B.A.: Fiz. Tverd. Tela **6** (1964) 2862; Sov. Phys. Solid State (English Transl.) **6** (1965) 2278.
64Wie Wieder, H.H.: J. Appl. Phys. **35** (1964) 1224.
65Bin Binggeli, B., Fatuzzo, E.: J. Appl. Phys. **36** (1965) 1431.
65Los Lösche, A., Windsch, W.: Phys. Status Solidi **11** (1965) K55.
65Min Minaeva, K.A., Levanyuk, A.P.: Izv. Akad. Nauk SSSR, Ser. Fiz. **29** (1965) 978; Bull. Acad. Sci. USSR, Phys. Ser. (English Transl.) **29** (1965) 978.
65Rud Rudyak, V.M., Baranov, A.I.: Izv. Akad. Nauk SSSR, Ser. Fiz. **29** (1965) 951; Bull. Acad. Sci. USSR, Phys. Ser. (English Transl.) **29** (1965) 955.
66Bli Blinc, R., Lahajnar, G., Pintar, M., Zupancic, I.: J. Chem. Phys. **44** (1966) 1784.
66Fou Fousek, J., Safrankova, M., Kaczer, J.: Appl. Phys. Lett. **8** (1966) 192.
66Gam Gammon, R.W., Cummins, H.Z.: Phys. Rev. Lett. **17** (1966) 193.
66Gon Gonzalo, J.A.: Phys. Rev. **144** (1966) 662.
66Iva1 Ivanov, N.R., Zotov, V.F.: Kristallografiya **11** (1966) 924; Sov. Phys. Crystallogr. (English Transl.) **11** (1967) 781.
66Iva2 Ivanov, N.R., Shuvalov, L.A.: Kristallografiya **11** (1966) 614; Sov. Phys. Crystallogr. (English Transl.) **11** (1967) 534.
66Kol Koldobskaya, M.F., Meleshina, V.A., Rez, I.S., Mironova, Z.A., Gavrilova, I.V., Safronov, G.M.: Kristallografiya **11** (1966) 785; Sov. Phys. Crystallogr. (English Transl.) **11** (1967) 665.
66Sta Stankowski, J: Proceeding of the International Meeting on Ferroelectricity, Prague, 1966; Prague: Institute of Physics of the Czechoslovak Academy of Science, 1966. Vol. 2, p. 364.
66Str Strukov, B.A., Kristallografiya **11** (1966) 892; Sov. Phys. Crystallogr. (English Transl.) **11** (1967) 757.
66Vas Vasilevskaya, A.S., Sonin, A.S., Slepkov, I.A.: Kristallografiya **11** (1966) 749; Sov. Phys. Crystallogr. (English Transl.) **11** (1967) 640.
66War Wartewig, S., Windsch, W.: Phys. Status Solidi **17** (1966) K221.
67Bjo Bjorkstam, J.L.: Phys. Rev. **153** (1967) 599.
67Bli Blinc, R., Pintar, M., Zupancic, I.: J. Phys. Chem. Solids **28** (1967) 405.
67Saw Sawada, A., Abe, R.: Jpn. J. Appl. Phys. **6** (1967) 699.
67Son1 Sonin, A.S., Vasilevskaya, A.S.: Fiz. Tverd. Tela **9** (1967) 1951; Sov. Phys. Solid State (English Transl.) **9** (1968) 1536.
67Son2 Sonin, A.S., Vasilevskaya, A.S.: Fiz. Tverd. Tela **9** (1967) 451; Sov. Phys. Solid State (English Transl.) **9** (1967) 386.
67Son3 Sonin, A.S., Suvorov, V.S.: Fiz. Tverd. Tela **9** (1967) 1829; Sov. Phys. Solid State (English Transl.) **9** (1967) 1437.
67Vas Vasilevskaya, A.S., Perfilova, V.E., Sonin, A.S.: Izv. Akad. Nauk SSSR, Ser. Fiz. **31** (1967) 1132; Bull. Acad. Sci. USSR, Phys. Ser. (English Transl.) **31** (1967) 1149.
67Win Windsch, W., Welter, M.: Z. Naturforsch. **22a** (1967) 1.
68Bre1 Brezina, B., Galanov, E.K., Ivanov, N.R., Kislovskii, L.D., Shuvalov, L.A.: Kristallografiya **13** (1968) 821; Sov. Phys. Crystallogr. (English Transl.) **13** (1969) 710.
68Bre2 Brezina, B., Smutny, F.: Czech. J. Phys. B **18** (1968) 393.
68Chi Chincholkar, V.S., Unruh, H.-G.: Phys. Status Solidi **29** (1968) 669.
68Gon Gonzalo, J.A.: Phys. Rev. **144** (1968) 662.
68Iwa Iwasaki, H., Toyoda, H., Ohtsuka, M.: Jpn. J. Appl. Phys. **7** (1968) 787.
68Lom Lomova, L.G., Sonin, A.S., Regul′skaya, T.A.: Kristallografiya **13** (1968) 90; Sov. Phys. Crystallogr. (English Transl.) **13** (1968) 68.
68Min Minaeva, K.A., Strukov, B.A., Varnstorff, K.: Fiz. Tverd. Tela **10** (1968) 2125; Sov. Phys. Solid State (English Transl.) **10** (1969) 1665.
68Mor Moravec, F., Konstantinova, V.P.: Kristallografiya **13** (1968) 284; Sov. Phys. Crystallogr. (English Transl.) **13** (1968) 221.

69Gur Gurevich, V.M.: Elektroprovodnost Segnetelektrikov, Moskva: Izdatelstovo Komiteta Standartov, Mer I Izmeritel′nykh Priboroy pri Sovete Ministrov SSSR 1969; Electric Conductivity of Ferroelectrics, Jerusalem: Israel Program for Scientific Translations, 1971 (English Transl.).

69Hay Hayashi, M., Mishima, H.: Jpn. J. Appl. Phys. **8** (1969) 968.

69Kat Kato, T., Abe, R.: J. Phys. Soc. Jpn. **26** (1969) 948.

69Lut Luther, G., Müser, H.E.: Z. Naturforsch. **24a** (1969) 389.

69Min Minaeva, K.A., Levanyuk, A.P., Strukov, B.A.: Izv. Akad. Nauk SSSR, Ser. Fiz. **33** (1969) 328; Bull. Acad. Sci. USSR, Phys. Ser. (English Transl.) **33** (1969) 304.

69Pet Petroff, J.F.: Phys. Status Solidi **31** (1969) 285.

70Kat Kato, T., Abe, R.: J. Phys. Soc. Jpn. **29** (1970) 389.

70Min Minaeva, K.A., Strukov, B.A., Huang, H.C.: Fiz. Tverd. Tela **12** (1970) 1584; Sov. Phys. Solid State (English Transl.) **12** (1970) 1256.

70Tak Takagi, M., Suzuki, S., Watanabe, H.: J. Phys. Soc. Jpn. **28** (1970) Suppl., 369.

70Tar Taraskin, S.A., Strukov, B.A., Meleshina, V.A.: Fiz. Tverd. Tela **12** (1970) 1386; Sov. Phys. Solid State (English Transl.) **12** (1970) 1089.

70Tel Tello, M.J., Gonzalo, J.A.: J. Phys. Soc. Jpn. **28** (1970) Suppl., 199.

71Baj Bajak, I.L.: Fyz. Cas. **21** (1971) 90.

71Bli Blinc, R., Mali, M., Osredkar, R., Prelesnik, A., Zupancic, I., Ehrenberg, L.: J. Chem. Phys. **55** (1971) 4843.

71Bre Brezina, B.: Mater. Res. Bull. **6** (1971) 401.

71Cha Chabin, M., Gilletta, F.: C. R. Acad. Sci. (Paris), Ser. B **272** (1971) 243.

71Fuj Fujii, Y., Yamada, Y.: J. Phys. Soc. Jpn. **30** (1971) 1676.

71Hay Hayashi, M.: J. Phys. Soc. Jpn. **31** (1971) 1450.

71Hel Helwig, J., Albers, J.: Phys. Status Soldi (a) **7** (1971) 151.

71Kev Keve, E.T., Bye, K.L., Whipps, P.W., Annis, A.D.: Ferroelectrics **3** (1971) 39.

71LeB Le Bihan, R., Maussion, M.: C. R. Acad. Sci. (Paris), Ser. B **272** (1971) 1010.

72Bro Brosowski, G., Luther, G., Müser, H.E.: Phys. Status Solidi (a) **14** (1972) K15.

72Izr Izrael, A., Petroff, J.F., Authier, A.: J. Cryst. Growth **16** (1972) 131.

72Kat Kato, T., Abe, R.: J. Phys. Soc. Jpn. **32** (1972) 717.

72Mor Mori, K., Hayashi, M.: J. Phys. Soc. Jpn. **33** (1972) 1396.

72Nak Nakatani, N.: J. Phys. Soc. Jpn. **32** (1972) 1556.

72Ser Serdobol'skaya, O.Yu., Kuak, T.T.: Fiz. Tverd. Tela **14** (1972) 2443; Sov. Phys. Solid State (English Transl.) **14** (1973) 2114.

73Hat Hatano, J., Suda, F., Futama, H.: Jpn. J. Appl. Phys. **12** (1973) 1644.

73Ito Itoh, K., Mitsui, T.: Ferroelectrics **5** (1973) 235.

73Jaq Jaque, F., Herreros, J.M., Sanchez, C.: Solid State Commun. **12** (1973) 63.

73Kat Kato, T., Abe, R.: J. Phys. Soc. Jpn. **35** (1973) 1643.

73Kay Kay, M.I., Kleinberg, R.: Ferroelectrics **5** (1973) 45.

73Lut Luther, G.: Phys. Status Solidi (a) **20** (1973) 227.

73Mat Matsuda, T., Abe, R.: J. Phys. Soc. Jpn. **35** (1973) 1790.

73Mer Mercado, A., Gonzalo, J.A.: Ferroelectrics **5** (1973) 229.

73Pol Polcarova, M., Janta, J.: Czech. J. Phys. B **23** (1973) 331.

73Pop Poplavko, Yu.M., Pereverzeva, L.P., Meriakri, V.V., Ushatkin, E.F., Ogurtsov, S.V., Yashchishin, P.I.: Fiz. Tverd. Tela **15** (1973) 1250; Sov. Phys. Solid State (English Transl.) **15** (1973) 842.

73Pur Pura, B., Przedmojski, J.: Phys. Lett. A **43** (1973) 217.

74Fuj Fujimoto, M., Dressel, L.A.: Ferroelectrics **8** (1974) 611.

74Gil Gillespie, S., Schürmann, H.K., Gunton, J.D., Mihalisin, T.: Solid State Commun. **15** (1974) 1753.

74God Godefroy, L., Jullien, P., Morlon, B., Godefroy, G.: Ferroelectrics **8** (1974) 421.

74Ima Imai, K.: J. Phys. Soc. Jpn. **36** (1974) 1069.

74Kat Kato, T., Abe, R.: J. Phys. Soc. Jpn. **36** (1974) 1065.

74Lop Lopez Rodriguez, V., Gonzalez Ibeans, J.: Ferroelectrics **6** (1974) 203.

74Pop Poplavko, Yu.M., Pereverzeva, L.P., Yashchishin, P.I., Mariakri, V.V., Ushatkin, E.F., Ogurtsov, S.V.: Ukr. Fiz. Zh. **19** (1974) 1688.

74Sta1 Stankowski, J., Galezewski, A., Waplak, S., Gruszczynska, U., Gierszal, H.: Ferroelectrics **6** (1974) 209.

74Sta2 Stankowski, J., Waplak, S., Yurin, V.A.: Phys. Status Solidi (a) **22** (1974) K41.

74Sta3 Stankowski, J., Wieckowski, A., Hedewy, S.: J. Magn. Reson. **15** (1974) 498.

74Ste Stepien-Damm, J.A., Suski, T., Meysner, L., Hilczer, B., Lukaszewicz, K.: Bull. Acad. Pol. Sci. Ser. Sci. Chim. **22** (1974) 685.

74Vol Völkel, G., Bartuch, U., Brunner, W., Windsch, W.: Phys. Status Solidi (a) **25** (1974) 591.

74Win Windsch, W., Kunze, R., Völkel, G.: Phys. Status Solidi (a) **26** (1974) K175.

74Zer Zerem, J.Z., Halperin, A.: Ferroelectrics **7** (1974) 205.

75Bee Beerman, H.P.: Infrared Phys. **15** (1975) 225.

75Fuj Fujimoto, M., Dressel, L.A.: Ferroelectrics **9** (1975) 221.

75Had1 Hadni, A., Thomas, R.: C. R. Acad. Sci. (Paris), Ser. B **280** (1975) 95.

75Had2 Hadni, A., Thomas, R.: Phys. Status Solidi (a) **31** (1975) 71.

75Kev Keve, E.T.: Philips Tech. Rev. **35** (1975) 247.

75Mey Meyer, K.P., Pawlaczyk, Cz., Hilczer, B., Scholz, R.: Krist. Tech. **10** (1975) 759.

75Nak Nakatani, N.: J. Phys. Soc. Jpn. **39** (1975) 741.

75Ste Stepisnik, J., Slak, J.: J. Chem. Phys. **62** (1975) 34.

75Str Strukov, B.A., Minaeva, K.A., Teleshevskii, V.I., Shirina, N.G., Kkhanna, S.K.: Izv. Akad. Nauk SSSR, Ser. Fiz. **39** (1975) 758; Bull. Acad. Sci. USSR, Phys. Ser. (English Transl.) **39**, No. 4 (1975) 101.

75Wie Wieckowski, A., Kulinski, W.: Acta Phys. Pol. A **47** (1975) 481.

75Win Windsch, W., Völkel, G.: Ferroelectrics **9** (1975) 187.

76Buc Buchheim, A., Grande, S., Rosenberger, H., Schnabel, B., Voigtsberger, B.: Ann. Phys. (Leipzig) **33** (1976) 374.

76Cer Cervenka, P.O., Prasad Rao, A.D., Porto, S.P.S.: Ferroelectrics **11** (1976) 511.

76Dis Distler, G.I., Shenyavskaya, L.A.: Krist. Tech. **11** (1976) 383.

76Ehs Ehses, K.H., Müser, H.E.: Ferroelectrics **12** (1976) 247.

76Fle1 Fletcher, S.R., Keve, E.T., Skapski, A.C.: Ferroelectrics **14** (1976) 775.

76Fle2 Fletcher, S.R., Keve, E.T., Skapski, A.C.: Ferroelectrics **14** (1976) 789.

76Kot Kotake, Y., Miyagawa, I.: J. Chem. Phys. **64** (1976) 3169.

76Mor Morrison, I.E.G., Rees, L.V.C., Silver, J., White, E.A.D.: J. Chem. Soc. Dalton Trans. (1976) 1103.

76Mul1 Müller, D.: Solid State Commun. **19** (1976) 1067.

76Mul2 Müller, D.: Ferroelectrics **13** (1976) 431.

76Sad Sader, E., Harnik, E.: Phys. Lett. A **58** (1976) 199.

76Wur Würfel, P., Batra, I.P.: Ferroelectrics **12** (1976) 55.

76Yag Yagi, T., Tokunaga, M., Tatsuzaki, I.: J. Phys. Soc. Jpn. **40** (1976) 1659.

76Yur Yurin, V.A., Waplak, S., Stankowski, J., Ankudinov, M.A., Zheludev, I.S.: Kristallografiya **21** (1976) 327; Sov. Phys. Crystallogr. (English Transl.) **21** (1976) 177.

77Bot Böttcher, R., Heinhold, D., Windsch, W.: Chem. Phys. Lett. **49** (1977) 148.

77Cho Choe, H.M., Judy, J.H., Van Der Ziel, A.: Ferroelectrics **15** (1977) 181.

77Hat Hatano, J., Suda, F., Futama, H.: J. Phys. Soc. Jpn. **43** (1977) 1933.

77Hau Haussühl, S., Albers, J.: Ferroelectrics **15** (1977) 73.

77Kaw Kawashima, R., Tokunaga, M., Tatsuzaki, I.: J. Phys. Soc. Jpn. **42** (1977) 903.

77Kom Komlyakova, N.S., Likhov, A.B., Malek, Z., Rudyak, V.M., Shuvalov, L.A.: Kristallografiya **22** (1977) 566; Sov. Phys. Crystallogr. (English Transl.) **22** (1977) 323.

77Lus Luspin, Y., Hauret, G.: Ferroelectrics **15** (1977) 43.

77Sad Sader, E., Harnik, E.: J. Appl. Phys. **48** (1977) 3607.

77Sus Suski, T.: Acta Univ. Wratislav. No. 341 (1977) 54.

77Tar Taraskin, S.A., Strukov, B.A., Fedorikhin, V.A., Belugina, N.V., Meleshina, V.A.: Fiz. Tverd. Tela **19** (1977) 2936; Sov. Phys. Solid State (English Transl.) **19** (1977) 1721.

77Tyl Tylczynski, Z.: Acta Phys. Pol. A **51** (1977) 249.

77Vaz Vazquez, F., Gonzalo, J.A.: Ferroelectrics **16** (1977) 223.
77Win Winterfeldt, V., Schaack, G., Klöpperpieper, A.: Ferroelectrics **15** (1977) 21.
78Fel Felix, P., Gamot, P., Lacheau, P., Raverdy, Y.: Ferroelectrics **17** (1978) 543.
78Lil Lillicrap, B.J., Wood, J.D.C.: J. Mater. Sci. **13** (1978) 681.
78Owe Owens, F.J.: J. Phys. Chem. Solids **39** (1978) 291.
78Rom Romanjuk, N.A., Andriyevskij, B.V., Zheludev, I.S.: Ferroelectrics **21** (1978) 333.
78Sta1 Stankowska, J., Polovinko, I., Stankowski, J.: Ferroelectrics **21** (1978) 529.
78Sta2 Stankowski, J.: Ferroelectrics **20** (1978) 109.
78Tak Takahashi, K., Takagi, M.: J. Phys. Soc. Jpn. **44** (1978) 1266.
78Wel Welter, M., Kröber, T., Wartewig, S., Windsch, W.: Mol. Phys. **36** (1978) 1385.
78Win Windsch, W., Völkel, G.: Ferroelectrics **17** (1978) 491.
79Bot Böttcher, R., Heinhold, D., Windsch, W.: Chem. Phys. Lett. **65** (1979) 452.
79Deg Deguchi, K.: J. Phys. Soc. Jpn. **47** (1979) 153.
79Ema1 Ema, K., Katayama, M., Ikeda, Y., Hamano, K.: J. Phys. Soc. Jpn. **46** (1979) 347.
79Ema2 Ema, K., Hamano, K., Ikeda, Y.: J. Phys. Soc. Jpn. **46** (1979) 345.
79Glo Glogarova, M., Janovec, V., Tikhomirova, N.A.: J. Phys. (Paris) **40** Suppl. C3 (1979) 502.
79Hof Hoffmann, S.K., Szczepaniak, L.S.: J. Magn. Reson. **36** (1979) 359.
79Lil Lillicrap, B.J., Wood, J.D.C., Wood, V.M., Shaw, N.: J. Phys. D **12** (1979) 633.
79Paw Pawlaczyk, Cz., Luther, G., Müser, H.E.: Phys. Status Solidi (b) **91** (1979) 627.
79Sha Shaulov, A., Bell, M.I., Smith, W.A.: J. Appl. Phys. **50** (1979) 4913.
80Baj Bajak, I.L., Brezina, B.: Acta Phys. Slovaca **30** (1980) 77.
80Dev Devyatkov, M.N., D'yakonov, G.I.: Vestn. Mosk. Univ., Ser. 3, Fiz. Astron. **35** (1980) 77; Moscow Univ. Phys. Bull. (English Transl.) **35** (1980) 83.
80Ehs1 Ehses, K.-H., Meister, H.: Ferroelectrics **25** (1980) 577.
80Ehs2 Ehses, K.-H.: Ferroelectrics **25** (1980) 573.
80Ima Imai, K.: J. Phys. Soc. Jpn. **49** (1980) 2263; Erratum **50** (1981) 2130.
80Jar Jaroma-Weiland, G., Krajewski, T.: Acta Phys. Pol. A **58** (1980) 617.
80Kra Krajewski, T., Breczewski, T.: Ferroelectrics **25** (1980) 547.
80Miy Miyakawa, K., Yagi, T.: J. Phys. Soc. Jpn. **49** (1980) 1881.
80Mot Motegi, H., Ibaraki, K., Nakamura, E.: Jpn. J. Appl. Phys. **19** (1980) L433.
80Mus Müser, H.E., Helwig, J., Barth, E.: Ferroelectrics **25** (1980) 371.
80Pol Polovinko, I., Stankowska, J., Stankowski, J.: Ferroelectrics **25** (1980) 523.
80Ram Ramos, S., Del Cerro, J., Zamora, M.: Phys. Status Solidi (a) **61** (1980) 307.
80Sch Schmitt, H., Müser, H.E., Mengelkoch, O., Sterta, W.: Ferroelectrics **25** (1980) 499.
80Sta Stankowski, J., Malinowski, W.: Acta Phys. Pol. A **58** (1980) 773.
80Str Strukov, B.A., Sigov, A.S., Fedorikhin, V.A. Taraskin, S.A.: Pis'ma Zh. Eksp. Teor. Fiz **31** (1980) 184; JETP Lett. (English Transl.) **31** (1980) 169.
80Tik Tikhomirova, N.A., Pikin, S.A., Shuvalov, L.A., Dontsova, L.I., Popov, E.S., Shilnikov, A.V., Bulatova, L.G.: Ferroelectrics **29** (1980) 145.
80Vol Volkov, A.A., Kozlov, G.V., Lebedev, S.P.: Kratk. Soobshch. Fiz., Sb. Akad. Nauk SSSR, Fiz. Inst. P.N. Lebedeva **5** (1980) 39; Sov. Phys. Lebedev Inst. Rep. (English Transl.) **5** (1980) 25.
81Don Dontsova, L.I., Popov, E.S., Shil'nikov, A.V., Bulatova, L.G., Tikhomirova, N.A., Shuvalov, L.A.: Kristallografiya **26** (1981) 758; Sov. Phys. Crystallogr. (English Transl.) **26** (1981) 430.
81Hab Habrylo, S., Koralewski, M.: Acta Phys. Pol. A **60** (1981) 147.
81Had Hadni, A., Thomas, R.: Thin Solid Films **81** (1981) 247.
81Kit Kitaeva, V.F., Ryvkin, V.A., Yurin, V.A., Sobolev, N.N.: Kratk. Soobshch. Fiz., Sb. Akad. Nauk SSSR, Fiz. Inst. P.N. Lebedeva **6** (1981) 40; Sov. Phys. Lebedev Inst. Rep. (English Transl.) **6** (1981) 37.
81Law Lawless, W.N.: Phys. Rev. B **23** (1981) 2421.
81Mon Montoto, L., Jaque, F.: Ferroelectrics **38** (1981) 959.
81Nak Nakatani, N.: Jpn. J. Appl. Phys. **20** (1981) 2281.
81Par Parpia, D.Y.: J. Cryst. Growth **54** (1981) 347.
81Pol Polomska, M., Hilczer, B., Michalczyk, M.: Ferroelectrics **39** (1981) 1217.

81Rom1 Romanyuk, N.A., Kostetskii, A.M.: Kristallografiya **26** (1981) 125; Sov. Phys. Crystallogr. (English Transl.) **26** (1981) 67.
81Rom2 Romanyuk, N.A., Andrievskii, B.V., Gaba, V.M.: Opt. Spektrosk. **50** (1981) 126; Opt. Spectrosc. (English Transl.) **50** (1981) 65.
81Rud Rudyak, V.M., Bogomolov, A.A., Bolshakova, N.M., Dabizha, T.A., Zharov, S.Yu.: Ferroelectrics **33** (1981) 25.
81Tyl1 Tylczynski, Z.: Physica B **111** (1981) 267.
81Tyl2 Tylczynski, Z.: Acta Phys. Pol. A **59** (1981) 195.
81Yur Yurin, V.A., Kitaeva, V.F., Rivkin, V.A., Zheludev, I.S.: Ferroelectrics **39** (1981) 1185.
82Kor Koralewski, M., Habrylo, S.: Ferroelectrics **46** (1982) 13.
82Ram Ramos, S., Del Cerro, J.: Ferroelectrics **46** (1982) 1.
82Slo Slosarek, G., Idziak, S., Pislewski, N., Stankowski, J.: Phys. Status Solidi (b) **110** (1982) 233.
82Str Strukov, B.A., Spiridonov, T.P., Minaeva, K.A., Fedrikhin, V.A., Davtyan, A.V.: Kristallografiya **27** (1982) 313; Sov. Phys. Crystallogr. (English Transl.) **27** (1982) 190.
82Tyl Tylczynski, Z.: Acta Phys. Pol. A **62** (1982) 373.
83Ami Amin, M., Abd-Elghani, S., Elkonsol, S., Riyad, M.A.: Ferroelectrics **47** (1983) 245.
83Jar Jaroszyk, F., Kudynski, R.: Mater. Sci. **9** (1983) 165.
83Kob Kobayashi, J., Uesu, Y., Takehara, H.: J. Appl. Crystallogr. **16** (1983) 212.
83Kus Kusto, W.J.: Ber. Bunsenges. Phys. Chem. **87** (1983) 284.
83Man Mangin, J., Hadni, A.: Phys. Rev. B **27** (1983) 7730.
83Nov Novik, V.K., Gavrilova, N.D., Galstyan, G.T.: Kristallografiya **28** (1983) 1165; Sov. Phys. Crystallogr. (English Transl.) **28** (1983) 684.
83Str Strukov, B.A., Davtyan, A.V., Minaeva, K.A., Gornaev, A.A.: Izv. Akad. Nauk SSSR, Ser. Fiz. **47** (1983) 611; Bull. Acad. Sci. USSR, Phys. Ser. (English Transl.) **47**, No. 3 (1983) 189.
83Szu Szuba, S.: Acta Phys. Pol. A **64** (1983) 39.
83Tsu Tsujimi, Y., Yagi, T., Tatsuzaki, I.: J. Phys. Soc. Jpn. **52** (1983) 1469.
84Ami Amin, M., Darwish, K.A., Ibrahim, S.S.: Ferroelectrics **59** (1984) 233.
84Bha Bhalla, A.S., Fang, C.S., Cross, L.E., Xi, Y.: Ferroelectrics **54** (1984) 151.
84Dun Dunk, A., Saunders, G.A.: J. Mater. Sci. **19** (1984) 125.
84Had Hadni, A., Thomas, R.: Ferroelectrics **59** (1984) 221.
84Kor Koralewski, M., Habrylo, S.: Ferroelectrics Lett. **2** (1984) 81.
84Pra Pradhan, M.M., Garg, R.K., Arora, M.: Ferroelectrics **56** (1984) 251.
84Sto Stoyanov, S.R., Michailov, M.P., Stankowska, J.: Acta Phys. Pol. A **65** (1984) 141.
84Tak Takayama, Y., Deguchi, K., Nakamura, E.: J. Phys. Soc. Jpn. **53** (1984) 4121.
84Tsu Tsujimi, Y.: J. Phys. Soc. Jpn. **53** (1984) 827.
84Vas Vasil'ev, A.B., Kislovskii, L.D., Mednikov, S.V., Chernov, S.F., Shuvalov, L.A.: Fiz. Tverd. Tela **26** (1984) 893; Sov. Phys. Solid State (English Transl.) **26** (1984) 543.
85Aba Abass, A.K., Al-Eithan, F.Y.M., Misho, R.H.: Phys. Status Solidi (a) **89** (1985) 225.
85Bal Balloomal, L.S., Amin, M., Badawy, M.M.: Ferroelectrics Lett. **4** (1985) 159.
85Bot Böttcher, R., Heinhold, D., Windsch, W.: Chem. Phys. **93** (1985) 339.
85Bre1 Brezina, B., Havrankova, M.: Cryst. Res. Technol. **20** (1985) 781.
85Bre2 Brezina, B., Havrankova, M.: Cryst. Res. Technol. **20** (1985) 787.
85Fer Ferrer-Anglada, N., Filippini, V., Franco, G., Bandet, J.: Jpn. J. Appl .Phys. **24** (1985) Suppl. 24-2, 646.
85Ito Itoh, K., Nishikori, A., Yokomizo, H., Nakamura, E.: Jpn. J. Appl. Phys. **24** (1985) Suppl. 24-2, 594.
85Nak1 Nakatani, N.: Jpn. J. Appl. Phys. **24** (1985) Suppl. 24-2, 583.
85Nak2 Nakatani, N.: Jpn. J. Appl. Phys. **24** (1985) L528.
85Pyk Pykacz, H., Mroz, J.: Acta Phys. Pol. A **67** (1985) 571.
85Sol Solans, X., Franco, F., Miravitlles, C.: Ferroelectrics **62** (1985) 59.
85Vin Vindsh, V., Rakhimov, I., Sarnatskii, V.M., Charnaya, E.V., Shutilov, V.A.: Fiz. Tverd. Tela **27** (1985) 1671; Sov. Phys. Solid State (English Transl.) **27** (1985) 1005.
85Vol Volk, T.R., Rakhimov, I., Sarnatskii, V.M., Charnaya, E.V., Shuvalov, L.A., Shutilov, V.A.: Fiz. Tverd. Tela **27** (1985) 3613; Sov. Phys. Solid State (English Transl.) **27** (1985) 2176.

85Wol Wolniewicz, H.: Mater. Sci. **11** (1985) 27.
85Zav Zavorotnyi, V.F., Poplavko, Yu.M.: Fiz. Tverd. Tela **27** (1985) 3681; Sov. Phys. Solid State (English Transl.) **27** (1985) 2217.
86Bot Böttcher, R., Windsch, W.: Z. Naturforsch. **41a** (1986) 436.
86Che Cheng, Z.-X., Cheng, Y.-F.: Acta Phys. Sin. **35** (1986) 643 (in Chinese).
86Ger Gerbaux, X., Hadni, A.: Ferroelectrics **70** (1986) 175.
86Hat Hatta, I., Ema, K., Kato, R., Maesono, A.: Kotai Butsuri **21** (1986) 277.
86Kur Kuramoto, K., Motegi, H., Nakamura, E., Kosaki, K.: J. Phys. Soc. Jpn. **55** (1986) 377.
86Mey Meyer, K.-P.: Phys. Status Solidi (a) **94** (1986) K1.
86Mil Milovidova, S.D, Sidorkin, A.S., Savvinov, A.M., Maslakov, A.I.: Fiz. Tverd. Tela **28** (1986) 2541; Sov. Phys. Solid State (English Transl.) **28** (1986) 1423.
86Nak Nakatani, N.: Jpn. J. Appl. Phys. **25** (1986) 27.
86Tik Tikhomirova, N.A., Dontsova, L.I., Ginzberg, A.V., Chebotarev, A.A., Shuvalov, L.A.: Fiz. Tverd. Tela **28** (1986) 3319; Sov. Phys. Solid State (English Transl.) **28** (1986) 1869.
86Vik Vikhnin, V.S., Rakhimov, I.K., Sarnatskii, V.M., Charnaya, E.V., Shutilov, V.A.: Kristallografiya **31** (1986) 198; Sov. Phys. Crystallogr. (English Transl.) **31** (1986) 118.
86Vil Villar, R., Gmelin, E., Grimm, H.: Ferroelectrics **69** (1986) 165.
86Zio Ziolo, J., Fugiel, B., Pawlik, J.: Ferroelectrics **70** (1986) 129.
87Bre Brezina, B., Havrankova, M.: Cryst. Res. Technol. **22** (1987) 753.
87Gaf Gaffar, M.A., Mebed, M.M., Abu-El-Fadl, A.: Phys. Status Solidi (a) **104** (1987) 879.
87Jim Jimenez, F., Ramos, S., Del Cerro, J., Jimenez, B.: Cryst. Lattice Defects Amorphous Mater. **15** (1987) 399.
87Per Perez, R., Toribio, E., Gorri, J.A., Benadero, L.: Ferroelectrics **74** (1987) 3.
87Sta Stankowska, J., Jasinski, T.: Acta Phys. Pol. A **71** (1987) 959.
87Suc Suchkova, M.A., Kessenikh, G.G., Kondratkov, A.I., Serdobol'skaya, O.Yu.: Fiz. Tverd. Tela **29** (1987) 2290; Sov. Phys. Solid State (English Transl.) **29** (1987) 1319.
87Tas Tashiro, K., Yagi, N., Kobayashi, M., Kawaguchi, T.: Jpn. J. Appl. Phys. **26** (1987) 699.
87Yus Yushin, N.K., Smirnov, S.I., Turovets, A.G., Linnik, V.G., Agishev, B.A.: Pis'ma Zh. Tekh. Fiz. **13** (1987) 374; Sov. Tech. Phys. Lett. (English Transl.) **13** (1987) 154.
87Zha Zhang, K., Song, J., Wang, M., Fang, C., Lu, M.: J. Cryst. Growth **82** (1987) 639.
88Fug Fugiel, B., Pardala, M., Ziolo, J.: Solid State Commun. **65** (1988) 389.
88Kon1 Kondratkov, A.I., Serdobol'skaya, O.Yu.: Fiz. Tverd. Tela **30** (1988) 649; Sov. Phys. Solid State (English Transl.) **30** (1988) 371.
88Kon2 Kondratkov, A.I., Serdobol'skaya, O.Yu.: Fiz. Tverd. Tela **30** (1988) 1174; Sov. Phys. Solid State (English Transl.) **30** (1988) 678.
88Mro Mroz, M., Bobrowicz, L., Nawrocik, W.: Acta Phys. Pol. A **74** (1988) 767.
88Tik Tikhomirova, N.A., Dontsova, L.I., Ginzberg, A.V., Dorogin, V.I., Shuvalov, L.A., Bulatova, L.G., Chumakova, S.P.: Fiz. Tverd. Tela **30** (1988) 724; Sov. Phys. Solid State (English Transl.) **30** (1988) 414.
88Zhe Zheng, J., Fan, J., Che, Y., Shen, P., Zhang, S., Zhu, Y., Wen, J., Wang, H.: J. Chin. Rare Earth Soc. **6** (1988) 41 (in Chinese).
89DeL De La Pascua, M., Lorenzo, J.E., Gonzalo, J.A.: Acta Phys. Pol. A **76** (1989) 677.
89Don Dontsova, L.I., Tikhomirova, N.A., Shuvalov, L.A.: Ferroelectrics **97** (1989) 87.
89Dvo Dvornikova, A.E., Serdobol'skaya, O.Yu.: Fiz. Tverd. Tela **31** (1989) 223; Sov. Phys. Solid State (English Transl.) **31** (1989) 672.
89Gal Galiyarova, N.M.: Fiz. Tverd. Tela **31** (1989) 248; Sov. Phys. Solid State (English Transl.) **31** (1989) 1977.
89Hil Hilczer, B., Szczesniak, L., Meyer, K.-P.: Ferroelectrics **97** (1989) 59.
89LeB Le Bihan, R.: Ferroelectrics **97** (1989) 19.
89Mat Matyjasek, K., Stankowska, J.: Ferroelectrics **98** (1989) 87.
89Nak Nakatani, N.: Ferroelectrics **97** (1989) 127.
89Oka Okaz, A.M., El-Osaily, M., Kassem, M.E., Hamed, A.E.: Phase Transitions **18** (1989) 35.
89Pop Poprawski, R., Kolarz, A.: J. Phys. Chem. Solids **30** (1989) 693.
89Ram Ramos, S., Jimenez, F., Del Cerro, J.: Phase Transitions **18** (1989) 43.

89Slo Slosarek, G., Heuer, A., Zimmermann, H., Haeberlen, U.: J. Phys. Condens. Matter **1** (1989) 5931.
89Sog Sogr, A.A.: Ferroelectrics **97** (1989) 47.
89Tom Tomita, N., Orihara, H., Ishibashi, Y.: J. Phys. Soc. Jpn. **58** (1989) 1190.
89Tse Tsedrik, M.S., Margolin, L.N., Gontarev, V.F., Misko, A.S.: Cryst. Res. Technol. **24** (1989) 167.
89Wol Wolniewicz, H.: Mater. Sci. **15** (1989) 17.
90Bei Beige, H., Diestelhorst, M., Forster, R., Albers, J., Petersson, J.: Z. Naturforsch. **45a** (1990) 958.
90del de la Pascua, M., Sanz, G., Gonzalo, J.A.: Ferroelectrics **106** (1990) 45.
90Dya Dyakin, V.V., Lysenko, V.N., Ogenko, V.M., Polovina, A.I., Chuiko, A.A.: Dokl. Akad. Nauk SSSR **310** (1990) 579; Sov. Phys. Dokl. (English Transl.) **35** (1990) 58.
90Hal Halacinski, B., Kotlicka, E., Latuszek, A.: Acta Phys. Slovaca **40** (1990) 32.
90Kas Kassem, M.E., Hamed, A.E., Kandil, S.H., Stankowska, J.: Phase Transitions **21** (1990) 49.
90Myt Mytsyk, B.G., Osyka, B.V., Andrushchak, A.S., Petrushko, R.S: Izv. Akad. Nauk SSSR, Ser. Fiz. **54** (1990) 1150; Bull. Acad. Sci. USSR, Phys. Ser. (English Transl.) **54**, No.6 (1990) 121.
90Nak Nakatani, N.: Jpn. J. Appl. Phys. **29** (1990) 2774.
90Ros Rosenman, G.I., Malyshkina, O.V., Chepelev, Yu.L.: Ferroelectrics **110** (1990) 99.
90Sta Stankowska, J., Czarnecka, A., Kwitowska, G.: Ferroelectrics **108** (1990) 325.
90Str Strukov, B.A., Belov, A.A., Sorkin, E.L.: Fiz. Tverd. Tela **32** (1990) 3126; Sov. Phys. Solid State (English Transl.) **32** (1990) 1814.
90Wic Wicker, A., Legrand, J.F., Lotz, B., Wittmann, J.C.: Ferroelectrics **106** (1990) 51.
90Yao Yao, Y., Li, F., Lin, X., Zhao, Z., Wang, M.: Ferroelectrics **101** (1990) 267.
91Bog Bogomolov, A.A., Dabizha, T.A.: Ferroelectrics **118** (1991) 15.
91Cac Cach, R., Mroz, J., Haden, D.: Acta Phys. Pol. A **79** (1991) 905.
91Jim Jimenez, F., Ramos, S., del Cerro, J.: Ferroelectrics **118** (1991) 71.
91Kas Kassem, M.E., Elkhatib, A.M., Hamed, A.E., Kandil, S.H.: Ferroelectrics Lett. **13** (1991) 73.
91Kob Kobayashi, J., Uchino, K., Matsuyama, H., Saito, K.: J. Appl. Phys. **69** (1991) 409.
91Mon Montemezzani, G., Hulliger, J., Günter, P., Fousek, J.: Phys. Status Solidi (a) **127** (1991) 529.
91Mos Mostad, A., Natarajan, S.: Z. Kristallogr. **197** (1991) 209.
91Nak Nakatani, N.: Jpn. J. Appl. Phys. **30** (1991) 1024.
91Nov Novikov, V.N., Novik, V.K., Esengaliev, A.B., Gavrilova, N.D.: Ferroelectrics **118** (1991) 59.
91Sch Schirmer, G., Milsch, B.: Exp. Tech. Phys. **39** (1991) 547.
91Str Strukov, B.A., Belov, A.A., Sorkin, E.L.: Fiz. Tverd. Tela **33** (1991) 691; Sov. Phys. Solid State (English Transl.) **33** (1991) 394.
91Vol Völkel, G., Pöppl, A., Böttcher, R., Metz, H., Simon, T., Klöpperpieper, A.: Ser. Fiz. Uniw. im. Adama Mickiewicza Poznaniu **67** (1991) 153; Radio Microwave Spectrosc. Proc. Conf. RAMIS-91.
91Wol Wolniewicz, H.: Mater. Sci. **17** (1991) 23.
92del de la Pascua, M., Hu, Z., Ramirez, R., Koralewski, M., Gonzalo, J.A.: Ferroelectrics Lett. **14** (1992) 91.
92Dro Drozhdin, S.N., Kamysheva, L.N.: Fiz. Tverd. Tela **34** (1992) 2797; Sov. Phys. Solid State (English Transl.) **34** (1992) 1496.
92Dzi1 Dziedzic, J., Wolniewicz, H.: Mater. Sci. **18** (1992) 81.
92Dzi2 Dziedzic, J., Wolniewicz, H.: Mater. Sci. **18** (1992) 41.
92Elk Elkhatib, A.M., Kassem, M.E., El-Samahy, A.E., Hamed, A.E., Aly, E.H.: Radiat. Eff. Defects Solids **124** (1992) 391.
92FeL Fe Lapena, M., Ramirez, R., Gonzalo, J.A., Koralewski, M.: Ferroelectrics **125** (1992) 1.
92Jim Jimenez-Morales, F.: Ferroelectrics **134** (1992) 213.
92Kor Koralewski, M., Jachnik, W., Jasinski, T.: Ferroelectrics **129** (1992) 165.
92Str Strukov, B.A., Belov, A.A.: Ferroelectrics **126** (1992) 299.
93Cha Charnaya, E.V., Kuleshov, A.A., Radzhabov, A.K., Rakhimov, I.K., Shuvalov, L.A.: Ferroelectrics **143** (1993) 143.
93Dzi Dziedzic, J., Wolniewicz, H.: Mater. Sci. **19** (1993/95) 35.
93Kor Koralewski, M., Noheda, B., Lifante, G., Gonzalo, J.A.: Solid State Commun. **85** (1993) 783.
93Kus Kushnir, O.S., Shopa, Y.I., Vlokh, O.G.: Ferroelectrics **143** (1993) 187.

94Hub Hubert Joe, I., Aruldhas, G., Anbukumar, S., Ramasamy, P.: Cryst. Res. Technol. **29** (1994) 685.
94Igl Iglesias, T., Noheda, B., Lifamte, G., Gonzalo, J.A.: Ferroelectrics Lett. **17** (1994) 47.
94Jim Jimenez, B., Jimenez, R.: Ferroelectrics **154** (1994) 125.
94Kam Kaminsky, W.: Phase Transitions **52** (1994) 235.
94Kor Koralewski, M., Jimenez, B., De Frutos, J., Noheda, B., Gonzalo, J.A.: Ferroelectrics **157** (1994) 263.
94Lal1 Lal, R.B., Batra, A.K., Trolinger, J.D., Wilcox, W.R., Steiner, B.: Ferroelectrics **158** (1994) 81.
94Lal2 Lal, R.B., Etminan, S., Batra, A.K.: Proc. IEEE Int. Symp. Appl. Ferroelectr. **9**th (1994), p. 695.
94Lut Lüthi, R., Haefke, H., Gutmannsbauer, W., Meyer, E., Howald, L., Güntherodt, H.-J.: J. Vac. Sci. Technol. B **12** (1994) 2451.
94Osa Osak, W., Tkacz-Smiech, K., Strzalkowska, C.: Ferroelectrics **158** (1994) 331.
94Prz Przeslawski, J., Iglesias, T., Lifante, G., Gonzalo, J.A.: Ferroelectrics Lett. **18** (1994) 75.
94San Santra, L., Verma, A.L., Bajpai, P.K., Hilczer, B., Huong, P.V.: J. Phys. Chem. Solids **55** (1994) 405.
94Sre Sreekumar, R., Philip, J.: Ferroelectrics **160** (1994) 23.
95Bie Biedrzycki, K., Markowski, L.: Ferroelectrics **172** (1995) 405.
95Blu Bluhm, H., Schwarz, U.D., Meyer, K.-P., Wiesendanger, R.: Appl. Phys. A **61** (1995) 525.
95Fan Fang, C.S., Liu, H., Zhuo, H.S., Wang, M., Xu, D.: Cryst. Res. Technol. **30** (1995) 785.
95Jin1 Jin, B.M., Bhalla, A.S.: Ferroelectrics **173** (1995) 97.
95Jin2 Jin, B.M., Erdei, S., Bhalla, A.S.: Ferroelectrics **173** (1995) 105.
95Kam Kamysheva, L.N., Kosareva, O.A., Drozhdin, S.N., Golitsyna, O.M.: Kristallografiya **40** (1995) 93; Crystallogr. Rep. (English Transl.) **40** (1995) 82.
95Mel Meleshina, V.A., Belugina, N.V., Schlemmbach, H., Windsch, W., Gavrisch, L.: Kristallografiya **40** (1995) 863; Crystallogr. Rep. (English Transl.) **40** (1995) 798.
95Mih Mihaylova, E., Stoyanov, S.: Ferroelectrics **174** (1995) 283.
95Nak Nakatani, N, Hayakawa, K., Inoue, H.: Jpn. J. Appl. Phys. **34** (1995) 5453.
95Oza Ozaki, T., Fujii, K., Ohgami, J.: J. Phys. Soc. Jpn. **64** (1995) 2282.
95Sta Stankowska, J., Czarnecka, A., Mielcarek, S.: Ferroelectrics **172** (1995) 221.
96Cha Chang, J.-M., Batra, A.K., Lal, R.B.: J. Cryst. Growth **158** (1996) 284.
96Ohg Ohgami, J., Sugawara, Y., Morita, S., Nakamura, E., Ozaki, T.: Jpn. J. Appl. Phys. **35** (1996) 5174.
96Sak Sakai, A., Araya, A.: Physica B **219**/**220** (1996) 529.

No. 60A-2 $(NH_2CH_2COOH)_3 \cdot H_2SeO_4$, Triglycine selenate (TGSe)

(M = 370.18; [D: 387.28])

1a Ferroelectricity in TGSe was discovered by Matthias et al. in 1956. 56Mat

b

phase	II	I
state	F	P
crystal system	monoclinic	monoclinic
space group	$P2_1 - C_2^{2}$ [a])	$P2_1/m - C_{2h}^{2}$ [a])
Θ [°C]	22 [D: 35 [b])]	

[a]) 57Pep

[b]) 76Ges1

P_s || [010]
$\rho = 1.845_2 \cdot 10^3$ kg m^{-3} at 20 °C. 57Pep
Transparent, colorless. 58Nit
Cleavage plane: (010).

2a Crystal growth: evaporation or slow cooling from aqueous solution. 58Nit
Solubility in H_2O: see Fig. 60A-1-001 in No. 60A-1.

3a Two axial systems are used as in the case of TGS. See subsection 3a in No. 60A-1.
Unit cell parameters (Hoshino's system):
a = 9.5028(6) Å, b = 12.8279(6) Å, c = 5.8564(4) Å, β = 110.565(6)° at 24 °C (phase I). 79Yam
Table 60A-2-001.
For deuterated crystal (DTGSe), see Table 60A-2-005, Table 60A-2-008.

b Crystal structure: isomorphous with TGS.
Z = 2. 79Yam
Table 60A-2-002, Table 60A-2-003, Table 60A-2-004, Table 60A-2-005, Table 60A-2-006, Table 60A-2-007, Table 60A-2-008. Table 60A-2-009, Table 60A-2-010.

4 Thermal expansion: Fig. 60A-2-001, Fig. 60A-2-002, Fig. 60A-2-003, Fig. 60A-2-004.
For γ-irradiated crystal: Fig. 60A-2-005, Fig. 60A-2-006.

5a Dielectric constant: Fig. 60A-2-007, Fig. 60A-2-008, Fig. 60A-2-009, Fig. 60A-2-010, Fig. 60A-2-011.
Dielectric loss at low frequency: Fig. 60A-2-007;
see also 95Prz, 90Gri, 85Shu
Dielectric constant of γ-irradiated crystal: see 88Sta1, 91Str3
Effect of hydrostatic pressure on dielectric constant: Fig. 60A-2-012, Fig. 60A-2-013, Fig. 60A-2-014, Fig. 60A-2-015; see also 79Kaf, 86Zan
Phase diagram in regard to p: Fig. 60A-2-016, Fig. 60A-2-017.
Phase diagram for deuteration rate: Fig. 60A-2-018.
Tricritical point induced by hydrostatic pressure and deutration: Fig. 60A-2-019.
Effect of uniaxial pressure on dielectric constant: see 92Ham
Effect of uniaxial pressure on Θ_f: Fig. 60A-2-020; see also 92Ham
See also Table 60A-1-012 in No. 60A-1.
Θ_f of γ-irradiated crystal: see 88Sta1
Dielectric properties of α-alanine doped crystal: see 89Sta, 78Var
Dielectric properties of VO^{2+} doped crystal: see 88Cza

b	Nonlinear dielectric properties: Fig. 60A-2-021, Fig. 60A-2-022, Fig. 60A-2-023, Fig. 60A-2-024, Fig. 60A-2-025; see also Fig. 60A-2-010 and Effect of pressure on nonlinear dielectric properties: Fig. 60A-2-026, Fig. 60A-2-027, Fig. 60A-2-028.	80Sch
	See also	89Fug
	Effect of γ-irradiation on dielectric nonlinear properties: see	94Str
	Second harmonic generation due to nonlinear dielectric properties: Fig. 60A-2-029.	
c	Spontaneous polarization: Fig. 60A-2-030, Fig. 60A-2-031; see also Effect of hydrostatic pressure on spontaneous polarization: Fig. 60A-2-032, Fig. 60A-2-033.	94Igl2
	Effect of uniaxial pressure on spontaneous polarization: see	92Ham
	Spontaneous polarization of γ-irradiated crystal: see	88Sta1, 94Str
	Coercive field: see	78Hat
	Coercive field and internal bias field of γ-irradiated crystal: see	88Sta1
d	Pyroelectric properties: see	73Tse, 78Man, 89Wan
6a	Heat capacity: Fig. 60A-2-034, Fig. 60A-2-035; see also Effect of hydrostatic pressure on heat capacity: Fig. 60A-2-036, Fig. 60A-2-037. Heat capacity of γ-irradiated crystal: Fig. 60A-2-038; see also	78Ema 93Str, 94Kas
	Transition entropy: $\Delta S_m = 2.39$ J K^{-1} mol^{-1}.	68Str
b	Thermal conductivity: Fig. 60A-2-039.	
7a	Piezoelectric constant: Fig. 60A-2-040; see also	82Var
8a	Elastic stiffness: Table 60A-2-011; see also Elastic compliance: Fig. 60A-2-041, Fig. 60A-2-042. Ultrasonic wave velocity: Fig. 60A-2-043, Fig. 60A-2-044, Fig. 60A-2-045. Effect of hydrostatic pressure on ultrasonic wave velocity: Fig. 60A-2-046. Ultrasonic wave velocity of γ-irradiated crystal: Fig. 60A-2-047. Absorption coefficient of ultrasonic wave: Fig. 60A-2-048, Fig. 60A-2-049.	83Kha
9a	Refractive index: Fig. 60A-2-050, Fig. 60A-2-051. Birefringence: Fig. 60A-2-052; see also	88Kor2, 80Iva
	Optical axial angle: Fig. 60A-2-053, Fig. 60A-2-054. Infrared absorption: Fig. 60A-2-055; see also Fig. 60A-1-117, Fig. 60A-1-118 in No. 60A-1. Absorption in the ultraviolet region: Fig. 60A-2-056.	
b	Electrooptic constant: see	74Sir
c	Piezooptical effect: see	80Iva
d	Optical activity: Fig. 60A-2-057, Fig. 60A-2-058.	
10a	Raman scattering: Fig. 60A-2-059, Fig. 60A-2-060.	
b	Brillouin scattering: Fig. 60A-2-061; see also	82Yam, 96Fur
11	Electrical conductivity: Fig. 60A-2-062, Fig. 60A-2-063; see also	84Ami

13a	NMR: Table 60A-2-012; Fig. 60A-2-064, Fig. 60A-2-065, Fig. 60A-2-066. Electric field gradient tensor: see	 75Ale, 76Ale
b	ESR for Cr^{3+} doped crystal: see Table 60A-1-028, Fig. 60A-1-161 in No. 60A-1. For Cu^{2+} doped crystal: Table 60A-2-013; see also For γ-irradiated crystal: see	 81Sta 71Suz
15a	Domain structure: 180° domains are observed by means of etching method , powder deposition technique, and nematic liquid crystal method. Fig. 60A-2-067; see also	70Kon 77Hat, 78Sud 79Tik 76Sta
b	Domain switching: Fig. 60A-2-068; see also	89San
16	Etchant for revealing domain: 10 % aqueous solution of ammonia, and mixture of acetic acid and ethyl alcohol.	70Kon 89San

Table 60A-2-001. $(NH_2CH_2COOH)_3 \cdot H_2SeO_4$ (TGSe). Unit cell parameters at T = 17, 27, and 39.6 °C [77Ole].

	17 °C	27 °C	39.6 °C
a [Å]	9.544	9.530	9.540
b [Å]	12.719	12.761	12.845
c [Å]	5.841	5.861	5.863
β [°]	110.46	110.52	110.86

Table 60A-2-002. $(NH_2CH_2COOH)_3 \cdot H_2SeO_4$ (TGSe). Fractional coordinates of nonhydrogen atoms in phase I (24 °C) [79Yam].

	x	y	z
Se	0.9990(1)	0.2500	0.2250(1)
O(1)	0.8433(4)	0.2500	–0.0158(6)
O(2)	0.9636(5)	0.2500	0.4788(6)
O(3)	1.0923(3)	0.1458(2)	0.2036(5)
O(11)	0.5984(4)	0.2500	0.0577(7)
O(12)	0.4820(6)	0.2637(33)	0.6559(7)
C(11)	0.4809(5)	0.2500	0.8594(10)
C(12)	0.3341(5)	0.2500	0.9078(10)
N(1)	0.3385(7)	0.2097(7)	1.1544(12)
O(31)	0.7810(3)	0.4975(3)	0.2349(5)
O(32)	0.5434(3)	0.4763(3)	0.2153(6)
C(31)	0.6877(4)	0.4700(3)	0.3225(7)
C(32)	0.7325(4)	0.4306(3)	0.5786(7)
N(3)	0.8986(4)	0.4294(3)	0.6970(5)

Table 60A-2-003. $(NH_2CH_2COOH)_3 \cdot H_2SeO_4$ (TGSe). Anisotropic temperature parameter for nonhydrogen atoms in phase I (24 °C) [79Yam]. U_{ij} [$\cdot 10^{-2}$ Å^2] is defined by Eq. (d) in Introduction.

	U_{11}	U_{22}	U_{33}	U_{12}	U_{13}	U_{23}
Se	1.83(1)	1.88(2)	2.28(2)	0	1.01(1)	0
O(1)	2.31(15)	5.46(25)	2.60(10)	0	0.70(12)	0
O(2)	4.72(22)	4.01(21)	2.51(15)	0	1.96(15)	0
O(3)	3.95(14)	2.29(11)	5.27(15)	1.05(11)	2.44(12)	0.43(11)
O(11)	2.16(16)	7.05(19)	3.66(19)	0	1.07(14)	0
O(12)	3.94(24)	8.01(201)	3.60(21)	–1.44(19)	1.10(19)	0.52(46)
C(11)	2.42(20)	3.67(26)	3.50(23)	0	1.02(17)	0
C(12)	2.25(20)	4.43(31)	3.97(26)	0	0.94(19)	0
N(1)	2.75(27)	8.16(63)	4.51(33)	1.29(30)	2.13(26)	0.18(33)
O(31)	3.86(13)	6.20(21)	3.80(14)	–0.48(14)	1.20(12)	1.33(14)
O(32)	2.94(13)	6.87(23)	5.22(17)	1.25(15)	0.88(12)	0.99(16)
C(31)	3.21(16)	2.72(16)	4.12(18)	–0.10(14)	1.26(14)	0.03(14)
C(32)	3.70(18)	3.53(19)	3.84(18)	–0.32(15)	1.53(15)	0.24(15)
N(3)	4.16(16)	3.22(16)	2.68(13)	–0.49(13)	0.77(12)	0.21(12)

Table 60A-2-004. $(NH_2CH_2COOH)_3 \cdot H_2SeO_4$ (TGSe). Fractional coordinates and mean square displacements of hydrogens in phase I (24 °C) [79Yam].

	x	*y*	*z*	$\overline{u^2}$ [10^{-2} Å^2]
H(1)	0.687(11)	0.250	1.012(18)	6.6(33)
H(2)	0.281(7)	0.316(5)	0.851(11)	6.0(20)
H(4)	0.412(9)	0.149(7)	1.175(14)	0.5(19)
H(5)	0.256(10)	0.183(7)	1.200(16)	2.0(24)
H(6)	0.398(10)	0.250	1.174(16)	5.4(28)
H(7)	0.531(8)	0.489(6)	0.088(12)	0.0(16)
H(13)	0.689(6)	0.472(5)	0.675(10)	4.1(17)
H(14)	0.699(6)	0.365(5)	0.588(10)	4.1(17)
H(15)	0.936(6)	0.496(4)	0.715(10)	3.3(15)
H(16)	0.910(5)	0.397(4)	0.836(9)	2.4(13)
H(17)	0.937(8)	0.387(6)	0.616(12)	7.0(24)

Table 60A-2-005. $(ND_2CH_2COOD)_3 \cdot D_2SeO_4$ (DTGSe). Fractional coordinates of nonhydrogen atoms in phase I (37 °C) [79Yam]. Unit cell parameters: a = 9.5118(8) Å, b = 12.8321(6) Å, c = 5.8557(5) Å, β = 110.539(5)°.

	x	*y*	*z*
Se	0.9987(0)	0.2500	0.2242(1)
O(1)	0.8436(3)	0.2500	–0.0166(5)
O(2)	0.9627(4)	0.2500	0.4753(5)
O(3)	1.0926(2)	0.1462(2)	0.2039(4)
O(11)	0.5980(3)	0.2500	0.0568(5)
O(12)	0.4818(5)	0.2517(36)	0.6554(7)
C(11)	0.4793(4)	0.2500	0.8593(8)
C(12)	0.3347(4)	0.2500	0.9089(8)
N(1)	0.3584(5)	0.2082(5)	1.1529(9)
O(31)	0.7807(2)	0.4973(2)	0.2342(4)
O(32)	0.5445(2)	0.4720(2)	0.2162(4)
C(31)	0.6882(3)	0.4706(2)	0.3225(5)
C(32)	0.7342(3)	0.4299(3)	0.5803(6)
N(3)	0.8983(3)	0.4302(2)	0.6968(4)

Table 60A-2-006. $(ND_2CH_2COOD)_3 \cdot D_2SeO_4$ (DTGSe). Anisotropic temperature parameters for nonhydrogen atoms in phase I (37 °C) [79Yam]. U_{ij} [$\cdot 10^{-2}$ Å^2] is defined by Eq. (d) in Introduction.

	U_{11}	U_{22}	U_{33}	U_{12}	U_{13}	U_{23}
Se	1.96(1)	1.87(1)	2.31(1)	0	0.83(1)	0
O(1)	2.36(12)	6.12(20)	2.53(13)	0	0.46(10)	0
O(2)	4.89(17)	4.03(16)	2.67(13)	0	1.90(13)	0
O(3)	4.04(11)	2.51(9)	5.51(12)	1.04(8)	2.14(10)	0.20(9)
O(11)	2.26(13)	7.95(25)	3.57(15)	0	0.89(11)	0
O(12)	4.60(21)	9.72(179)	3.76(18)	1.59(71)	1.35(16)	–0.96(55)
C(11)	2.43(17)	3.79(21)	4.09(21)	0	0.75(15)	0
C(12)	2.32(17)	4.52(24)	4.24(22)	0	0.81(16)	0
N(1)	3.01(23)	7.90(45)	4.02(25)	0.84(24)	1.75(20)	0.63(25)
O(31)	3.88(11)	5.85(15)	4.15(11)	–0.38(11)	1.04(9)	1.39(11)
O(32)	3.30(11)	6.96(18)	5.74(14)	1.16(12)	0.78(10)	0.75(13)
C(31)	3.48(13)	3.05(14)	4.18(15)	0.43(11)	0.92(12)	0.09(12)
C(32)	4.06(16)	3.91(16)	4.28(16)	–0.18(13)	1.70(13)	0.47(13)
N(3)	4.47(13)	2.89(11)	2.65(10)	–0.36(10)	0.52(9)	0.25(9)

Table 60A-2-007. $(ND_2CH_2COOD)_3 \cdot D_2SeO_4$ (DTGSe). Fractional coordinates and mean square displacements of hydrogens and deuteriums in phase I (37 °C) [79Yam].

	x	y	z	$\overline{u^2}$ [10^{-2} Å^2]
D(1)	0.693(6)	0.250	1.021(10)	3.0(15)
H(2)	0.275(5)	0.312(3)	0.841(7)	5.1(14)
D(4)	0.432(9)	0.363(7)	1.175(14)	4.4(25)
D(5)	0.264(9)	0.316(6)	1.169(14)	4.6(26)
D(6)	0.399(8)	0.250	1.275(13)	7.4(25)
D(7)	0.516(19)	0.490(15)	0.065(25)	3.8(46)
H(13)	0.694(4)	0.473(3)	0.684(6)	1.7(09)
H(14)	0.695(4)	0.363(3)	0.577(6)	2.5(10)
D(15)	0.932(4)	0.494(3)	0.706(7)	1.7(10)
D(16)	0.924(4)	0.409(3)	0.836(6)	2.6(10)
D(17)	0.937(5)	0.386(4)	0.609(6)	5.4(14)

Table 60A-2-008. $(ND_2CH_2COOD)_3 \cdot D_2SeO_4$ (DTGSe). Fractional coordinates of nonhydrogen atoms in phase II (21 °C) [79Yam]. Unit cell parameters: a = 9.415(2) Å, b = 12.836(2) Å, c = 5.839(1) Å, β = 110.547(19)°.

	x	y	z
Se	0.99847(5)	0.25000(0)	0.22525(7)
O(1)	0.8429(4)	0.2492(11)	–0.0152(6)
O(2)	0.9632(4)	0.2473(11)	0.4791(6)
O(3)	1.0893(9)	0.1501(7)	0.1973(19)
O(4)	1.0951(10)	0.3570(6)	0.2118(20)
O(11)	0.5986(4)	0.2611(12)	1.0605(7)
O(12)	0.4821(6)	0.2695(9)	0.6577(8)
C(11)	0.4809(6)	0.2599(16)	0.8635(10)
C(12)	0.3351(5)	0.2588(16)	0.9116(10)
N(1)	0.3597(6)	0.2132(5)	1.1579(10)
O(21)	0.2204(10)	0.5109(8)	0.7777(20)
O(22)	0.4588(10)	0.5373(7)	0.8096(16)
C(21)	0.3191(13)	0.5343(11)	0.6868(22)
C(22)	0.2827(12)	0.5746(12)	0.4360(23)
N(2)	0.1132(11)	0.5734(7)	0.3008(18)
O(31)	0.7834(11)	0.5048(8)	0.2450(19)
O(32)	0.5504(11)	0.4847(8)	0.2450(17)
C(31)	0.6965(14)	0.4748(10)	0.3334(27)
C(32)	0.7474(10)	0.4342(8)	0.5990(19)
N(3)	0.9125(11)	0.4335(9)	0.6977(21)

Table 60A-2-009. $(ND_2CH_2COOD)_3 \cdot D_2SeO_4$ (DTGSe). Anisotropic temperature parameters for nonhydrogen atoms in phase II (21 °C) [79Yam]. U_{ij} [$\cdot 10^{-2}$ Å^2] is defined by Eq. (d) in Introduction.

	U_{11}	U_{22}	U_{33}	U_{12}	U_{13}	U_{23}
Se	1.790(15)	1.646(14)	2.044(15)	–0.231(45)	1.155(17)	–0.050(40)
O(1)	2.26(14)	5.19(26)	2.53(13)	–0.66(45)	0.70(16)	–0.28(34)
O(2)	4.29(19)	3.41(24)	2.30(13)	–0.91(40)	2.80(19)	–0.42(25)
O(3)	2.65(34)	2.88(40)	4.28(45)	1.31(28)	1.43(43)	0.24(23)
O(4)	4.24(47)	1.37(30)	5.36(50)	–0.62	4.02	–0.23
O(11)	2.05(15)	7.04(50)	3.43(17)	0.85(37)	1.24(18)	0.39(27)
O(12)	4.37(24)	8.05(80)	3.58(20)	–1.74(36)	1.98(26)	0.04(21)
C(11)	2.54(20)	4.52(56)	3.32(21)	0.69(45)	1.48(23)	–0.21(32)
C(12)	2.04(18)	3.74(40)	4.06(23)	0.20(47)	1.21(23)	0.46(36)
N(1)	1.76(21)	6.32(39)	3.84(26)	0.65(21)	0.21(27)	0.54(16)
O(21)	2.55(35)	4.78(41)	3.65(39)	–0.43(29)	1.07(39)	0.44(21)
O(22)	2.74(27)	3.95(31)	4.79(42)	0.55(22)	0.53(37)	–0.15(19)
C(21)	3.14(45)	3.19(50)	2.73(36)	0.44(37)	1.54(45)	0.35(23)
C(22)	2.71(43)	5.41(57)	3.05(41)	–0.08(39)	0.53(45)	0.22(25)
N(2)	5.73(38)	1.99(28)	2.15(28)	–0.74(25)	1.10(35)	0.00(15)
O(31)	4.11(43)	5.41(44)	3.15(35)	–0.50(33)	1.63(41)	1.23(21)
O(32)	3.07(33)	7.34(64)	4.65(42)	1.33(36)	1.74(40)	0.71(27)
C(31)	2.40(39)	2.02(38)	6.06(67)	0.26(29)	1.23(54)	0.46(27)
C(32)	1.86(30)	2.84(31)	2.89(35)	–0.32(24)	1.16(37)	0.53(17)
N(3)	2.85(32)	3.62(41)	2.68(35)	–0.45(20)	0.53(36)	0.57(20)

Table 60A-2-010. $(ND_2CH_2COOD)_3 \cdot D_2SeO_4$ (DTGSe). Fractional coordinates and mean square displacements of hydrogens and deuteriums in phase II (21 °C) [79Yam].

	x	y	z	$\overline{u^2}$ [10^{-2} Å^2]
D(1)	0.695(7)	0.260(15)	1.012(11)	1.6(18)
H(2)	0.274(14)	0.313(11)	0.812(24)	3.8(45)
H(3)	0.286(15)	0.188(12)	0.894(25)	4.8(45)
D(4)	0.430(12)	0.151(10)	1.188(19)	5.2(34)
D(5)	0.248(14)	0.192(10)	1.177(22)	7.6(44)
D(6)	0.417(13)	0.222(12)	1.364(20)	8.2(47)
D(7)	0.473(16)	0.482(12)	0.920(22)	9.2(52)
H(8)	0.311(14)	0.519(11)	0.329(25)	1.9(39)
H(9)	0.293(21)	0.640(14)	0.431(34)	5.0(61)
D(10)	0.075(15)	0.496(9)	0.289(26)	1.1(35)
D(11)	0.070(19)	0.605(13)	0.189(32)	4.0(51)
D(12)	0.048(19)	0.607(12)	0.424(30)	3.9(33)
H(13)	0.697(15)	0.484(11)	0.709(25)	1.7(39)
H(14)	0.709(19)	0.358(13)	0.358(33)	3.4(51)
D(15)	0.925(18)	0.500(11)	0.681(31)	4.4(52)
D(16)	0.927(22)	0.409(14)	0.854(34)	6.6(65)
D(17)	0.942(19)	0.388(12)	0.589(29)	3.3(00)

Table 60A-2-011. $(NH_2CH_2COOH)_3 \cdot H_2SeO_4$ (TGSe). Elastic stiffness constant $c_{\lambda\mu}$ [$\cdot 10^{10}$ N m^{-2}] at 30 °C [78Min].

c_{11}	3.42(6)	c_{12}	–2.30(80)
c_{22}	3.10(6)	c_{13}	1.33(6)
c_{33}	2.27(4)	c_{15}	0.21(2)
c_{44}	0.81(2)	c_{23}	1.76(60)
c_{55}	1.10(2)	c_{25}	–0.70(25)
c_{66}	0.52(1)	c_{35}	–0.50(5)
		c_{46}	0.14(1)

Table 60A-2-012. $(NH_2CH_2COOH)_3 \cdot H_2SeO_4$ (TGSe). Principal components of ^{77}Se chemical shift and their direction cosines with respect to the a^*, b, c frame [80Mos]. σ_{av}: average of the principal components, $\Delta\sigma = \sigma_{zz} - (\sigma_{xx} + \sigma_{yy})/2$, $\eta = (\sigma_{yy} - \sigma_{xx})/(\sigma_{zz} - \sigma_{av})$. The a^* axis is normal to the bc plane.

T [°C]	Principal components of the chemical shift tensor relative to liquid H_2SeO_4		Direction cosines			σ_{av}	Anisotropy $\Delta\sigma$	Anisotropy parameter η
		[10^{-6}]						
30 °C	σ_{xx}	17	–0.378,	0,	0.926			
(phase I)	σ_{yy}	–13	0,	1.0,	0	–17(3)	–56	0.8
	σ_{zz}	–54	–0.926,	0,	0.378			
–12 °C	$\sigma_{xx}(1)$	19	–0.395,	0.442,	0.806			
(phase II)	$\sigma_{yy}(1)$	–15	–0.123,	0.844,	–0.523	–16	–54	0.94
	$\sigma_{zz}(1)$	–52	0.910,	0.305,	0.279			
	$\sigma_{xx}(2)$	20	–0.391,	–0.463,	0.795			
	$\sigma_{yy}(2)$	–15	0.106,	0.836,	0.539	–15	–53	0.98
	$\sigma_{zz}(2)$	–51	0.914,	–0.295,	0.278			

Table 60A-2-013. $(NH_2CH_2COOH)_3 \cdot H_2SeO_4$ (TGSe). Spin Hamiltonian parameters of the $^{63}Cu^{2+}$ glycine complex and direction cosines of the local crystal field axes in a^*, b, c frame [96Hof]. The a^* axis is normal to the bc plane.

g	A [10^{-2} m^{-1}]
$g_z = 2.2596(3)$	$A_z = 151.2(5)$
$g_y = 2.0647(5)$	$A_y = 2.5(5)$
$g_x = 2.0529(5)$	$A_z = 42.2(5)$

	Direction cosines		
	a^*	b	c
Z	0.1771	± 0.8309	–0.5273
Y	0.8213	± 0.1701	0.5442
X	0.5380	± 0.5304	–0.6561

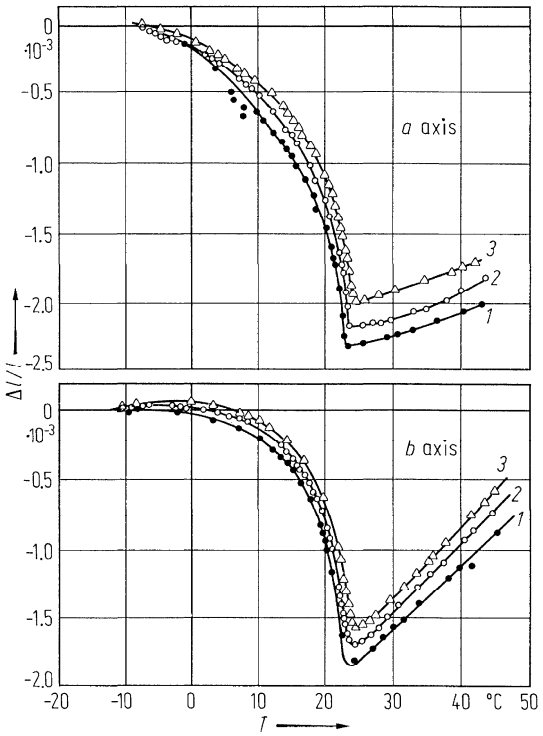

Fig. 60A-2-001. $(NH_2CH_2COOH)_3 \cdot H_2SeO_4$ (TGSe). $\Delta l/l$ vs. T [73Var]. $\Delta l/l$: linear thermal expansion. Parameter: E_{bias}. Curve *1*: $E_{bias} = 0$; *2*: $E_{bias} = 50$ kV m^{-1}; *3*: $E_{bias} = 200$ kV m^{-1}.

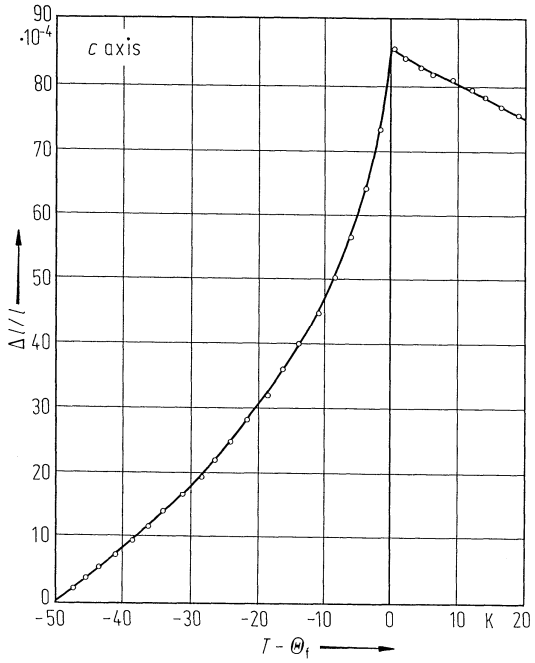

Fig. 60A-2-002. $(NH_2CH_2COOH)_3 \cdot H_2SeO_4$ (TGSe). $\Delta l/l$ vs. $T - \Theta_f$ [80Sta]. $\Delta l/l$: linear thermal expansion along the *c* axis.

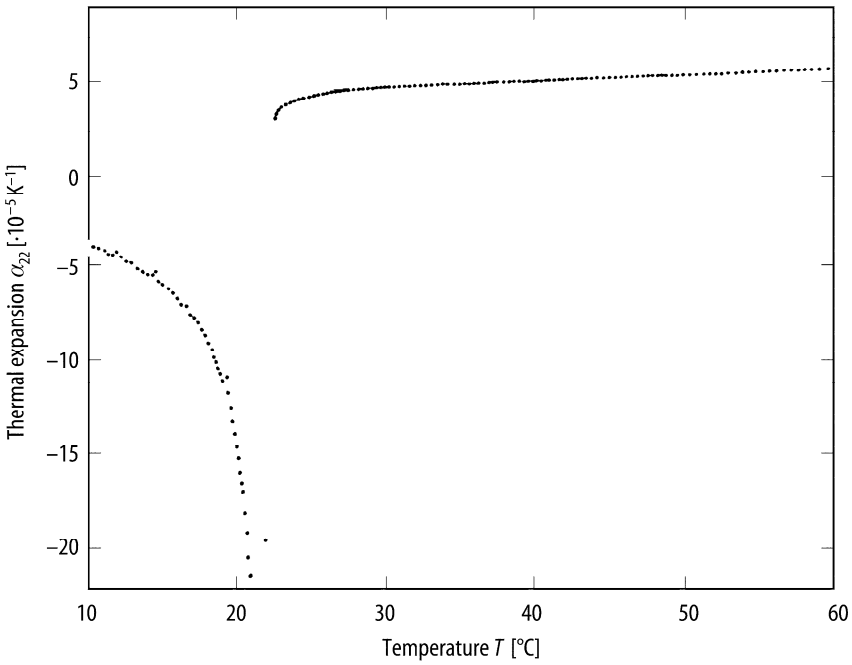

Fig. 60A-2-003. $(NH_2CH_2COOH)_3 \cdot H_2SeO_4$ (TGSe). α_{22} vs. T [80Deg]. α_{22}: linear thermal expansion coefficients along the *b* axis.

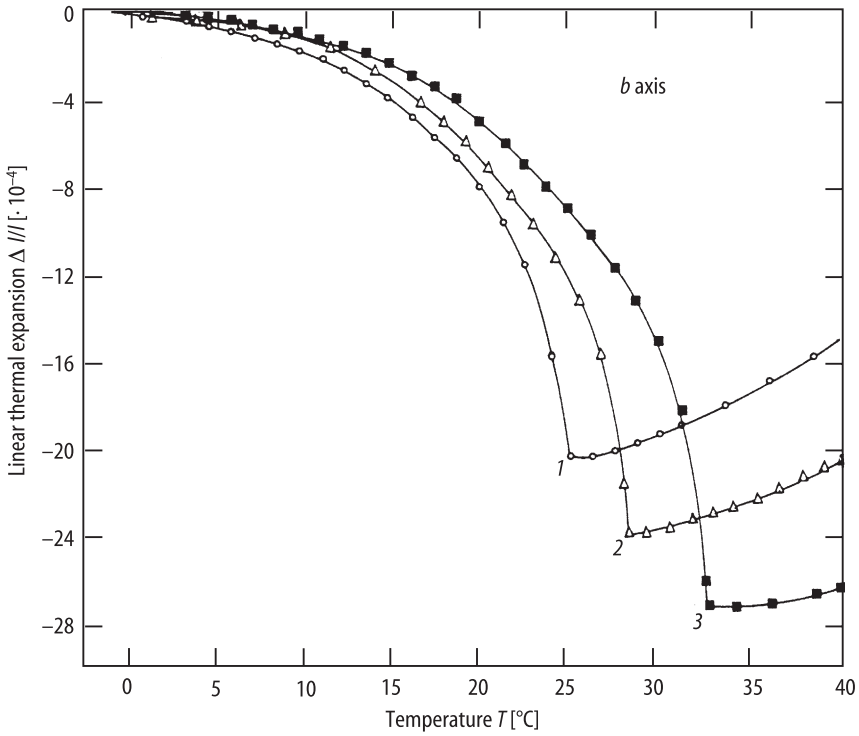

Fig. 60A-2-004. $[(NH_2CH_2COOH)_3 \cdot H_2SeO_4]_{1-x}[(ND_2CH_2COOD)_3 \cdot D_2SeO_4]_x$ ($TGSe_{1-x}DTGSe_x$). $\Delta l/l$ vs. T [90Ham]. $\Delta l/l$: linear thermal expansion along the *b* axis. Parameter: x. Curve *1*: x = 0.35; *2*: x = 0.65; *3*: x = 0.90.

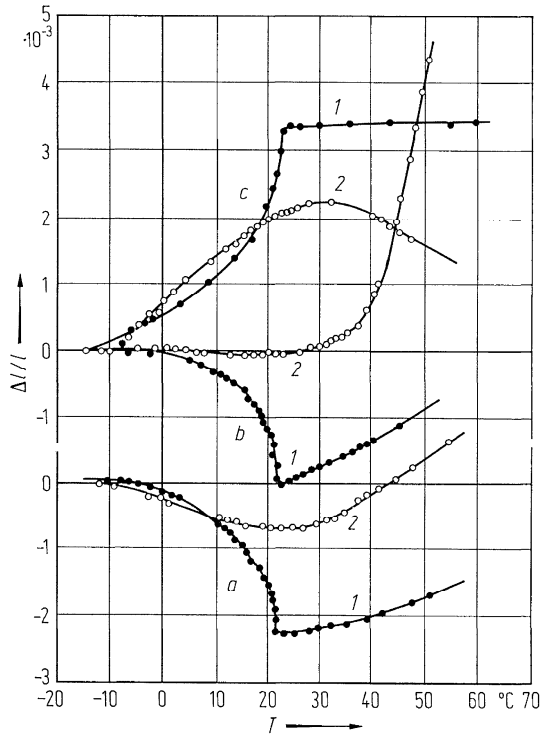

Fig. 60A-2-005. $(NH_2CH_2COOH)_3 \cdot H_2SeO_4$ (TGSe). $\Delta l/l$ vs. T [73Var]. $\Delta l/l$: linear thermal expansion along the a, b, c axes. Curves *1*: before γ-irradiation. Curves *2*: after γ-irradiation of 500 mR.

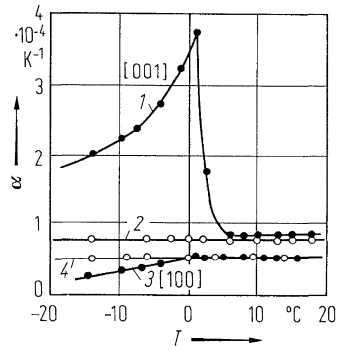

Fig. 60A-2-006. $(NH_2CH_2COOH)_3 \cdot H_2SeO_4$ (TGSe). α vs. T [73Var]. α: linear thermal expansion coefficients along the [100] and [001] directions. Curves *1*, *3*: before γ-irradiation. Curves *2*, *4*: after γ-irradiation of 500 mR.

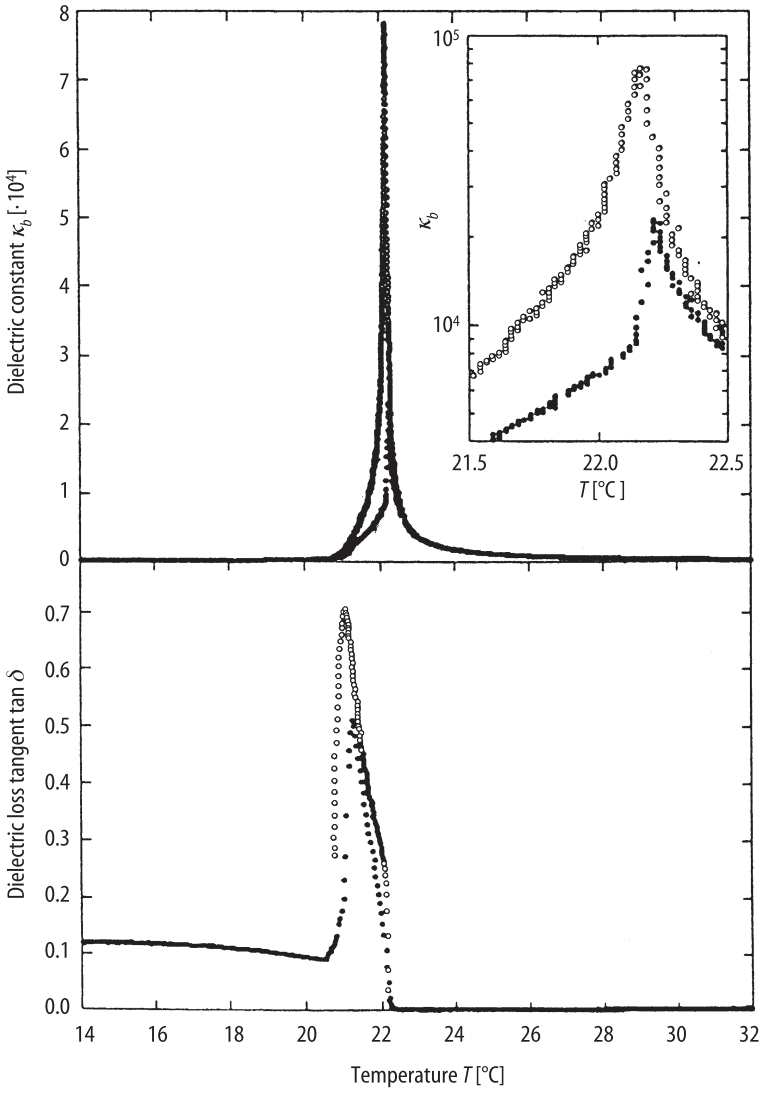

Fig. 60A-2-007. $(NH_2CH_2COOH)_3 \cdot H_2SeO_4$ (TGSe). κ_b, tan δ vs. T [94Igl1]. f = 1 kHz. Full circle: heating; open circle: cooling.

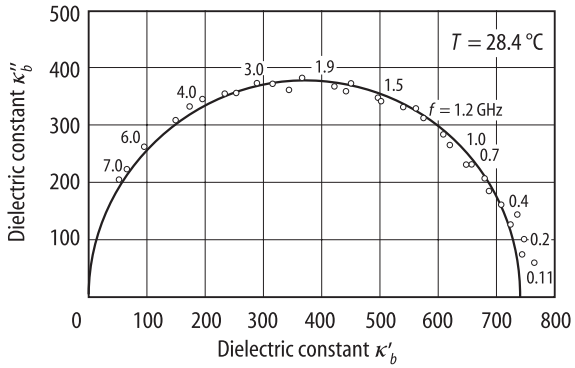

Fig. 60A-2-008. $(NH_2CH_2COOH)_3 \cdot H_2SeO_4$ (TGSe). Cole-Cole plot of the complex dielectric constant [74Lut].

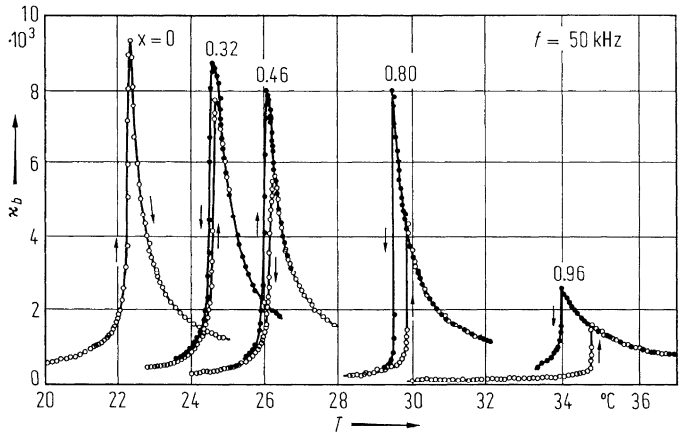

Fig. 60A-2-009. $[(NH_2CH_2COOH)_3 \cdot H_2SeO_4]_{1-x}[(ND_2CH_2COOD)_3 \cdot D_2SeO_4]_x$ ($TGSe_{1-x}DTGSe_x$). κ_b vs. T [76Ges1]. Parameter: x.

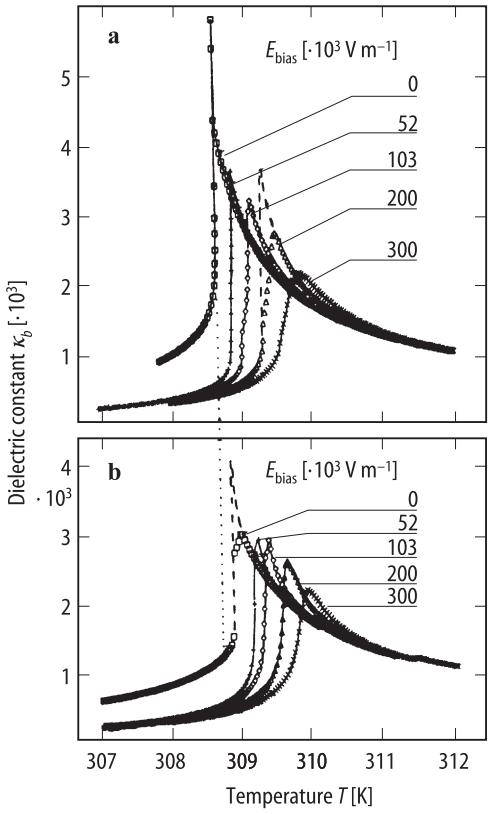

Fig. 60A-2-010. $(ND_2CH_2COOD)_3 \cdot D_2SeO_4$ (DTGSe). κ_b vs. T [95Fug]. Parameter: E_{bias}. (**a**) heating; (**b**) cooling. Amplitude of applied ac field is 44 V m^{-1}. f = 1 kHz.

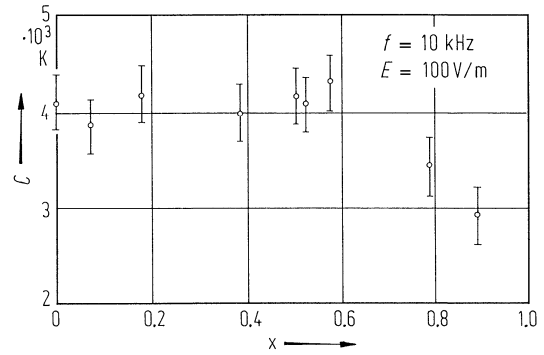

Fig. 60A-2-011. $[(NH_2CH_2COOH)_3 \cdot H_2SeO_4]_{1-x}[(ND_2CH_2COOD)_3 \cdot D_2SeO_4]_x$ ($TGSe_{1-x}DTGSe_x$). *C* vs. x [82Tak]. *C*: Curie-Weiss constant.

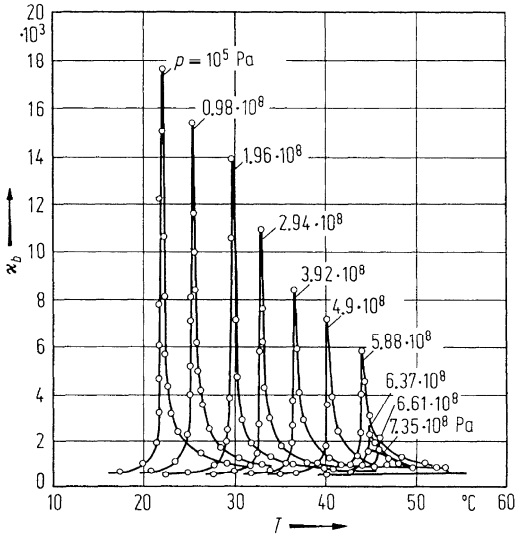

Fig. 60A-2-012. $(NH_2CH_2COOH)_3 \cdot H_2SeO_4$ (TGSe). κ_b vs. *T* [68Pol2]. Parameter: *p*.

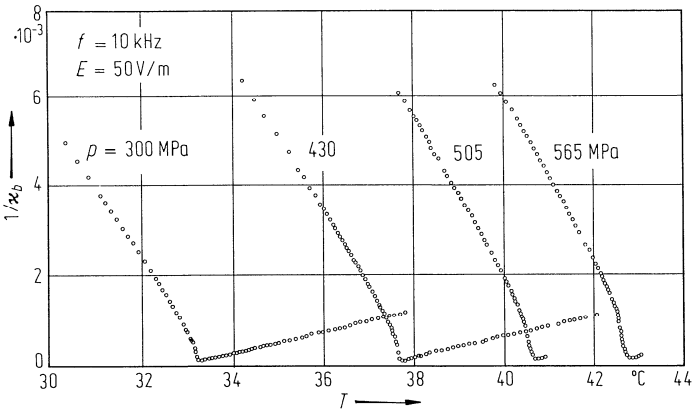

Fig. 60A-2-013. $(NH_2CH_2COOH)_3 \cdot H_2SeO_4$ (TGSe). κ_b^{-1} vs. *T* [80Yam]. Parameter: hydrostatic pressure, *p*.

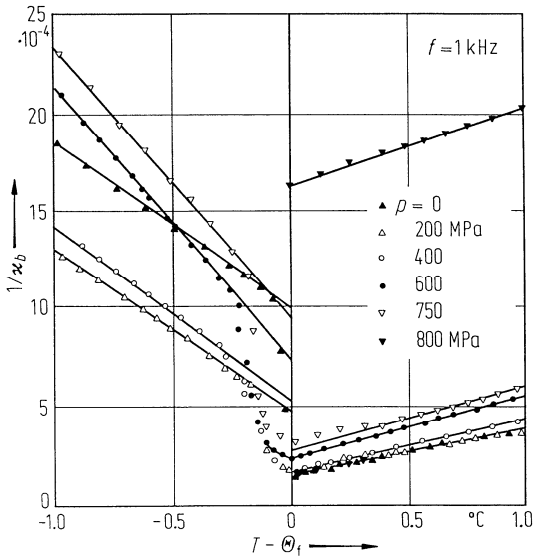

Fig. 60A-2-014. Deuterated triglycine selenate (DTGSe). κ_b^{-1} vs. $T - \Theta_t$ [79Che2]. Parameter: hydrostatic pressure, p.

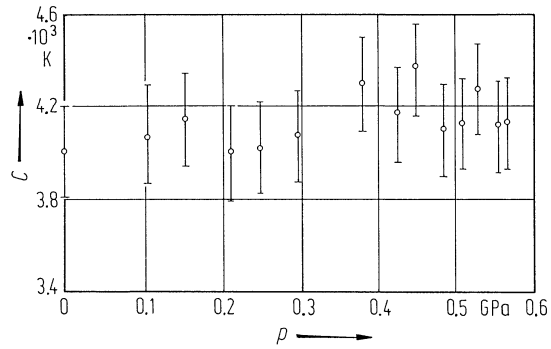

Fig. 60A-2-015. $(NH_2CH_2COOH)_3 \cdot H_2SeO_4$ (TGSe). C vs. p [80Yam]. C: Curie-Weiss constant, p: hydrostatic pressure.

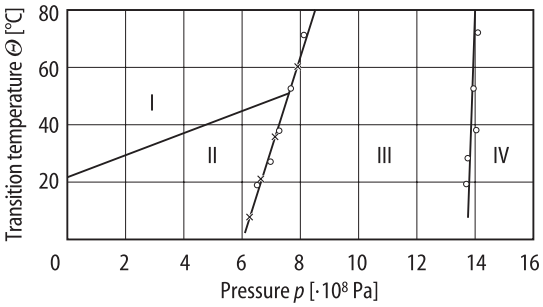

Fig. 60A-2-016. $(NH_2CH_2COOH)_3 \cdot H_2SeO_4$ (TGSe). Phase diagram [70Myl]. Full circle: by [70Myl], cross: by [68Pol1].

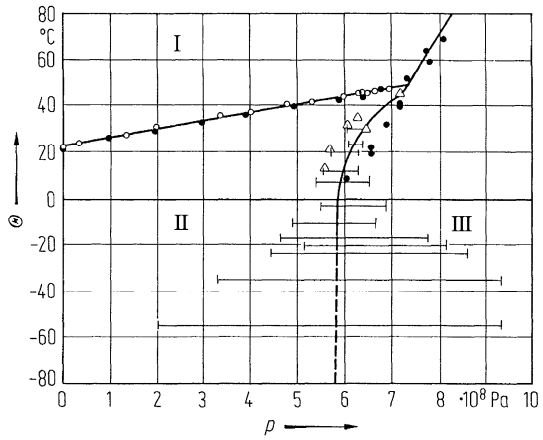

Fig. 60A-2-017. $(NH_2CH_2COOH)_3 \cdot H_2SeO_4$ (TGSe). Phase diagram. Full circles, triangles: [68Pol2]; open circles, bars: [74Ges].

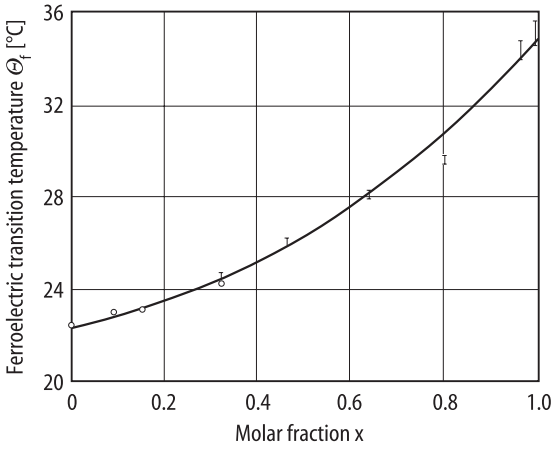

Fig. 60A-2-018. $[(NH_2CH_2COOH)_3 \cdot H_2SeO_4]_{1-x}[(ND_2CH_2COOD)_3 \cdot D_2SeO_4]_x$ ($TGSe_{1-x}DTGSe_x$). Θ_f vs. x [76Ges1]. Vertical bars show thermal hysteresis of the ferroelectric transition.

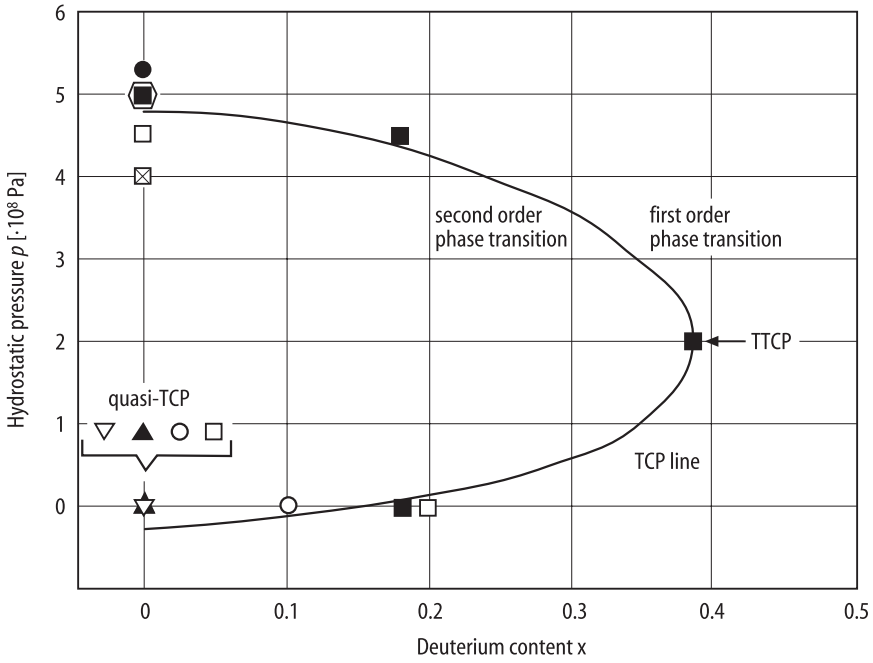

Fig. 60A-2-019. $[(NH_2CH_2COOH)_3 \cdot H_2SeO_4]_{1-x}[(ND_2CH_2COOD)_3 \cdot D_2SeO_4]_x$ ($TGSe_{1-x}DTGSe_x$). Tricritical line in the *p*-x space [96Kor]. *p*: hydrostatic pressure, x: deuterium content. TTCP: tetracritical point. Open squares: [76Shu]; open circles: [76Ges1]; full circle [76Ges2]; full triangle: [77Hat]; crossed square: [79Che1]; hexagon: [80Yam]; full squares: [82Tak]; open triangle: [94Igl1].

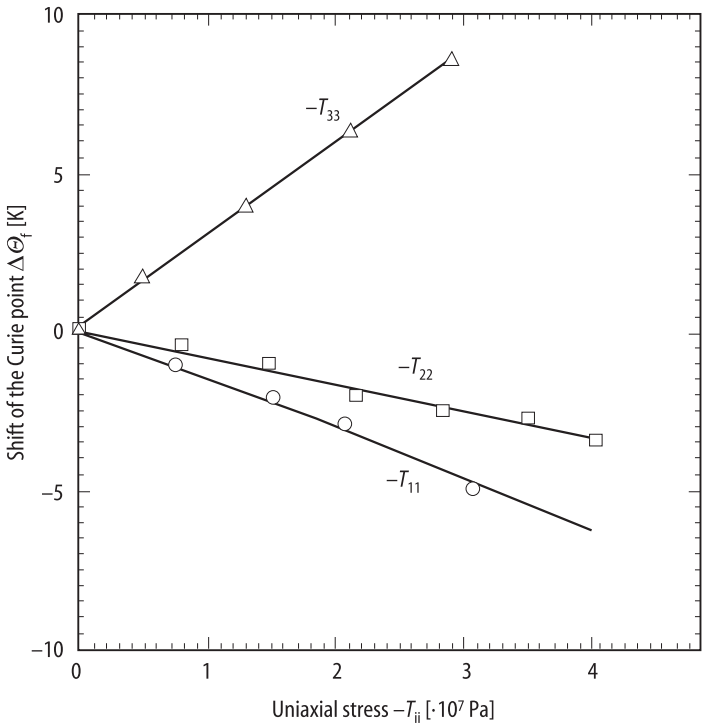

Fig. 60A-2-020. $(NH_2CH_2COOH)_3 \cdot H_2SeO_4$ (TGSe). $\Delta\Theta_f$ vs. $-T_{ii}$ [96Kor]. $\Delta\Theta_f$: shift of the Curie point, $-T_{ii}$: uniaxial stress. The orthogonal axial system ($x, y \parallel b, z \parallel c$) is adopted.

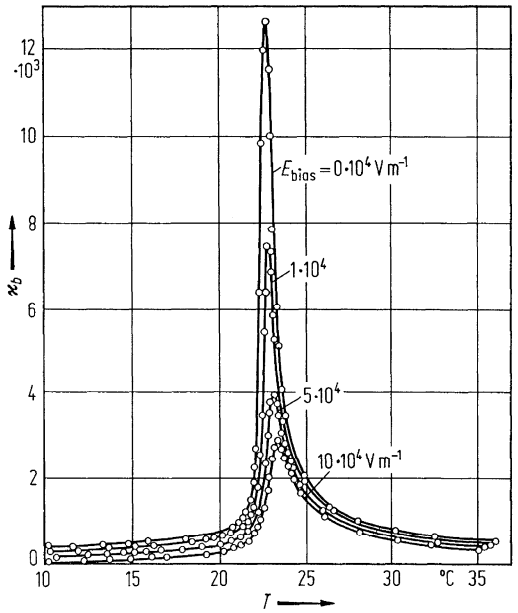

Fig. 60A-2-021. $(NH_2CH_2COOH)_3 \cdot H_2SeO_4$ (TGSe). $\varkappa_b$ vs. T [71Zar]. Parameter: E_{bias}.

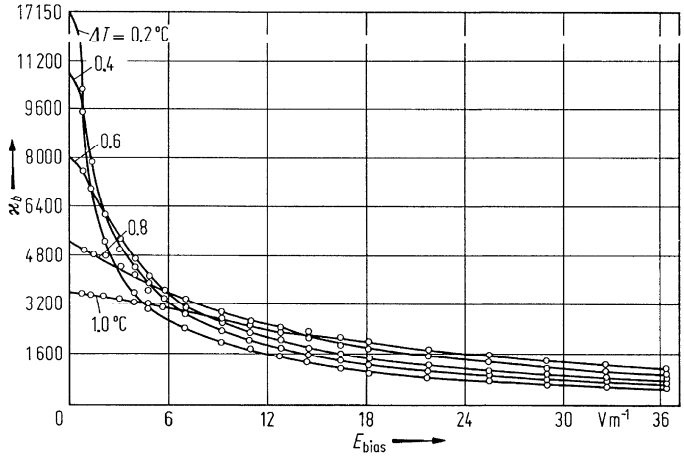

Fig. 60A-2-022. $(NH_2CH_2COOH)_3 \cdot H_2SeO_4$ (TGSe). $\varkappa_b$ vs. E_{bias} [71Zar]. Parameter: $\Delta T = T - \Theta_f$.

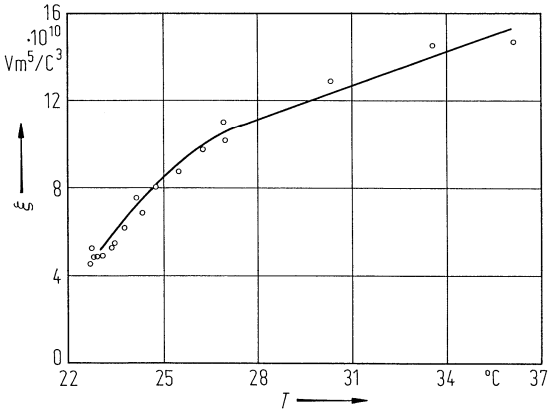

Fig. 60A-2-023. $(NH_2CH_2COOH)_3 \cdot H_2SeO_4$ (TGSe). ξ vs. T [80Sch]. ξ: coefficient of power series expansion of electric field strength, $E = (1/\chi_p)P + \xi P^3 + \zeta P^5$.

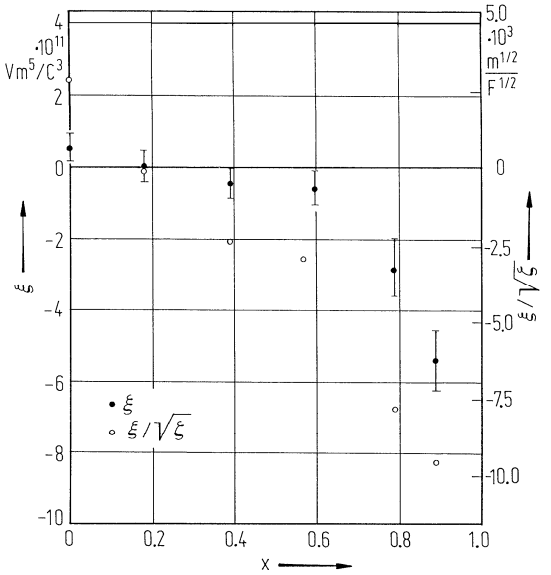

Fig. 60A-2-024. $[(NH_2CH_2COOH)_3 \cdot H_2SeO_4]_{1-x}[(ND_2CH_2COOD)_3 \cdot D_2SeO_4]_x$ ($TGSe_{1-x}DTGSe_x$). ξ, $\xi/\sqrt{\zeta}$ vs. x [82Tak]. ξ, ζ: coefficients of power series expansion of electric field strength, see caption of Fig. 60A-2-023.

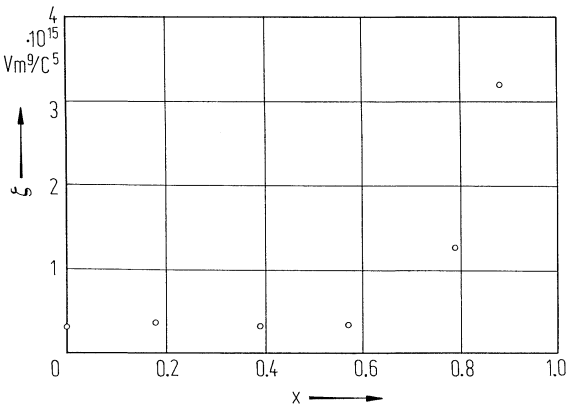

Fig. 60A-2-025. $[(NH_2CH_2COOH)_3 \cdot H_2SeO_4]_{1-x}[(ND_2CH_2COOD)_3 \cdot D_2SeO_4]_x$ ($TGSe_{1-x}DTGSe_x$). ζ vs. x [82Tak]. ζ: coefficient of power series expansion of electric field strength, see caption of Fig. 60A-2-023.

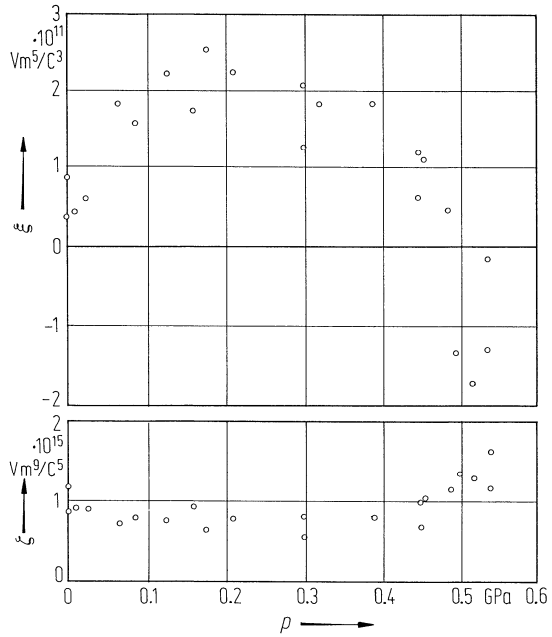

Fig. 60A-2-026. $(NH_2CH_2COOH)_3 \cdot H_2SeO_4$ (TGSe). ξ, ζ vs. p [80Sch]. ξ, ζ: coefficients of power series expansion of electric field strength, see caption of Fig. 60A-2-023. p: hydrostatic pressure.

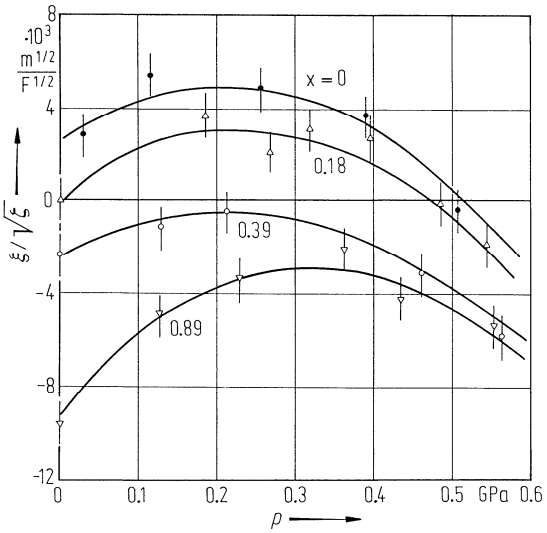

Fig. 60A-2-027. $[(NH_2CH_2COOH)_3 \cdot H_2SeO_4]_{1-x}[(ND_2CH_2COOD)_3 \cdot D_2SeO_4]_x$ ($TGSe_{1-x}DTGSe_x$). $\xi/\sqrt{\zeta}$ vs. p [82Tak]. Parameter: x. ξ, ζ: coefficients of power series expansion of electric field strength, see caption of Fig. 60A-2-023. p: hydrostatic pressure.

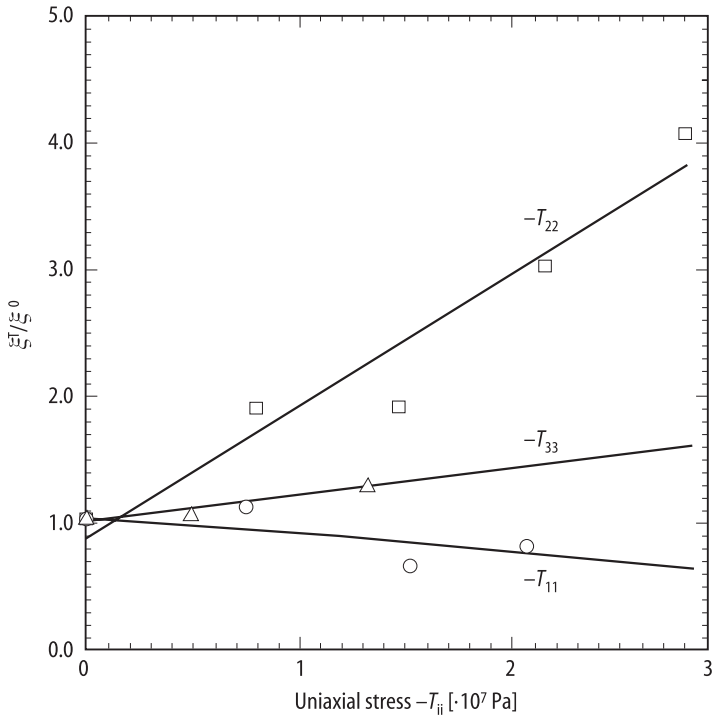

Fig. 60A-2-028. $(NH_2CH_2COOH)_3 \cdot H_2SeO_4$ (TGSe). ξ^T/ξ^0 vs. $-T_{ii}$ [96Kor]. $-T_{ii}$: uniaxial stress. The orthogonal axial system (x, $y \parallel b$, $z \parallel c$) is adopted. ξ^T, ξ^0: coefficient of power series expansion of electric field strength under uniaxial stress $-T_{ii}$ and no pressure, respectively, see caption of Fig. 60A-2-023.

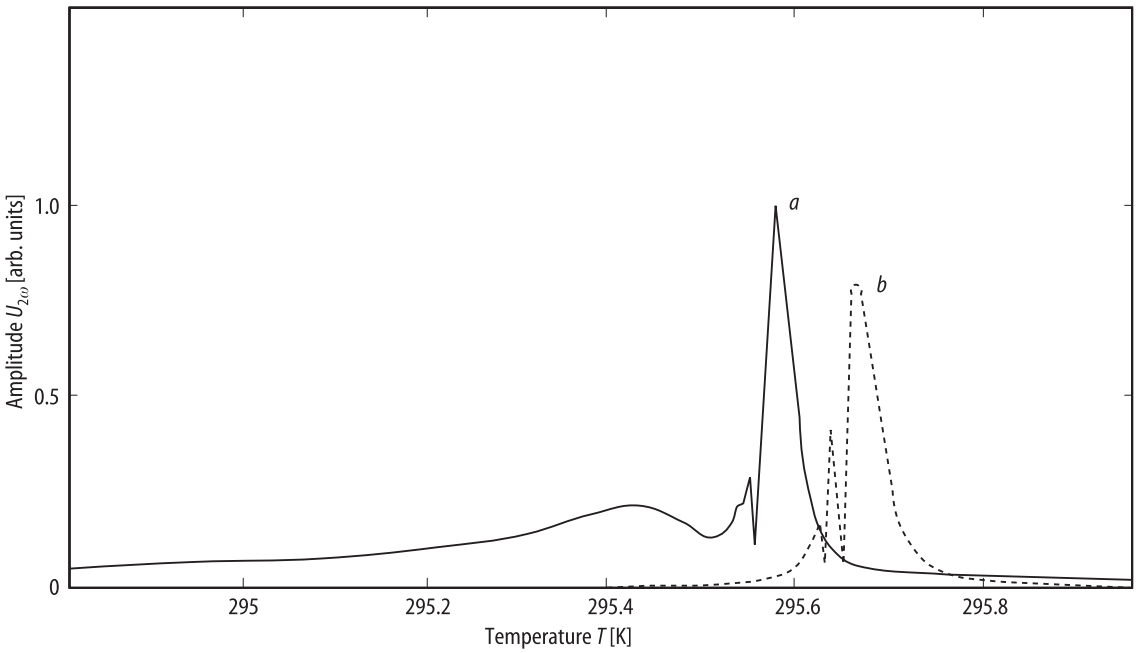

Fig. 60A-2-029. $(NH_2CH_2COOH)_3 \cdot H_2SeO_4$ (TGSe). $U_{2\omega}$ vs. T [89Kal]. $U_{2\omega}$: amplitude of second harmonic voltage. Curve *a*: cooling. Curve *b*: heating. f = 20 kHz, V = 200 mV, sample thickness = 2.12 mm.

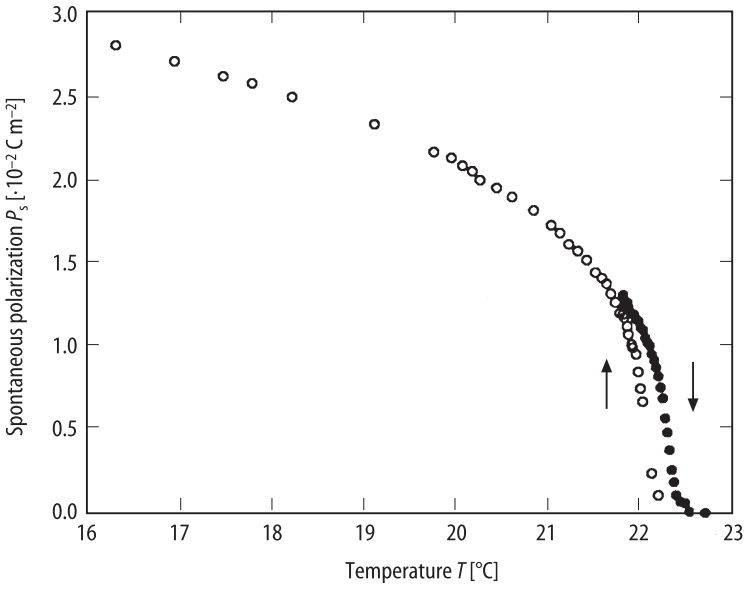

Fig. 60A-2-030. $(NH_2CH_2COOH)_3 \cdot H_2SeO_4$ (TGSe). P_s vs. T [94Igl1]. Full circle: heating; open circle: cooling.

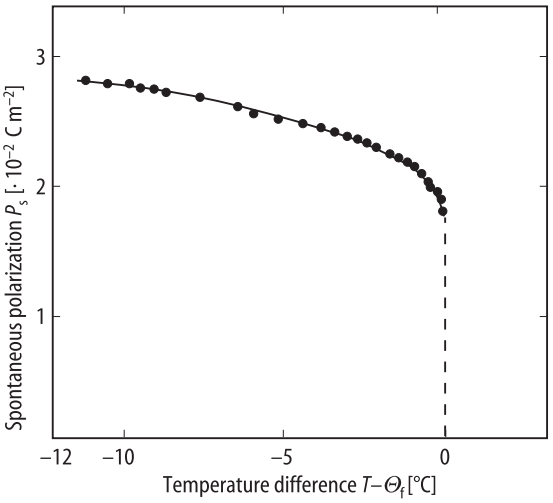

Fig. 60A-2-031. $(ND_2CH_2COOD)_3 \cdot D_2SeO_4$ (DTGSe). P_s vs. $T - \Theta_f$ [88Sta2]. P_s was measured during cooling.

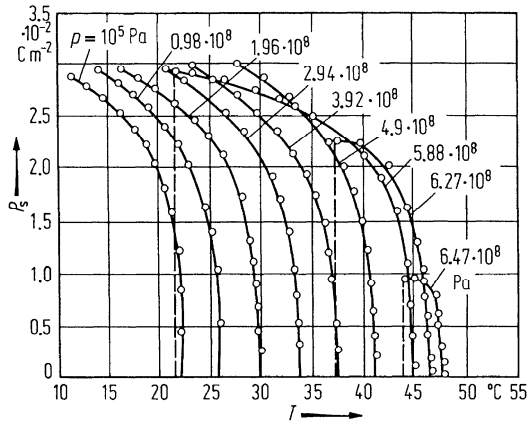

Fig. 60A-2-032. $(NH_2CH_2COOH)_3 \cdot H_2SeO_4$ (TGSe). P_s vs. T [68Pol2]. Parameter: hydrostatic pressure, p.

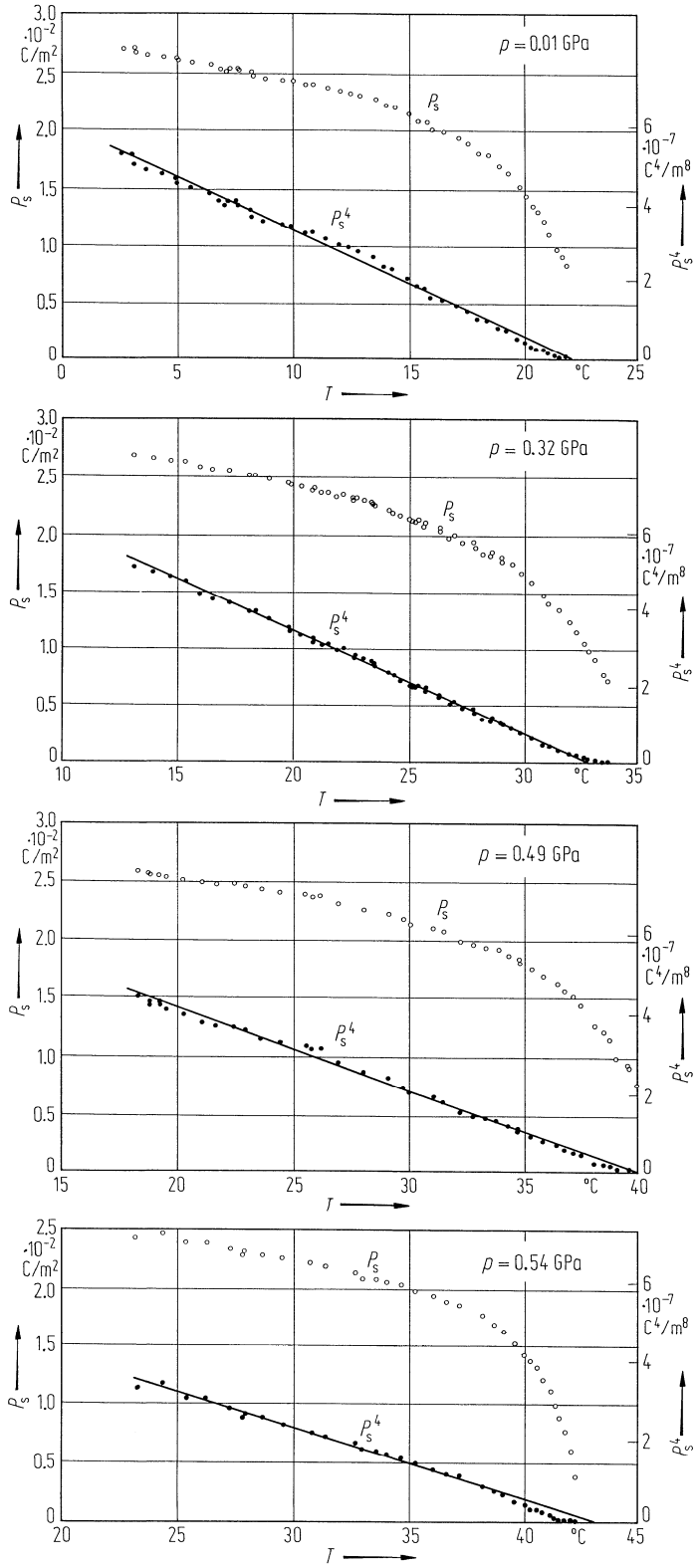

Fig. 60A-2-033. $(NH_2CH_2COOH)_3 \cdot H_2SeO_4$ (TGSe). P_s, P_s^4 vs. T [80Yam]. Parameter: hydrostatic pressure, p.

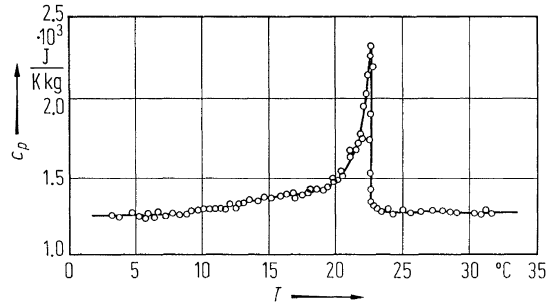

Fig. 60A-2-034. $(NH_2CH_2COOH)_3 \cdot H_2SeO_4$ (TGSe). c_p vs. T [68Str]. c_p: specific heat capacity at constant pressure.

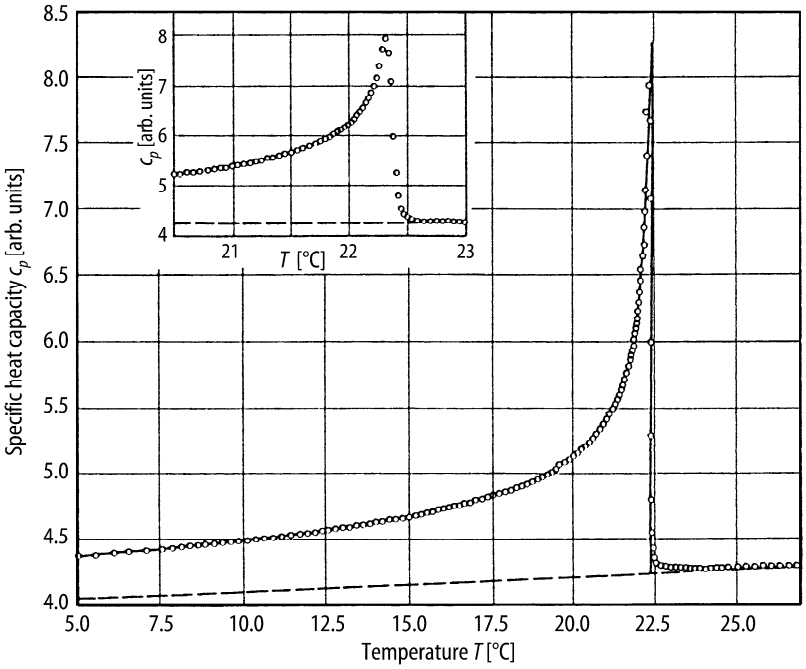

Fig. 60A-2-035. $(NH_2CH_2COOH)_3 \cdot H_2SeO_4$ (TGSe). c_p vs. T [77Ema]. c_p: specific heat capacity at constant pressure.

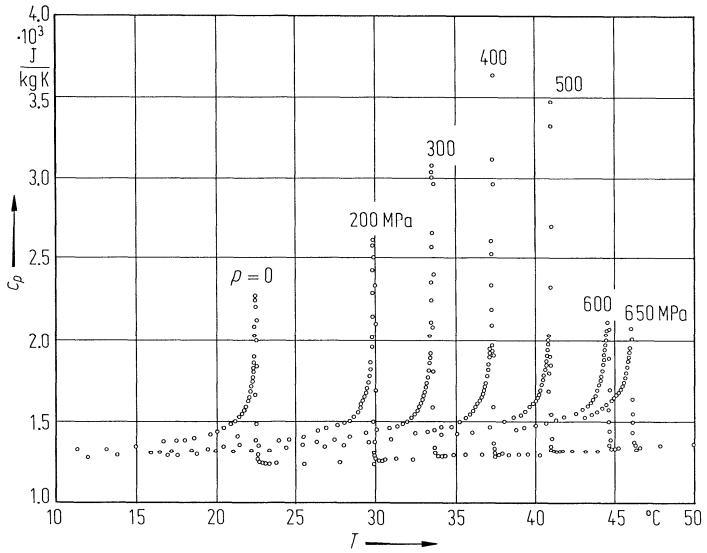

Fig. 60A-2-036. $(NH_2CH_2COOH)_3 \cdot H_2SeO_4$ (TGSe). c_p vs. T [79Che1]. Parameter: hydrostatic pressure, p. c_p: specific heat capacity at constant pressure.

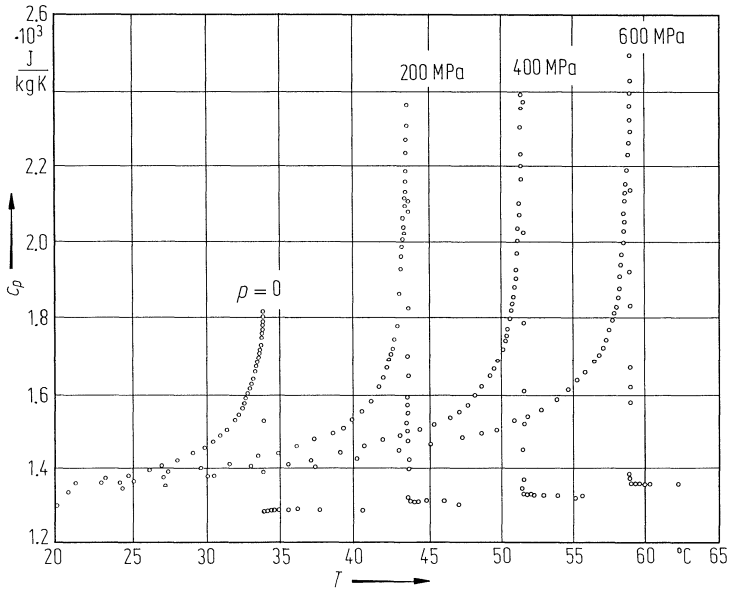

Fig. 60A-2-037. Deuterated triglycine selenate (DTGSe). c_p vs. T [79Che2]. Parameter: hydrostatic pressure, p. c_p: specific heat capacity at constant pressure.

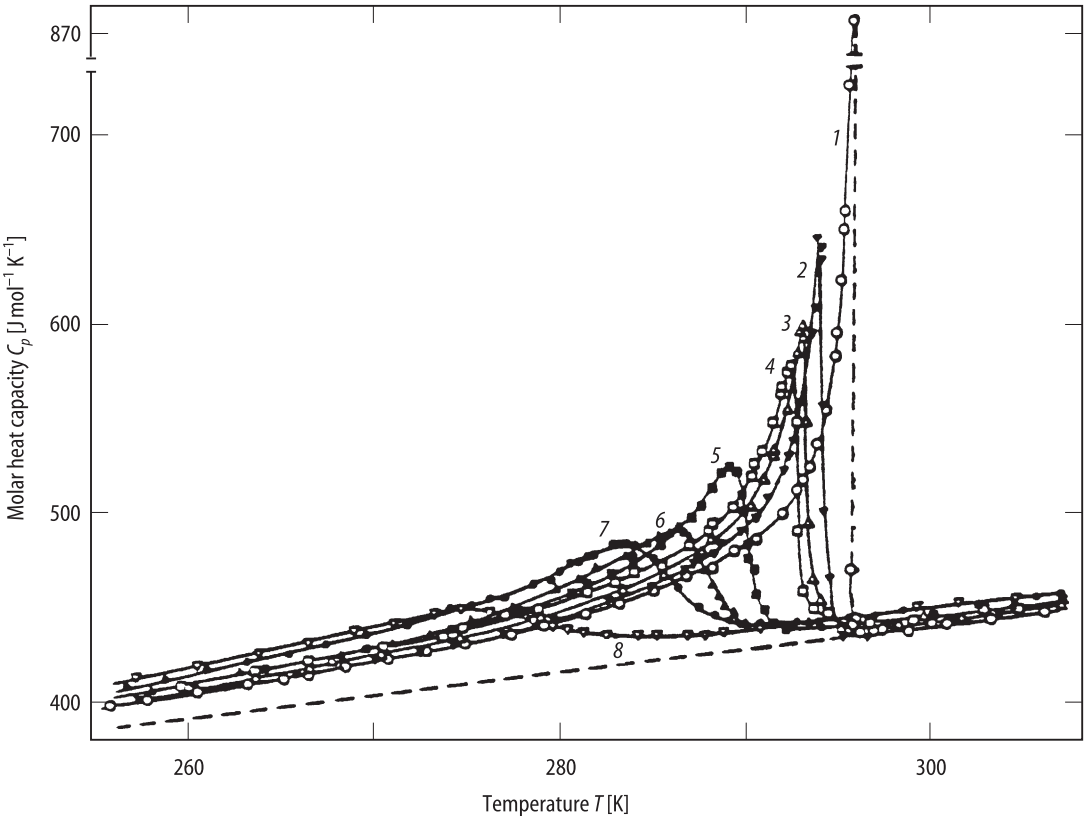

Fig. 60A-2-038. $(NH_2CH_2COOH)_3 \cdot H_2SeO_4$ (TGSe). C_p vs. T [91Str1]. C_p: molar heat capacity at constant pressure. Parameter: γ-radiation dose. *1*: 0; *2*: 0.5 MR; *3*: 1.0 MR; *4*: 2.0MR; *5*: 4.0 MR; *6*: 7.0 MR; *7*: 11 MR; *8*: 20 MR.

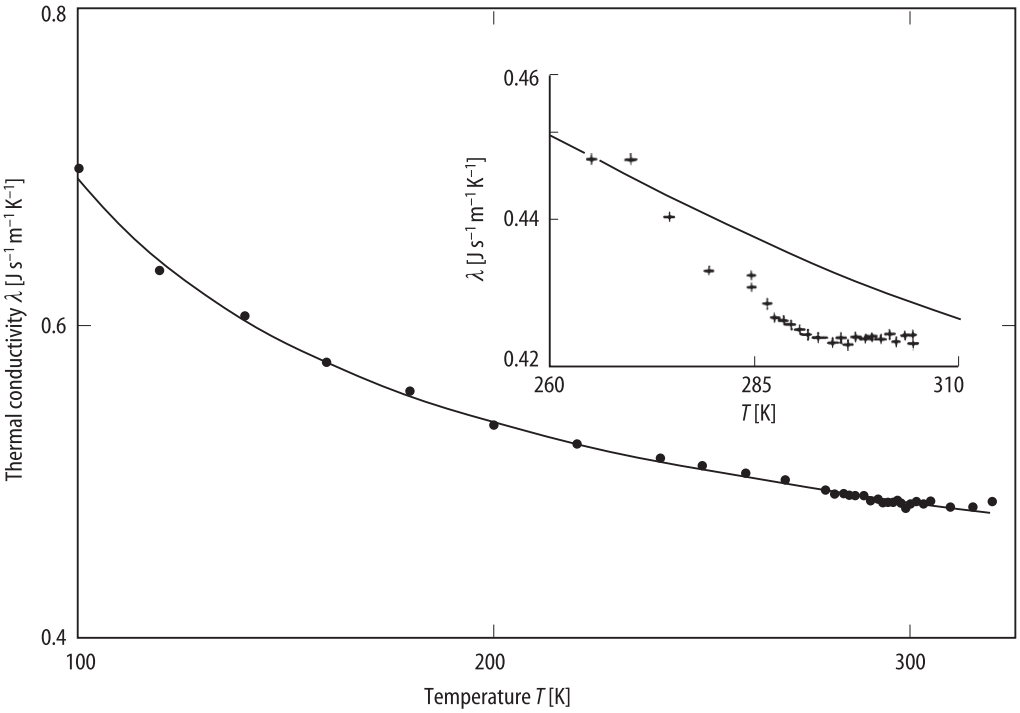

Fig. 60A-2-039. $(NH_2CH_2COOH)_3 \cdot H_2SeO_4$ (TGSe). λ vs. T [91Str2]. λ: thermal conductivity along the *a* axis.

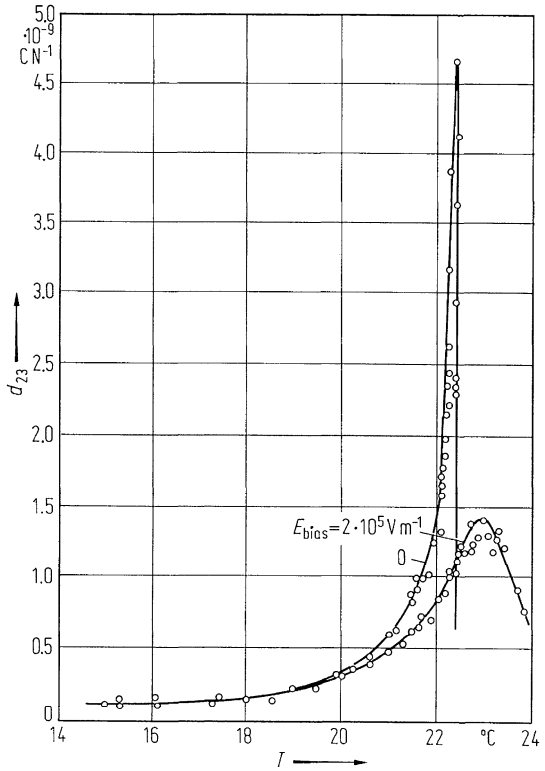

Fig. 60A-2-040. $(NH_2CH_2COOH)_3 \cdot H_2SeO_4$ (TGSe). d_{23} vs. T [74Var].

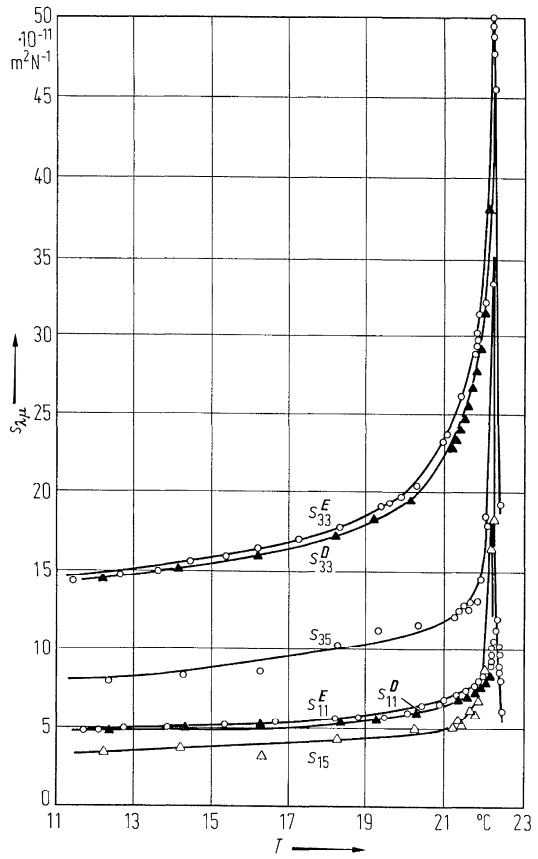

Fig. 60A-2-041. $(NH_2CH_2COOH)_3 \cdot H_2SeO_4$ (TGSe). $s_{\lambda\mu}$ vs. T [74Var].

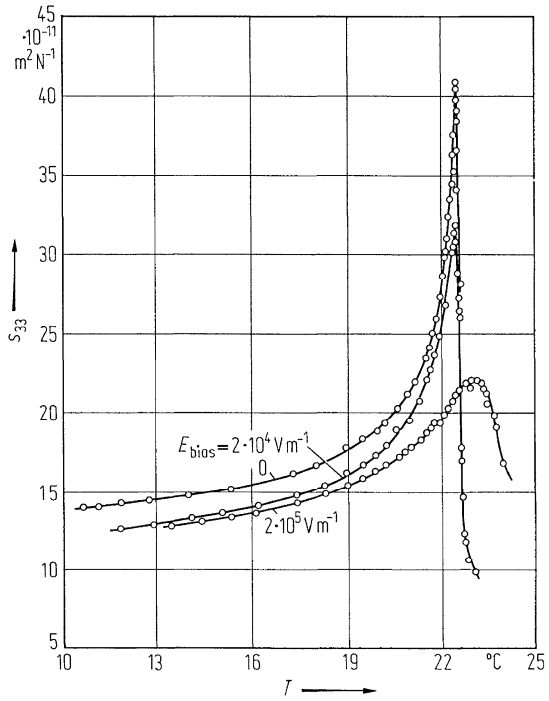

Fig. 60A-2-042. $(NH_2CH_2COOH)_3 \cdot H_2SeO_4$ (TGSe). s_{33} vs. T [74Var]. Parameter: E_{bias}.

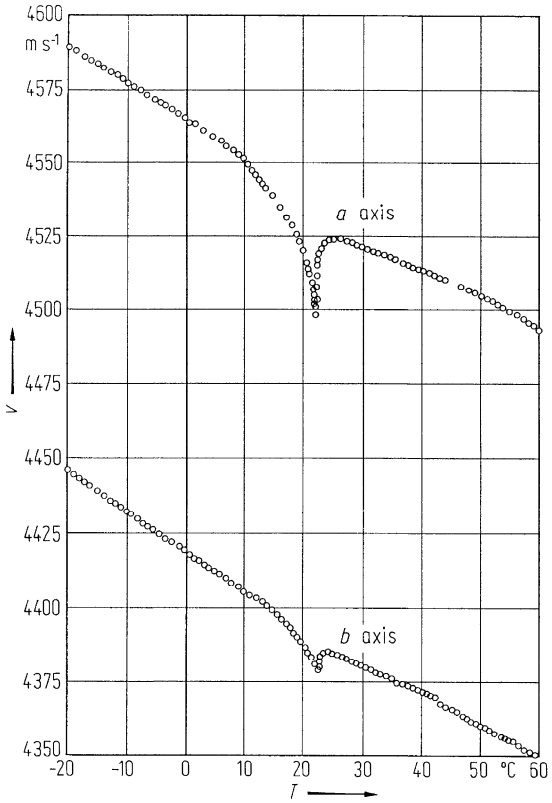

Fig. 60A-2-043. $(NH_2CH_2COOH)_3 \cdot H_2SeO_4$ (TGSe). v vs. T [75Tod]. v: velocity of the longitudinal ultrasound propagating along the a and b axes. $f = 10$ MHz.

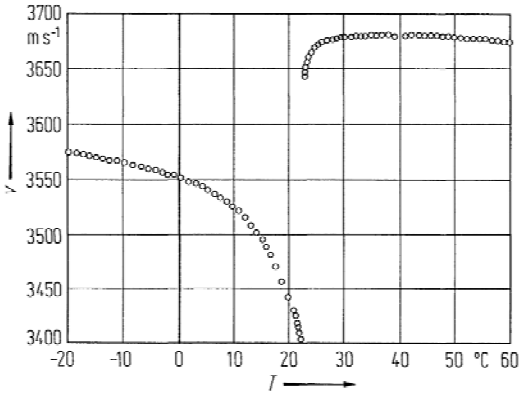

Fig. 60A-2-044. $(NH_2CH_2COOH)_3 \cdot H_2SeO_4$(TGSe). v vs. T [75Tod]. v: velocity of the longitudinal ultrasound propagating along the c axis. $f = 10$ MHz.

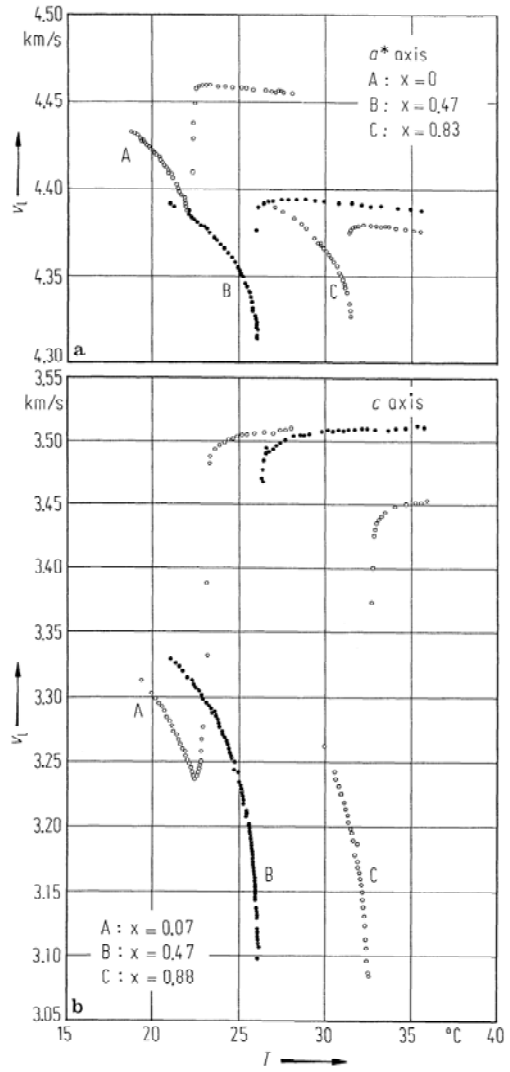

Fig. 60A-2-045. $[(NH_2CH_2COOH)_3 \cdot H_2SeO_4]_{1-x}[(ND_2CH_2COOD)_3 \cdot D_2SeO_4]_x$ ($TGSe_{1-x}DTGSe_x$). v_l vs. T [84Tak]. Parameter: x. v_l: velocities of the longitudinal sound waves propagating along the normal to the bc plane (**a**) and along the c axis (**b**). $f = 10$ MHz.

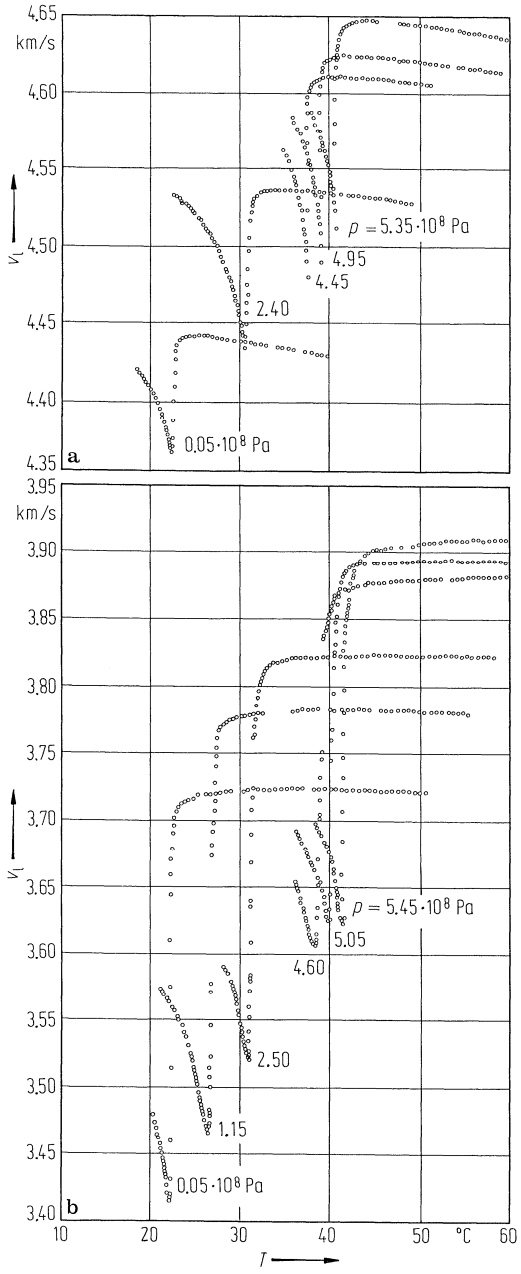

Fig. 60A-2-046. $(NH_2CH_2COOH)_3 \cdot H_2SeO_4$ (TGSe). v_1 vs. T [81Tak]. Parameter: hydrostatic pressure, p. v_1: velocities of the longitudinal sound waves propagating along the normal to the *bc* plane (**a**) and along the *c* axis (**b**). $f = 10$ MHz.

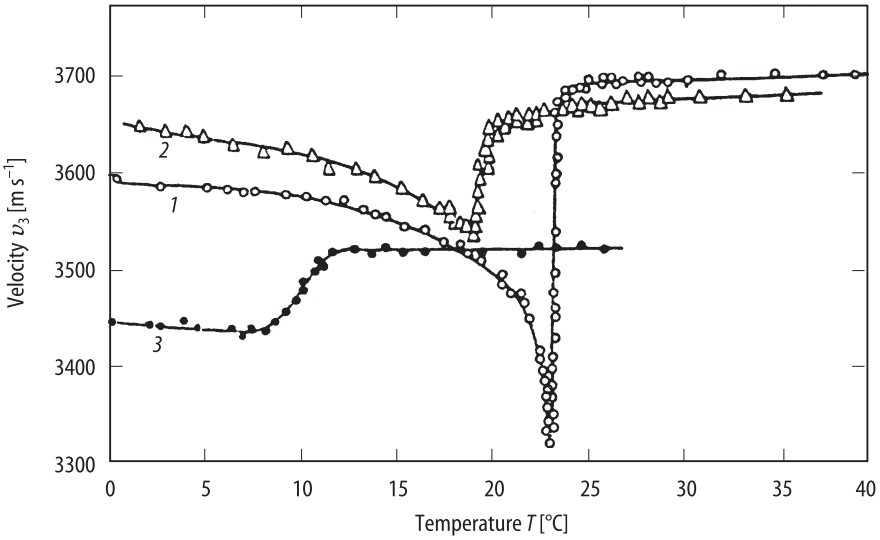

Fig. 60A-2-047. $(NH_2CH_2COOH)_3 \cdot H_2SeO_4$ (TGSe). v_3 vs. T [89Str]. Parameter: γ-radiation dose. Curve *1*: before irradiation; *2*: after irradiation of 3 MR; *3*: after irradiation of 10 MR. v_3: velocities of the longitudinal ultrasound propagating along the *c* axis. $f = 10$ MHz.

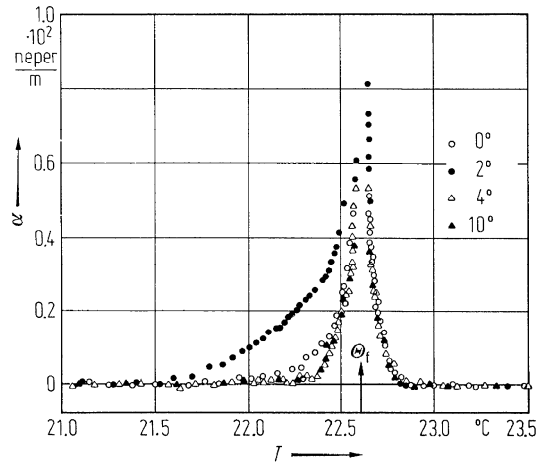

Fig. 60A-2-048. $(NH_2CH_2COOH)_3 \cdot H_2SeO_4$ (TGSe). α vs. T [74Tod]. α: absorption coefficients of the quasi-longitudinal ultrasound propagating in the *bc* plane with angles 0°, 2°, 4°, and 10° to the *c* axis. $f = 10$ MHz.

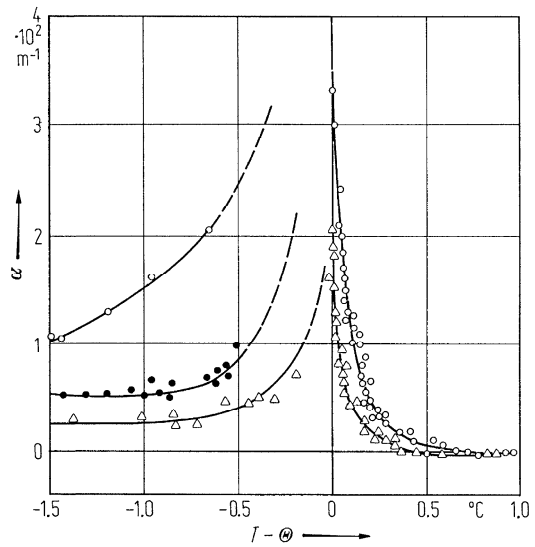

Fig. 60A-2-049. $(NH_2CH_2COOH)_3 \cdot H_2SeO_4$ (TGSe). α vs. $T - \Theta$ [67Min]. α: absorption coefficients of the longitudinal ultrasound propagating along the c axis. Parameter: f. Triangles: 5 MHz; full circles: 10 MHz; open circles: 15 MHz.

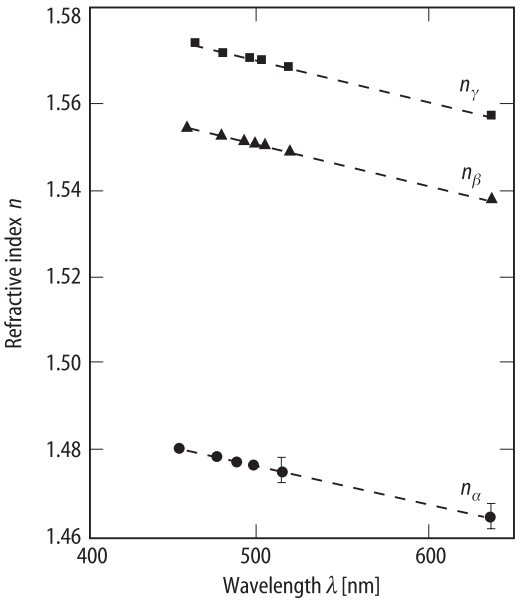

Fig. 60A-2-050. $(NH_2CH_2COOH)_3 \cdot H_2SeO_4$ (TGSe). n_a, n_β, n_γ vs. λ [88Bur]. $n_\alpha = n_b$. $T = 18$ °C.

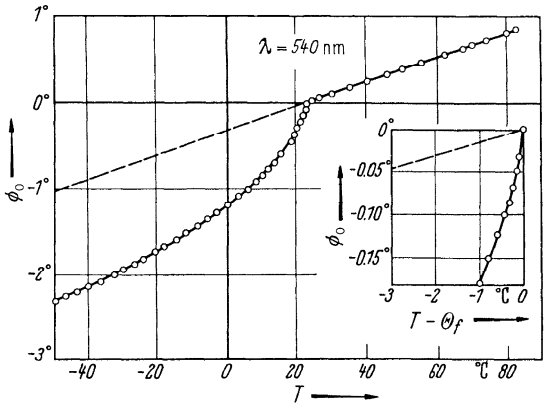

Fig. 60A-2-051. $(NH_2CH_2COOH)_3 \cdot H_2SeO_4$ (TGSe). ϕ_o vs. T [66Iva1]. ϕ_o: rotation angle of the optical indicatrix around the b axis.

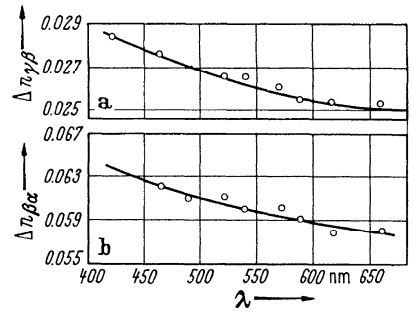

Fig. 60A-2-052. $(NH_2CH_2COOH)_3 \cdot H_2SeO_4$ (TGSe). $\Delta n_{\gamma\beta}$, $\Delta n_{\beta\alpha}$ vs. λ [66Iva2]. (**a**) $\Delta n_{\gamma\beta} = n_\gamma - n_\beta$. (**b**) $\Delta n_{\beta\alpha} = n_\beta - n_\alpha$. $T = 21$ °C.

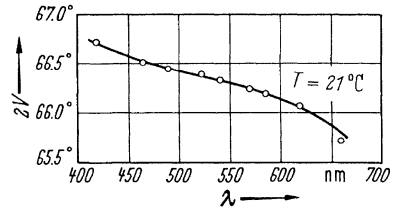

Fig. 60A-2-053. $(NH_2CH_2COOH)_3 \cdot H_2SeO_4$ (TGSe). $2V$ vs. λ [66Iva2]. $2V$: optical axial angle.

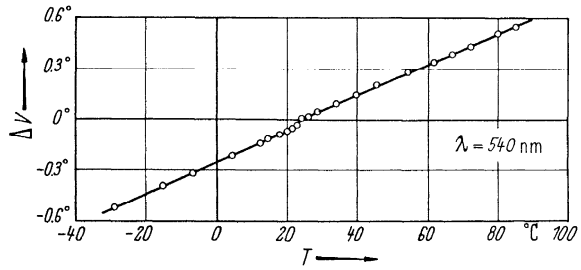

Fig. 60A-2-054. $(NH_2CH_2COOH)_3 \cdot H_2SeO_4$ (TGSe). ΔV vs. T [66Iva1]. $\Delta V = V(T) - V(\Theta_{II-I})$. $2V(T)$: optical axial angle at T [°C].

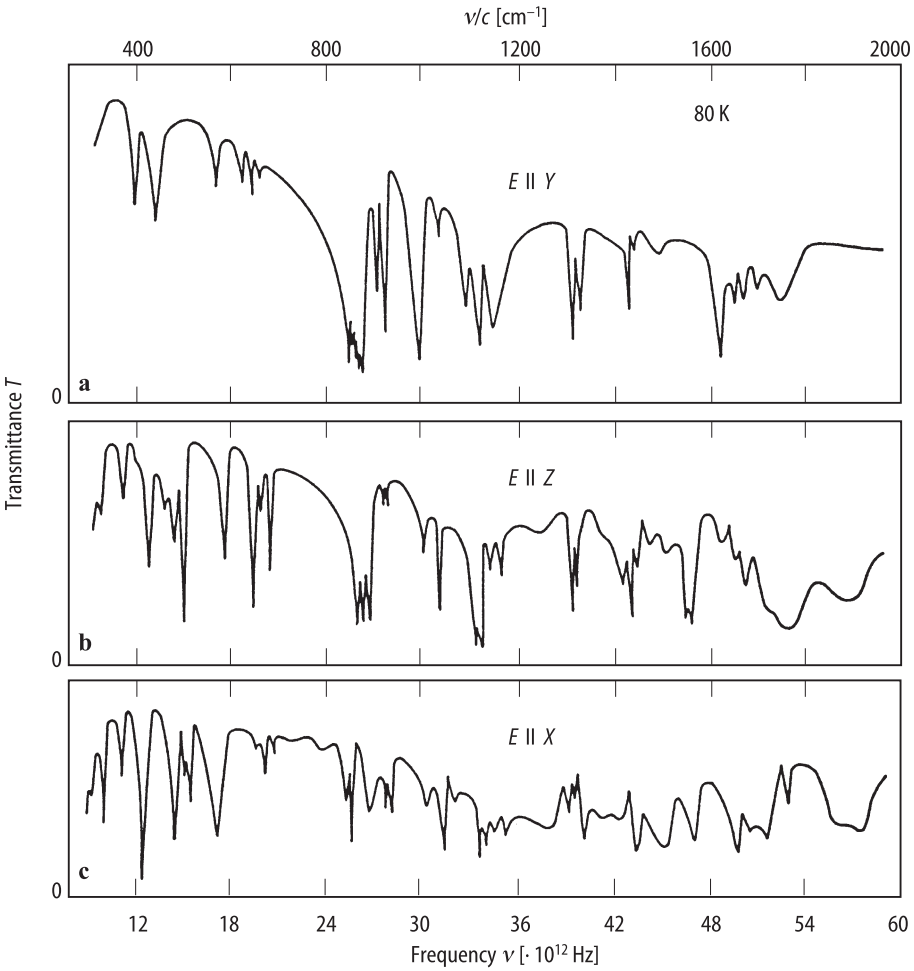

Fig. 60A-2-055. $(NH_2CH_2COOH)_3 \cdot H_2SeO_4$ (TGSe). T vs. ν [77Ger]. T: transmittance of infrared radiation at 80 K. Polarization of the light: (**a**) || Y, (**b**) || Z, (**c**) || X. The orthogonal axial system (X, Y || b, Z || c) is adopted. Thickness of the sample is less than 1 mm.

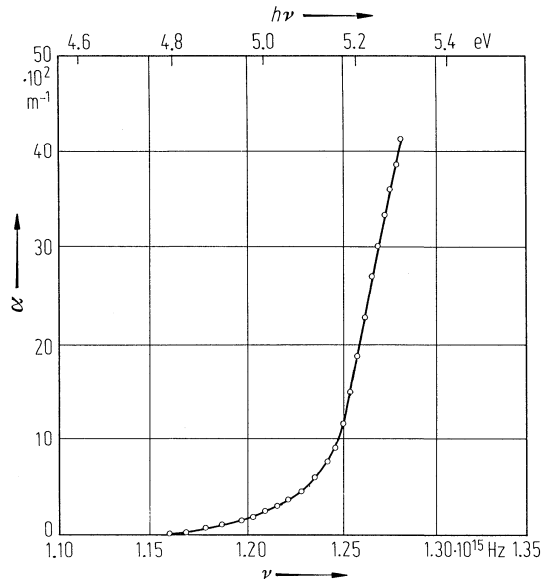

Fig. 60A-2-056. $(NH_2CH_2COOH)_3 \cdot H_2SeO_4$ (TGSe). α vs. ν [87AlE]. α: optical absorption coefficient along the b axis. $T = 290$ K.

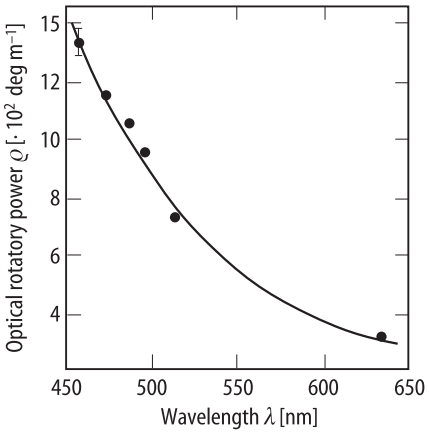

Fig. 60A-2-057. $(NH_2CH_2COOH)_3 \cdot H_2SeO_4$ (TGSe). ρ vs. λ [88Kor1]. ρ: optical rotatory power under the application of voltage $E_2 = 200$ kV m^{-1}. $T = 285$ K.

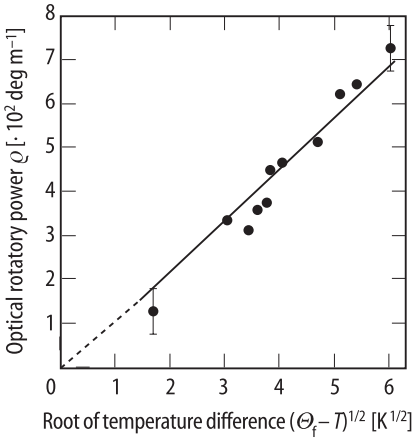

Fig. 60A-2-058. $(NH_2CH_2COOH)_3 \cdot H_2SeO_4$ (TGSe). ρ vs. $(\Theta_f - T)^{1/2}$ [88Kor1]. ρ: optical rotatory power at $\lambda = 632.8$ nm under the application of voltage $E_2 = 150$ kV m^{-1}.

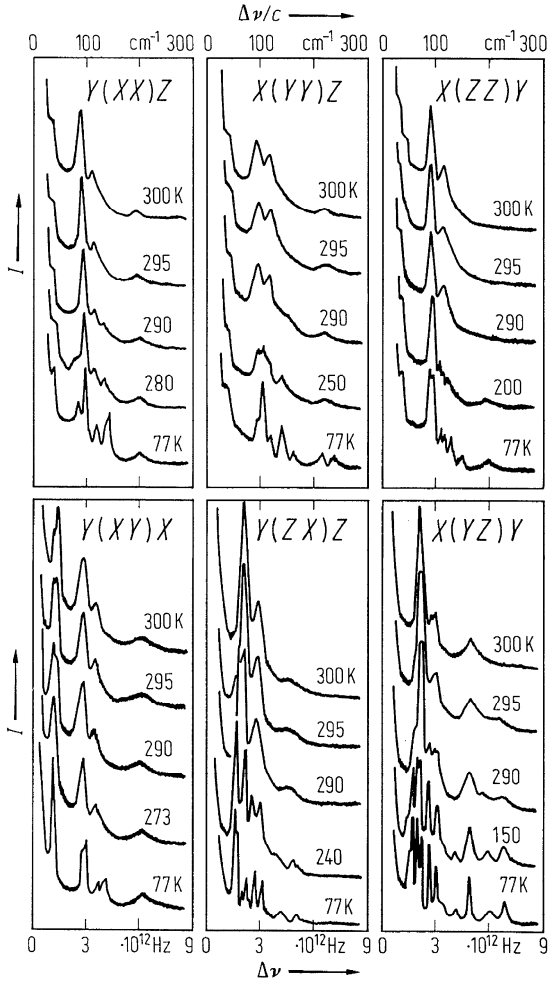

Fig. 60A-2-059. $(NH_2CH_2COOH)_3 \cdot H_2SeO_4$ (TGSe). I vs. $\Delta\nu$ [77Kan]. I: Raman scattering intensity. Parameter: T.

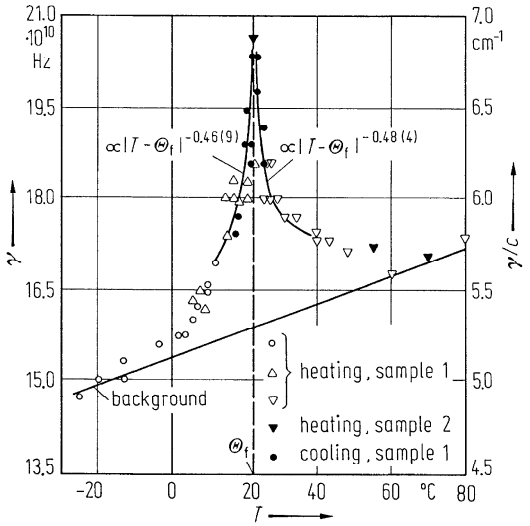

Fig. 60A-2-060. $(NH_2CH_2COOH)_3 \cdot H_2SeO_4$ (TGSe). γ vs. T [77Sch]. γ: half line width at half maximum of the Raman spectrum of the lowest TO-phonon mode (ν_o/c = 37.4 cm^{-1}) at Θ_f. The smooth curve is a least square fit to the data.

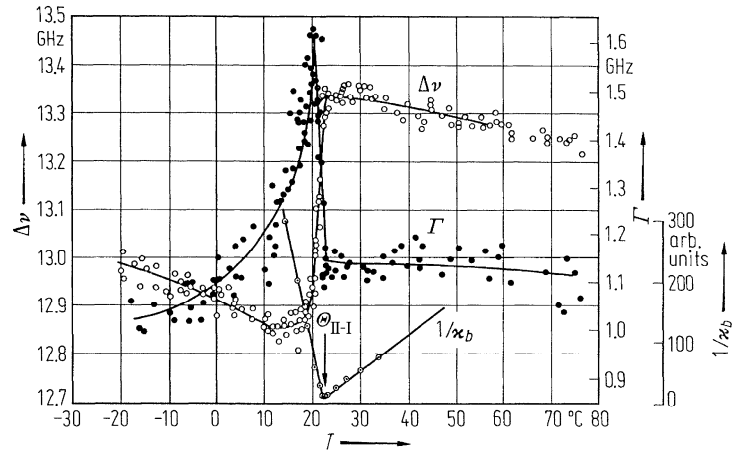

Fig. 60A-2-061. $(NH_2CH_2COOH)_3 \cdot H_2SeO_4$ (TGSe). $\Delta\nu$, Γ, κ_b^{-1} vs. T [76Yag]. $\Delta\nu$: frequency shift of Brillouin scattering; c_{33}-mode. Γ: full line width at half maximum.

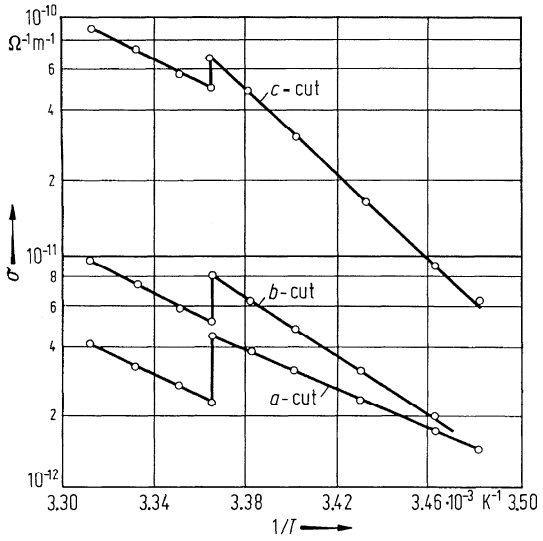

Fig. 60A-2-062. $(NH_2CH_2COOH)_3 \cdot H_2SeO_4$ (TGSe). σ vs. $1/T$ [69Son]. σ was measured by two terminal method. Applied voltage $E = 120$ kV m^{-1}.

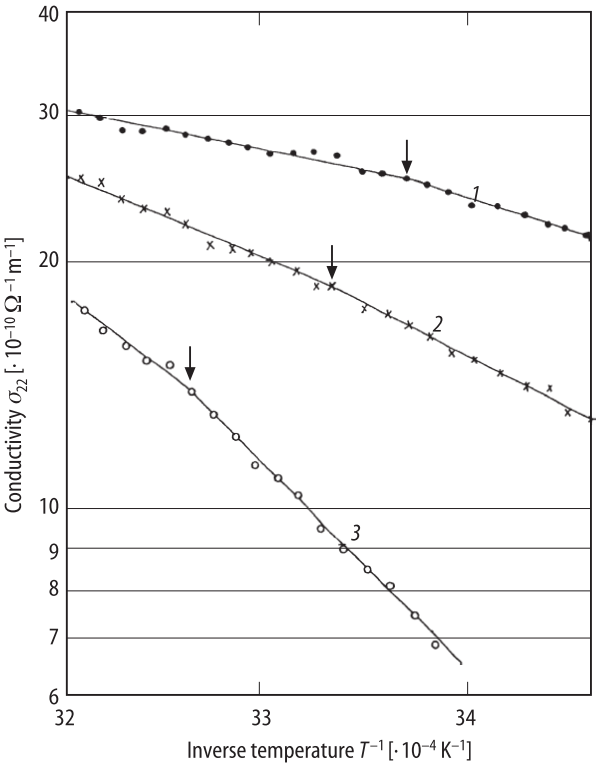

Fig. 60A-2-063. $[(NH_2CH_2COOH)_3 \cdot H_2SeO_4]_{1-x}[(ND_2CH_2COOD)_3 \cdot D_2SeO_4]_x$ ($TGSe_{1-x}DTGSe_x$). σ_{22} vs. $1/T$ [91Ham]. Parameter: x. Curve *1*: x = 0.27; *2*: x = 0.55; *3*: x = 0.90. σ_{22} was measured during cooling. Applied voltage $E = 1000$ kV m^{-1}. Arrows indicate the transition point.

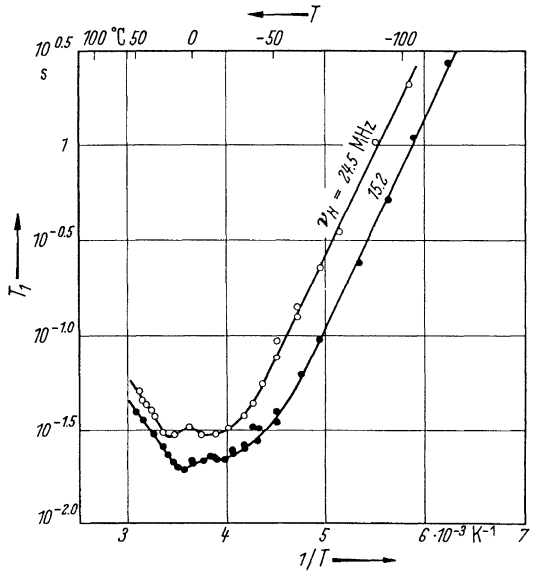

Fig. 60A-2-064. $(NH_2CH_2COOH)_3 \cdot H_2SeO_4$ (TGSe). T_1 vs. $1/T$ [66Bli]. T_1: spin lattice relaxation time for proton. ν_H: Larmor frequency of proton.

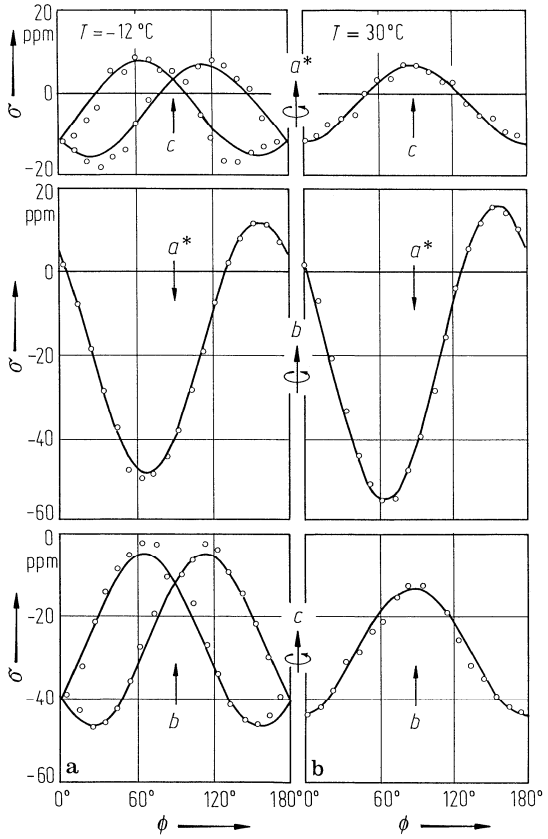

Fig. 60A-2-065. $(NH_2CH_2COOH)_3 \cdot H_2SeO_4$ (TGSe). σ vs. ϕ [80Mos]. Parameter: T. σ: chemical shift of ^{77}Se nuclei at (**a**) $T = -12$ °C and (**b**) $T = 30$ °C relative to liquid selenic acid H_2SeO_4. ϕ: rotation angle. $\nu_L = 11.46$ MHz.

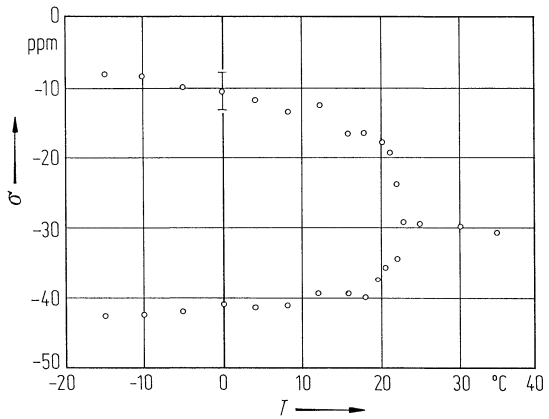

Fig. 60A-2-066. $(NH_2CH_2COOH)_3 \cdot H_2SeO_4$ (TGSe). σ vs. T [80Mos]. σ: chemical shift of ^{77}Se nuclei relative to liquid selenic acid H_2SeO_4. $\boldsymbol{H} \perp \boldsymbol{c}$, $\angle(\boldsymbol{H}, \boldsymbol{a}^*) = 45°$. $\nu_L = 11.46$ MHz.

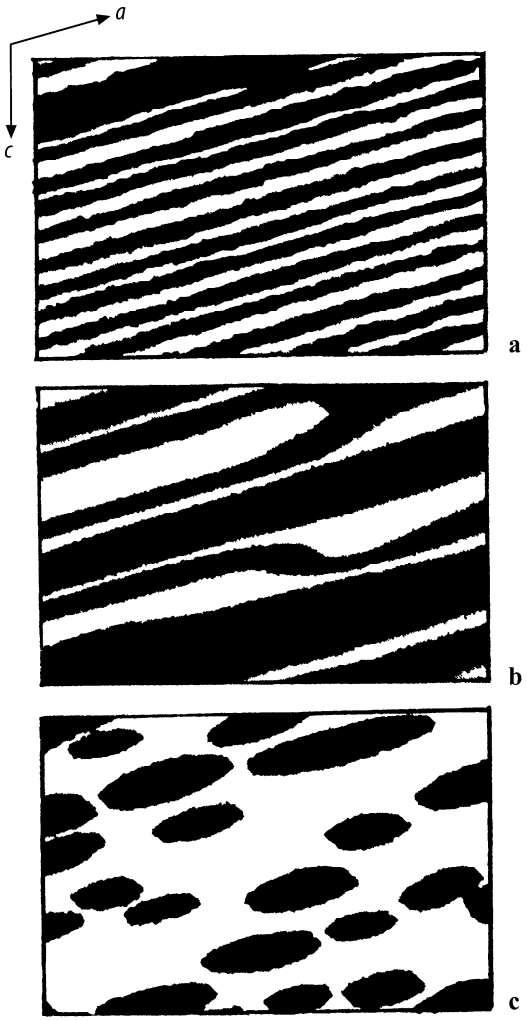

Fig. 60A-2-067. $(NH_2CH_2COOH)_3 \cdot H_2SeO_4$ (TGSe). Domain patterns obtained on the (010) surface by powder-deposition technique [77Hat]. Black regions are negative domains covered by the carbon powders. (**a**) Striped domains parallel to the (001) planes. (**b**) Coarse striped domains. (**c**) Restricted lenticular domains.

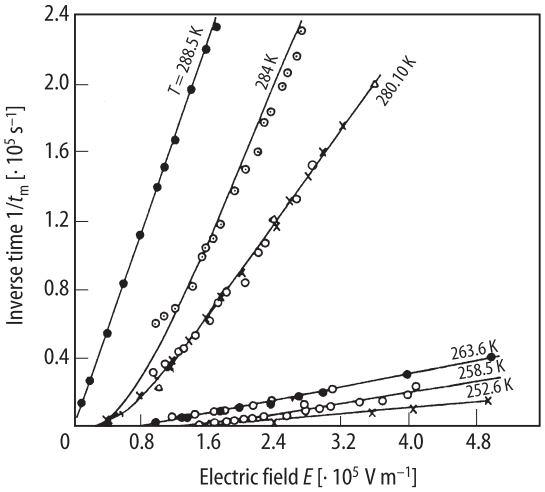

Fig. 60A-2-068. $(NH_2CH_2COOH)_3 \cdot H_2SeO_4$ (TGSe). $1/t_m$ vs. E [86San]. Parameter: T. t_m: time corresponding to the maximum switching current.

References

56Mat Matthias, B.T., Miller, C.E., Remeika, J.P.: Phys. Rev. **104** (1956) 849.
57Pep Pepinsky, R., Okaya, Y., Jona, F.: Bull. Am. Phys. Soc. [2] **2** (1957) 220.
58Nit Nitsche, R.: Helv. Phys. Acta **31** (1958) 306.
66Bli Blinc, R., Lahajnar, G., Pintar, M., Zupancic, I.: J. Chem. Phys. **44** (1966) 1784.
66Iva1 Ivanov, N.R., Shuvalov, L.A.: Kristallografiya **11** (1966) 614; Sov. Phys. Crystallogr. (English Transl.) **11** (1967) 534.
66Iva2 Ivanov, N.R., Zotov, V.F.: Kristallografiya **11** (1966) 924; Sov. Phys. Crystallogr. (English Transl.) **11** (1967) 781.
67Min Minaeva, K.A., Levanyuk, A.P., Strukov, B.A., Koptsik, V.A.: Fiz. Tverd. Tela **9** (1967) 1220; Sov. Phys. Solid State (English Transl.) **9** (1967) 950.
68Pol1 Polandov, I.N., Mylov, V.P., Churagulov, B.R.: Dokl. Akad. Nauk SSSR **178** (1968) 1293; Sov. Phys. Dokl. (English Transl.) **13** (1968) 145.
68Pol2 Polandov, I.N., Mylov, V.P., Strukov, B.A., Varikash, V.M.: Fiz. Tverd. Tela **10** (1968) 1377; Sov. Phys. Solid State (English Transl.) **10** (1968) 1092.
68Str Strukov, B.A., Taraskin, S.A., Koptsik, V.A., Varikash, V.M.: Kristallografiya **13** (1968) 541; Sov. Phys. Crystallogr. (English Transl.) **13** (1968) 447.
69Son Sonin, A.S., Plotinskii, V.N.: Fig. 167 in: Gurevich, V.M.: Elektroprovodnost' Segnetoelektoelektrikov, Moskva: Izdatel'stvo Komiteta Standartov, Mer Iizmeritel'nykh Priboroy pri Sovete Ministrov SSSR 1969; Electric Conductivity of Ferroelectrics, Jerusalem: Israel Program for Scientific Transaction 1971.
70Kon Konstantinova, V.P., Stankovskaya, Ya.: Kristallografiya **15** (1970) 382; Sov. Phys. Crystallogr. (English Transl.) **15** (1970) 325.
70Myl Mylov, V.P., Churagulov, B.R., Leonidova, G.G.: Fiz. Tverd. Tela **12** (1970) 1288; Sov. Phys. Solid State (English Transl.) **12** (1970) 1012.
71Suz Suzuki, I., Abe, R.: J. Phys. Soc. Jpn. **31** (1971) 179.
71Zar Zarembovskaya, T.A., Varikash, V.M.: Fiz. Tverd. Tela **13** (1971) 3537; Sov. Phys. Solid State (English Transl.) **13** (1972) 2989.
73Tse Tsedrik, M.S., Margolin, L.N., Gontarev, V.F.: Krist. Tech. **8** (1973) 513.
73Var Varikash, V.M., Zarembovskaya, T.A.: Izv. Vyssh. Uchebn. Zaved. Fiz., 1973, 141.
74Ges Gesi, K., Ozawa, K.: J. Phys. Soc. Jpn. **37** (1974) 1053.
74Lut Luther, G., Birkenheier, C., Brosowski, G., Müser, H.E., Petersson, J.: Ferroelectrics **8** (1974) 569.
74Sir Sirota, N.N., Korina, R.V.: Krist. Tech. **9** (1974) 55.
74Tod Todo, I., Tatsuzaki, I.: J. Phys. Soc. Jpn. **37** (1974) 1477.
74Var Varikash, V.M., Sarembovskaja, T.A.: Krist. Tech. **9** (1974) 685.
75Ale Aleksandrova, I.P., Repeta, V.S., Konstantinova, V.P.: Izv. Akad. Nauk SSSR, Ser. Fiz. **39** (1975) 922; Bull. Acad. Sci. USSR, Phys. Ser. (English Transl.) **9**, No. 5 (1975) 27.
75Tod Todo, I.: J. Phys. Soc. Jpn. **9** (1975) 1538.
76Ale Aleksandrova, I.P., Repeta, V.S., Chekmasova, T.I., Konstantinova, V.P.: Fiz. Tverd. Tela **18** (1976) 1311; Sov. Phys. Solid State (English Transl.) **18** (1976) 754.
76Ges1 Gesi, K.: J. Phys. Soc. Jpn.**41** (1976) 565.
76Ges2 Gesi, K., Ozawa, K.: J. Phys. Soc. Jpn. **40** (1976) 599.
76Shu Shuvalov, L.A., Baranov, A.I., Shirokov, A.M., Konstantinova, V.P.: Ferroelectrics **14** (1976) 699.
76Sta Stankowska, J., Czarnecka, A., Kaluba, M.: Acta Phys. Pol. A **50** (1976) 823.
76Yag Yagi, T., Tokunaga, M., Tatsuzaki, I.: J. Phys. Soc. Jpn. **40** (1976) 1659.
77Ema Ema, K., Hamano, K., Kurihara, K., Hatta, I.: J. Phys. Soc. Jpn. **43** (1977) 1954.
77Ger Gerbaux, X., Hadni, A., Waldschmidt, J.M.: Opt. Commun. **21** (1977) 425.
77Hat Hatano, J., Suda, F., Futama, H.: J. Phys. Soc. Jpn. **43** (1977) 1933.
77Kan Kaneko, N., Takahashi, H., Higasi, K.: J. Phys. Chem. Solids **38** (1977) 849.
77Ole Olejnik, S., Lukaszewicz, K.: Acta Univ. Wratislav. No. 341 (1977) 43.
77Sch Schaack, G., Winterfeldt, V.: Ferroelectrics **15** (1977) 35.

78Ema Ema, K., Hamano, K.: Ferroelectrics **20** (1978) 193.
78Hat Hatano, J.: J. Phys. Soc. Jpn. **45** (1978) 1291.
78Man Mangin, J., Hadni, A.: J. Phys. (Paris) Lett. **39** (1978) 447.
78Min Minaeva, K.A., Baryshnikova, E.V., Strukov, B.A., Varikash, V.M.: Kristallografiya **23** (1978) 646; Sov. Phys. Crystallogr. (English Transl.) **23** (1978) 361.
78Sud Suda, F., Hatano, J., Futama, H.: J. Phys. Soc. Jpn. **44** (1978) 244.
78Var Varikash, V.M., Tarasevich, E.V., Pupkevich, P.A.: Krist. Tech. **13** (1978) 693.
79Che1 Chernenko, V.A., Polandov, I.N., Strukov, B.A., Novik, V.K.: Fiz. Tverd. Tela **21** (1979) 258; Sov. Phys. Solid State (English Transl.) **21** (1979) 154.
79Che2 Chernenko, V.A., Polandov, I.N., Baranov, A.I.: Fiz. Tverd. Tela **21** (1979) 1381; Sov. Phys. Solid State (English Transl.) **21** (1979) 798.
79Kaf Kafadarova, E.A., Polandov, I.N., Petrov, V.M., Popov, A.N.: Fiz. Tverd. Tela **21** (1979) 620; Sov. Phys. Solid State (English Transl.) **21** (1979) 368.
79Tik Tikhomirova, N.A., Dontsova, L.I., Pikin, S.A., Shuvalov, L.A.: Pis'ma Zh. Eksp. Teor. Fiz. **29** (1979) 37; JETP Lett. (English Transl.) **9** (1979) 34.
79Yam Yamada, M.: Master Thesis, Hokkaido University (1979).
80Deg Deguchi, K., Sumi, T., Nakamura, E.: Phys. Lett. A **80** (1980) 403.
80Iva Ivanov, N.R.: J. Phys. Soc. Jpn. **49** (1980) Suppl. B, 160.
80Mos Moskvich, Yu.N., Sukhovskii, A.A., Sorokin, A.V., Lundin, A.G.: Fiz. Tverd. Tela **22** (1980) 232; Sov. Phys. Solid State (English Transl.) **22** (1980) 135.
80Sch Schmitt, H., Müser, H.E., Mengelkoch, O., Sterta, W.: Ferroelectrics **25** (1980) 499.
80Sta Stankowski, J., Malinowski, W.: Acta Phys. Pol. A **58** (1980) 773.
80Yam Yamashita, H., Takeuchi, Y., Tatsuzaki, I.: J. Phys. Soc. Jpn. **49** (1980) 1874.
81Sta Stankowski, J.: Phys. Rep. **77** (1981) 1.
81Tak Takeuchi, Y., Yamashita, H., Tatsuzaki, I.: J. Phys. Soc. Jpn. **50** (1981) 2022.
82Tak Takeuchi, Y., Tatsuzaki, I.: J. Phys. Soc. Jpn. **51** (1982) 545.
82Var Varikash, V.M., Shuvalov, L.A., Tarasevich, E.V., Lagutina, J.P.: Ferroelectrics **42** (1982) 47.
82Yam Yamashita, H., Tatsuzaki, I.: J. Phys. Soc. Jpn. **51** (1982) 1453.
83Kha Khanna, S.K.: Phys. Status Solidi (b) **116** (1983) 173.
84Ami Amin, M., Balloomal, L.S., Badawy, M.M.: Ferroelectrics **56** (1984) 203.
84Tak Takeuchi, Y.: J. Phys. Soc. Jpn. **53** (1984) 3457.
85Shu Shuvalov, L.A., Gridnev, S.A., Popov, V.M., Kudaev, A.V.: Ferroelectrics Lett. **3** (1985) 103.
86San Sangunni, K.S., Ravi, R., Bhat, H.L., Narayanan, P.S.: Jpn. J. Appl. Phys. **25** (1986) 380.
86Zan Zankevich, V.A.: Fiz. Tverd. Tela **28** (1986) 603; Sov. Phys. Solid State (English Transl.) **28** (1986) 339.
87AlE Al-Eithan, F.Y.M., Al-Edani, M.C., Abass, A.K.: Phys. Status Solidi (a) **103** (1987) 571.
88Bur Burshtein, Z., Burger, A., Morgan, S., Silberman, E.: J. Opt. Soc. Am. A **5** (1988) 2010.
88Cza Czarnecka, A., Stankowska, J.: Ferroelectrics **81** (1988) 91.
88Kor1 Koralewski, M., Kubicki, M., Czarnecka, A.: Ferroelectrics **80** (1988) 265.
88Kor2 Koralewski, M., Glazer, A.M., Czarnecka, A.: Ferroelectrics **80** (1988) 261.
88Sta1 Stankowska, J., Hamed, A.E.: Acta Phys. Pol. A **74** (1988) 399.
88Sta2 Stankowska, J., Hamed, A.E.: Acta Phys. Pol. A **74** (1988) 37.
89Fug Fugiel, B.: Ferroelectrics **100** (1989) 175.
89Kal Kalisz, L., Fugiel, B., Ziolo, J.: Solid State Commun. **71** (1989) 679.
89San Sangunni, K.S., Bhat, H.L., Narayanan, P.S.: Ferroelectrics Lett. **10** (1989) 87.
89Sta Stankowska, J., Czarnecka, A., Tarnowka, D.: Acta Phys. Pol. A **76** (1989) 529.
89Str Strukov, B.A., Minaeva, K.A., Spiridonov, T.P.: Fiz. Tverd. Tela **31** (1989) 288; Sov. Phys. Solid State (English Transl.) **31** (1989) 515.
89Wan Wang, M., Fang, C.S., Zhuo, H.S.: Ferroelectrics **91** (1989) 365.
90Gri Gridnev, S.A., Prasolov, B.N., Dybova, O.V., Maksimova, N.G.: Izv. Akad. Nauk SSSR, Ser. Fiz. **54** (1990) 721; Bull. Acad. Sci. USSR, Phys. Ser. (English Transl.) **54**, No. 4 (1990) 115.
90Ham Hamed, A.E., Kassem, M.E., Kandil, S.H., El-Samahy, A.E.: Ferroelectrics **110** (1990) 119.
91Ham Hamed, A.E., Kassem, M.E., El-Osaily, M., Okaz, A.M.: Phase Transitions **29** (1991) 219.

91Str1 Strukov, B.A., Taraskin, S.A., Suvkhanov, A.B.: Izv. Akad. Nauk SSSR, Ser. Fiz. **55** (1991) 539; Bull. Acad. Sci. USSR, Phys. Ser. (English Transl.) **55**, No. 3 (1991) 119.
91Str2 Strukov, B.A., Belov, A.A.: Vestn. Moskov. Univ., Fiz. Astron. **32**, No. 2 (1991) 100; Moscow Univ. Phys. Bull. (English Transl.) **46**, No. 2 (1991) 98.
91Str3 Strukov, B.A., Taraskin, S.A., Belov, A.A.: Ferroelectrics **117** (1991) 77.
92Ham Hamed, A.E.: Phase Transitions **38** (1992) 43.
93Str Strukov, B.A., Taraskin, S.A., Song, Y.V., Varikash, V.M., Pupkevich, P.A.: Izv. Akad. Nauk SSSR, Ser. Fiz. **57**, No. 6 (1993) 12; Bull. Acad. Sci. USSR Phys. Ser. (English Transl.) **57** (1993) 963.
94Igl1 Iglesias, T., Noheda, B., Lifante, G., Gonzalo, J.A., Koralewski, M.: Phys. Rev. B **50** (1994) 10307.
94Igl2 Iglesias, T., Noheda, B., Gallego, B., Fernandez del Castillo, J.R., Lifante, G., Gonzalo, J.A.: Europhys. Lett. **28** (1994) 91.
94Kas Kassem, M.E., Hamed, A.E., Abulnasr, L., Abboudy, S.: Radiat. Phys. Chem. **44** (1994) 527.
94Str Strukov, B.A., Taraskin, S.A., Song, Y.W., Varikash, V.M., Pupkevich, P.A.: Phase Transitions **46** (1994) 239.
95Fug Fugiel, B., Westwanski, B., Pawlik, M., Paradala, M., Pawlik, J.: Ferroelectrics **166** (1995) 131.
95Prz Przeslawski, J., Iglesias, T., Gonzalo, J.A.: Solid State Commun. **96** (1995) 195.
96Fur Furuta, H., Yoshioka, S., Tsujimi, Y., Shimada, Y., Yagi, T.: Physica B **219**/**220** (1996) 541.
96Hof Hoffmann, S.K., Hilczer, W., Goslar, J.: J. Magn. Reson. A **122** (1996) 37.
96Kor Koralewski, M., Stankowska, J., Iglesias, T., Gonzalo, J.A.: J. Phys. C **8** (1996) 4079.

No. 60A-3 $(NH_2CH_2COOH)_3 \cdot H_2BeF_4$, Triglycine fluoroberyllate (TGFB)

(M = 312.22; [D: 329.33])

1a Ferroelectricity in TGFB was first reported by Pepinsky et al. in 1957. 57Pep

b

phase	II	I
state	F	P
crystal system	monoclinic	monoclinic
space group	$P2_1 - C_2^2$	$P2_1/m - C_{2h}^2$
Θ [°C]	72.82(5) [a])	

57Pep

[a]) 77Gor

Θ for deuterated crystal: see Fig. 60B-2-001 in No. 60B-2. See also 79Loi
P_s || [010]. 57Pep
$\rho = 1.631_5 \cdot 10^3$ kg m^{-1} at 20 °C. 57Pep
Transparent, colorless. 58Nit
Cleavage plane: (010).

2a Crystal growth: evaporation or cooling from aqueous solution. 58Nit, 66Wie

Solubility in H_2O: see Fig. 60A-1-001 in No. 60A-1.
Solubility of deuterated TGFB (DTGFB) in D_2O: see 79Loi

3a Unit cell parameters: a = 9.385(1) Å, b = 12.632(2) Å, c = 5.699(1) Å, β = 110.31° at 23 °C. 79Was

b Crystal structure: isomorphous with TGS, Z = 2. 73War
Table 60A-3-001, Table 60A-3-002, Table 60A-3-003, Table 60A-3-004, Table 60A-3-005, Table 60A-3-006, Table 60A-3-007.

4 Thermal expansion: Fig. 60A-3-001, Fig. 60A-3-002; see also 72Zar, 80Sta

Thermal expansion coefficients: Fig. 60A-3-003.

5a Dielectric constant: Fig. 60A-3-004, Fig. 60A-3-005, Fig. 60A-3-006; see also 66Str, 78Fel

For Cu^{2+}-, Cr^{3+}-doped crystal: see 73Sta
Phase diagram in regard to p: Fig. 60A-3-007.
Change of Θ for uniaxial pressure: see Table 60A-1-012 in No. 60A-1.
Dielectric constants in far-infrared region: see Fig. 60A-3-023, Fig. 60A-3-024 in subsection 9a.

b Nonlinear dielectric properties: Fig. 60A-3-008, Fig. 60A-3-009.
$E = (T - \Theta)P/\varepsilon_0 C + \xi P^3 + \zeta P^5$, $C = 2.5 \cdot 10^3$ K, $\xi = 2.4 \cdot 10^{11}$ V m^5 C^{-3}, 77Gor
$\zeta = 4.2 \cdot 10^{14}$ V m^9 C^{-5}, Θ = 72.82(5) °C.
See also 66Wie

c Spontaneous polarization: Fig. 60A-3-010, Fig. 60A-3-011, Fig. 60A-3-012; see also 57Hos, 66Str, 73Tse

For Cu^{2+}-, Cr^{3+}-doped crystal: see 73Sta
Coercive field: Fig. 60A-3-013, Fig. 60A-3-014; see also 66Wie
For Cu^{2+}-, Cr^{3+}-doped crystal: see 73Sta

d	Pyroelectric coefficient: Fig. 60A-3-006, Fig. 60A-3-015; see also	73Tse, 81Mat
	For L-α-alanine-doped crystal (LATGFB): see	88Cho
6a	Heat capacity: Fig. 60A-3-016, Fig. 60A-3-017; see also	66Str, 83Ema
	Transition heat and transition entropy: ΔQ_m = 1670 J mol^{-1}, ΔS_m = 4.89 J K^{-1} mol^{-1}.	57Hos
b	Thermal conductivity: Fig. 60A-3-018; see also	78Fel
	Thermal diffusivity: see	78Fel
7a	Piezoelectric constant at high pressure: Fig. 60A-3-019. Piezoelectric properties of irradiated crystal and L-α-alanine-doped crystal (LATGFB): see	82Var
8a	Ultrasonic attenuation: Fig. 60A-3-020.	
9a	Refractive indices: n_a = 1.526, n_b = 1.502, n_c = 1.526 for λ = 632.8 nm. Birefringence: Fig. 60A-3-021. Far-infrared absorption: Fig. 60A-3-022. Far-infrared and infrared spectra: Fig. 60A-3-023, Fig. 60A-3-024. Infrared transmission: Fig. 60A-3-025. Reflectance spectra in the 5 to 22 eV region: see	73Mer2 78Rom
c	Piezooptic constant: Fig. 60A-3-026. See also Table 60A-1-020 in No. 60A-1.	
10a	Raman scattering: see	90YiJ
b	Brillouin scattering: see	73Mer2
11	Electric conduction: Table 60A-3-008; Fig. 60A-3-027.	
13a	NMR: Table 60A-3-009; Fig. 60A-3-028, Fig. 60A-3-029, Fig. 60A-3-030, Fig. 60A-3-031.	
b	ESR for Cu^{2+}-doped crystal: Table 60A-3-010, Table 60A-3-011; Fig. 60A-3-032, Fig. 60A-3-033. For Cr^{3+}-doped crystal: see Table 60A-1-028 and Fig. 60A-1-161 in No. 60A-1; see also	 78Wap, 81Sta
15a	Domain structure was observed by etching method.	73Sta
b	Domain switching: Fig. 60A-3-034, Fig. 60A-3-035.	
16	Etchant for revealing domain structure: 10 % aqueous solution of NH_4OH.	73Sta

Table 60A-3-001. $(NH_2CH_2COOH)_3 \cdot H_2BeF_4$ (TGFB). Fractional coordinates and isotropic temperature parameters in phase I (85 °C) [73War]. B is defined by Eq. (e) in Introduction. Unit cell parameters: a = 9.401(1) Å, b = 12.627(1) Å, c = 5.713 Å, β = 110.13(1)° at 85 °C.

	x	y	z	B [Å^2]
F(3)	0.0830(5)	0.1503(3)	0.1983(8)	4.12(8)
O(3)	0.2187(6)	0.5002(4)	0.7649(10)	4.73(11)
O(4)	0.4547(6)	0.5275(5)	0.7790(10)	5.13(12)
O(2)	0.4878(9)	0.2655(11)	0.6594(16)	5.11(20)
C(3)	0.3112(7)	0.5285(6)	0.6722(12)	3.63(13)
C(4)	0.2644(7)	0.5710(7)	0.4110(13)	4.08(13)
N(2)	0.0972(6)	0.5727(5)	0.2961(10)	3.85(11)
N(1)	0.3490(15)	0.2144(13)	0.1502(26)	6.14(34)
Be	0.9966(11)	0.25	0.2222(20)	2.49(18)
F(1)	0.8456(6)	0.25	–0.0022(10)	3.61(11)
F(2)	0.9676(6)	0.25	0.4737(11)	4.18(12)
O(1)	0.5995(9)	0.25	0.0615(15)	4.94(17)
C(1)	0.5791(12)	0.25	0.8633(20)	4.12(20)
C(2)	0.3268(12)	0.25	0.8977(21)	4.45(21)

Table 60A-3-002. $(NH_2CH_2COOH)_3 \cdot H_2BeF_4$ (TGFB). Fractional coordinates and temperature parameters in phase II (23 °C) [79Was]. The anisotropic temperature parameter U_{ij} [$\cdot 10^{-2}$ Å] is defined by Eq. (d) in Introduction. U is defined as $U = B/4$. B: isotropic temperature parameter defined by Eq. (e) in Introduction.

Atom	x	y	z	U_{11}	U_{22}	U_{33}	U_{23}	U_{13}	U_{12}
Be	0.9964(6)	0.25	0.2281(12)	1.85(11)	1.88(6)	1.87(8)	–0.14(9)	0.74(6)	–0.02(6)
F(1)	0.8435(4)	0.2513(5)	0.0010(5)	1.75(8)	3.89(7)	2.53(8)	0.08(6)	0.46(6)	0.05(6)
F(2)	0.9684(3)	0.2463(4)	0.4770(5)	4.39(7)	3.42(7)	2.38(6)	–0.21(6)	1.88(5)	–0.10(6)
F(3)	1.0821(4)	0.1487(4)	0.1955(6)	2.56(6)	2.38(8)	3.73(7)	–0.04(7)	1.40(5)	0.58(7)
F(4)	1.0853(5)	0.3500(4)	0.2055(6)	3.08(6)	2.35(8)	3.63(6)	0.28(7)	0.86(6)	–0.75(7)
O(11)	0.5991(2)	0.2610(4)	1.0742(5)	1.83(9)	5.59(10)	3.22(8)	0.35(7)	0.98(7)	–0.16(6)
O(12)	0.4859(3)	0.2744(5)	0.6617(7)	3.68(8)	6.43(9)	3.04(8)	0.27(6)	1.09(8)	–0.72(7)
C(11)	0.4806(3)	0.2652(5)	0.8675(6)	2.20(6)	2.52(6)	3.04(6)	0.02(4)	0.84(8)	–0.22(6)
C(12)	0.3318(3)	0.2590(6)	0.9142(7)	1.88(7)	3.36(9)	3.73(6)	0.56(5)	0.72(8)	0.19(5)
N(1)	0.3486(4)	0.2131(6)	0.1579(8)	2.22(8)	5.19(10)	3.78(4)	0.05(7)	1.68(9)	0.46(7)
O(21)	0.2222(2)	0.5095(5)	0.7795(6)	2.63(8)	4.32(9)	3.02(5)	0.97(9)	0.66(8)	–0.27(6)
O(22)	0.4642(2)	0.5353(4)	0.8087(7)	2.08(8)	4.49(9)	3.19(5)	0.73(8)	0.17(6)	0.30(9)
C(21)	0.3194(2)	0.5359(6)	0.6915(7)	2.28(7)	1.18(10)	2.37(6)	0.30(6)	0.43(7)	0.07(10)
C(22)	0.2755(3)	0.5728(5)	0.4251(8)	2.21(7)	3.87(9)	2.71(9)	0.44(8)	0.91(8)	0.05(9)
N(2)	0.1099(4)	0.5724(4)	0.2974(8)	2.75(8)	2.56(4)	1.86(10)	0.31(7)	0.27(7)	–0.30(8)
O(31)	0.7916(2)	0.5040(4)	0.2473(6)	2.93(8)	4.91(6)	2.87(9)	1.21(8)	0.86(7)	–0.47(9)
O(32)	0.5561(3)	0.4853(5)	0.2566(7)	2.51(5)	7.06(4)	3.79(5)	1.50(6)	1.16(8)	1.52(8)
C(31)	0.7043(2)	0.4783(6)	0.3513(8)	2.68(6)	2.55(5)	2.73(8)	0.09(8)	0.96(7)	0.35(5)
C(32)	0.7566(2)	0.4317(5)	0.6108(8)	2.83(7)	3.09(6)	2.69(8)	0.61(10)	1.15(9)	0.24(8)
N(3)	0.9222(5)	0.4222(4)	0.7128(9)	2.91(8)	2.60(6)	2.21(7)	0.04(8)	0.57(9)	–0.49(6)

Atom	x	y	z	U
H(11)	0.4265(10)	0.1538(9)	0.1858(9)	0.0320(2)
H(12)	0.2697(9)	0.2878(8)	1.1837(11)	0.0311(1)
H(13)	0.3945(10)	0.2531(11)	1.3053(11)	0.0315(2)
H(14)	0.2799(12)	0.1941(11)	0.8377(11)	0.0307(1)
H(15)	0.2638(11)	0.2885(9)	0.7873(10)	0.0304(2)
H(16)	0.6851(10)	0.2429(9)	1.0326(10)	0.0305(1)
H(21)	0.0804(10)	0.5044(11)	0.2044(10)	0.0328(2)
H(22)	0.0735(10)	0.5939(11)	0.1019(11)	0.0364(1)
H(23)	0.0859(9)	0.6145(12)	0.4119(10)	0.0373(3)
H(24)	0.3196(11)	0.5353(11)	0.6563(11)	0.0351(4)
H(25)	0.3136(11)	0.6428(10)	0.5961(10)	0.0304(3)
H(26)	0.5080(9)	0.5158(10)	0.9802(11)	0.0392(2)
H(31)	0.9833(9)	0.4770(8)	0.7070(10)	0.0330(4)
H(32)	0.9618(10)	0.4021(11)	0.8827(11)	0.0315(2)
H(33)	0.9500(10)	0.3819(10)	0.6278(12)	0.0298(3)
H(34)	0.7065(11)	0.3648(11)	0.5990(10)	0.0305(2)
H(35)	0.7248(10)	0.4692(11)	0.7231(11)	0.0316(3)

Table 60A-3-003. $(NH_2CH_2COOH)_3 \cdot H_2BeF_4$ (TGFB). Interatomic distances and bond angles in phase I (85 °C) [73War].

Bond lengths [Å]		Bond lengths [Å]		Bond angles [°]	
Be –F(1)	1.552(10)	O(3)–C(3)	1.217(10)	F(2)–Be–F(3)	110.52
–F(2)	1.553(15)	O(4)–C(3)	1.276(08)	F(2)–Be–F(1)	111.27
–F(3)	1.528(08)	C(3)–C(4)	1.503(10)	F(1)–Be–F(3)	106.81
F(1)–F(2)	2.563(08)	C(4)–N(2)	1.481(09)	O(1)–C(1)–O(2)	120.81
–F(3)	2.473(06)	N(1)–F(3)	2.732(17)	O(1)–C(1)–C(2)	117.51
F(2)–F(3)	2.533(08)	–O(4)	2.937(17)	O(2)–C(1)–C(2)	120.76
F(3)–F(4)	2.516(10)	–O(2)	2.824(16)	N(1)–C(2)–C(1)	108.37
O(1)–C(1)	1.297(12)	N(2)–F(1)	2.955(08)	O(3)–C(3)–O(4)	125.83
O(2)–C(1)	1.213(16)	–F(2)	2.767(08)	O(3)–C(3)–C(4)	121.91
C(1)–C(2)	1.516(18)	–F(4)	2.865(09)	O(4)–C(3)–C(4)	112.26
C(2)–N(1)	1.445(19)	O(4)–O(6)	2.471(11)	N(2)–C(4)–C(3)	110.43
		O(1)–F(1)	2.464(11)		

Table 60A-3-004. $(NH_2CH_2COOH)_3 \cdot H_2BeF_4$ (TGFB). Interatomic distances and bond angles in phase II (23 °C) [79Was].

Bond lengths [Å]		Bond angles [°]	
Glycine I			
C(11)–O(11)	1.311(9)	O(11)–C(11)–O(12)	125.0(8)
C(11)–O(12)	1.197(10)	O(11)–C(11)–C(12)	112.8(7)
C(11)–C(12)	1.511(10)	O(12)–C(11)–C(12)	122.8(8)
C(12)–N(1)	1.462(11)	C(11)–C(12)–N(1)	112.7(6)
Glycine II			
C(21)–O(21)	1.230(11)	O(21)–C(21)–O(22)	125.7(8)
C(21)–O(22)	1.289(10)	O(21)–C(21)–C(22)	120.9(7)
C(21)–C(22)	1.502(11)	O(22)–C(21)–C(22)	113.3(8)
C(22)–N(2)	1.469(10)	C(21)–C(22)–N(2)	111.8(7)
Glycine III			
C(31)–O(31)	1.210(12)	O(31)–C(31)–O(32)	125.7(8)
C(31)–O(32)	1.309(11)	O(31)–C(31)–C(32)	122.7(8)
C(31)–C(32)	1.506(12)	O(32)–C(31)–C(32)	111.6(8)
C(32)–N(3)	1.463(11)	C(31)–C(32)–N(3)	111.2(7)

Donor-acceptor	D–A	D–H	H–A
O(11)–H(16)–F(1)	2.472(7)	0.917(25)	1.560(21)
N(1)–H(11)–O(22)	2.818(8)	1.020(23)	1.809(35)
N(1)–H(12)–F(3)	2.708(6)	0.801(27)	1.957(25)
N(1)–H(13)–O(12)	2.810(8)	0.946(26)	1.930(18)
C(12)–H(14)		0.984(29)	
C(12)–H(15)		0.796(32)	
O(22)–H(26)–O(32)	2.476(9)	0.952(20)	1.530(21)
N(2)–H(21)–F(4)	2.853(8)	0.902(38)	2.022(38)
N(2)–H(22)–F(1)	2.951(9)	1.081(36)	2.285(23)
N(2)–H(22)–F(3)	2.925(6)	1.081(36)	1.941(35)
N(2)–H(23)–F(2)	2.770(8)	0.935(38)	1.902(36)
C(22)–H(24)		0.862(38)	
C(22)–H(25)		0.978(37)	
N(3)–H(31)–F(3)	2.911(8)	0.906(35)	2.372(35)
N(3)–H(32)–F(4)	2.842(7)	0.943(20)	1.919(21)
N(3)–H(32)–F(1)	2.958(7)	0.943(20)	2.415(38)
N(3)–H(33)–F(2)	2.708(6)	0.806(32)	1.951(36)
C(32)–H(34)		0.961(38)	
C(32)–H(35)		0.925(30)	

Table 60A-3-005. $(NH_2CH_2COOH)_3 \cdot H_2BeF_4$ (TGFB). Displacements of atoms from the best fit planes of the glycine molecules (GI, II, III) in phase I (85 °C) [73War].

Atom	GI [Å]	GII, GIII [Å]
N	+0.246	–0.021
C^N	–0.048	–0.001
C	+0.056	+0.004
O	0.000	–0.001
O^N	–0.009	–0.002

Table 60A-3-006. $(NH_2CH_2COOH)_3 \cdot H_2BeF_4$ (TGFB). Displacements of atoms from the best fit planes of the glycine molecules (GI, II, III) in phase II (23 °C) [79Was].

GI	[Å]	GII	[Å]	GIII	[Å]
O(11)	0.0016	O(21)	–0.0004	O(31)	–0.0016
O(12)	0.0019	O(22)	–0.0004	O(32)	–0.0013
C(11)	–0.0048	C(21)	0.0011	C(31)	0.0041
C(12)	0.0013	C(22)	–0.0003	C(32)	0.0011
N(1)	–0.4544	N(2)	0.0009	N(3)	0.0024

Table 60A-3-007. $(NH_2CH_2COOH)_3 \cdot H_2BeF_4$ (TGFB). Configuration of BeF_4^{2-} ion in phase II (23 °C) [79Was].

Bond distances [Å]		Bond angles [°]	
Be–F(1)	1.564(9)	F(1)–Be–F(2)	111.34(7)
–F(2)	1.531(9)	F(1)–Be–F(3)	105.90(6)
–F(3)	1.557(12)	F(1)–Be–F(4)	106.84(7)
–F(4)	1.544(12)	F(2)–Be–F(4)	111.95(7)
		F(3)–Be–F(4)	110.23(6)
		F(2)–Be–F(3)	110.36(7)

Table 60A-3-008. $(NH_2CH_2COOH)_3 \cdot H_2BeF_4$ (TGFB). Activation energy ΔU estimated from electric conductivity. Ionic conductivity $\sigma = \sigma_o \exp(-\Delta U/kT)$ [61Gur].

Estimated from	Ferroelectric phase	Paraelectric phase
σ_a	0.93 eV	0.64 eV
σ_b	0.76	0.70
σ_c	0.72	0.65

Table 60A-3-009. Deuterated triglycine fluoroberyllate (DTGFB). e^2qQ/h [kHz], η for ^{9}Be and direction cosines λ, μ, ν of the principal axes of the electric field gradient tensors in the crystal fixed coordinate system a^*, b, c [71Bli].

	T = 361 K	T = 340 K	T = 340 K
e^2qQ/h	130(3)	126(3)	126(3)
η	0.43(3)	0.64(3)	0.64(3)
ϕ_{zz} λ	±0.370	0.363	–0.363
μ	0.000	0.152	0.152
ν	±0.929	0.920	–0.920
ϕ_{yy} λ	±0.929	0.828	–0.828
μ	0.000	0.400	0.400
ν	0.370	–0.392	0.392
ϕ_{xx} λ	0.000	–0.428	0.428
μ	1.000	0.904	0.904
ν	0.000	0.020	0.020

Table 60A-3-010. $(NH_2CH_2COOH)_3 \cdot H_2BeF_4$ (TGFB):Cu^{2+}. ESR data [67Sta, 72Sta].

Paramagnetic center	S	**H**	ν [GHz]	T	g-factor	FS [10^{-2} m^{-1}]	HFS [10^{-2} m^{-1}]	Comment
Cu^{2+}	1/2	(3)	≈ 9	–100...120 °C	$g_{\parallel}$ = 2.24 $g_{\perp}$ = 2.06		$^nA_{\parallel}$ = 132 $^nA_{\perp}$ = 32	for FS due to two-ion aggregate; see Fig. 60A-3-032
Cu^{2+}	2	(5)	9.4	160 K	g_z = 2.12 g_y = 2.15 g_x = 2.08	D = 1080 E = 300		temperature change; see Fig. 60A-3-033

Table 60A-3-011. $(NH_2CH_2COOH)_3 \cdot H_2BeF_4$ (TGFB):Cu^{2+}. Spin Hamiltonian parameters of copper aggregates with spin S = 2 [72Mac].

D	E	a	b	c	g_x	g_y	g_z
[10^2 m^{-1}]							
0.108	0.030	–0.003	0	0.009	2.08	2.15	2.12

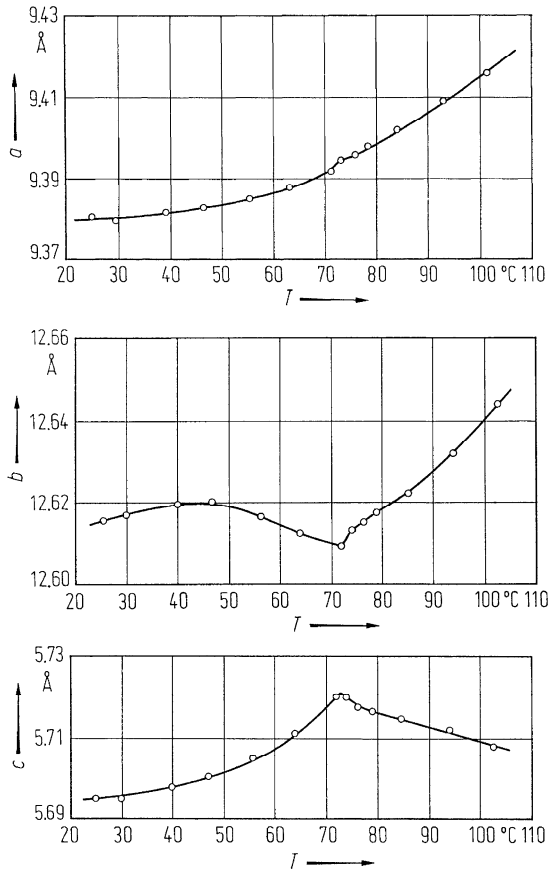

Fig. 60A-3-001. $(NH_2CH_2COOH)_3 \cdot H_2BeF_4$ (TGFB). *a*, *b*, *c* vs. *T* [77Was]. *a*, *b*, *c*: unit cell parameters.

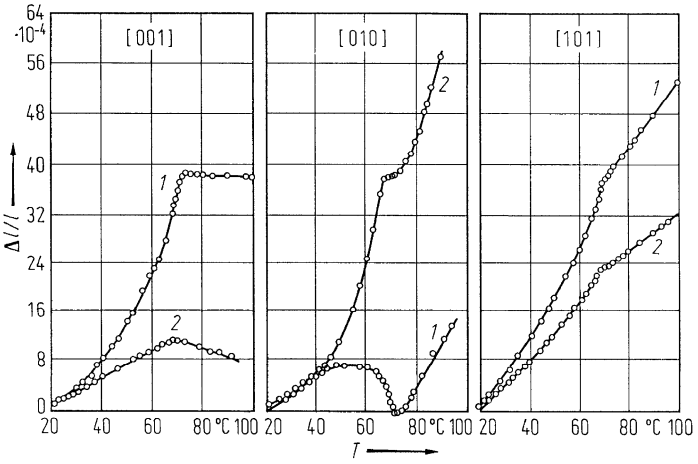

Fig. 60A-3-002. $(NH_2CH_2COOH)_3 \cdot H_2BeF_4$ (TGFB). $\Delta l/l$ vs. *T* [72Var]. $\Delta l/l$: linear thermal expansion along the [001], [010] and [101] directions. Curves *1*: unirradiated. Curves *2*: after γ-irradiation of 500 mR.

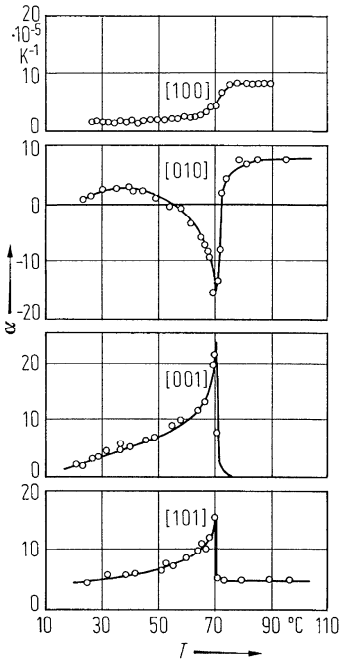

Fig. 60A-3-003. $(NH_2CH_2COOH)_3 \cdot H_2BeF_4$ (TGFB). α vs. T [72Zar]. α: linear thermal expansion coefficients along the [100], [010], [001] and [101] directions.

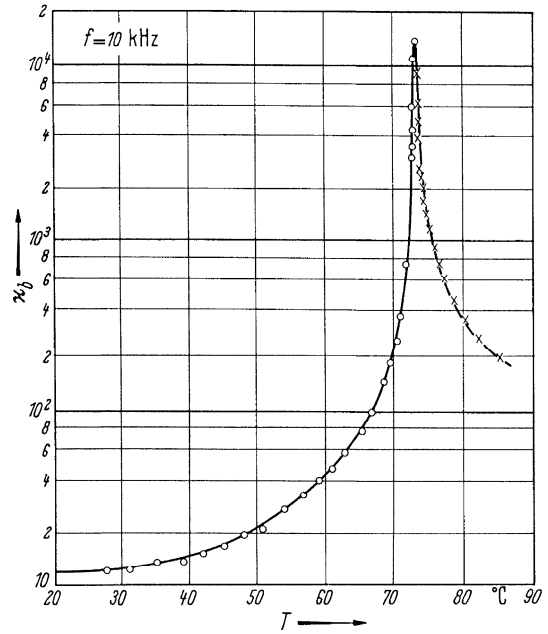

Fig. 60A-3-004. $(NH_2CH_2COOH)_3 \cdot H_2BeF_4$ (TGFB). κ_b vs. T [66Wie].

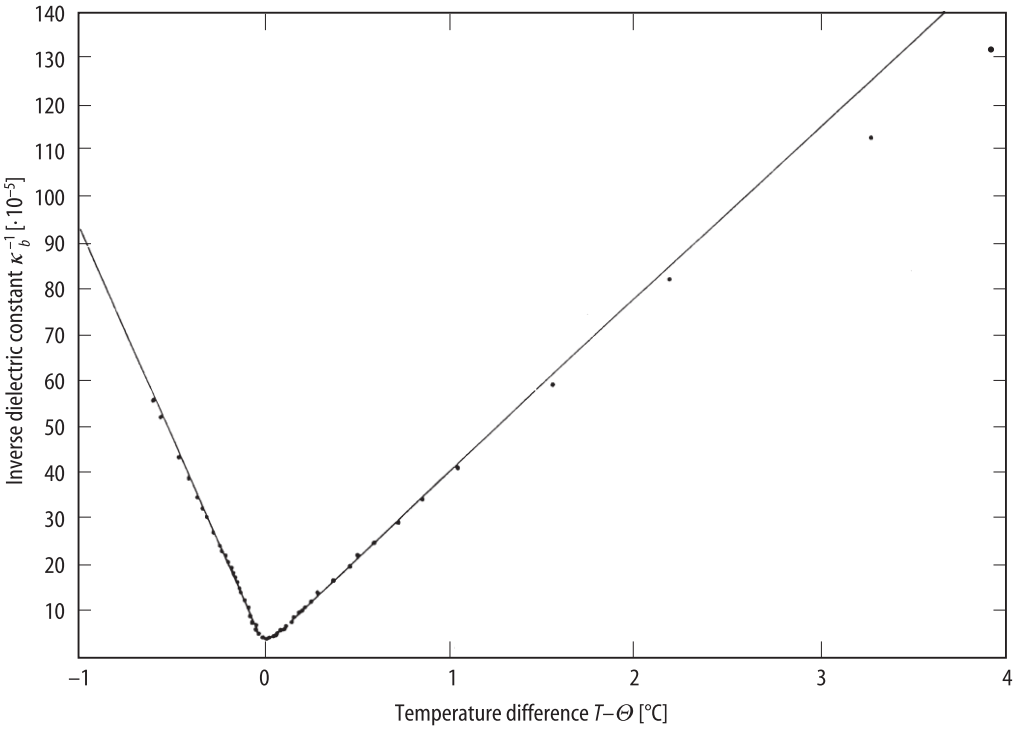

Fig. 60A-3-005. $(NH_2CH_2COOH)_3 \cdot H_2BeF_4$ (TGFB). κ_b^{-1} vs. $T - \Theta$ [73Mer1]. Θ = 73.30(5) °C. f = 1 kHz.

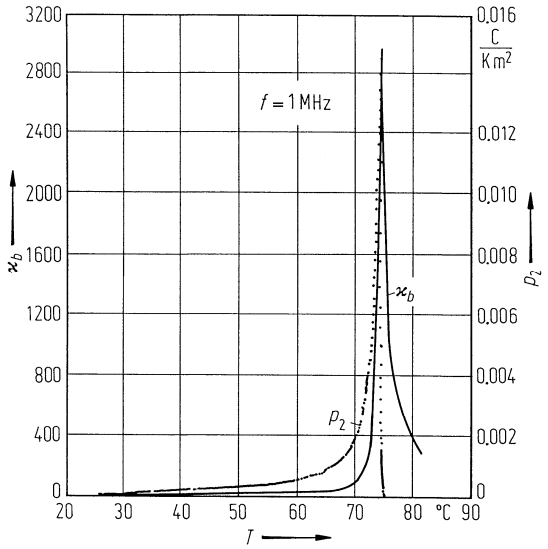

Fig. 60A-3-006. $(ND_2CH_2COOD)_3 \cdot D_2BeF_4$ (DTGFB). $\varkappa_b$, p_2 vs. T [80Dou]. p_2: pyroelectric coefficient along the b axis.

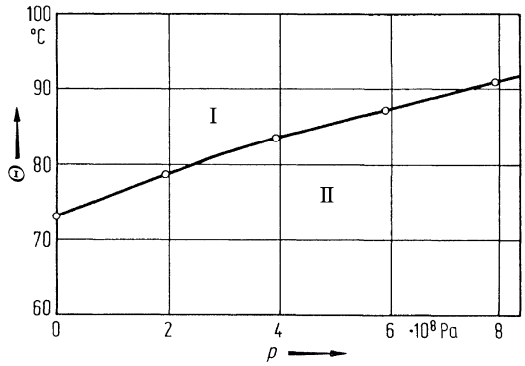

Fig. 60A-3-007. $(NH_2CH_2COOH)_3 \cdot H_2BeF_4$ (TGFB). Phase diagram [67Myl].

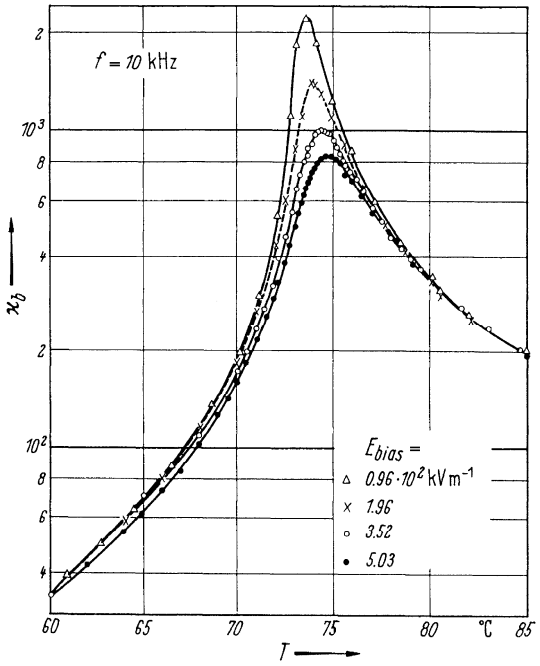

Fig. 60A-3-008. $(NH_2CH_2COOH)_3 \cdot H_2BeF_4$ (TGFB). κ_b vs. T [66Wie]. Parameter: E_{bias}.

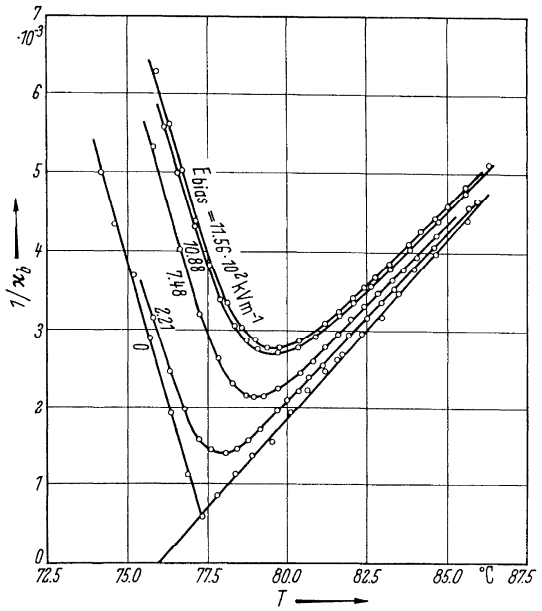

Fig. 60A-3-009. $(ND_2CH_2COOD)_3 \cdot D_2BeF_4$ (DTGFB). κ_b^{-1} vs. T [66Bre]. Parameter: E_{bias} .

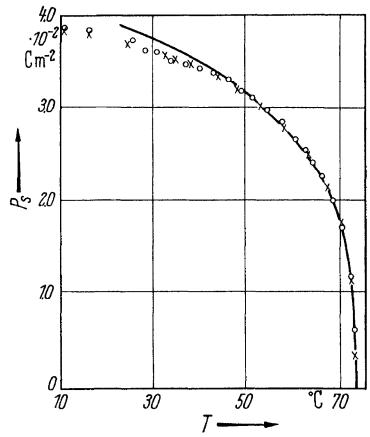

Fig. 60A-3-010. $(NH_2CH_2COOH)_3 \cdot H_2BeF_4$ (TGFB). P_s vs. T [66Wie].

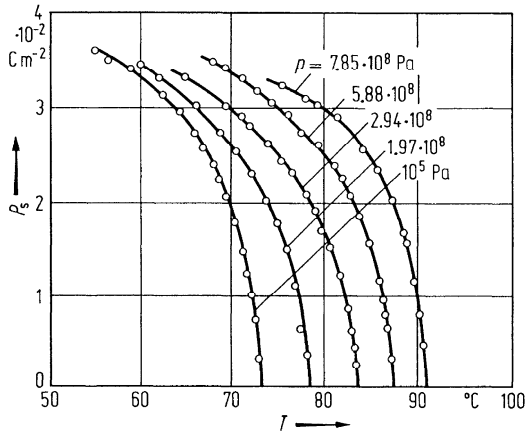

Fig. 60A-3-011. $(NH_2CH_2COOH)_3 \cdot H_2BeF_4$ (TGFB). P_s vs. T [67Myl]. Parameter: p.

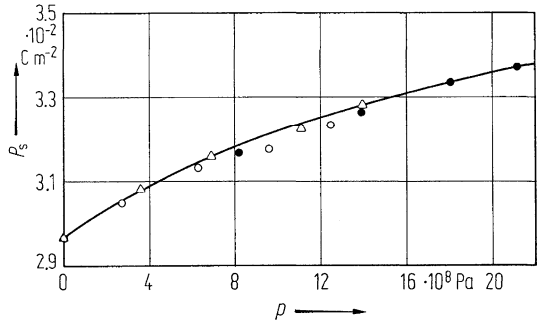

Fig. 60A-3-012. $(NH_2CH_2COOH)_3 \cdot H_2BeF_4$ (TGFB). P_s vs. p at RT [74Sta]. Open circle, full circle, triangle: by different specimens.

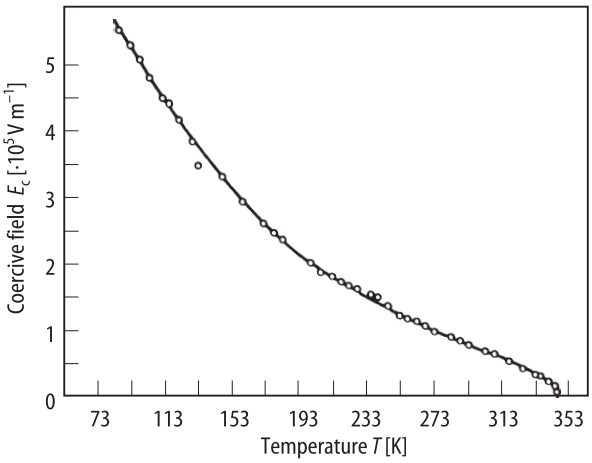

Fig. 60A-3-013. $(NH_2CH_2COOH)_3 \cdot H_2BeF_4$ (TGFB). E_c vs. T [74Sta].

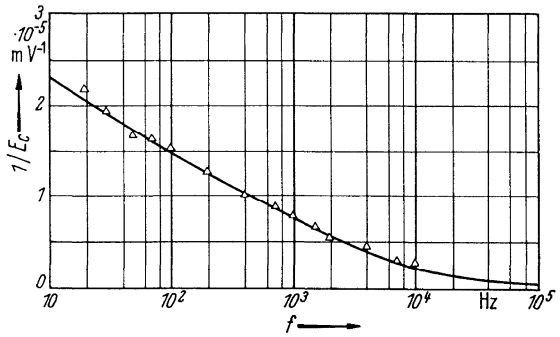

Fig. 60A-3-014. $(NH_2CH_2COOH)_3 \cdot H_2BeF_4$ (TGFB). $1/E_c$ vs. f [58Pul].

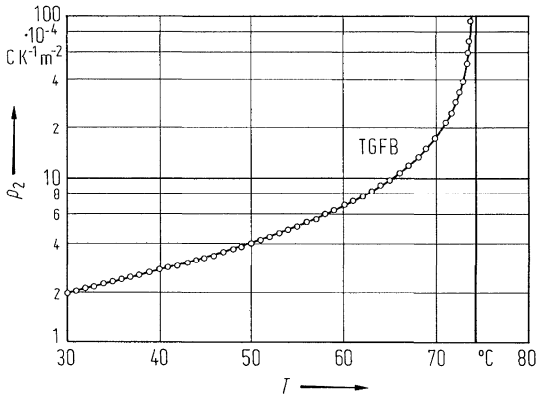

Fig. 60A-3-015. $(NH_2CH_2COOH)_3 \cdot H_2BeF_4$ (TGFB). p_2 vs. T [78Fel]. p_2: pyroelectric coefficient along the b axis.

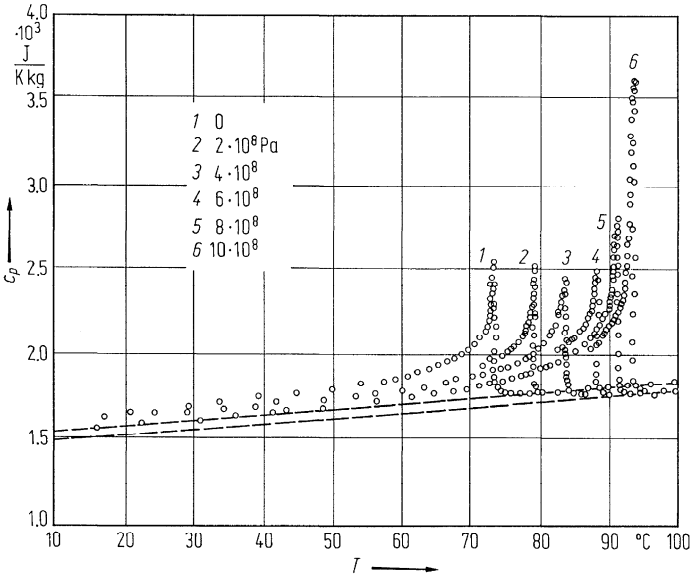

Fig. 60A-3-016. $(NH_2CH_2COOH)_3 \cdot H_2BeF_4$ (TGFB). c_p vs. T [79Che]. Parameter: p.

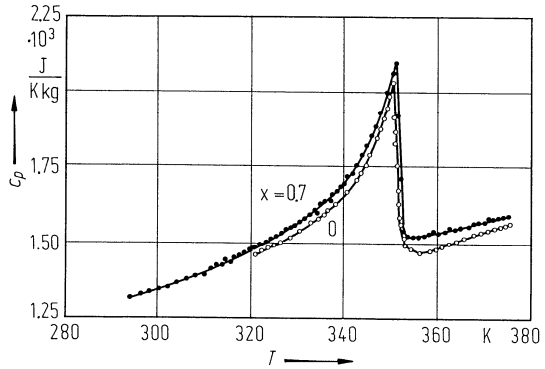

Fig. 60A-3-017. $[(NH_2CH_2COOH)_3 \cdot H_2BeF_4]_{1-x}[(ND_2CH_2COOD)_3 \cdot D_2BeF_4]_x$ ($TGFB_{1-x}DTGFB_x$). c_p vs. T [81Loi]. Parameter: x.

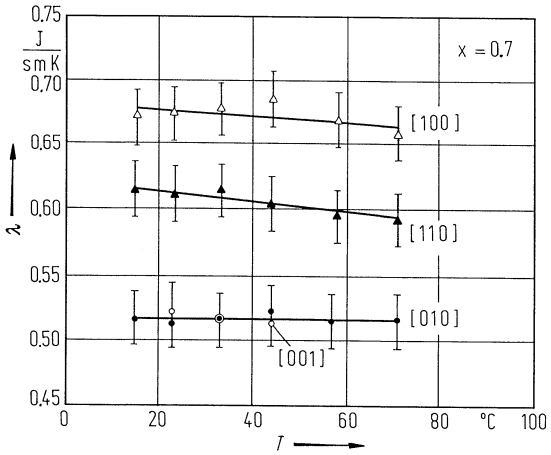

Fig. 60A-3-018. $[(NH_2CH_2COOH)_3 \cdot H_2BeF_4]_{1-x}[(ND_2CH_2COOD)_3 \cdot D_2BeF_4]_x$ ($TGFB_{1-x}DTGFB_x$, x = 0.7). λ vs. T [81Loi]. λ: thermal conductivity.

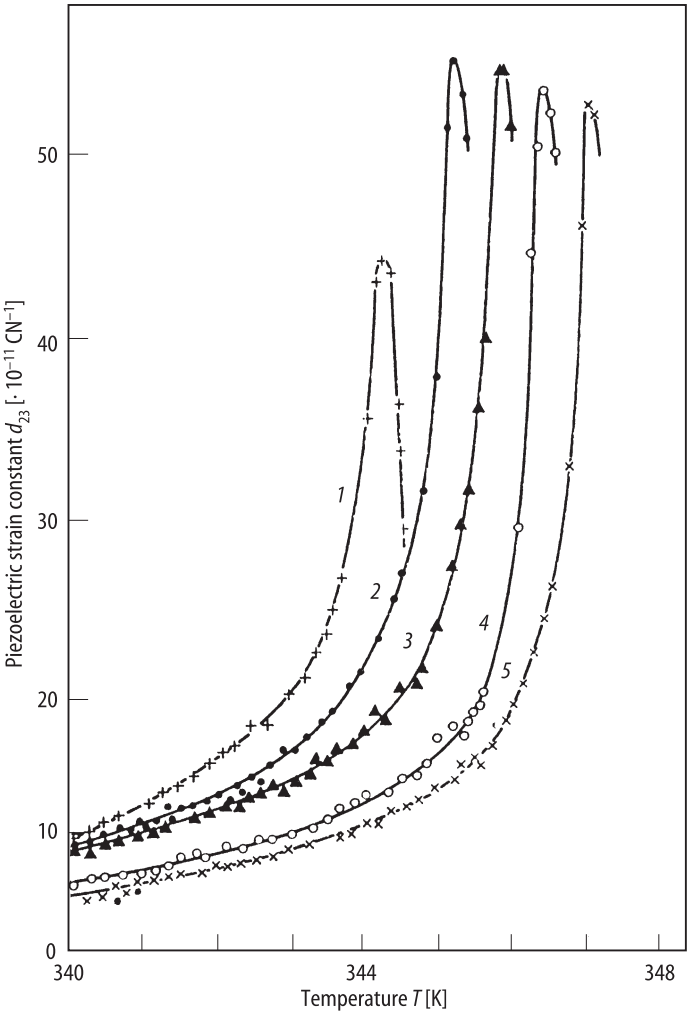

Fig. 60A-3-019. $(NH_2CH_2COOH)_3 \cdot H_2BeF_4$ (TGFB). d_{23} vs. T [83Zan]. Parameter: *p. 1*: p = 0.1 MPa; *2*: 20 MPa; *3*: 40 MPa; *4*: 90 MPa; *5*: 110 MPa.

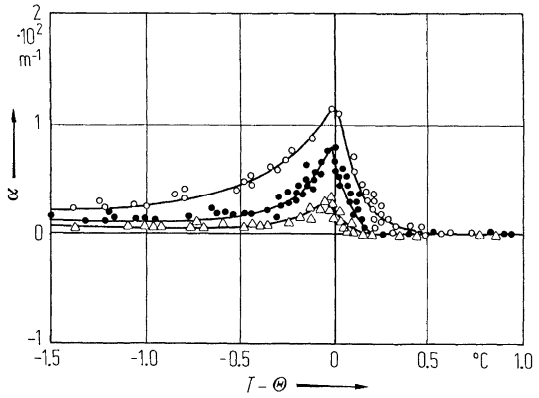

Fig. 60A-3-020. $(NH_2CH_2COOH)_3 \cdot H_2BeF_4$ (TGFB). α vs. $T - \Theta$ [67Min]. α: absorption coefficients of the longitudinal ultrasound propagating along the *c* axis. Parameter: *f*. Triangles: f = 5 MHz; full circles: 10 MHz; open circles: 15 MHz.

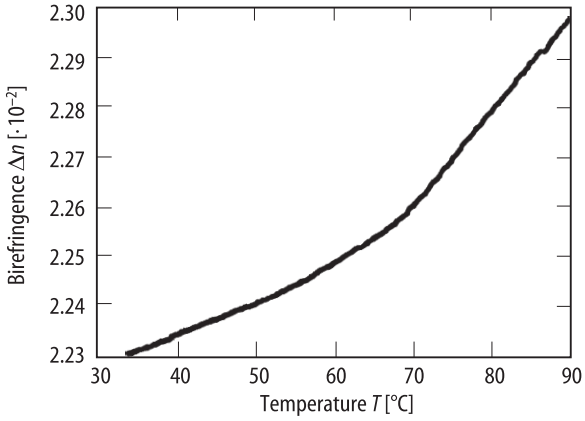

Fig. 60A-3-021. $(NH_2CH_2COOH)_3 \cdot H_2BeF_4$ (TGFB). Δn vs. T [94Ort]. Δn: birefringence along the b axis.

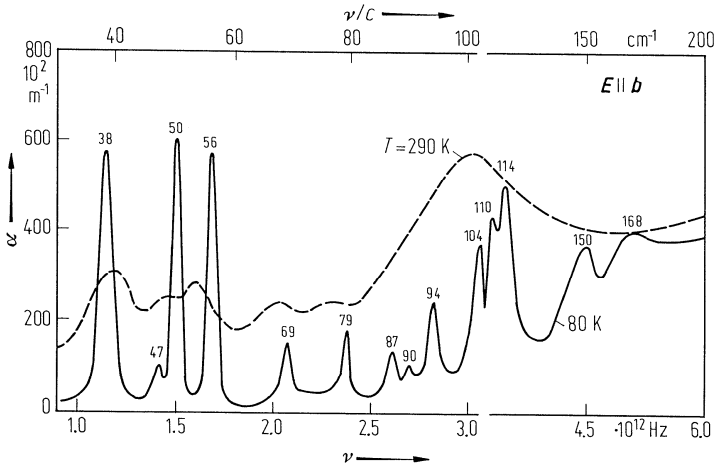

Fig. 60A-3-022. $(NH_2CH_2COOH)_3 \cdot H_2BeF_4$ (TGFB). α vs. ν [79Ver]. Parameter: T. α: far-infrared absorption coefficient along the c axis. $\boldsymbol{E} \parallel \boldsymbol{b}$. Full curve: $T = 80$ K, dashed curve: $T = 290$ K.

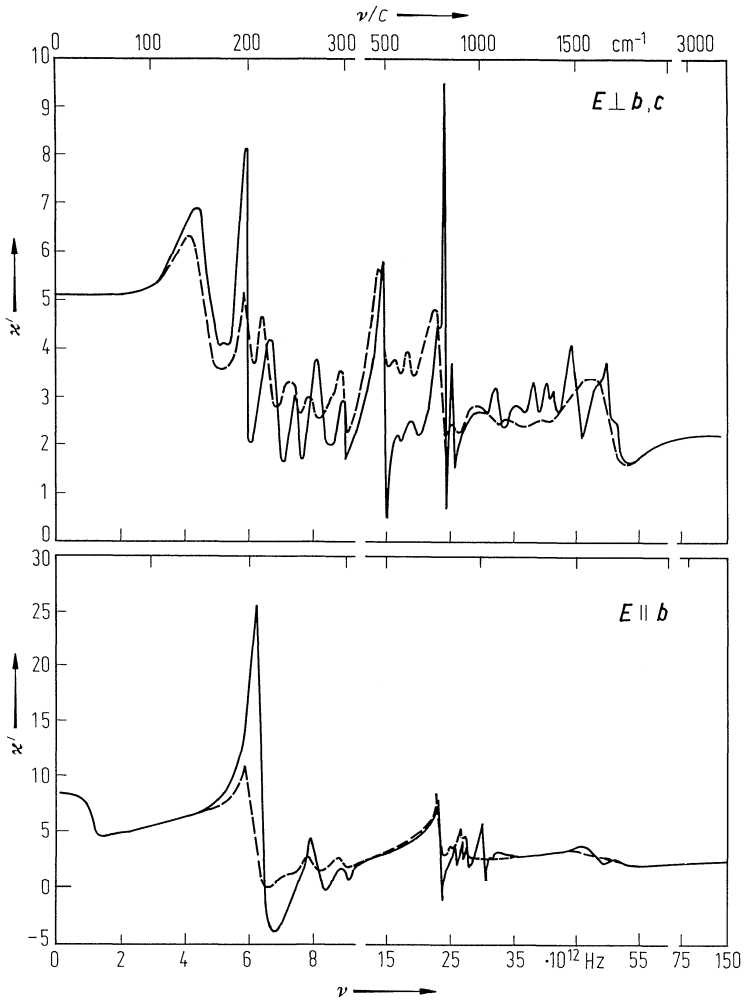

Fig. 60A-3-023. $(NH_2CH_2COOH)_3 \cdot H_2BeF_4$ (TGFB). κ' vs. ν [79Ver]. Parameter: T. Full curves: $T = 80$ K, dashed curves: $T = 290$ K. The curves were obtained from reflectivity data using Kramers-Kronig relation.

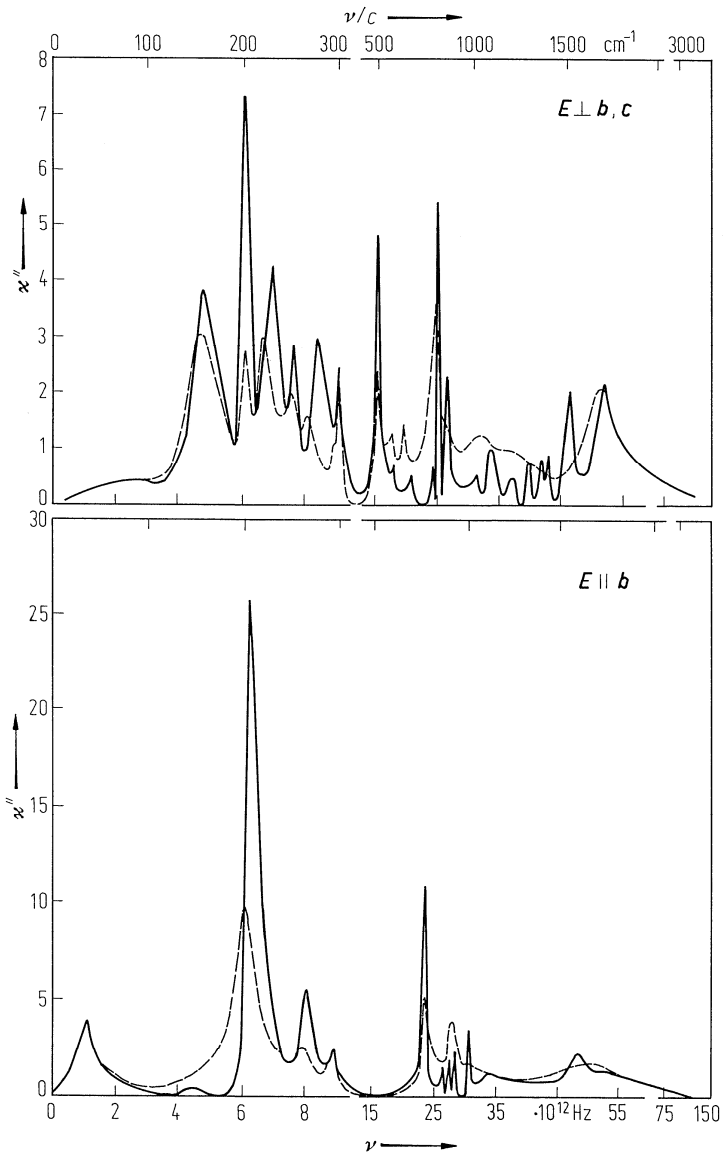

Fig. 60A-3-024. $(NH_2CH_2COOH)_3 \cdot H_2BeF_4$ (TGFB). κ'' vs. ν [79Ver]. Parameter: T. Full curves: $T = 80$ K, dashed curves: $T = 290$ K. The curves were obtained from reflectivity data using Kramers-Kronig relation.

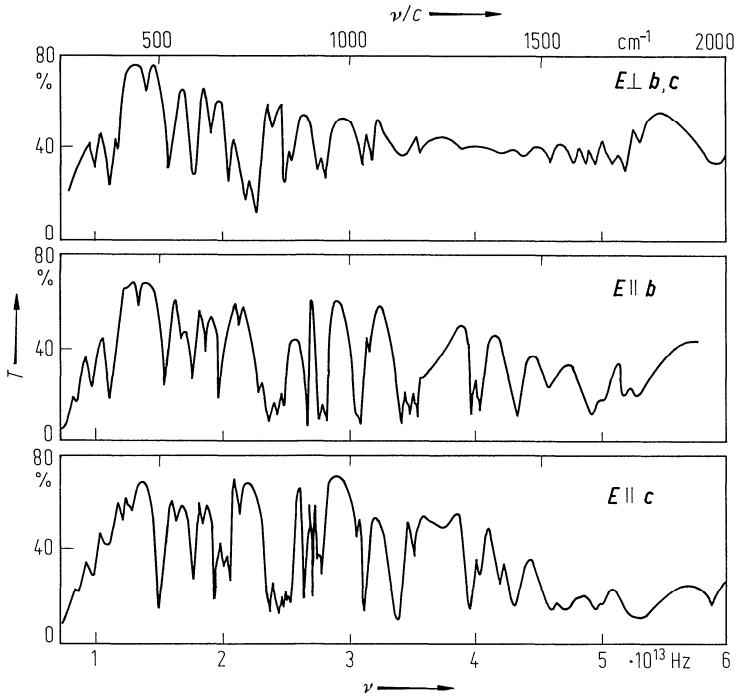

Fig. 60A-3-025. $(NH_2CH_2COOH)_3 \cdot H_2BeF_4$ (TGFB). T vs. ν [79Ver]. T: transmission. $T = 80$ K.

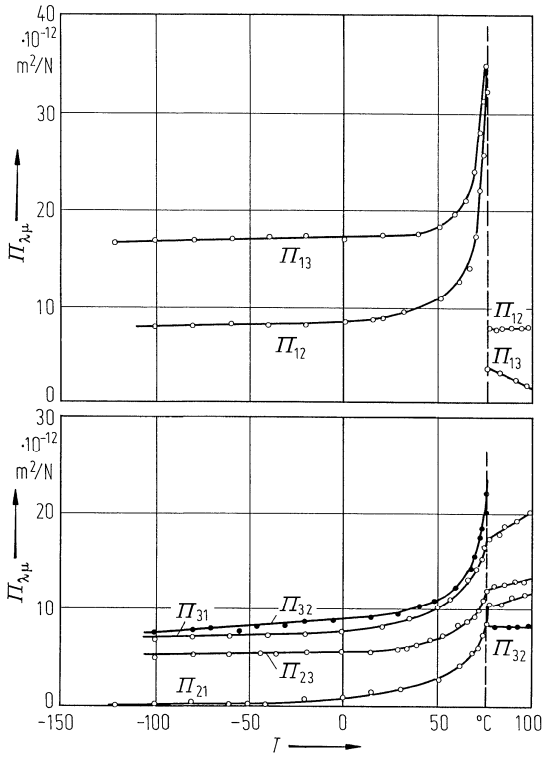

Fig. 60A-3-026. $(NH_2CH_2COOH)_3 \cdot H_2BeF_4$ (TGFB). $\Pi_{\lambda\mu}$ vs. T [83Rom]. $\Pi_{\lambda\mu}$: piezooptic constant for **T**. $\lambda = 632.8$ nm.

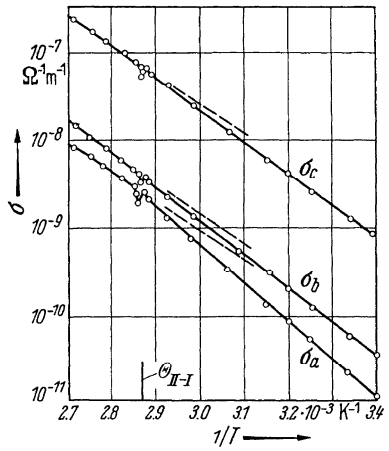

Fig. 60A-3-027. $(NH_2CH_2COOH)_3 \cdot H_2BeF_4$ (TGFB). σ_a, σ_b, σ_c vs. $1/T$ [61Gur].

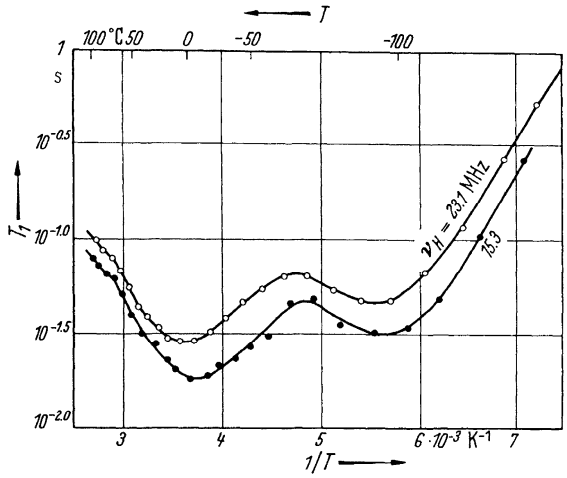

Fig. 60A-3-028. $(NH_2CH_2COOH)_3 \cdot H_2BeF_4$ (TGFB). T_1 vs. $1/T$ [66Bli]. T_1: spin-lattice relaxation time for proton. ν_H: Larmor frequency of proton.

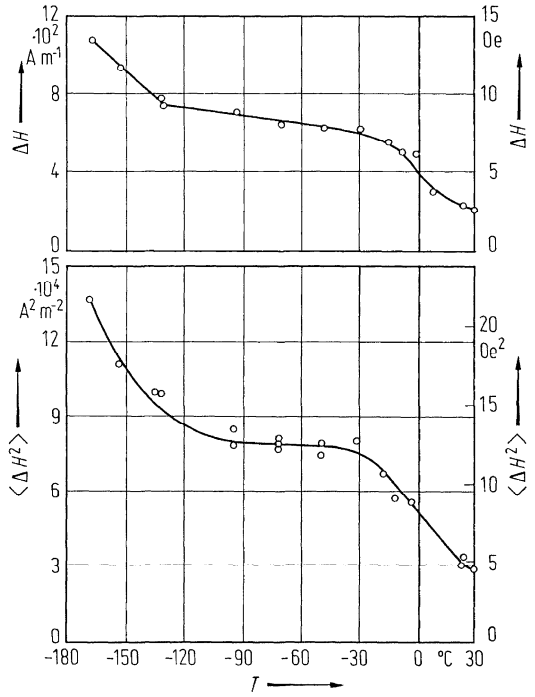

Fig. 60A-3-029. $(NH_2CH_2COOH)_3 \cdot H_2BeF_4$ (TGFB). ΔH, $\langle \Delta H^2 \rangle$ vs. T [63Bli]. ΔH, $\langle \Delta H^2 \rangle$: line width and second moment of ^{19}F magnetic resonance absorption in powdered TGFB, respectively.

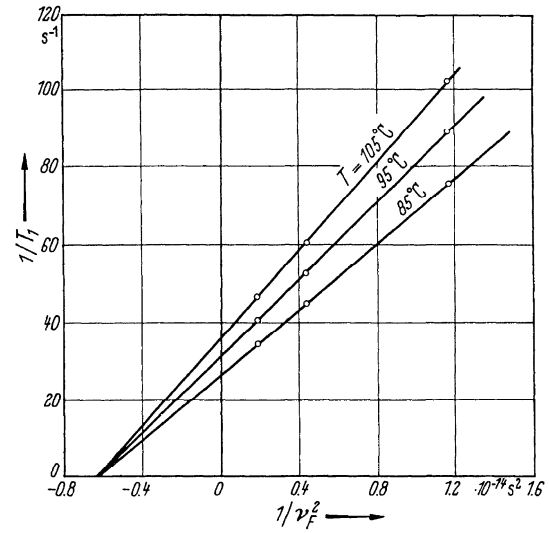

Fig. 60A-3-030. $(NH_2CH_2COOH)_3 \cdot H_2BeF_4$ (TGFB). $1/T_1$ of ^{19}F vs. $1/\nu_F^2$ [66Bli]. Parameter: T. ν_F: Larmor frequency of ^{19}F.

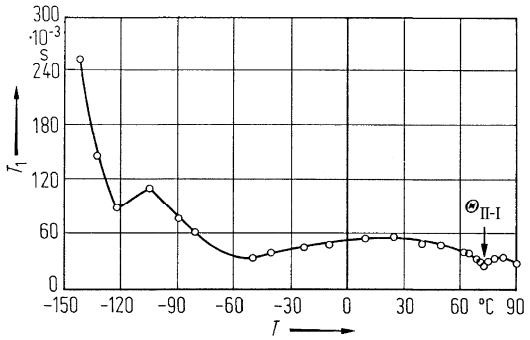

Fig. 60A-3-031. $(NH_2CH_2COOH)_3 \cdot H_2BeF_4$ (TGFB). T_1 vs. T [76Mul]. T_1: spin-lattice relaxation time of ^{19}F at 27 MHz.

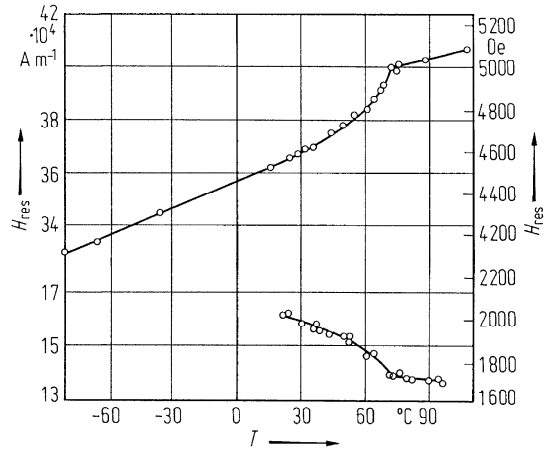

Fig. 60A-3-032. $(NH_2CH_2COOH)_3 \cdot H_2BeF_4$ (TGFB):Cu^{2+}. H_{res} vs. T [67Sta]. H_{res}: ESR magnetic field strength due to Cu^{2+} ion pair. See also Table 60A-3-010.

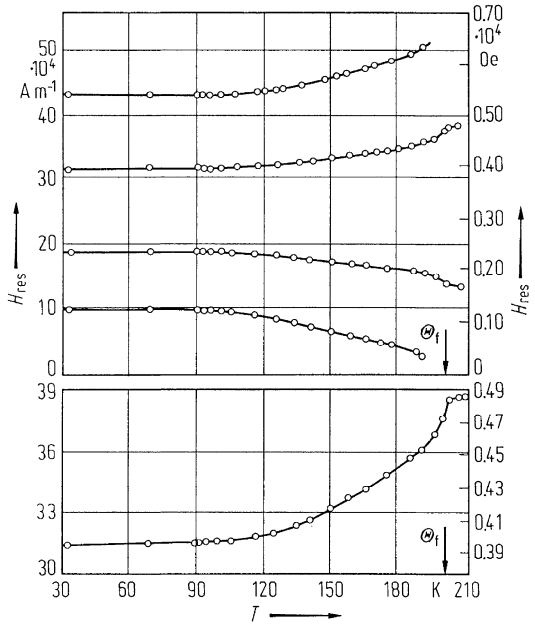

Fig. 60A-3-033. $(NH_2CH_2COOH)_3 \cdot H_2BeF_4$ (TGFB):Cu^{2+}. H_{res} vs. T [72Sta]. H_{res}: resonant field strength due to four-copper complex. See also Table 60A-3-010.

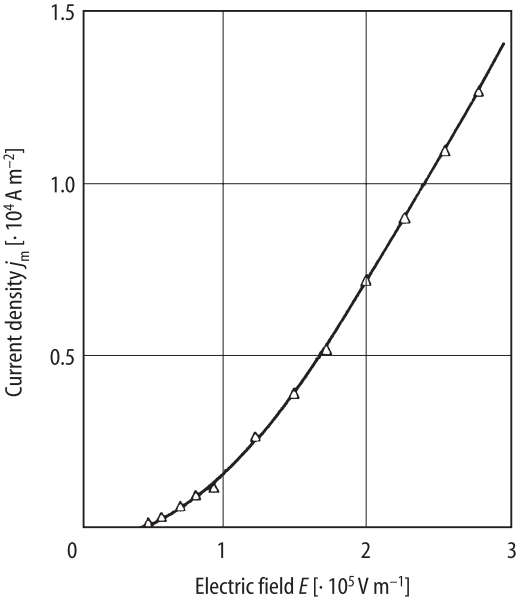

Fig. 60A-3-034. $(NH_2CH_2COOH)_3 \cdot H_2BeF_4$ (TGFB). j_m vs. E [58Pul]. j_m: maximum switching current density.

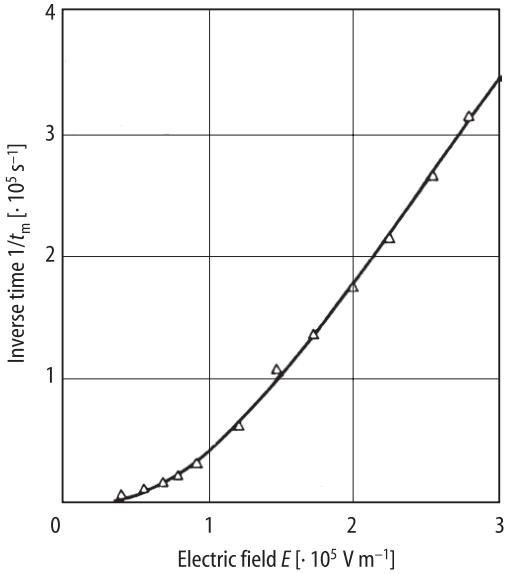

Fig. 60A-3-035. $(NH_2CH_2COOH)_3 \cdot H_2BeF_4$ (TGFB). $1/t_m$ vs. E [58Pul]. t_m: time corresponding to the maximum switching current.

References

57Hos Hoshino, S., Mitsui, T., Jona, F., Pepinsky, R.: Phys. Rev. **107** (1957) 1255.
57Pep Pepinsky, R., Okaya, Y., Jona, F.: Bull. Am. Phys. Soc. [2] **2** (1957) 220.
58Nit Nitsche, R.: Helv. Phys. Acta **31** (1958) 306.
58Pul Pulvari, C.F., Kuebler, W.: J. Appl. Phys. **29** (1958) 1742.
61Gur Gurevich, V.M., Zheludev, I.S.: Kristallografiya **6** (1961) 778; Sov. Phys. Crystallogr. (English Transl.) **6** (1962) 624.
63Bli Blinc, R., Zupancic, I.: J. Phys. Chem. Solids **24** (1963) 1379.
66Bli Blinc, R., Lahajnar, G., Pintar, M., Zupancic, I.: J. Chem. Phys. **44** (1966) 1784.
66Bre Brezina, B., Smutny, F.: Proceeding of the International Meeting on Ferroelectricity, held at Prague (1966), Prague: Institute of Physics of the Czechoslovak Academy of Science 1966. Vol. 2, p. 182.
66Str Strukov, B.A., Taraskin, S.A., Koptsik, V.A.: Zh. Eksp. Teor. Phys. **51** (1966) 1037; Sov. Phys. JETP (English Transl.) **24** (1967) 692.
66Wie Wieder, H.H., Parkerson, C.R.: J. Phys. Chem. Solids **27** (1966) 247.
67Min Minaeva, K.A., Levanyuk, A.P., Strukov, B.A., Koptsik, V.A.: Fiz. Tverd. Tela **9** (1967) 1220; Sov. Phys. Solid State (English Transl.) **9** (1967) 950.
67Myl Mylov, V.P., Polandov, I.N., Strukov, B.A.: Fiz. Tverd. Tela **9** (1967) 3012; Sov. Phys. Solid State (English Transl.) **9** (1968) 2375.
67Sta Stankowski, J.: Phys. Status Solidi **24** (1967) 451.
71Bli Blinc, R., Slak, J., Stepisnik, J.: J. Chem. Phys. **55** (1971) 4848.
72Mac Mackowiak, M., Kurzynski, M.: Phys. Status Solidi (b) **51** (1972) 841.
72Sta Stankowski, J., Mackowiak, M.: Phys. Status Solidi (b) **51** (1972) 449.
72Var Varikash, V.M., Zarembovskaya, T.A., Lagutina, Zh.P.: Kristallografiya **17** (1972) 473; Sov. Phys. Crystallogr. (English Transl.) **17** (1973) 768.
72Zar Zarembovskaya, T.A., Varikash, V.M., Pupkevich, P.A.: Izv. Vyssh. Uchebn. Zaved. Fiz., 1972, 153.
73Mer1 Mercado, A., Gonzalo, J.A.: Phys. Rev. B **7** (1973) 3074.
73Mer2 Mercado, A., Gonzalo, J.A.: Ferroelectrics **5** (1973) 229.
73Sta Stankowska, J.: Acta Phys. Pol. A **43** (1973) 603.
73Tse Tsedrik, M.S., Margolin, L.N., Gontarev, V.F.: Krist. Tech. **8** (1973) 513.
73War Warkusz, F., Lukaszewicz, K.: Bull. Acad. Polon. Sci., Ser. Sci. Chim. **21** (1973) 275.
74Sta Stankowski, J., Galezewski, A., Waplak, S., Gruszczynska, U., Gierszal, H.: Ferroelectrics **6** (1974) 209.
76Mul Muller, D., Petersson, J.: Phys. Status Solidi (b) **78** (1976) 191.
77Gor Gordon, J.E., Boal, D.G.: Ferroelectrics **17** (1977) 411.
77Was Was'kowska, A.: Acta Univ. Wratislav. No. 341 (1977) 47.
78Fel Felix, P., Gamot, P., Lacheau, P., Raverdy, Y.: Ferroelectrics **17** (1978) 543.
78Rom Romanjuk, N.A., Andriyevskij, B.V., Zheludev, I.S.: Ferroelectrics **21** (1978) 333.
78Wap Waplak, S., Stankowski, J.: Acta Phys. Pol. A **54** (1978) 465.
79Che Chernenko, V.A., Polandov, I.N.: Fiz. Tverd. Tela **21** (1979) 1846; Sov. Phys. Solid State (English Transl.) **21** (1979) 1059.
79Loi Loiacono, G.M., Osborne, W.N., Delfino, M., Kostecky, G.: J. Cryst. Growth **46** (1979) 105.
79Ver Vergnat-Grandjean, D., Vergnat, P., Gerbaux, X., Hadni, A.: J. Phys. C **12** (1979) 3343.
79Was Waskowska, A., Olejnik, S., Lukaszewicz, K., Ciechanowicz-Rutkowska, M.: Ferroelectrics **22** (1979) 855.
80Dou Dougherty, J.P., Seymour, R.J.: Rev. Sci. Instrum. **51** (1980) 229.
80Sta Stankowski, J., Malinowski, W.: Acta Phys. Pol. A **58** (1980) 773.
81Loi Loiacono, G.M., Kostecky, G.: Thermochim. Acta **45** (1981) 133.
81Mat Mathur, S.C., Batra, A.K., Singh, H., Mansingh, A.: Ferroelectrics **39** (1981) 1197.
81Sta Stankowski, J.: Phys. Rep. **77** (1981) 1.
82Var Varikash, V.M., Shuvalov, L.A., Tarasevich, E.V., Lagutina, J.P.: Ferroelectrics **42** (1982) 47.
83Ema Ema, K.: J. Phys. Soc. Jpn. **52** (1983) 2798.

83Rom Romanyuk, N.A., Mytsyk, B.G., Varikash, V.M.: Fiz. Tverd. Tela **25** (1983) 1670; Sov. Phys. Solid State (English Transl.) **25** (1983) 962.
83Zan Zankevich, V.A., Gover, G.A., Varikash, V.M., Khachatryan, Yu.M.: Izv. Akad. Nauk SSSR, Ser. Fiz. **47** (1983) 776; Bull Acad. Sci. USSR, Phys. Ser. (English Transl.) **47**, No. 4 (1983) 150.
88Cho Chobot, G.M., Kurilovich, N.F., Varikash, V.M., Shuvalov, L.A.: Kristallografiya **33** (1988) 925; Sov. Phys. Crystallogr. (English Transl.) **33** (1988) 547.
90YiJ Yi, J., Lan, G., Li, B., Hu, S., Wang, H., Zheng, J.: Ferroelectrics **101** (1990) 251.
94Ort Ortega, J., Folcia, C.L., Etxebarria, J., Breczewski, T.: Ferroelectrics **152** (1994) 355.